University of Nottingham
UK | CHINA | MALAYSIA

Analysing the role of medulloblastoma exosomes as biomarkers and their functional contribution to metastasis

Hannah K. Jackson BSc, MRes

Thesis submitted to the University of Nottingham for the degree of Doctor of Philosophy

March 2021

Children's Brain Tumour Research Centre

Abstract

Introduction: Recurrent/metastatic medulloblastoma is a devastating disease with an abysmal prognosis of less than 10% five-year survival. Whilst primary tumours can be classified based on epigenetic and transcriptomic features, there is very little information regarding molecular signatures of metastatic tumours. The secretion of extracellular vesicles (EVs) has emerged as a pivotal mediator for communication in the tumour microenvironment during metastasis. The most investigated EVs are exosomes, nanovesicles secreted by all cell types and able to cross the blood-brain-barrier. The role of exosomes as vehicles for cell-to-cell communication between a tumour and its microenvironment is a relatively new concept, with only limited study of this potential mechanism in medulloblastoma. This study aims to gain insight into the differences between exosomes of primary and metastatic medulloblastoma cell lines to better understand how exosomal cargo may account for differences seen between these phenotypes and to identify their applicability as a prognostic biomarker of increased metastatic potential.

Methods and Results: Metastatic medulloblastoma cells were found to secrete markedly more exosomes compared to non-metastatic primary cells. Additionally, metastatic exosomes significantly enhanced the migration and invasiveness of primary and non-malignant cells in a transwell migration assay. Moreover, we demonstrated that the pro-migratory function of metastatic exosomes was, in part, due to tumour-promoting proteins EMMPRIN and MMP-2 enriched on their external surface. Furthermore, using zymography assay, metastatic exosomes were shown to potentiate medulloblastoma migration resulting in degradation of extracellular matrix components, via the active protease, MMP-2, on their surface. In support of this, stable genetic knockdown of MMP-2 or EMMPRIN antagonised the pro-migratory function of exosomes.

Next generation sequencing was utilised to characterise exosomal RNA cargo (mRNA and miRNA). Hierarchical clustering, demonstrated that metastatic exosomes had

distinct genetic cargoes compared to primary and normal exosomes. Further characterisation of the RNA delineated target pathways of importance for medulloblastoma progression and interaction with the surrounding microenvironment, in agreement with the pro-migratory phenotype conferred by metastatic exosomes.

Differential gene expression analysis of mRNA sequencing data, identified *PCAT1, PAPPA2* and *POU5F1B* as highly enriched in metastatic exosomes compared to their matched primary counterpart. These genes had previously been implicated in cancer progression in other cancer types, and in this study their high expression correlated with poor overall survival and tumour metastasis in medulloblastoma. A number of miRNAs were also identified which were differentially secreted in metastatic exosomes relative to primary and normal exosomes, yielding a candidate set of exosomal miRNAs as potential metastatic medulloblastoma biomarkers. Notably, several of the candidate miRNAs (miR-382-5p, miR-381-3p, miR-346, miR-628-5p) were detected at substantially higher levels in metastatic disease CSF samples, compared to matched CSF samples from their primary tumour.

Conclusion: This study demonstrates the importance of exosomes in creating a favourable environment to drive medulloblastoma metastasis, either through extracellular matrix signalling, via surface-bound proteins, or through intracellular delivery of their RNA cargo to recipient cells. Our observations have also highlighted the possibility of CSF-derived exosomal miRNAs as biomarkers for metastatic medulloblastoma.

Acknowledgements

For me, these are the most important pages of my thesis because without those mentioned here, none of the other pages would have been possible. There are so many others beyond those mentioned here who have helped and supported me and for that, I am truly grateful.

First of all, I wish to express my deepest gratitude to my fantastic supervisor, Dr Beth Coyle, for your continual guidance and encouragement, which has been a constant source of motivation. You have been a supervisor, mentor and friend to me over the past four years and it has been a privilege to work with you. To my supervisor Dr Ian Kerr, your support and advice has been invaluable, you have always been there when I have needed you. I am truly grateful for your kindness and reassurance over the years; not forgetting your dry sense of humour too! I thank you both for believing in me, I could not have asked for better supervisors.

A special thanks are owed to Dr Franziska Linke for always steering me in the right direction. I am in awe of your drive and skill, you are the best postdoc I could have ever wished for.

To my dearest friends, Sophie, Macha, Christine, Alice, Louisa and James, you have been my constant support network throughout this PhD and I will forever be grateful for your friendship. I cannot imagine my PhD without you all by my side. Soph, you have been the best friend to me for over a decade, I certainly wouldn't be where I am now if it wasn't for you.

I would also like to express my gratitude to all my lovely fellow CBTRC members and friends who I have had the privilege to work with. Thank you for making it the most joyful, friendly and caring work environment. A special thank you to Catherine, Phoebe, Alina, Louise, Michaela, Jasper, James and Josh. A big thank you to everyone in the

Kerr lab, Parth, Debs, James and Simon, your patience, expertise and kindness always made me feel so welcome.

I would like to extend my thanks to The James Tudor Foundation, without whom this project would not have been possible; your support has not gone unappreciated.

To my loved ones, I owe my family for believing in me and caring so much. My parents, grandparents, sister, aunts and cousins, I am deeply grateful for your never ending support. To my Grandads, I hope I have made you proud.

Not forgetting my four-legged family, Brunni, Heidi and Kiki, your constant cuddles and companionship is incomparable.

To Jay, my greatest team mate, I am forever grateful for your ability to make me smile even through the hard times. Thank you for supporting my pursuit of a scientific career and always believing in me, you have truly helped me forward every step of the way. To my wonderful sister Lauren, I could never thank you enough for being my greatest cheerleader and for your absolute confidence in me. Your love and support has always kept me smiling.

To Mum and Dad, who I dedicate this thesis to. I couldn't have done any of this without your unconditional love, guidance and encouragement. You are my biggest motivators and you have always filled me with the confidence that I am capable of doing anything I put my mind to. I am so proud to be your daughter.

List of publications and grants

Original articles:

Sabnis, D. H. *et al.* (2019) 'A role for ABCB1 in prognosis, invasion and drug resistance in ependymoma', Scientific Reports, 9(1). doi: 10.1038/s41598-019-46700-z.

Théry, C. *et al.* (2018) 'Minimal information for studies of extracellular vesicles 2018 (MISEV2018): a position statement of the International Society for Extracellular Vesicles and update of the MISEV2014 guidelines', Journal of Extracellular Vesicles, 7(1). doi: 10.1080/20013078.2018.1535750.

Conference abstracts:

Jackson, H. K. *et al.* (2018) 'MBRS-21. Extracellular vesicles from metastatic medulloblastoma cell lines carry mRNAs known to correlate with metastatic disease', Neuro-Oncology, 20(suppl_2), pp. i132–i132. doi: 10.1093/neuonc/noy059.466.

Jackson, H. K. *et al.* (2020a) 'MBRS-27. Exosomes carry distinct miRNAs that drive medulloblastoma progression', Neuro-Oncology, 22(Supplement_3), pp. iii403–iii403. doi: 10.1093/neuonc/noaa222.542.

Jackson, H. K. *et al.* (2020b) 'MBRS-28. Exosomes drive medulloblastoma metastasis in a MMP-2 and EMMPRIN dependent manner', Neuro-Oncology, 22(Supplement_3), pp. iii403–iii403. doi: 10.1093/neuonc/noaa222.543.

Grants:

2020: Awarded the James Tudor Foundation Travel grant **(£2,234)**

2019: Co-applicant BBSRC research summer experience placement **(£500)**

2018: Awarded the School of medicine postgraduate research travel grant **(£600.00)**

2018: Awarded the University of Nottingham graduate school travel grant **(£578.25)**

2017: Co-applicant for a grant application to secure funding for my PhD **(£89,950)**

Table of Contents

List of Figures

List of Tables

List of common abbreviations

ANOVA	analysis of variance
BBB	blood-brain barrier
BME	Base membrane extract
CNS	central nervous system
CSF	cerebrospinal fluid
CSRT	craniospinal radiotherapy
DMEM	Dulbecco's modified eagle's medium
DMSO	Dimethyl N3-sulfoxide
ECM	extracellular matrix
EGF	epidermal growth factor
EMMPRIN	extracellular matrix metalloproteinase inducer
EMT	epithelial to mesenchymal transition
EpCAM	epithelial cell adhesion and activation molecule
ESCA	oesophageal carcinoma
ESCRT	endosomal sorting complexes required for transport
EV	extracellular vesicle
EXO	exosome
FBS	foetal bovine serum
FDR	false discovery rate
FGF	fibroblast growth factor
FP	forward primer
GAPDH	glyceraldehyde 3-phosphate dehydrogenase
GBM	glioblastoma multiforme

GO	gene ontology
GSEA	gene set enrichment analysis
HNSC	head and neck squamous cell carcinoma
IGF	insulin-like growth factor
ILVs	intraluminal vesicles
INS	insulin
ISEV	International Society of Extracellular Vesicles
KEGG	kyoto encyclopedia of Genes and Genomes
LAM111	laminin-111
M-stage	metastatic staging
MBEN	medulloblastoma with extensive nodularity
NSCLC	non-small cell lung cancer
LC/A	large cell/anaplastic
lncRNA	long non-coding RNA
MAPK	mitogen-activated protein kinase
MDS	multidimensional scaling
miRNA	micro RNA
MMP	matrix-metalloproteinase
MRI	magnetic resonance imaging
mRNA	messenger RNA
MV	microvesicles
MVB	multivesicular body
NanoFCM	nanoscale flow cytometry
NGS	next-generation sequencing
NTA	nanoparticle tracking analysis

PAPPA	pappalysin-2
PCA	principal component analysis
PCAT1	prostate cancer associated transcript 1
PI3K	phosphoinositide 3-kinase
POU5F1B	POU Class 5 Homeobox 1B
RFU	relative fluorescence unit
RP	reverse primer
RPM	reads per million
SD	standard deviation
SEC	size-exclusion chromatography
SEM	standard error of the mean
TEM	transmission electron microscopy
UMI	unique molecular index
WHO	World Health Organisation
WNT	wingless
YBX1	Y-box-binding protein 1

Chapter 1

Introduction

Chapter 1. Introduction

Cancer is one of the leading causes of death worldwide, accounting for an estimated 9.6 million deaths, or one in six deaths in 2019 (WHO, 2019). The cancer burden continues to rise globally due to the growing and ageing world population (Sung *et al.*, 2021). Childhood cancer is rare, with the overall incidence rates varying between 50 and 200 per million children globally (WHO, 2019). The pattern of cancer in children differs considerably to cancer in adults. In general, leukaemia constitutes around a third of all cancers in childhood. Brain and central nervous system (CNS) tumours represent the second most prevalent cancer in children, accounting for approximately 25% of all paediatric cancers. They also remain the leading cause of cancer-related mortality and morbidity in children. Among those who do survive, it is thought that over 60% develop substantial health, neurological, behavioural and developmental sequelae caused by current treatment protocols (Kessler and Bhatt, 2018; Pollack, Agnihotri and Broniscer, 2019). Over the past two decades the cure rates of patients with paediatric brain tumours has improved. However, the outcome has remained the same for these tumours, due to intractable drug resistance, metastatic nature and the limited number of clinical trials being conducted for patients with these tumours (Miklja *et al.*, 2019). This coupled with the unique nature of the microenvironment of the central nervous system and poor drug access, means that brain tumours represent a difficult medical challenge (D'Asti *et al.*, 2012, 2016). It is clear that further research is required, to better understand the mechanisms driving drug resistance and metastasis, and to target these in a way that improves survival rates with reduced associated complications.

There are over 100 different subtypes of brain and CNS tumours, with presentation depending on age, histology and location of the tumour. The most common paediatric brain tumours are classified into three distinct groups; medulloblastomas, ependymomas and astrocytomas. This classification is based on the origin of the

tissue, histopathological features of the malignancy, and the location of the tumour. The focus of this project is medulloblastoma, the most prevalent malignant paediatric brain tumour.

1.1 Medulloblastoma

Medulloblastoma is an embryonal tumour of the cerebellum and is classified as a highly malignant grade IV tumour according to the World Health Organisation (WHO), implying a high proliferative potential and aggressive nature (Louis *et al.*, 2016). The peak age of diagnosis is ~3-9 years of age, although tumours can occur during the first year of life or during adulthood in some individuals. Tumours are highly invasive and commonly disseminate, frequently metastasising to the leptomeningeal space of the spinal cord and brain (Ramaswamy *et al.*, 2017). In fact, 30% of medulloblastoma patients display metastases at diagnosis and almost all patients exhibit metastasis at relapse (Zapotocky *et al.*, 2018).

Classical symptoms of patients suffering with medulloblastoma include, morning headaches, nausea and vomiting (associated with elevated intracranial pressure), double vision (associated with cranial nerve dysfunction), ataxic gait with unsteadiness and papilledema (associated with dysfunction of the cerebellar vermis) (Angelini *et al.*, 2016; Northcott *et al.*, 2019). Patients with a suspected medulloblastoma are diagnosed by cranial and spinal magnetic resonance imaging (MRI), revealing a mass in the posterior fossa region. Patients may also display evidence of metastases, as assessed by spinal MRI and cytological assessment of the lumbar cerebral spinal fluid (CSF) (Van Ommeren *et al.*, 2020).

1.1.1 Medulloblastoma tumour classification

Primarily, medulloblastoma was regarded as a single tumour entity, with prognosis being based on clinical factors including, metastatic status, histology and extent of resection. The 2007 WHO brain tumour classification aimed to move towards a more biological sub-grouping approach, with medulloblastoma divided into four different histological variants: classical, desmoplastic, medulloblastoma with extensive

nodularity (MBEN) and large cell/ anaplastic (Louis *et al.*, 2007). In recent years, advances in transcriptomics and high-throughput methods has allowed medulloblastoma to be further classified into four distinct molecular subgroups: Wingless (WNT), Sonic Hedgehog (SHH), Group 3 and Group 4 (Louis *et al.*, 2016). The WNT and SHH subgroups were named from the signalling pathways playing the most significant roles in the pathogenesis of that subgroup. The underlying biology driving the remaining two subgroups is less well understood. Therefore, the agreement was to retain generic names for these groups. The four core molecular subgroups are distinct genetically, epigenetically and phenotypically and are associated with different risks and prognosis. Due to the heterogeneity of medulloblastoma tumours, more recently the four subgroups were further subcategorised into 12 subtypes with distinct somatic copy-number aberrations, activated pathways, and clinical outcomes (Cavalli *et al.*, 2017).

1.1.1.1 Histological characteristics of medulloblastoma

Traditionally, the diagnosis of medulloblastoma has been established by histopathological evaluation. As previously mentioned, a total of four morphologies have been distinguished; classical, desmoplastic, MBEN and large cell/ anaplastic (Figure 1.1).

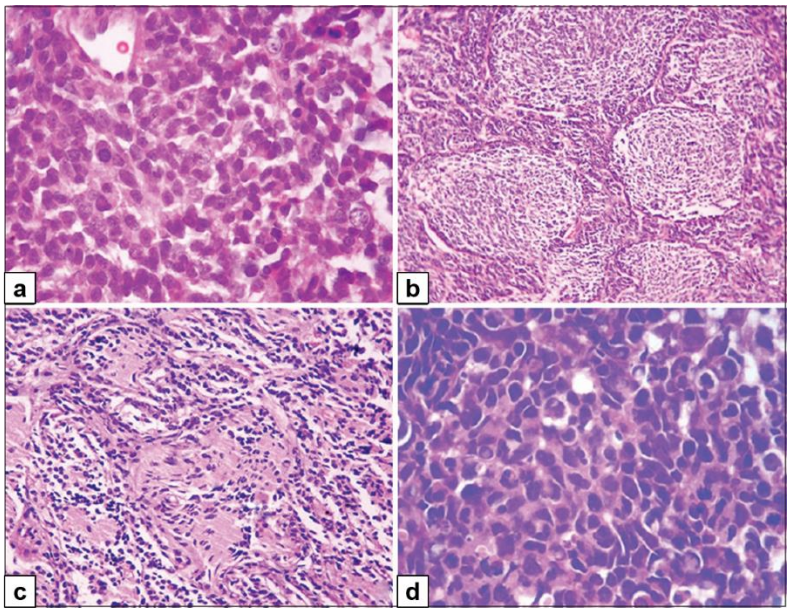

Figure 1.1 Histological variants of medulloblastoma

Microphotographs showing (A) classic medulloblastoma, characterised by sheets of small cells with a high nuclear to cytoplasmic ratio. (B) Desmoplastic subtype, characterised by reticulin-free nodules surrounded by proliferating cells which produce an extracellular matrix rich in reticulin. (C) Medulloblastoma with extensive nodularity, characterised by large reticulin-free nodules populated with small rounded cells. (D) Large cell/anaplastic subtype, displaying characteristic cells with prominent nucleoli and large nuclei embedded in a background of cells. Image adapted from (Orr, 2020).

Classic medulloblastoma, which represents the majority of medulloblastoma tumours (~70%), are characterised by sheets of pleomorphic, small, round cells usually with a high nuclear to cytoplasmic ratio. Homer-Wright rosettes, indicating neuroblastic differentiation, are present in some classic tumours (Northcott *et al.*, 2019). Desmoplastic tumours are characterised by reticulin-free nodules, surrounded by proliferating cells which produce an extracellular matrix rich in reticulin. Tumours of this pathology represent 7% of all medulloblastomas. Desmoplastic tumours arise in the cerebellar hemispheres usually in children below the age of 3 and are associated with a favourable outcome (Orr, 2020). Large cell/anaplastic (LC/A) medulloblastoma compromises the most undifferentiated tumours and accounts for around 10-20% of diagnosed medulloblastomas. LC/A tumours are characterized by large round cells with prominent nucleoli and large nuclei embedded in a background of cells (Figure 2D). These tumours, known for their aggressive behaviour, often metastasise via the

CSF and outside the central nervous system (Taylor *et al.*, 2012). MBEN tumours constitute the remaining 5% of medulloblastomas and are indicative of a favourable outcome. Like desmoplastic subtype, MBEN is also characterised by reticulin-free nodules, however in this instance these are larger and populated with small rounded cells (Cavalli *et al.*, 2017).

1.1.1.2 Molecular characteristics of medulloblastoma subgroups

With the arrival of microarray, and later deep sequencing gene technologies, our molecular understanding of medulloblastoma has been revolutionised. Medulloblastoma is no longer regarded as a single entity; instead expression profiling identified discrete molecular subgroups within medulloblastoma, and in 2012 a consensus on medulloblastoma subgroups emerged proposing four distinct molecular subgroups. The four groups are distinct in terms of histology, genetic profiles, pathway signatures and are associated with different risks and outcomes, as summarised in (Table 1.1)

Based on the significance of molecular subgrouping for medulloblastoma tumours, the most recent update of the WHO classification of CNS tumours now classifies medulloblastomas according to their molecular characteristics as well as histopathological features (Louis *et al.*, 2016). The following section will discuss each of the medulloblastoma molecular subgroups in further detail.

Table 1.1 Molecular subgroups of medulloblastoma

Based on data from the following references (Northcott *et al.*, 2012; Taylor *et al.*, 2012; Juraschka and Taylor, 2019)

	WNT	SHH	Group 3	Group 4
Age Group				
Gender ♀:♂	1 : 1	1 : 1	1 : 2	1 : 3
Anatomic location				
Histology	Classic, rarely LCA.	Desmoplastic, classic, LCA.	Classic, LCA.	Classic, LCA.
Prevalence	10%	30%	25%	35%
Prognosis	Very good	Infants good, others intermediate	Poor	Intermediate
Metastasis	Rare	Uncommon	Very frequent	Frequent
Proposed cell of origin	Progenitor cells in the lower rhombic lip	Granular precursors of the external granule layer	Neural stem cells	Unipolar brush cells
Genetic Alterations	*CTNNB1, DDX3X, SMARCA4, TP53* mutation.	*PTCH1, SMO, SUFU, TP53* mutation, *GLI2, MYCN* amplification.	*GLI1, GFLB* activation, *MYC, OTX-2* amplification, *SMARCA4* mutation.	*KDM6A* mutation, *SNCAIP* duplication, *CDK6, MYCN* amplification.

1.1.1.2.1 WNT subgroup

WNT subgroup is the most understood of the medulloblastoma tumours, however is the least frequently occurring, accounting for only 10% of all medulloblastoma tumours. Tumours typically reside in the midline region of the fourth vertical and infiltrate the brain stem. Almost all WNT tumours studied exhibit classic histology and rarely metastasize (Ramaswamy *et al.*, 2016).

Up to 90% of WNT tumours harbour somatic activating mutations in exon 3 of *CTNNB1* which encodes β-catenin, this leads to an accumulation of nuclear β-catenin which is a characteristic observed in WNT patients and can be analysed by immunohistochemical staining for β-catenin. Alternatively, patients can be screened

for hotspot mutations in exon 3 of *CTNNB1* by sequencing (Ramaswamy *et al.*, 2017). Patients with WNT tumours who lack somatic *CTNNB1* mutations often contain constitutional variants of tumour suppressor gene *APC* (Kessler and Bhatt, 2018). Another hallmark feature of WNT tumours is monosomy 6, which is present in 80% of patients, typically co-occurring with *CTNNB1* mutations. Other than monosomy 6, it is uncommon to see other regions of genetic amplification or deletion in the genome of patients with WNT tumours (Northcott *et al.*, 2012; Cavalli *et al.*, 2017).

Patients with WNT tumours have a very good long term prognosis in comparison to other subgroups, with survival rates likely to exceed 90% (Taylor *et al.*, 2012). This may be a result of alterations in the brain vasculature in these patients. Indeed, several studies on human and mouse WNT medulloblastomas, revealed WNT tumours lacked an intact blood-brain barrier (BBB) (Phoenix *et al.*, 2017). This leaky vasculature was suggested to render them more accessible to systemic chemotherapies, providing a potential biological explanation for the favourable treatment response of patients with WNT tumours, although further validation is required.

1.1.1.2.2 SHH subgroup

Demographically, SHH tumours account for around 30% of medulloblastoma tumours, and have a balanced sex ratio and a bimodal peak age incidence, most often occurring in infants and adults. They classically arise in the cerebellar hemispheres, and are thought to arise from granule cell precursors of the external granule layer (Huang *et al.*, 2016). SHH tumours can have classic, LC/A and desmoplastic/nodular histology, with the desmoplastic/nodular variant exclusively classified to this group (Kool *et al.*, 2014; Cavalli *et al.*, 2017).

As the name suggests, SHH medulloblastomas are characterised by activation of the SHH signalling pathway, a pathway involved in cerebellar development. The majority of patients harbour germline or somatic mutations in critical genes of the pathway. These mutations include, loss-of-function mutations or deletions in *PTCH1* (43% of patients), loss-of-function mutations or deletions in *SUFU* (10%), activating mutations

in *SMO* (9%), *GLI1* or *GLI2* amplifications (9%) and *MYCN* amplifications (7%) (Northcott *et al.*, 2012; Kool *et al.*, 2014). In addition, recurrent alterations in the *TP53* signalling pathway (9.4%) and the PI3K pathway (10%) may also act as key drivers of tumorigenesis in this subgroup (Northcott *et al.*, 2012).

Patients with SHH tumours have an intermediate prognosis with a 5-year survival rate of approximately 75% (Kool et al., 2012). However, around 15-20% of patients present with metastatic disease and are considered to be at higher risk than patients who are non-metastatic. SHH tumours usually recur locally in the original resection cavity, with leptomeningeal dissemination more common in infant patients compared to adults (Taylor *et al.*, 2012).

1.1.1.2.3 Group 3

Group 3 tumours confer the worst prognosis, with less than 50% 5-year survival (Ramaswamy *et al.*, 2016). Demographically, Group 3 tumours occur most frequently in males and are present in both children and infants, but are seldom seen in adults. The majority of Group 3 tumours exhibit classic histology, however Group 3 also encapsulates the majority of LC/A tumours. (Kool *et al.*, 2008; Kim *et al.*, 2011). This subgroup accounts for around 25% of all medulloblastoma tumours and is associated with very high rates of metastasis (Northcott *et al.*, 2012). Radiographically, these tumours are located in the midline vermin adjacent to the fourth ventricle (Zapotocky *et al.*, 2018).

Approximately 40-45% of patients with Group 3 medulloblastomas present with metastatic disease. Unlike SHH tumours, Group 3 tumours recur distantly, away from the primary tumour site. However, despite the extremely aggressive nature of Group 3 tumours, a recent study by Zapotocky *et al.,* noted that more than half of the Group 3 tumours analysed in their cohort did not exceed a diameter of 35 mm, making them significantly smaller than SHH and Group 4 tumours (Zapotocky *et al.*, 2018).

Group 3 tumours likely arise from a neural stem cell population (Robinson *et al.*, 2019). Unlike, WNT and SHH no germline mutations associated with a predisposition to

Group 3 are known. Nonetheless, a commonly occurring cytogenetic alternation is focal, high-level amplifications of the *MYC* proto-oncogene, an event that often co-occurs with *PVT1-MYC* fusions (Ramaswamy *et al.*, 2017). Unfortunately, *MYC* expression alone is not a prognostic indicator of Group 3 as *MYC* is downstream target of the WNT pathway, thus is also observed in WNT tumours (Rudin *et al.*, 2009). *MYC* amplification has been observed in around 17% of Group 3 tumours and is indicative of a high risk of recurrence and low survival rates. Amplification of the medulloblastoma oncogene *OTX2* is also common in Group 3 tumours (Adamson *et al.*, 2010). Cytogenetic events are also common in this subgroup. Isochromosome 17q is present in 40-50% of cases, and other common events are loss of chromosomes 8, 10q and 16q and gain of 1q, 7, and 18 (Kool *et al.*, 2008; Northcott et al., 2012). NPR3 has been proposed as an immunohistochemical marker for Group 3 tumours (Northcott *et al.*, 2011).

1.1.1.3 Group 4

Group 4 medulloblastomas are the most prevalent tumours, accounting for 35-40% of all medulloblastoma diagnoses (Kool *et al.*, 2014). They typically occur in childhood and adolescents and are far more frequent in males (3:1 gender ratio). Patients with Group 4 medulloblastoma tumours have an intermediate prognosis, with an overall 5-year survival of 75% (Northcott *et al.*, 2011). The cell of origin of Group 4 tumours has not been definitively established, however these tumours appear to have transcriptional similarities to unipolar brush cells (Robinson *et al.*, 2019).

Despite the fact that Group 4 tumours account for over 35% of all medulloblastomas, the molecular pathogenesis of these tumours are less understood and are least represented among the current established cell lines (Ivanov *et al.*, 2016). As seen in Group 3 patients, isochromosome 17q is also observed in Group 4 tumours, however it is more frequent in Group 4 (66%) compared with Group 3 tumours (26%). Deletions of chromosome 17p is also seen in Group 4 tumours, however has rarely been observed in WNT or SHH subgroups. Group 4 tumours are currently identified through

transcriptional profiling and *KCNA1* has been proposed as the marker for immunohistochemistry (Kim *et al.*, 2011; Northcott *et al.*, 2019).

Tumours of this subtype frequently disseminate, with 30-40% of patients exhibiting metastases at diagnosis (Northcott *et al.*, 2012). Comparable to Group 3 tumours, distal metastases at recurrence are more common than local disease (Ramaswamy *et al.*, 2017).

1.1.1.4 Further stratification of medulloblastoma subgroups

While molecular subgrouping has substantially advanced the understanding of medulloblastoma, the importance of heterogeneity within medulloblastoma subgroups was unknown. Thus, there have been numerous attempts to further subcategorise the subgroups. The most notable by Cavalli *et al.,* who built on the classification of medulloblastoma into subgroups, using integrated analysis of DNA methylation, gene expression, copy number alterations, and clinical data revealing the existence of twelve subtypes of medulloblastoma (Figure 1.2) (Cavalli *et al.*, 2017).

Cavalli *et al.,* suggested the existence of two WNT subtypes; WNTα and WNTβ constituting 70% and 30% of WNT tumours respectively. WNTα encompassed mainly children, had a similar prognosis to WNTβ and has ubiquitous monosomy 6. WNTβ comprised older children and adults, who were frequently diploid for chromosome 6.

Four clinically and cytogenetically distinct SHH subtypes have been described; SHHα, SHHβ, SHHγ, and SHHδ. SHHα primarily affect children aged 3-16 years, have the worst prognosis and are enriched for *TP53* mutations and *MYCN*/*GLI2* amplification. SHHβ also have a poor prognosis, predominantly occur in infants and are frequently metastatic. SHHγ tumours have a balanced genome, are associated with a good outcome and typically display MBEN histology. Finally, the SHHδ subtype occurs mainly in adults and tumours are enriched for *TERT* promoter mutations (Cavalli *et al.*, 2017; Juraschka and Taylor, 2019).

Three distinct subtypes of Group 3 tumours have now emerged; Group 3α, Group 3β and Group 3γ. Group 3α tumours occur in infants and despite being frequently metastatic are associated with a better outcome, Group 3β were predominantly displayed in older children and featured *OTX2* gain, *DDX3*1 loss, and high *GFI1/GFI1B* expression, and Group 3γ encompassed mainly infants, is characterised by *MYC* amplification and a high rate of metastasis. Group 3γ has the worst outcome of all medulloblastomas.

Group 4 tumours were also subdivided into three subtypes; Group 4α, Group 4β and Group 4γ. Molecular features associated with these subtypes include *MYCN* and *CDK6* amplification in Group 4α, *SNCAIP* duplication in Group 4β, and *CDK6* amplification in Group 4γ. Unlike the other subgroups, there was no significant difference in overall survival or metastatic dissemination.

The identification of clinically and biologically different subtypes within each of the four core subgroups of medulloblastoma has further refined our understanding of the genomic landscape of medulloblastoma, will simplify the identification of targets for therapy, and could allow for therapies effective across subtypes (Cavalli *et al.*, 2017).

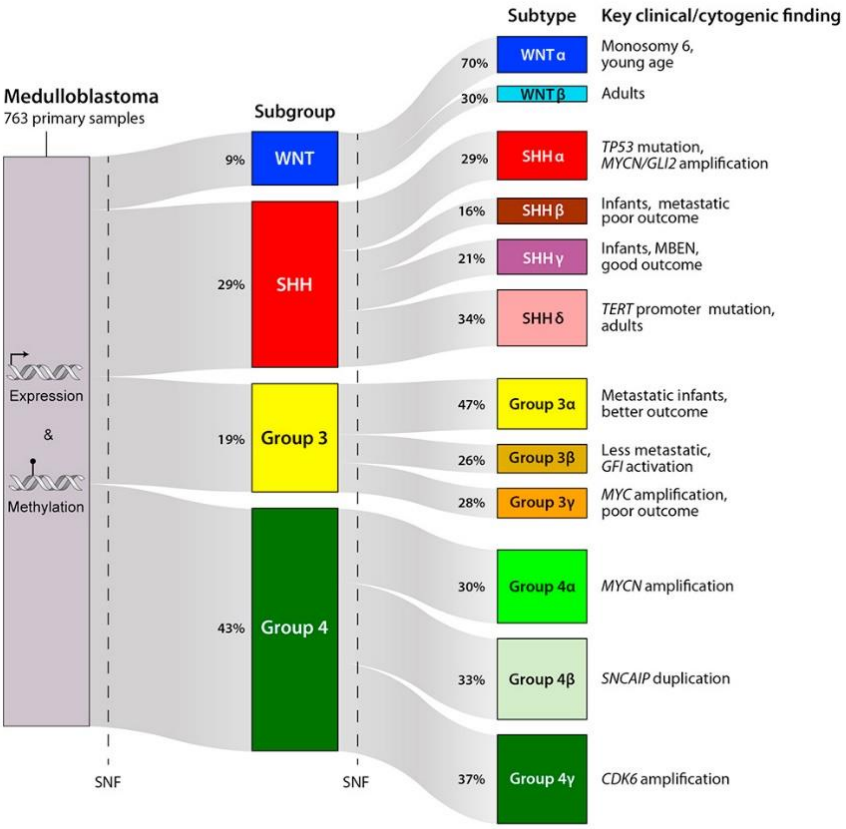

Figure 1.2 Intertumoral heterogeneity within medulloblastoma subgroups

Schematic representation of the classification of medulloblastoma into subgroups. In 2017 Cavalli *et al.,* used integrated analysis of DNA methylation, gene expression, copy number alterations, and clinical data to analyse 763 primary medulloblastoma samples. This revealed the existence of twelve subtypes within the classic four molecular subgroups of medulloblastoma (WNT, SHH, Group 3 and Group 4). Diagram taken from Cavalli *et al.,* 2017.

1.1.2 Risk stratification

Historically, prognosis of a patient with medulloblastoma relied primarily on extent of surgical resection, age at diagnosis, histological subtypes, presence of metastases and occasionally genetic and pathological factors including presence of *MYCN* amplifications. However, an updated risk stratification proposal for medulloblastoma patients aged 3-17 was developed (Ramaswamy *et al.*, 2016; Juraschka and Taylor, 2019), taking into account subgroup status and select genetic and cytogenetic aberrations to more precisely predict outcome. This stratification ascribes patients to one of four risk groups; low risk (>90% survival), standard risk (75%-90% survival),

high risk (50-75% survival) and very high risk (<50% survival). The four risk categories are summarized below (Table 1.2).

Table 1.2 Proposed risk stratification for medulloblastoma

Based on data from Ramaswamy *et al.,* 2016

Risk category	Low	Standard	High	Very high
Survival (%)	>90	75-90	50-75	<50
WNT	Non-metastatic under age of 16			
SHH		Non-metastatic, *TP53* WT and no *MYCN* amplification	All *MYCN* amplified non-infant metastatic, *TP53* WT	*TP53* mutation
Group 3		Non-metastatic, no *MYC* amplification		metastatic, with *MYC* amplification
Group 4	Non-metastatic chromosome 11 loss	Non-metastatic, no chromosome 11 loss	Metastatic	

1.1.3 Medulloblastoma treatment

The current treatment of medulloblastoma is based on risk stratification. Patients characterised as standard risk involves complete surgical resection, followed by craniospinal radiotherapy (CSRT) and maintenance chemotherapy. Despite the fact CSRT is an effective therapy and has dramatically increased overall survival, it leads to irreparable damage to the surrounding cells and numerous adverse clinical effects including neurocognitive and psychological health impairments, hearing loss, infertility and hormonal imbalances. Clinical trials have tested combination adjuvant chemotherapy or multimodal therapies to limit these adverse effects (Kessler and Bhatt, 2018).

Patients with high-risk medulloblastoma require more aggressive treatments. High risk patients above the age of three are treated with high-dose chemotherapy and radiotherapy. Patients below the age of three are considered high-risk due to the avoidance of radiotherapy, this is to prevent neurocognitive impairment which could

likely have devastating long term effects. Therefore, adjuvant chemotherapy is the main treatment used in children, examples include methotrexate, carboplatin, cisplatin, vincristine, lomustine and etoposide (Ramaswamy *et al.*, 2017; Menyhárt and Győrffy, 2020).

Trade-offs between the side effects of current treatment protocols and the potential of improved survival have caused survival rates to remain stagnant over the past three decades (Juraschka and Taylor, 2019). Complete surgical resection can lead to complicated neurological defects- cerebellar mutism occurs in approximately 25% of medulloblastoma patients. Radiotherapy and chemotherapy, particularly in infants, are associated with neurocognitive impairment, hearing loss, short stature, pituitary hormone deficiency, cerebrovascular disease and secondary malignancies (Orr, 2020). These factors all have significant impacts on the quality of life of medulloblastoma patients and increase the urgency to identify more effective treatments to maximise treatment efficacy but also reduce the long-term sequelae of current therapies.

1.1.4 Medulloblastoma metastasis

Metastasis describes the dissemination of tumour cells to distant organs or parts of the body resulting in the formation of secondary tumours. It is defined as one of the six classical hallmarks of cancer (Hanahan and Weinberg, 2011). The occurrence of metastases often confers a devastating clinical fate and is responsible for over 90% of cancer-related deaths (Gupta and Massagué, 2006).

Metastasis is a complex, multistep process dependent on intrinsic and external environmental factors. The initial steps of the metastatic process requires the cells to acquire an invasive phenotype and lose their adhesion to the stroma (Friedl, 2009), this results in degradation of the surrounding tissue at the primary tumour site, followed by breakdown of the basement membranes of blood, lymphatic vessels or the leptomeninges (Chambers, Groom and MacDonald, 2002). This process is termed intravasation and allows tumour cells to migrate around the body via the lymph or

circulatory system or along surfaces across body cavities. After successful intravasation, some of the tumour cells eventually adhere to blood vessel walls and can invade (extravasation) and migrate into the local tissue, here they are capable of forming a secondary tumour. The process of metastasis is considered highly inefficient as only 0.01% of tumour cells which reach the blood stream succeed in establishing a secondary metastatic tumour (Fidler, 1970). A recent study in mice, has also suggested that cancer cells rarely form metastatic tumours alone, and travelling in groups increases their chances of survival and forming a new metastasis (Cheung *et al.*, 2016).

Epithelial to mesenchymal transition (EMT) often initiates the multistep metastatic process. EMT refers to epithelial tumour cells acquiring a mesenchymal phenotype under the influence of cancer-associated fibroblasts (CAFs). Tumour cells undergoing EMT lose their cell-cell junctions and epithelial polarity, and enter a low proliferative state with an increased invasive and migratory capacity (Diepenbruck and Christofori, 2016). Molecular markers of EMT include an increased expression of *vimentin* as a mesenchymal marker and loss of *E-cadherin* and *β-cadherin* as epithelial markers (Figure 5.). A spindle-like cell shape is also characteristic of cells undergoing EMT (Dudás *et al.*, 2018). These morphological changes are regulated by three transcriptional factors, *Snail, Zeb* and *Twist*. Once the tumours have reached the distant metastatic site the reverse process takes place. Mesenchymal to epithelial reverting transition (MErT) returns tumour cells to a high proliferative state and allows for the formation of secondary tumours (Steinbichler *et al.*, 2018).

Metastatic sites are not chosen randomly, and different types of cancers appear to favour particular organs as secondary tumour sites (Lu and Kang, 2007). This idea was originally postulated by Stephen Paget in 1889 who suggested that metastasis was not a random event. Instead, it was hypothesised that initiating cancer cells “seed” require a certain affinity to a particular organ “soil” to establish tumour growth, because they offer a compatible microenvironment (Paget, 1889). This has allowed for

metastatic patterns to be predicted for almost all cancer types. Fidler et al., supported this hypothesis in 1970, showing metastatic cancer cells from certain tumour sites displayed high incidence of metastatic ability to specific organs, independent of the anatomy of the blood and lymphatic vessels which drain the primary tumour (Fidler, 1970).

1.1.4.1 Features of medulloblastoma metastasis

Metastasis and recurrence are accountable for 95% of medulloblastoma associated deaths (Menyhárt and Győrffy, 2020). The predominant pattern of metastatic dissemination for medulloblastoma tumours is leptomeningeal metastasis (Figure 1.3), where tumour cells invade and colonise the cerebral spinal fluid (CSF) pathways and are transported around the CNS (Fults, Taylor and Garzia, 2019). The leptomeninges are the two innermost layers of tissues that protect the brain and spinal cord and consist of the arachnoid mater and the pia mater, between which circulates the CSF in the subarachnoid space (Sakka, Coll and Chazal, 2011).

The particular molecular mechanisms necessary for medulloblastoma tumours to disseminate and survive in the leptomeningeal space are poorly understood, and there are no therapies that target this paramount clinical problem (Fults, Taylor and Garzia, 2019). Leptomeningeal metastasis can also occur during surgery via the placement of shunts which are designed to drain CSF. Medulloblastoma can block the flow of CSF resulting in an increased intracranial pressure, shunts are used to drain CSF into the abdominal cavity, which can result in peritoneal metastasis (Greenfield and Bilsky, 2005). Occasionally, medulloblastoma tumour cells disseminate from the cerebellum and invade into the adjacent substance of the brain tissue, this is termed parenchymal metastasis (Rochkind *et al.*, 1991).

The fact that medulloblastomas rarely metastasise outside CNS and spread exclusively to the spinal leptomeninges, has fostered the belief that medulloblastoma cells spread directly through the CSF, not the bloodstream. However, recent experimental evidence challenges this, suggesting a potential route for cells via a

haematogenous route for distant leptomeningeal sites (Van Ommeren *et al.*, 2020). Further studies regarding the incidence of haematogenous dissemination and whether there is subgroup specificity should be conducted to advance the understanding of this method of metastatic dissemination.

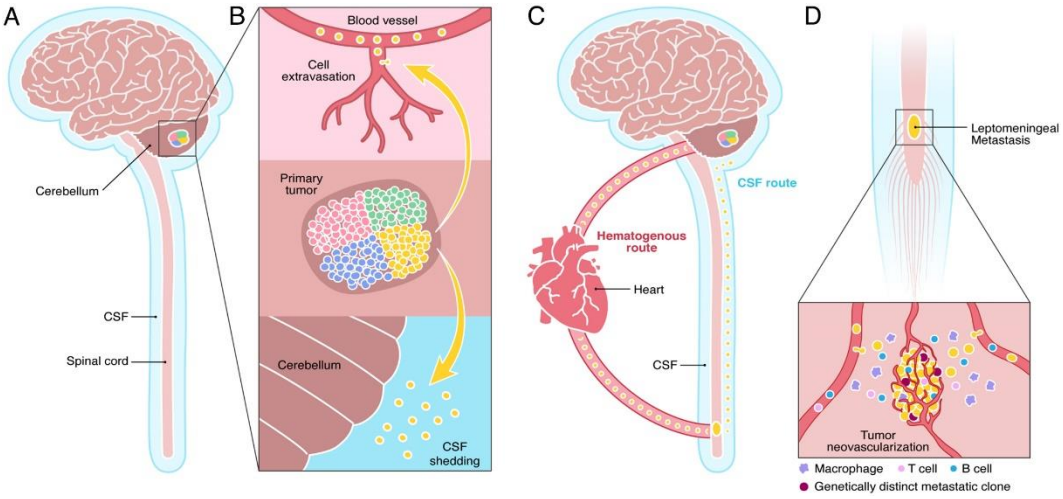

Figure 1.3 Mechanisms of medulloblastoma metastasis

(A) The primary tumour in the cerebellum consists of a heterogonous population of cells, of which some cells may have metastatic potential. (B) Metastatic cells can either shed from the tumour into the CSF circulation or extravasate into the local blood circulation. (C) Metastatic cells circulate via the CSF or a haematogenous route to distant leptomeningeal sites. (D) Metastatic cells then undergo further genetic divergence in the metastatic site, undergoing complex interactions with the tumour microenvironment. Image taken from Juraschka and Taylor *et al.,* 2019.

1.1.4.2 Medulloblastoma subgroup specific metastatic behaviour

As alluded to previously, metastatic dissemination in medulloblastoma is highly subgroup specific, with dissemination at diagnosis principally enriched in Group 3 and Group 4 tumours, and moderately rare in WNT and SHH tumours. The pattern of relapse within each subgroup is also highly specific; SHH medulloblastomas recur most frequently in resection cavities in the tumour bed, in comparison Group 3 and Group 4 tumours recur almost exclusively with metastatic dissemination, further from their primary tumour cavity (Ramaswamy *et al.*, 2016; Fults, Taylor and Garzia, 2019). In addition focal relapses are more frequently observed in Group 4 tumours, whilst in Group 3 tumours, diffuse multifocal or laminar relapses are most frequently observed

(Ramaswamy *et al.*, 2016). Limited studies of matched primary and metastatic tumours, have suggested that despite retaining the same subgroup at recurrence, the matched tumours were genetically distinct. It was suggested that only rare cells within the primary tumour have the ability to metastasize and this sub clone drives clonal selection in the metastases (Wang *et al.*, 2015).

Patterns of medulloblastoma dissemination can be largely categorised into nodular (formation of small nodules on the leptomeningeal surface) and diffuse (laminar coatings across the leptomeninges), with nodular metastasis displaying a significantly more favourable patient outcome (Dufour *et al.*, 2012). Most recently, nodular and diffuse patterns of metastatic dissemination were found to be highly subgroup specific (Zapotocky *et al.*, 2018). It was observed that SHH medulloblastomas spread exclusively in a nodular manner, Group 3 tumours mainly display laminar metastases and Group 4 tumours exhibited both of these patterns. It was also observed that Group 3 primary tumours have an increased propensity to metastasize at an earlier stage from smaller primary tumours (Zapotocky *et al.*, 2018). Not only do these findings further support the heterogeneous behaviours of medulloblastoma tumours, but they could also further refine radiological descriptions of the four subgroups and allow for pre-surgical diagnosis of medulloblastoma tumours.

1.2 Tumour microenvironment

The tumour mass consists not only of a heterogeneous population of cancer cells, but also a microenvironment made up of benign surrounding cells, growth factors, cytokines and extracellular matrix (ECM) proteins, collectively known as the tumour microenvironment (Bissel & Radisky 2001). Tumour progression is highly influenced by reciprocal interactions between cancer cells with their environment, which ultimately determines successful establishment of metastatic sites.

1.2.1 Matrix-metalloproteinases

Escalating evidence supports the view that extracellular proteinases, such a matrix-metalloproteinases (MMPs), facilitate many of the changes in the microenvironment during tumour progression. MMPs are calcium-dependent, zinc-containing endopeptidases and are capable of degrading almost all proteins found in the ECM, and can therefore disrupt the balance between growth and antigrowth signals in the tumour microenvironment (Egeblad and Werb, 2002). MMPs can either be bound to the cell membrane or secreted from the cytosol into the extracellular environment (Koyama, 2004). To date 23 MMPs have been discovered in humans. These cleave specific peptides abundant in the ECM, with the most typical substrates being many collagen types, laminin, gelatin and fibronectin (Isaacson *et al.*, 2017).

The complexity of the tumour microenvironment allows for multilevel regulation of MMPs. They are synthesised as inactive zymogens and once secreted must be activated by proteolytic cleavage in order to become functional (Sternlicht and Werb, 2001; Isaacson *et al.*, 2017). Proteolytic activity of MMPs can be regulated at various levels, including gene expression, presence of specific inhibitors, compartmentalization and pro-enzyme activation (Kessenbrock, Plaks and Werb, 2010). Moreover, there are several proteases that can mediate the conversion of zymogens to active enzymes, including plasmin, furin or active MMP itself (Sternlicht and Werb, 2001).

MMPs have been implicated in cancer progression for over 40 years (Liotta *et al.,* 1980) and overexpression of MMPs has been considered as potential diagnostic and prognostic markers in numerous types of cancer (Isaacson *et al.*, 2017). Indeed, several MMPs have been shown to be upregulated in liquid biopsies from patients with cancer by as much as 10-fold compared to healthy controls. Furthermore, the level of upregulation positively correlated with stage and metastatic dissemination (Isaacson *et al.*, 2017). Additionally, where MMP upregulation is perceived, numerous studies have documented increased proliferation, invasion, migration, inflammation, neoplastic progression, and a positive correlation with disease recurrence (Isaacson *et al.*, 2017). In this context, enzymatic activity of MMP-2 and MMP-9 were increased in the blood of patients with advanced NSCLC that did not respond to treatment and had disease progression (Gonzalez-Avila *et al.*, 2019). In addition, MMP-9 was found to be elevated in urine samples of patients with bladder cancer with poor prognosis (Offersen *et al.*, 2010), moreover elevated MMP-11 was identified as a biomarker for metastatic breast cancer (González de Vega *et al.*, 2019).

Although evidence has shown a wide range of biological functions of MMPs in cancer, as detailed above, a fundamental role is their degradation and remodelling of the ECM, paving the way through to create a migratory pathway for tumour cell invasion (Isaacson *et al.*, 2017). Cell migration can be enhanced by overexpression of MMPs, whilst treatment with MMP inhibitors results in reduced migration (Nabeshima *et al.*, 2002). Several studies have demonstrated mechanisms to localise MMP to the cell surface which proved essential for cell migration, and would appear the most logical mechanism to allow migration through the ECM. The presence of active MMP-2 on the surface of human melanoma cells was insufficient for invasion. Its more specialized localization, together with MT1-MMP, to the invasion front of cells was essential for invasion and subsequent migration (Nabeshima *et al.*, 2002).

With regards to medulloblastoma, regional distributions of MMPs in medulloblastoma tumours showed that MMP-2 and MMP-9 had the highest expression. Additionally,

increased expression levels of MMP-2 and MMP-9 have been associated with medulloblastoma dissemination and advanced tumour stage (Bodey et al., 2000; Vince et al., 2001). The overexpression of MMP-9 has also been positively correlated to chemo and radio resistant medulloblastoma cells (Ganji *et al.*, 2011). A study by Rao and colleagues, concluded that targeting MMP-9 by RNA interference (RNAi) inhibited medulloblastoma tumour growth *in vitro* and decreased cell viability (Rao *et al.*, 2007). The same group also inhibited MMP-2 in medulloblastoma cells which resulted in repression of stem cell tropism towards tumour cells (Bhoopathi *et al.*, 2012).

1.2.2 Extracellular matrix metalloproteinase inducer

Induction of MMPs is due in part to extracellular matrix metalloproteinase inducer (EMMPRIN), a highly glycosylated glycoprotein commonly enriched on the surface of tumour cells (Gabison *et al.*, 2005). EMMPRIN has been associated with tumour progression and poor patient outcome (Ju *et al.*, 2008; Menck *et al.*, 2015) and has been shown to promote metastasis and invasion via stimulating MMP synthesis in neighbouring cells (Tang *et al.*, 2005).

Overexpression of EMMPRIN alone or in combination with other factors, especially VEGF and MMP-2, can predict the prognosis and stage of various cancers (Bi *et al.*, 2012; Xin *et al.*, 2016). Additionally, where EMMPRIN upregulation is detected, numerous studies have documented increased tumour cell invasion, migration, angiogenesis, anti-apoptosis and drug resistance through its association with numerous proteins, such as; MMP-2, MMP-9, Fascin, Ki-67 and VEGF (reviewed by Xin *et al.*, 2016).

Expression levels of EMMPRIN have been correlated with poor patient outcome in several brain tumours. For example, EMMPRIN on the surface of glioma cells has been shown to strengthen tumour progression, and the expression of EMMPRIN mRNA and protein were found to be significantly higher in gliomas compared to normal brain samples (Kaushik, Hahn and Yong, 2015; Li *et al.*, 2017). EMMPRIN has also been associated with poor survival outcome in an astrocytoma patient cohort (Tsai *et al.*,

2013). EMMPRIN has not been extensively studied in medulloblastoma, however it has been demonstrated that EMMPRIN was upregulated in medulloblastoma tissues compared with normal control tissue and high levels of EMMPRIN positively correlated with a worse prognosis (Chu *et al.*, 2011), suggesting that EMMPRIN plays an active role in medulloblastoma tumourigenesis and may represent a negative prognostic factor.

1.3 Extracellular vesicles

Intercellular communication is a vital hallmark of multicellular organisms and can be facilitated through direct cell-to-cell contact or through the transfer of secreted molecules. Extracellular vesicles (EVs) are a heterogeneous group of circulating, cell-derived membranous structures released by most cell types. An assortment of molecules including, proteins, mRNA, miRNA and lipids can be loaded either as vesicular cargo or as components of the EVs membrane (Azmi, Bao and Sarkar, 2013). The relative protection of the cargo allows for molecules, which might be unstable or ineffective if secreted alone, to be carried through the extracellular space and remain viable within the luminal space of the EV (Raposo and Stoorvogel, 2013). EV based communication not only allows for individual molecules to be transferred to a recipient cell, but also potentially a combination of complementary molecules could be offloaded to a target cell to deliver a more effective signal (Azmi, Bao and Sarkar, 2013). EVs are capable of local and systemic trafficking and have been isolated from a wide range of biological fluids including blood, cerebral spinal fluid and saliva (Sato-Kuwabara *et al.*, 2015). Surface glycans, phospholipids and proteins allow specific ECM components and recipient cells to be targeted, and EVs are widely considered as an additional mechanism for intercellular communication.

More recently, pathological roles of EVs have been recognised in diseases such as cancers, neurodegenerative disorders, and infectious diseases. Additionally their roles in protection, repair and regeneration present exciting possibilities to be explored.

Understandably, EV science has achieved widespread interest and enthusiasm, however, in this expanding field much remains unknown regarding biogenesis, secretion, targeting and fate of these vesicles.

1.3.1 EV classification

Based on size and biogenesis, EVs have been stratified into three classes; exosomes, microvesicles and apoptotic bodies. It must be emphasised that there is much controversy regarding nomenclature and size of different vesicles (Witwer *et al.*, 2013). However, basic requirements of criteria for EVs have been established (Lötvall *et al.*, 2014; Théry *et al.*, 2018) and each class is loosely defined by size, though the more robust defining feature is their mode of biogenesis, (summarised in Table 1.3).

Exosomes will be the main focus of my project; however, the remaining two classes will also be explained in more detail below.

Table 1.3 Characteristics of extracellular vesicle populations

Based on data from the following references (Lötvall *et al.*, 2014; Théry *et al.*, 2018)

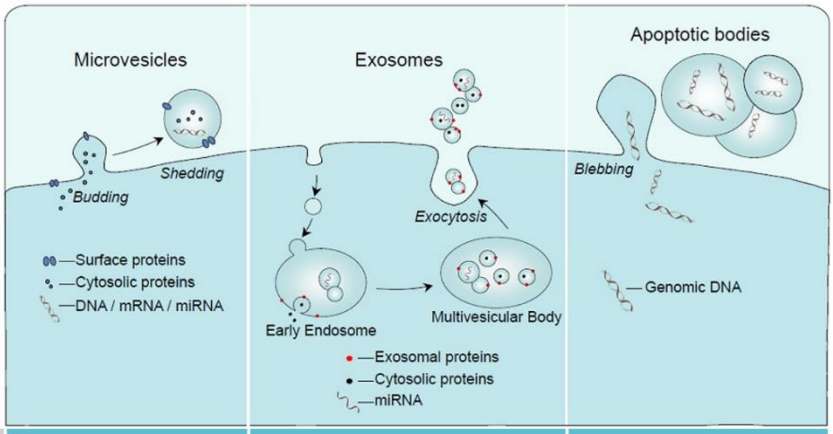

Characteristics	Microvesicles	Exosomes	Apoptotic bodies
Diameter (nm)	200-1000	30-100	800-5,000
Shape	Heterogeneous	Spheroid	Heterogeneous
Sedimentation (x *g*)	10,000-20,000	100,000	2,000
Markers	CD40 ligand, Integrins, Selectins	Tetraspanins (CD63, CD81, CD9) ESCRT components (tsg10), Alix	Histones
Lipids	Phosphatidylserine	Cholesterol, ceramide, lipid rafts	Not determined
Cellular origin	Surface budding	Multivesicular endosomes	Surface blebbing

1.3.2 Exosomes

Exosomes are considered the smallest (30-100 nm in diameter) class of EVs and are derived from the endo-lysosomal pathway (El Andaloussi *et al.*, 2013). The pathway is initiated by the inward budding of the producing cells plasma membrane, incorporating surface molecules from the producing cell into the early endosome as it is formed. Various separate mechanisms have been implicated in driving this process of endocytosis, which are broadly separated as clathrin-dependent and -independent mechanisms. Clustering of molecules on the membrane, relevant as cargo or machinery for budding, initiates the secondary invagination into the lumen of early endosomes, forming multiple intraluminal vesicles (ILVs) (Simons and Raposo, 2009). During this process, cytosolic proteins, nucleic acids and lipids are sorted into the ILVs

(Grant and Donaldson, 2009). This process often allows for the identification of the cellular origin of exosomes, due to the membrane components shared with the producing cell. However, due to numerous shared characteristics between cell types, certain exosome populations cannot be indistinguishable from one another. It has also been observed that relevant molecular components are also delivered from the Golgi apparatus, perhaps providing a more selective mechanism of exosomal cargo loading (El Andaloussi *et al.*, 2013).

The formation of ILVs requires two distinct processes. Initially, the endosome membrane is reorganized and becomes highly enriched for tetraspanins (Pols and Klumperman, 2009), with CD9 and CD63 thought to play critical roles in exosome formation. Subsequently, the endosomal sorting complexes required for transport (ESCRTs) are recruited to the site of ILV formation (Colombo *et al.*, 2013).

As the early endosome matures into a late endosome with free ILVs within, it is descriptively termed a multivesicular body (MVB, Figure 1.4). In general, MVBs can be processed via two different routes; they can either enter the lysosomal pathway whereby fusion with a lysosome ensures degradation of their contents and recycling of vesicular components, or they can fuse with the producing cells plasma membrane and release their cargo as exosomes into the extracellular space (Gruenberg and Stenmark, 2004).

A variety of mechanisms have been proposed for the release of exosomes. Overexpression or knockdown of cortactin has been show to increase or decrease exosome secretion, respectively (Sinha *et al.*, 2016). Rab GTPases, the largest family of small GTPases (Stenmark, 2009) are well known for their diverse rolls in membrane trafficking. Interestingly, several Rabs have been shown to play a role in exosome secretion, however the extent of their involvement is not known and often data is cell line specific. For example, overexpression of Rab11 repressed exosome secretion in human leukemic cells (Savina, Vidal and Colombo, 2002). Additionally, depletion of Rab11 in Drosophila reduced the secretion of Evi-bearing exosomes (Koles *et al.*,

2012). On the contrary, knockdown of Rab11 in HeLa cells was not found to affect exosome release (Ostrowski *et al.*, 2010). Small GTPases of other families such as the Rho/Rac/cdc42 family have also been implicated in exosome secretion. In particular, RhoA effector citron kinase was shown to enhance the production of exosomes (Loomis *et al.*, 2006).

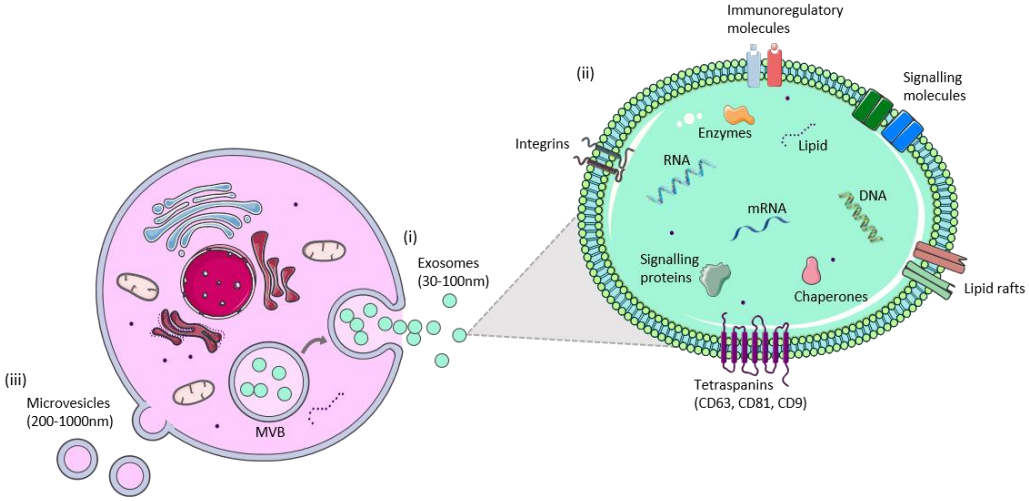

Figure 1.4 Biogenesis and composition of exosomes

Exosomes are derived from internal vesicles (IV) stored in multivesicular endosomes (MVB). MVE are part of the endosomal compartment and contain internalized proteins, mRNA and miRNAs. MVE fuse with the cellular plasma membrane and release their cargo as exosomes into the extracellular space (i). Exosomes are 30 to 100 nm in size, they have a lipid bilayer membrane and contain a variety of cellular components. These include, multiple proteins, lipids, RNAs (mRNA, miRNA, ncRNA) and DNA. The exosome membrane contains various proteins involved in targeting and adhesion (tetraspanins and integrins), antigen presentations (immunoregulatory molecules such as MHC I and II) and membrane trafficking (lipid rafts) (ii). The biogenesis of microvesicles occurs at the surface of the cells by outward budding of the membrane (iii). Schematic created using Servier Medical ART.

1.3.3 Microvesicles

Microvesicles constitute a more heterogeneous and larger population of extracellular vesicles, ranging from 100-1000 nm in diameter (Table 1.3). Unlike exosomes, the biogenesis of microvesicles occurs at the surface of the cells by outward budding and fission of the plasma membrane, followed by the subsequent release of vesicles into the extracellular space (Raposo and Stoorvogel, 2013). The mechanisms involved in the biogenesis of microvesicles are still being revealed. However, the molecular machineries involved in exosome biogenesis appear to partly overlap with

microvesicles, including ESCRT proteins, although further research is needed to investigate this (Colombo *et al.*, 2013).

Studies of pure microvesicles populations are limited as they were originally pelleted together with exosomes at the 100,000 x *g* ultracentrifugation step. It is only more recently that microvesicles have been accepted as a distinct extracellular vesicle population and isolated separately from exosomes at around 10,000-20,000 x *g* (Menck *et al.*, 2015).

1.3.4 Apoptotic bodies

Of the three different subpopulations of extracellular vesicles, apoptotic bodies are the least well characterised. They range from around 800-5,000 nm in diameter and are released by cells undergoing programmed cell death/apoptosis. Cells undergo several steps during apoptosis including cell shrinkage, chromatin condensation, nuclear fragmentation, membrane blebbing and then the cells break down into apoptotic bodies (Reed, 2000). Apoptotic bodies can be isolated at 2,000 x *g* (Crescitelli *et al.*, 2013). They consist of cytoplasm with tightly packed organelles and sometimes contain a nuclear fragment which can be visualised by electron microscopy. The organelle integrity is maintained and is enclosed by an intact plasma membrane. After release, apoptotic bodies are quickly phagocytosed by neoplastic cells, macrophages or parenchymal cells and degraded inside phagolysosomes (Reed, 2000). There are similarities between apoptotic bodies and the two smaller classes of EVs, but the focus for studies into intercellular communication has tended more towards microvesicles and exosomes.

1.3.5 Extracellular vesicle isolation and characterisation

With the complexity and variety integral to EV biology, there are often difficulties discriminating one EV class from another, not least associated with the physical problems of separating one class from another. It has been reported that mixed populations of EVs have often mistakenly been identified as exosomes in the literature (Théry *et al.*, 2018) causing much confusion. Accordingly, the International Society of

Extracellular Vesicles (ISEV) has called for the reporting of minimal requirements in EV studies. ISEV recommends that each preparation on EVs be; 1) defined by quantitative measure of the source of EVs (e.g. number of secreting cells, volume of biofluid, mass of tissue); 2) characterised to the extent possible to determine abundance of EVs (total particle number and/or protein or lipid content); 3) tested for presence of components associated with EV subtypes; and 4) tested for the presence of non-vesicular components. The most routinely used methods for the isolation and characterisation of exosomes will be discussed below, although new separation methods are constantly arising. In a recent survey, new separation options included microfluidics, field-flow and tangential flow (Nieuwland *et al.*, 2020; Royo *et al.*, 2020).

1.3.5.1 Differential and density gradient ultracentrifugation

Ultracentrifugation is still the most widely applied method for separating exosomes from cells, apoptotic bodies and microvesicles (Nieuwland *et al.*, 2020). This approach is used by many due to its ease and high yield of relatively homogeneous population of exosomes. Isolation of exosomes by ultracentrifugation consists of several centrifugation steps to sediment cell debris, microvesicles and apoptotic bodies, followed by a high-speed ultracentrifugation step ranging from 100,000 to 120,000 x *g* (Théry *et al.*, 2006). Unfortunately, ultracentrifugation is not always appropriate for clinical samples due to large starting volumes required and user-dependent recovery rates. In line with this, a recent study, using the addition of spike-in exosome controls, determined that 100% exosome recovery in certain biological fluids could not be achieved (Van Deun *et al.*, 2017).

Density gradient centrifugation is seen as both a purification and detection method. Briefly, this method involves two centrifugation steps at 1,000 *x g* followed by addition of a 30% sucrose cushion, followed by differential ultracentrifugation. This yields exosome pellets with fewer contaminating large proteins or aggregates (Zhang *et al.*, 2015). This method relies on the floating densities of exosomes which range from 1.13 g ml-1 to 1.19 g ml-1 (Hugel *et al.*, 2005). More recently, Muller and colleagues,

identified a large loss in total numbers of exosomes recovered using a sucrose gradient cushion, however a lower ratio of contaminating protein, suggesting a purer isolation method (Muller *et al.*, 2014).

1.3.5.2 Exosome precipitation

Several commercial kits are available to precipitate exosomes, which are easy to use, do not require specialised equipment and do not require large starting volumes, allowing for easy integration into the clinic or research laboratory. Examples include ExoQuick™ (System Bioscience, California, USA) and Exo-Spin™ (Cell guidance Systems, Cambridge, UK). The exact mode of action of these kits has not yet been verified or disclosed, however these kits rely on polymer interactions to precipitate exosomes out of solution (Zarovni *et al.*, 2015). A big disadvantage of using exosome precipitation kits is the co-precipitation of other non-exosome contaminants, including polymeric materials and proteins, which greatly biases downstream RNA analysis of exosomal cargo (Zarovni *et al.*, 2015; Nieuwland *et al.*, 2020). Contamination from the reagents used in these kits could also affect assays of exosomal activity.

1.3.5.3 Ultrafiltration and size-exclusion chromatography

Ultrafiltration is a commonly used size-based exosome isolation techniques. Several groups have developed ultrafiltration as an alternative and rapid method of isolating exosomes. Ultrafiltration has also recently been recommended as an additional step within the ultracentrifugation protocol, to further purify exosome populations by removal of non-exosomal proteins or larger particles (Muller *et al.*, 2014). Ultrafiltration is much less time consuming than ultracentrifugation and no specialist equipment is required. Nevertheless, the use of force can cause breakage of larger vesicles which has the potential to skew the results of downstream analysis (Zarovni *et al.*, 2015).

Size-exclusion chromatography (SEC) is a column-based technique, allowing for the differential elution of smaller vesicles from non-membrane-bound proteins, but not from MVs or protein aggregates (Sidhom et al., 2020). Separation is achieved by passage through a column containing fine porous beads, in which the smaller molecules

traverse longer routes through the beads. While the larger components, including exosomes, move around the beads taking shorter routes and are eluted first. In a recent survey it was noted that the use of SEC for the isolation of exosomes has more than doubled since 2016 (Nieuwland *et al.*, 2020). SEC is efficient, with a 20 minute average processing time per sample, and has minimum impact on the integrity of EVs. However, compared to ultracentrifugation, the total number of isolated exosomes is reduced, as is the mRNA and protein yield (Sidhom, Obi and Saleem, 2020).

1.3.5.4 Transmission electron microscopy

Transmission electron microscopy (TEM) is a widely used technique to characterise the structure, morphology and size of various biological components. TEM currently offers the greatest resolution of any technique, allowing for the ultrastructure of exosomes to be revealed (Sidhom, Obi and Saleem, 2020). An important consideration when using TEM techniques is the sample preparation, which involves several extensive steps and may induce changes in the morphology of the EVs. The characteristic features of exosomes examined under TEM is a cup-shaped morphology, with diameters ranging from 30-100 nm (Raposo *et al.*, 1996). It is believed the cup-shaped morphology originates from the sample processing, during which exosomes suffer extensive dehydration and often collapse. To avoid the damage caused by TEM, cryo-EM is being applied for exosome analysis. Cryo-EM is free from the effects of dehydration and fixing, as samples are prepared in vitreous ice using liquid nitrogen temperatures, which causes no ultrastructure changes (Colombo *et al.*, 2013). In conjunction to standard image acquisition, antibodies conjugated to gold particles can allow specific maker proteins to be detected, adding to the morphological information that can be acquired (Raposo *et al.*, 1996; Sidhom, Obi and Saleem, 2020). Unfortunately, cryo-EM is not always accessible for EV characterisation due to the high cost of specialised equipment required.

1.3.5.5 Nanoparticle tracking analysis

Nanoparticle tracking analysis (NTA) is an attempt to quantify a broad population of vesicles without giving much morphological information. In this method, a laser beam is directed through the sample chamber and the vesicles in suspension in the path of the beam scatter light in a manner which can easily be detected via a microscope onto which a video camera is mounted. The camera captures a video file of vesicles moving under Brownian motion. The NTA software tracks particles individually using Stokes Einstein equation, calculating their diameters and concentration (Soo *et al.*, 2012). Sample preparation is very quick and samples can be recovered in their native form after measurements. In addition, the method can detect the presence of surface markers on EVs by the use of fluorescently labelled antibodies (Sidhom, Obi and Saleem, 2020).

1.3.5.6 Western blotting

Western blotting remains one of the most commonly used techniques for the characterisation of exosomes (Nieuwland *et al.*, 2020), due to its ease of use and ability to detect both surface and internal proteins. However, despite the fact that there are several protein markers widely cited within the literature as “exosome-specific” markers, none can distinguish between the different EV subtypes and rather should be identified as “exosome-enriched” proteins (Lötvall *et al.*, 2014; Théry *et al.*, 2018). Therefore, based on ISEV guidelines, it is suggestion that 3 or more proteins are reported in at least a semi-quantitative manner in any EV preparation. The guidelines recommend the assessment of both transmembrane and intra-luminal proteins that are expected to be present or enriched in EVs/exosomes. Many of these markers are associated with the biogenesis of EVs, including tetraspanins (CD63, CD9, CD81), membrane-binding proteins TSG101, annexins, and Rabs. Additionally, proteins not expected within EVs/exosomes should also be determined to rule out cellular contamination (Lötvall *et al.*, 2014; Théry *et al.*, 2018). The primary pitfall of western blotting for EV characterisation is the large amount of exosomal protein required for a

single preparation, additionally the reproducibility and specificity are often limited by the quality of the antibody used (Doyle and Wang, 2019).

1.3.5.7 Flow cytometry

Flow cytometry is a molecular approach, routinely used to characterise EV surface proteins. Unlike western blotting, flow cytometry allows for the observation of intact vesicles. Although, the size detection of particles by flow cytometry is limited to 300 nm and does, therefore, not allow for the direct detection of single exosomes (Vogel *et al.*, 2021). However, efforts have been made to modify flow cytometry machines available to allow EV scale detection (Campos-Silva *et al.*, 2019). More recently, dedicated flow cytometers with high sensitivity, allowing for measurements at the sub-micron scale have been developed (Sidhom, Obi and Saleem, 2020). The new generation of flow cytometers allows measurements of the size and structure of EVs down to 40 nm (Vogel *et al.*, 2021).

1.4 The significance of extracellular vesicles in cancer

Accumulating evidence indicates that extracellular vesicles play an intriguing and pivotal role in cancer progression. EVs have been implicated in a diverse range of physiological functions due to their capacity to transfer oncogenic proteins and nucleic acid cargo from a donor cell to a recipient. Tumour-derived EVs have been demonstrated to play a decisive role in tumorigenesis, promoting tumour growth and progression (Seo *et al.*, 2018), enhancing tumour cell migration and invasion (Huang *et al.*, 2020), developing drug resistance (Lv *et al.*, 2014) and performing immunosuppressive functions (Liu *et al.*, 2020). Therefore, the content of the vesicles is of great significance in the evolution of cancer.

1.4.1 EVs as mediators of intercellular communication in cancer

Extracellular vesicles have been implicated in numerous physiological and pathological processes, such as tumour initiation, growth, progression and metastasis. These effects are mainly attributed to their role as mediators of intercellular communication, as EVs can transfer oncogenic proteins and RNA from their cell of origin to recipient

cells. Exosomes from malignant cells have been shown to have the potential to induce transformation of normal cells. For example, Elmageed and colleagues showed that exosomes derived from prostate cancer cells induced clonal expansion of tumours through neoplastic reprogramming of patient-derived adipose stem cells (Elmageed *et al.*, 2014). The promoting effect of exosomes on tumour growth has also been widely reported; exosomes isolated from colon cancer cells enhance tumour cell growth of recipient cells in a time- and dose-dependent manner through shortening mitosis duration and activating STAT3 (Ren *et al.*, 2019). Similarly, exosomes derived from gastric cancer cells significantly increased the proliferation of less aggressive recipient cells. This increase in proliferation was accompanied by PI3K/Akt activation, PI3K inhibitors partially reduced the exosome induced proliferative effect (Qu *et al.*, 2009). The promoting roles of tumour cell proliferation, mediated by exosomes activating PI3K/Akt signalling, have also been observed in lung cancer cells (Li, Chen and Yi, 2021), gliomas cells (Skog *et al.*, 2008) and gastric cancer cells (Wang *et al.*, 2020).

In addition to influencing the local tumour microenvironment, there is also evidence to suggest EVs are involved in initiating and supporting tumour metastasis at distant sites. It has been reported that highly metastatic melanoma-derived exosomes “educate” bone marrow progenitor cells towards a pre-metastatic phenotype via the MET receptor, enhancing the metastatic ability of primary tumours (Peinado *et al.,* 2012). Similar results were also seen in gastrointestinal stromal tumour cell-derived exosomes containing protein tyrosine kinase, which converted progenitor smooth muscle cells to a pre-metastatic phenotype (Atay *et al.*, 2014). Protein profiles have also revealed the existence of surface-bound and soluble MMPs in EVs cultured from cell lines and bodily fluids (Shimoda and Khokha, 2017). Indeed, MT1-MMP, MMP-2 and MMP-9 existing in exosomes from tumour cells and corneal fibroblasts have been implicated in the degradation of the extracellular matrix. A similar mechanism was observed in a model of melanoma, whereby tumour-derived EVs containing MT1-MMP contributed to local tumour invasion and the establishment of distant metastases by regulation of Coronin 1C (Tagliatela *et al.*, 2020). Another noteworthy study examined

the potential role of exosomes in the phenomenon of metastatic organotrophism across a variety of cancer types (Hoshino *et al.*, 2015). This study implicated integrins on the surface of exosomes as a key factor determining the establishment of pre-metastatic niche sites in specific organs

EVs have also been shown to be critical for invadopodia biogenesis and activity. Invadopodia are actin-based protrusions formed in cancer and normal cells and are involved in multiple steps of the metastatic cascade. Knock-down of exosome secretion by Rab27a (critical for MVB docking) resulted in decreased numbers of invadopodia per cell, reducing cell migration (Paterson and Courtneidge, 2018). In total, these studies provide clear, compelling evidence to support a role of EVs in tumour biology and disease progression.

1.4.2 EVs as biomarkers in cancer

Aside from EVs being implicated in numerous physiological and pathological processes, several studies have shown that EVs can serve as potential biomarkers in cancer. A biomarker is a molecule which can be assessed for the definition of a biological status. This molecule can be descriptive for a healthy or pathogenic process, the response to a treatment, or prognostic for the future development of disease (Ilyin, Belkowski and Plata-Salamán, 2004). The National Cancer Institute (NCI) defines a tumour biomarker as “a substance found in tissue, blood, or other body fluids that may be a sign of cancer or certain benign (noncancerous) conditions” (National Cancer Institute, 2018a). An ideal biomarker should be detectable through non-invasive sampling, for example in a blood or tissue sample, and show a high specificity and sensitivity for the studied disease. A successful biomarker needs to have predictive function and correlate with disease progression or patient outcome (Kulasingam and Diamandis, 2008).

Extracellular vesicles are not only present in *in vitro* cell culture models, but have been detected *in vivo* in almost all body fluids including blood, cerebrospinal fluid, breast milk, ascites fluid, semen, urine and saliva (Raposo and Stoorvogel, 2013). EV cargo

comprises an abundance of biomolecules and current data suggests that EV cargo reflects the pathological state of their parent cell and might represent unique molecular profiles enriched for cell- and tissue-type specific markers. Consequently, since EVs closely represent the state of their originated cell and since they can be easily collected from nearly all bodily fluids, they represent a readily accessible source of cancer biomarkers. It has already been shown that the levels of exosomes are elevated in the plasma of some cancer patients as compared to healthy controls. For example, a study by Graves and colleagues demonstrated increased levels of extracellular vesicles in ascites fluid of ovarian cancer patients and that their amounts correlated with disease burden (Graves *et al.*, 2004). This was also confirmed for extracellular vesicles found in peripheral blood of gastric cancer patients (Baran *et al.*, 2010). In addition, the increased levels of exosomes have been correlated with the hypoxic, acidic microenvironment around tumours, which is hypothesised to stimulate the release of exosomes as well as their cell fusion capabilities (Parolini *et al.*, 2009; W. Liu *et al.*, 2020).

In different bodily fluids, in particular plasma and serum, EV biomarkers have been detected with great clinical value in numerous cancer types, as summarised in Table 1.4. Amongst the first reports exploring the potential role of extracellular vesicles as tumour biomarkers was a comparison of the content of glioblastoma EVs to their cells of origin (Skog *et al.*, 2008). It was reported that mRNA and miRNAs characteristic of glioma cells could be detected in serum EVs; a snapshot of the content of the secreting cell. This phenomenon has been demonstrated across multiple cancer types including lung (Li, Liu and Dong, 2021), breast (Di Modica *et al.*, 2017) and prostate (Donovan *et al.*, 2015). The correlation between tumour-EV and tumour-cell content is particularly valuable where the ability to conduct a tissue biopsy is limited, such as tumours of the brain or central nervous system. For example, a study by Shi and colleagues profiling exosomes from the CSF of seventy glioma patients showed that they contained significantly elevated levels of miR-21 relative to healthy controls, and EV miR-21 levels reflected tumour burden (Shi *et al.*, 2015). Prognostically informative

tumour-EV miRNA signatures have similarly been identified in EVs derived from; breast cancer patient plasma (Di Modica *et al.*, 2017), human colorectal cancer cell lines (Fu *et al.*, 2018) and exosomes isolated from patients with pancreatobiliary tract cancer (Machida *et al.*, 2016). Similarly, in a study of prostate cancer patients, Lie-Fu Ye and colleagues identified that a significant increase in the presence of mRNAs PCA and PRAC in urine-derived EVs was predictive of high-grade prostate cancer (Ye *et al.*, 2020). Taken together, these studies strongly suggest that tumour-EVs might be useful as easy non-invasive targets for early disease detection, monitoring or prognosis establishment in cancer.

Table 1.4 Extracellular vesicles as biomarkers in different cancer types

	Biomarker	Sample	Cancer type	Reference
Protein	CD63, HSP70, HSP90	Plasma	Melanoma	Logozzi *et al.*, 2009
	Survivin	Plasma	Prostate	Khan *et al.*, 2012
	PSA, PCA3	Urine	Prostate	Nilsson *et al.*, 2009
	CD24, ADAM10, EMMPRIN, claudin	Plasma and ascities	Ovarian	Kellar *et al.*, 2009
RNA	EGFRvIII	Serum	Glioblastoma	Skog *et al.*, 2008
	IL-8 and TGF-beta	Plasma	Glioma	Muller *et al.*, 2014
	PCA3, ERG	Urine	Prostate	Donovan *et al.*, 2015
	PCA, PRAC	Urine	Prostate	Lie-Fu Ye *et al.*, 2020
miRNA	miR-21	CSF	Glioma	Shi R *et al.*, 2015
	miR-21, miR-939, miR-373, and miR-1246	Plasma	Breast	Di Modica *et al.*, 2017
	miR-1246, miR-4644	Saliva	Pancreatobilliary tract	Machida *et al.*, 2016
	miR-92a, miR222	plasma	Colorectal	Pérez *et al.*, 2020

1.4.3 EVs in medulloblastoma

At the outset of this research there had only been two studies reporting a potential role for EVs in medulloblastoma, both of which used proteomic approaches to uncover the

potential roles of exosomal proteins in medulloblastoma progression. The first report of the characterisation and functional analysis of medulloblastoma exosomes was in 2012 by Epple and colleagues. Profiling studies on exosomes derived from a Group 3 medulloblastoma cell line (D283) was carried out to reveal the functional roles of exosomes which are relevant to medulloblastoma tumour progression, including their roles as growth stimulants and attractants for tumour cell migration *in vitro* (Epple *et al.*, 2012). Their results indicated a high proportion of nuclear proteins, but also the presence of common vesicular molecules, CD9 and CD63. Additionally, they identified the transcription factor HNF4A and suggested its role as a tumour suppressor in medulloblastoma. In support of this, inhibition of HNF4A with MEDICA 16, a known drug inhibitor, resulted in increased cell proliferation (Epple *et al.*, 2012).

Bisaro *et al.,* focused their attention on profiling exosomes derived from three SHH medulloblastoma cell lines grown as medullospheres (MBS). Medullospheres are obtained with serum-free media, enabling the formation and growth of spheres, and are thought to better recapitulate the multi-dimensional growth that exists in patient tumours (Edmondson *et al.*, 2014). Comparing protein content of exosomes isolated from MBS, with cells grown adherently, revealed that protein Hemopexin was limited to exosomes derived from MBS. Hemopexin is an iron carrier protein, iron depletion causes cell cycle arrest and leads to inhibition of cell proliferation (Smith and McCulloh, 2015). They found that treating MBS with iron chelators reduced the number and sizes of spheres, and the ability of the cells to form spheres (Bisaro *et al.*, 2015). Therefore, a role of extracellular vesicle-mediated iron metabolism in medulloblastoma progression and invasion was suggested, and the possibility of using iron-chelators in chemotherapy was revealed.

These results clearly indicate a role for exosomes in medulloblastoma tumourigenesis and are encouraging for future research efforts to understanding the effects of exosomal cargo on tumour progression and foster the translation of clinically relevant biomarkers for medulloblastoma.

1.5 Hypothesis and aims

As discussed, metastatic medulloblastoma is a devastating disease, with less than 10% 5-year survival. Primary tumours can be classified based on epigenetic and transcriptomic features, however there is very little information regarding molecular signatures of metastatic tumours. The secretion of extracellular vesicles has emerged as a pivotal mediator for communication in the tumour microenvironment during metastasis. The role of exosomes as vehicles for cell-to-cell communication between a tumour and its microenvironment is a relatively new concept, with only limited study of this potential mechanism in medulloblastoma.

We hypothesize that small vesicles, such as exosomes, are an important means of communication between medulloblastoma cells and their surroundings to drive mechanisms such as metastasis. The aims of this study are as follows:

Aim 1: Optimise a reliable method whereby sufficient amounts of high quality exosomes could be routinely obtained.

Aim 2: Investigate the influence of exosomes on the extracellular matrix and the ability of exosomes to transfer a migratory phenotype to recipient cells.

Aim 3: Characterise the exosomal RNA cargo of primary and metastatic cell lines to identify exosomal biomarkers of increased metastatic potential, and understand the long-term regulatory potential of exosomes via the intracellular delivery of RNA cargo to recipient cells.

Aim 4: Validate the abundance of candidate biomarkers in exosomes isolated from medulloblastoma patient CSF samples to understand the potential clinical utility of identified markers.

Chapter 2

Materials and Methods

Chapter 2. Materials and Methods

2.1 Tissue culture methods

2.1.1 Cell maintenance

Eleven cell lines were utilised in this study, clinical information for each cell line is listed in Table 2.1. Cell lines were grown at 37°C and 5% CO_2 in a humidifier incubator. To passage cells, they were washed twice in Hank's Balanced Salt solution (HBSS; Gibco, 14170). The cells were detached by incubation with 2 mL Trypsin-EDTA (Sigma, LH-SIG2044) for 5 minutes. The detached cells were collected and centrifuged at 100 x *g* for 5 minutes. Cell pellets were resuspended in fresh media and were split into standard treated T-75 tissue culture flasks (Corning, 430641U) in a ratio of 1:3-1:20 depending on their respective doubling times. All cell lines were routinely tested for contamination with Mycoplasma (VenorGem Kit Minerva Labs, Cambio). To maintain cells for long periods of time, they were frozen in 10% dimethyl sulfoxide (DMSO; Sigma, D2650) and 90% FBS. Cells were frozen at concentrations of 10^6 cells/mL as either 1 mL aliquots in cryovials (Alpha Laboratories, LW3532) or 0.5 mL aliquots in FluidX tubes (Brooks Life Sciences, 68-0703). Aliquots were placed at -80°C in a Mr FrostyTM (Thermo Fisher Scientific, 10110051) overnight before being transferred to liquid nitrogen for long-term storage.

2.1.1.1 Maintaining suspension cell lines

Suspension cells were subcultured by removing volumes of media containing suspension cells and replenishing with volumes of fresh media. Once a week the media containing suspension cells was transferred into a 50 mL tube and centrifuged at 100 x *g* for 5 minutes. Cell pellets were resuspended in ¼ conditioned media and ¾ fresh media and split into non-treated T-75 tissue culture flasks (Eppendorf; 0030711025) in a ratio of 1:2-1:5. To maintain suspension cells for long periods of time, they were frozen in Cellbanker® cryopreservation media (AMS Biotechnology Ltd., 11891) at a concentration of 10^6 cells/mL. 0.5 mL aliquots of cell suspension were then transferred

to FluidX tubes. For short-term storage samples were kept at -80°C (as tolerated in Cellbanker® media), for long-term storage vials were transferred to liquid nitrogen.

2.1.1.2 Cell counting

For cell counting, cells were first tyrpsinised and pelleted, after which they were suspended in growth media. Equal volumes of trypan blue (Sigma-Aldich T8154) and media were gently mixed. 10 µl of combined solution was then applied to a Neubauer Counting Chamber (VWR; 718605). The number of viable cells (clear cells that did not take up trypan blue) in the four corner squares of the chamber were counted. To determine the number of viable cells per mL of cell suspension, the following equation was utilised:

Cells per mL= (Average cells per square) x (Dilution factor: 2) x (1×10^4)

Table 2.1 Cell lines used in this study

Cell line	Subgroup	Metastatic stage	Growth type	Source	Reference
DAOY	SHH	Non-metastatic (M0)	Adherent	ATCC®HTB-186™	Jacobson *et al.*, 1985
UW228-3		Non-metastatic (M0)	Adherent	John R. Silber, University of Washington, Seattle	Keles *et al.*, 1995
ONS-76		Metastatic tumours at the right prepontine cistern (M2)	Adherent	Annette Künkele (Charité Universitätsmedizin, Berlin)	Yamada *et al.*, 1989
D283 Med	Group 3	Peritoneal metastasis and malignant ascites from laparotomy (M2)	Semi-adherent	ATCC® HTB-185™	Friedman *et al.*, 1985
HD-MB03		Spinal metastases at diagnosis (M3)	Semi-adherent	Till Milde (DKFZ, Heidelberg, Germany)	Milde *et al.*, 2012
D458*		Metastatic cells from CSF (M+)	Semi-adherent	John R. Silber, University of Washington, Seattle	Wikstrand *et al.*, 1991
D425*		Non-metastatic cells from primary tumour (M0)		Marcel Kool, German Cancer Research Centre	
CHLA-01*	Group 4	Non-metastatic primary tumour (M0)	Suspension	Professor Geoff Pilkington (University of Portsmouth, UK)	Xu *et al.*, 2012
CHLA-01R*		Recurrent metastatic cells from pleural fluid (M3)			
FB83	Foetal neuronal stem cells	N/A	Adherent	ATCC® HTB-185™	Ivanov *et al.*, 2016
HEK239T	Human embryonic kidney	N/A	Adherent	Ian Kerr, University of Nottingham	DuBridge RB, *et al.*, 1987

*cell lines with matched primary and metastatic pairs

2.1.2 Tissue culture media

Culture media information for the eleven cell lines utilised in this study can be found in Table 2.2.

Table 2.2 Culture media information for cell lines used in this study

Cell line	Culture media
DAOY	Dulbecco's Modified Eagle Serum/F-12 (DMEM; Gibco, 31885) + 15% foetal bovine serum (FBS; HyClone, SH30541.03) + 1% Sodium Pyruvate (Gibco, 11360070)
UW228-3	RPMI-1640 (Sigma-Aldrich; R8758) + 10% FBS
ONS-76	RPMI-1640 + 10% FBS
D283 Med	DMEM + 10% FBS
HD-MB03	RPMI-1640 + 10% FBS
D458	DMEM + 10% FBS
D425	
CHLA-01	DMEM F12 + 2% B27 (Gibco, 17504044) + 20 ng/mL recombinant human basic fibroblast growth factor (FGF; Gibco, PHG0266) + 20 ng/mL recombinant human epidermal growth factor (EGF; Gibco, PHG0315)
CHLA-01R	
FB83	DMEM + 10% FBS
HEK239T	DMEM + 10% FBS

2.1.3 Preparing cell pellets for molecular analysis

Cells were harvested into 50 mL tubes and centrifuged at 200 x *g* for 5 minutes. Cell pellets were resuspended in 1 mL of sterile PBS, transferred into a 1.5 mL Eppendorf and again centrifuged as above. The supernatant was discarded and the remaining cell pellet was snap frozen in liquid nitrogen and immediately stored at -80°C.

2.1.4 Generation of stable knockdown cell lines

Cell lines with stable knockdown of *BSG* and *MMP-2* expression were generated though shRNA-mediated gene silencing using commercialised virus particles. GIPZ™ Lentiviral particle starter kits (*BSG*; Horizon Discovery, VGH5526-EG4313, MMP-2; VGH5526-EG682) were used for subsequent transduction of CHLA-01R and D458 cell

lines, lentiviral DNA plasmid maps can be found in Appendix Figure 7. Lentiviral vectors can infect a broad range of cells, including dividing and non-dividing cells, and integrate into the genome of their target cells, which allows stable expression of the gene of interest. The transfection of cell lines was achieved following GIPZ™ lentiviral shRNA manual (Horizon Discovery). In brief, 5 x10^4 cells were seeded in 24-well plates and incubated at 37°C and 5% CO_2 overnight to allow cells to settle. Subsequently, cells were washed and trypsinised as previously described. Resulting pellets were resuspended in 1 mL of serum-free media and an appropriate amount of virus was added to achieve an MOI of 0.5 or 1 and centrifuged at 300 x *g* for 2 hours. Six hours post-transduction, an additional 1 mL of full media (containing serum) was added. 48-hours post-transduction, cells were examined microscopically for the presence of reporter gene (TurboGFP) expression. Selection of transfected cells was achieved by adding 1 µg/mL puromycin (Sigma) to the culture medium. In order to determine the minimum concentration of puromycin required to eliminate non-transduced cells, a puromycin kill curve was performed following the puromycin kill curve protocol (Sigma Aldrich). The Lentiviral transduced D458 and CHLA-01R were grown up to T75 flasks and frozen for long-term storage as previously described (2.1.3). *BSG* and *MMP-2* knockdown was confirmed by qRT-PCR (2.5.6) and western blot (2.3.1).

2.1.5 Assessment of cell viability and proliferation

2.1.5.1 PrestoBlue® assay

To measure changes in cell viability and proliferation of cells, the PrestoBlue® assay was used (ThermoFisher, Scientific). The PrestoBlue® Cell Viability Reagent is a resazurin-based solution that uses the reducing ability of living cells to quantitatively measure cell proliferation. Upon entering a living cell, PrestoBlue® reagent is reduced to resorufin which is red in colour and highly fluorescent. The health of the cell can be monitored by the change in fluorescence. Metabolically active cells continuously convert the PrestoBlue® reagent. Non-viable cells cannot reduce the indicator dye and therefore do not generate a change in signal.

2.1.5.2 Cell viability

To measure cell viability of cells grown in varying media conditions, 1 x 10^4 - 2.5 x 10^5 cells were seeded in triplicate in a 96-well-plate and incubated at 37°C and 5% CO_2 for 6 hours to allow the cells to settle. Subsequently, cells were incubated with 100 µl of culture media +10% PrestoBlue® for 1 hour at 37°C and 5% CO_2. The excitation at 586 nm was measured in triplicate in a photometer (FLUOstar Omega, BMG Labtech).

2.1.5.3 Cell proliferation

To measure cell proliferation upon treatment with varying exosome concentrations, 1 x 10^4 - 2.5 x 10^5 were seeded in duplicate in a 96-well-plate and incubated with exosomes at the indicated concentrations and time periods. Subsequently, cells were incubated with 100 µL of culture media +10% PrestoBlue for 1 hour at 37°C and 5% CO_2. The excitation at 586 nm was measured in a photometer and related to the excitation of the untreated control.

2.1.6 Cell invasion and migration assay in a modified Boyden chamber

Cell migration and invasion was quantified in a modified Boyden chamber assay. Briefly, the lower wells of the chamber were filled with DMEM +10% FBS (D425 and D458 cells) or EGF, FGF (20 ng/mL) and 2% B-27 (CHLA-01 and CHLA-01R cells) and sealed with a polycarbonate transwell insert with pore diameter of 8 µm (Greiner Bio-One Thincert, 662638). For invasion and migration experiments transwell inserts were coated with Collagen IV (Cultrex 3410-010-01) diluted to 200 µg/mL in H_2O and laminin 111 (Cultrex 3400-010-02) diluted to 100 µg/µl in serum-free media. This setting is thought to resemble the *in vivo* situation of tumour migration through the basement membrane. 1 x 10^5 cells were seeded in the upper wells in medium devoid of FBS. The chamber was incubated for 24 hours at 37°C, 5% CO_2 and subsequently the number of invasive cells in the lower chamber was quantified relative to the standard curve. For exosome treatments, cells were pre-treated with indicated

concentrations of exosomes 24 hours prior to the seeding of tumour cells in the upper wells.

2.1.6.1 Standard curve preparation

To quantify the number of migrating cells, a standard curve of known cell numbers was set up for every biological replicate, ranging from 0 to 5 x 10^5 cells. Cells were resuspended in 1x cell dissociation solution (AMSBIO, 3455-096-05). Subsequently, cells were incubated with PrestoBlue (dilution of 1:10) for 1 hour at 37°C and 5% CO_2. The excitation at 586 nm was measured in triplicate in a photometer.

2.2 Extracellular vesicle techniques

2.2.1 Particle-free FBS

Particle-free FBS was generated by the pelleting of extracellular vesicles by overnight ultracentrifugation at 100,000 x *g* at 4°C. Remaining supernatant was filter sterilised through a 0.22 µm filter (Millipore) and stored at -20°C.

2.2.2 Isolation of exosomes and microvesicles

To isolate exosomes and microvesicles from adherent and semi-adherent cell populations, cells were cultured in 10 T-75 flasks up to 30% confluence, washed twice with HBSS and incubated in media supplemented with particle-free FBS for 48 hours. Cell culture supernatants were collected and centrifuged for 5 minutes at 750 x *g* at 4°C to pellet cells. This was followed by centrifugation of the supernatant for 15 minutes at 1,500 x *g* at 4°C to pellet debris. The supernatant was then centrifuged for 35 minutes at 14,000 x *g* at 4°C to pellet the microvesicles. The microvesicle pellet was resuspended in PBS and centrifuged again for 35 minutes at 14,000 x *g* at 4°C to wash the pellet. The microvesicle pellet was then resuspended in PBS or lysis buffer and stored at -20°C for up to one week or -80°C for several months. For the isolation of exosomes, the supernatant from the 14,000 x *g* centrifugation step was filtered through a 0.22 µm filter (Millipore) to further purify exosome populations by removal of non-exosomal proteins or larger particles. The supernatant was then centrifuged for 2 hours

at 100,000 x *g* at 4°C. The pellet was washed by resuspending in PBS and centrifuged again for 2 hours at 100,000 x *g* at 4°C (Figure 2.1). The remaining pellet was then resuspended in PBS or lysis buffer and stored at -20°C for up to one week or -80°C for several months.

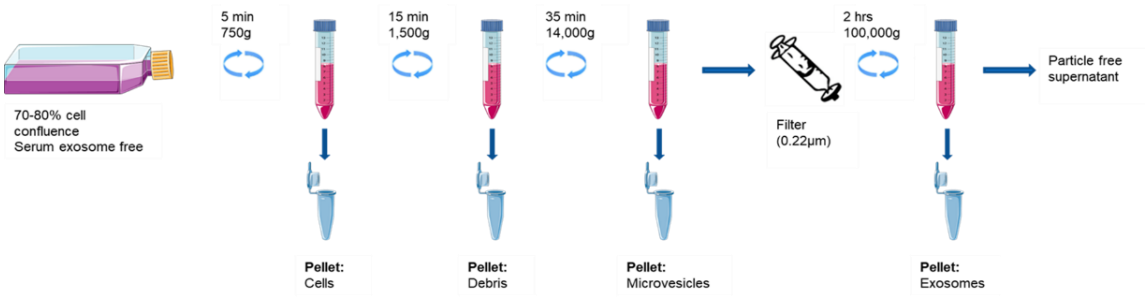

Figure 2.1 Schematic representation of EV isolation

Exosomes and microvesicle isolation method based on differential centrifugation and filtration steps, followed by a final ultracentrifugation step.

2.2.3 Isolation of CSF exosomes by size exclusion chromatography

Isolation of exosomes from patient samples was attempted using size exclusion chromatography qEV columns (Izon) according to the manufacturer's instructions. Briefly, cell culture supernatants were collected and centrifuged for 10 minutes at 1,500 x *g* to remove any cells and large particles. This was followed by centrifugation of the supernatant for 10 minutes at 10,000 x *g* to pellet remaining debris. The resultant supernatant was concentrated using 15 mL centrifugation filters (Amicon® Ultra), prior to loading in the qEV column. Fractions were collected and used immediately or stored at -20°C for up to one week or -80°C for several months.

2.3 Protein biochemistry

2.3.1 Antibodies used in this study

The antibodies used in this study are listed in Table 2.3.

Table 2.3 Antibodies used in this study

Cell line	Product number	Host species	Application	Product details
Annexin V	8555	Rabbit	Western blot (1:1000)	Cell signalling technology
CD9	13174	Rabbit	Western blot (1:1000)	Cell signalling technology
Histone 4	41328	Rabbit	Western blot (1:1000)	Cell signalling technology
EpCAM	2626	Rabbit	Western blot (1:1000)	Cell signalling technology
Alix	2171	Mouse	Western blot (1:1000)	Cell signalling technology
Anti-rabbit IgG, HRP-linked Antibody	7074	Goat	Western blot (1:2000)	Cell signalling technology
Anti-mouse IgG, HRP-linked Antibody	7076	Horse	Western blot (1:2000)	Cell signalling technology
MMP-2	86607	Mouse	Western blot (1:1000)	Abcam
EMMPRIN	46700	Mouse	Western blot (1:200)	Santa Cruz
PE-EMMPRIN	306211	Mouse	Flowcytometry (1:1000)	Biolegend
Biotin-MMP2	532001	Mouse	Flowcytometry (1:1000)	Biolegend
APC Streptavidin	405207	N/A	Flowcytometry (1:1000)	Biolegend
PE IgG1	400113	Mouse	Flowcytometry (1:1000)	Biolegend
APC IgG1	406609	Mouse	Flowcytometry (1:1000)	Biolegend

2.3.2 Protein isolation

For the isolation of protein from exosomes and cells, pellets were resuspended in 25-100 µl of lysis buffer (150 mM NaCl, 50 mM Tris pH 7.4, 0.1% SDS, 1% Triton X-100, supplemented with protease inhibitors) incubated for 20 minutes on ice and centrifuged for 30 minutes at 13,000 *x g* at 4°C. The supernatants were transferred to a clean Eppendorf and subjected to protein quantification as described in 2.3.3. Supernatants were collected and stored at -80°C.

2.3.3 Protein quantification by Bradford assay

The protein concentration in whole cell lysates and exosomes were quantified using a Bradford assay in relation to a Bovine Serum Albumin (BSA) standard curve (Bradford, 1976). Bradford assay was confirmed using the Protein Assay Dye Reagent (Biorad, 500-0006). This was diluted 1:4 in distilled water in a volume dependent on the number of samples to be tested (1 mL/sample). A 0.2% solution of BSA (Sigma-Alrich, A7906) was used to prepare standards from a concentration range of 0-40 µg/mL. Aliquots of unknown samples and BSA standards were loaded into a 96-well plate and loaded into the plate reader (FLUOstar Omega, BMG Labtech). The Bradford assay programme was selected and measurements of absorbance at 595 nm were determined.

2.3.4 SDS-PAGE

To analyse the protein expression of exosomes or whole cell lysates by western blotting, proteins were separated according to their molecule weight by discontinuous SDS polyacrylamide gel electrophoresis (SDS-PAGE) (Laemmli, 1970). This consists of two separate gels cast at different pH values. The resolving gel was prepared and after its polymerization (30-60 minutes) the stacking gel was layered on top and left to set for 60 minutes (Table 2.4). Protein samples (20 µg for exosomes and 10 µg for whole cell lysates) were mixed with sample buffer (Table 2.5) containing 5% β-mercaptoethanol, and heated for 5 minutes at 99°C. The prepared samples were then loaded onto the stacking gel and resolved in running buffer (Table 2.5) at 20 mA until samples reached the separating gel, at which point the current was increased to 40 mA for 60 minutes. To determine the protein sizes, a standard ECL rainbow protein ladder (Sigma RPN800E) was run as a molecular weight marker.

Table 2.4 Preparation of SDS-gels

Reagents	Resolving gel	Stacking gel
1M Tris pH 8.8	3.9 mL	n/a
1M Tris pH 6.8	n/a	0.65 mL
Distilled H_2O	1.9 mL	3.58 mL
Acrylamide (30%) (Sigma)	4 mL	0.67 mL
10% Ammonium Persulfate (APS, Sigma)	0.1 mL	0.05 mL
10% Sodium dodecyl sulfate (SDS, Sigma)	0.1 mL	0.05 mL
N,N,N′,N′-tetramethylethane-1,2-diamine (TEMED, Sigma)	0.01 mL	0.005 mL

2.3.5 Western blot

After electrophoresis, proteins were blotted onto a Hybond® Western blotting PVDF membrane (Scientific Lab Supplies 10600023) where they could then be detected by specific antibodies. The membrane was activated for 30 seconds in methanol, 3 minutes in water, and 10 minutes in transfer buffer (Table 2.5). The stacking gel was removed, and the resolving gel was placed on top of the activated membrane. The blot was covered in two sheets of filter paper on each side followed by two sponges, arranged in a transfer cassette. Blotting was performed in transfer buffer (Table 2.5) for 1 hour at 100 V at 4°C. After transfer, the binding capacity of the membrane was increased by drying for 10 minutes, followed by a rehydration step in TBS-T wash buffer. The membrane was routinely stained with Ponceau (Sigma) to confirm effective transfer.

Table 2.5 Buffers used for western blot

Buffer	Reagents
4 x SDS Sample Buffer	40% Glycerol (Courtner and Warner) 240mM TrisHCl pH 6.8 8% SDS 0.04% Bromophenol blue (Fisher)
10 x Running Buffer	250 mM Tris base 1.9 M Glycine 4% SDS
10 x Transfer Buffer	250 mM Tris base 1.9 M Glycine
1 x Transfer Buffer	100 mL 10x transfer buffer 200 mL Methanol 700 mL ddH_2O
10 x TBS	20 mM Tris Base pH 7.6 1.5 M NaCl
1 x TBS-T	100mL 10 x TBS 1mL Tween-20 (Sigma) 899mL ddH_2O

For protein detection, the membrane was blocked in blocking solution (TBS-T and 5% non-fat milk powder) for at least 60 minutes at room temperature on a rocker, to saturate non-specific antigen binding sites. The membrane was then rinsed in two changes of TBS-T (Table 2.5) and subsequently incubated in the appropriate primary antibody (Table 2.3) in TBS-T overnight at 4°C. The membrane was then rinsed several times in TBS-T over a 20-minute period. The membrane was then incubated in secondary antibody, in TBS-T for 1 hour at room temperature on the rocker. Following this, the membrane was rinsed several times in TBS-T over a 20-minute period.

Protein signals were detected using enhanced chemiluminescence (ECL) solution (Thermofisher Scientific). For proteins with particularly low expression Signalfire Elite (Cell Signalling 12757S) was used. Chemiluminescence was then measured in the LAS-3000 mini Biomolecular imager (GE Life Sciences) immediately after ECL incubation and digital images were saved. If further antibody staining was required, membranes were first washed briefly in TBS-T, following which ReBlot Plus Mild Antibody Stripping Solution (10x; Merck) was added and membranes incubated for 20

minutes at room temperature. After incubation, membranes were washed 2 x 2 minutes in TBS-T and the membrane was blocked again as previously described.

2.3.6 Detection of metalloproteinase activity by zymography

The activity of gelatinases MMP-2 and MMP-9 can be determined in cell culture supernatants or exosomes by gelatin zymography. Cell supernatants (15 µl) or exosomes (20 µg) were mixed with 4x loading buffer (Table 2.5), without β-mercaptoethanol, and loaded onto 10% SDS-PAGE gels (Table 2.4) which had been supplemented with 3 mg/mL gelatin (Sigma). Recombinant MMP-2 (Sigma) was also added as a reference marker. Electrophoresis was described as above, to separate protein according to their molecular weight. Subsequently, gels were incubated in renaturing buffer at room temperature for 30 minutes. To restore MMP activity, renaturing buffer was removed and replaced with developing buffer overnight at 37˚C. During which gelatinases degrade the gel. This degradation can be visualised by staining of the gels with Coomassie blue (staining solution) for 15 minutes under gentle agitation. To reduce background staining, gels were washed in de-staining solution for two hours to reveal the gelatinase bands. Gels were fixed in fixative solution for 15 minutes before gels were dried and photographed. All buffers and solutions used for zymography can be found in Table 2.6.

Table 2.6 Buffers and solutions used for zymography

Buffer	Reagents
10 x Running buffer	25mM Tris Base 192mM Glycine 0.1% SDS
10 x Developing buffer	Biorad 161076
Renaturing buffer	2.5% Triton-X-100 (Sigma, T8787)
Staining solution	40% Methanol 10% Glacial acetic acid (Sigma) 0.5% Coumassie blue R-250
De-staining solution	40% Methanol 10% Glacial acetic acid 50% Deionised water
Fixation buffer	5% Glycerine 30% methanol

2.3.7 Flow cytometry analysis

To determine surface exosomal EMMPRIN and MMP-2 by flow cytometry, exosomes (5 µg) suspended in PBS were incubated with flourochrome-labelled antibodies at the indicated concentrations (Table 2.3) for 30 minutes at room temperature in the dark. For unconjugated primary antibodies staining was performed for 20 minutes at room temperature, followed by incubation with fluorchrome-labelled anti-mouse secondary antibody for 20 minutes at room temperature in the dark. IgG1 antibodies were used as isotype matched negative controls. To remove unbound antibody, exosomes were washed in PBS by ultracentrifugation for 2 hours. Exosome pellets were resuspended in 200 µl PBS and fluorescence was measured by flow cytometry (MoFlo Astrios cell sorter). The flow cytometer was calibrated using control beads, which were then analysed as a reference for particle size. Forward scatter versus side scatter dot plots were used to gate exosome populations (Kaluza Analysis 2.1).

2.3.8 Flow nano analyzer (NanoFCM)

Exosome samples were diluted 1:10-1:100 and analysed using the Flow Nano Analyzer (NanoFCM), according to the manufacturers protocol (Tian *et al.*, 2020). Briefly, lasers were calibrated using 200 nm control beads (NanoFCM Inc.), which were analysed as a reference for particle concentration. A mixture of various sized beads (NanoFCM Inc.) were analysed to set a reference for size distribution. PBS was analysed as background signal. Particle concentration and size distribution were calculated using NanoFCM software (NanoFCM profession V1.0) and normalised to cell number and dilution necessary for adequate NanoFCM-reading. NanoFCM readings and instrument calibration were conducted by Dr Ben Peacock (NanoFCM application scientist).

2.4 Microscopy

2.4.1 Electron Microscopy

To visualise exosomes and microvesicles, vesicle pellets were resuspended in 2% paraformaldehyde and applied to a Cu-Rh formvar-coated 200 mesh grids (Agar

Scientific) for 3 minutes. Absorbing paper was used to gently remove any excess suspension. Negative contrast was achieved by incubating the grid for 30 seconds in 1% uranyl acetate, excess liquid was blotted off. Subsequent analysis of vesicles were carried out by JEOL 2100+ Transmission Electron Microscope (Philips) and iTEM software (Olympus). Sample processing and image acquisition was performed by Dr Zubair Nizamudeen.

2.4.2 Nanoparticle analysis

Nanoparticle Tracking Analysis (NTA) is a method used for the visualisation and analysis of nanometre particles in liquids ranging from a size of 10-1000 nm. The size of the particles are related to the rate of Brownian motion, temperature and the viscosity of the liquid and are not influenced by particle density or refractive index (Malvern). Each extracellular vesicle preparation was taken, and particle counts and size distribution were determined using NTA (NanoSight Ltd, Amesbury, UK). The instrument was configured with a 488 nm LM14 laser module and a high sensitivity digital camera system (OrcaFlash2.8, Hamamatsu C11440, NanoSight Ltd, Amesbury, UK). Prior to analysis of extracellular vesicle samples, 100 nm standard latex beads were tested as a control to confirm the NTA measurements were accurate. Samples were diluted in PBS, to a concentration between $2x10^6$ and $5x10^7$ particles/mL within the linear range of the instrument. Five replicate videos of 20 seconds were taken at 25°C, with samples under controlled flow, and analysed using NTA software (version 2.5), with the minimal expected particle size set to automatic, and camera sensitivity set at 12-16. The detection thresholds was set at 1-3, to reveal small particles.

2.5 Gene expression analysis

2.5.1 Total RNA isolation

RNA isolation from exosomes proved particularly challenging due to the low yields of RNA obtained, therefore several different RNA extraction methods were tested according to the manufacturer's instructions; mirVana (Ambion), Nucleospin RNA plus

(Agilent), TRIzol (Fisher), miRNeasy micro (Qiagen). In general, RNA yield and quality was most consistent when using the miRNeasy micro kit (Qiagen).

Therefore, the remainder of total RNA isolation from cultured cells or from extracellular vesicles was carried out using the spin column based miRNeasy Micro Kit (Qiagen) according to the manufacturer's instructions. Briefly, pellets were lysed in 700 µL of lysis reagent. The samples were vortexed for 15 seconds to help cell lysis and then incubated at room temperature for 5 minutes to allow dissociation of nucleoprotein complexes. 140 µL of chloroform was added to the samples for removal of cellular components. Samples were shaken vigorously for 15 seconds and incubated at room temperature for 3 minutes. Samples were centrifuged at 12,000 *x g* for 5 minutes at 4˚C. After centrifugation, the sample separates into 3 distinct phases; an upper colourless aqueous phase containing RNA, a white interphase and a lower pink organic phase. The upper aqueous phase was transferred into a new collection tube and 1.5 volumes of 100% ethanol was added and mixed thoroughly by pipetting up and down several times and subsequently applied onto a spin column containing glass fibre fleece. Columns were centrifuged at 8000 x *g* for 15 seconds at room temperature, this leads to the binding of nucleic acids to the column, whilst proteins and cellular debris are eluted. The columns containing the remaining RNA were washed once with RPE buffer then with 80% ethanol. The column was dried by a further centrifugation at 13,000 *x g* for 5 minutes, before 14 µL of nuclease-free water was added to the column for the elution of the isolated RNA. Concentration and purity of the RNA was measured by NanoDrop ND-1000 (2.5.3).

2.5.2 DNase treatment

To remove contaminating DNA, isolated RNA samples from cell lysates were treated with DNase enzyme. For every 10 µL of RNA 1.4 µL of DEPC treated water, 1.2 µL of RQ1 DNase and 1.4 µL of 10x RQ1 DNase buffer were added. The samples were then vortexed briefly and incubated for 30 minutes at 37˚C. 1.4 µL of RQ1 stop solution was

then added to inhibit DNase enzyme activity and the samples were incubated for a further 10 minutes at 65˚C.

2.5.3 Measuring RNA concentration and purity

Concentration and purity of RNA was determined using a NanoDrop 2000c spectrophotometer. The upper and lower pedestals were cleaned with nuclease-free water before being blanked at zero with 1 µL elution solution. 1 µL of RNA sample to be analysed was pipetted onto the lower pedestal and the concentration was derived from the absorbance at 260 nm. The ratio of absorbance at 260 nm and 280 nm was used to verify the purity of the RNA sample. A ratio of ~1.8-2.0 is ideal. The ratio of absorbance at 260 nm and 230 nm was used to verify the purity of nucleic acids. A ratio between ~2.0-2.2 is ideal. For exosomes and microvesicles, a 260/280 >1.7 was considered acceptable for further analysis.

2.5.4 Complementary DNA (cDNA) synthesis

To allow for the analysis of gene expression by qRT-PCR, the isolated RNA was transcribed into complementary DNA (cDNA). 100 ng of RNA was mixed with 1 µL of random primers (3 µg/µL; Invitrogen), 1 µL of oligoT_{25} (50 µM; Eurofins) and 1 µL of deoxynucleoside triphosphates (dNTPs; 25 mM; Thermo Scientific), made up to a total volume of 14 µL with dH_2O. The mixture was briefly centrifuged and incubated for 5 minutes at 65°C, followed by 1 minute incubation on ice. Following this, 1 µL of Superscript III Reverse Transcriptase (Invitrogen) was added to the mixture, along with 1 µL of Dithiothreitol (DTT; Invitrogen) and 4 µL of 5x first strand buffer (Invitrogen). The prepared reaction mixture was incubated in a thermal cycler (Techne TC-512) for 5 minutes at 25°C, 45 minutes at 50°C, followed by 15 minutes at 70°C to inactivate the reaction. For RNA extracted from whole cell lysates, the samples were diluted in a ratio of 1:10 with dH_2O and stored at -20°C.

2.5.5 Primer design

All primers used in this study are listed in Table 2.7 and were designed using NCBI primer blast (https://www.ncbi.nlm.nih.gov/tools/primer-blast/), subsequently open

online access tools, oligonucleotide properties calculator (http://OligoCalc.com) and OligoAnalyzer (https://eu.idtdna.com/pages/tools/oligoanalyzer) were utilised to predict the formation of primer dimers and hairpin structures.

Table 2.7 Primers used for qRT-PCR

Gene target		Sequence	Optimised annealing temperature
MMP-2	Forward	GCCTTTAACTGGAGCAAAAACAA	60
	Reverse	TCCATTTTCTTCTTCACTCATTG	
BSG	Forward	GTTCTTGCCTTTGTCATTCTG	60
	Reverse	TCACCATCATCTTCATCTACGA	
PAPPA2	Forward	ATTAATAACCGGGCCTACTGCAAC	60
	Reverse	GTCACAATCAGCAGCAAATGGAA	
POU5F1B	Forward	TTC ACA GGT GAT TAT GAT TTA AAG AGA	62
	Reverse	GCC TGG TGA AAT GAG CAA TTA	
GAPDH	Forward	ATGTTCGTCATGGGTGTGAA	60-62
	Reverse	GTCTTCTGGGTGGCAGTGAT	

2.5.5.1 Temperature gradient optimisation of primers

To determine the optimal annealing temperature for primers used in this study, gradient PCRs were performed. A cell line with high expression of the gene of interest was identified using the ProteinAtlas database (https://www.proteinatlas.org/) and a qRT-PCR was set up to test a range of annealing temperatures. 1 µL of cDNA was added to 14 µL of master mix (Table 2.8) for each temperature tested. Internal controls, NRT (no reverse transcription) and NTC (no template control), were included to check for genomic DNA contamination. The qRT-PCR was carried out according to the protocol (Table 2.9). The PCR products for each temperature were visualised on a 2% w/v agarose gel to verify a single gene product at the appropriate molecular weight and to identify the optimal annealing temperature that provided the highest yield and specificity. To test the efficiency of primers, a qRT-PCR was set up with a dilution series of control RNA.

2.5.6 Quantitative real-time PCR (qRT-PCR)

Changes in gene expression were analysed by quantitative real-time PCR (qRT-PCR) using SYBR green detection. The PCR technique amplifies DNA using DNA polymerase to synthesise new DNA from a template strand. PCR typically involves 35-40 cycles in which the gene of interest is amplified. Each PCR cycle consists of three main steps; initial DNA denaturation, followed by the annealing step of gene specific primers, and finally extension in which DNA polymerase synthesises the complementary DNA strand. The amount of DNA doubles with each cycle and every cycle involves a measurement of the fluorescence of SYBR green which emits a fluorescent signal when bound to double-stranded DNA. Therefore, the fluorescence increases with every cycle completed. The number of the cycle in which the fluorescence reaches the threshold level is called Ct value and was normalized to the expression of the house-keeping gene GAPDH (=ΔCt value).

For each gene 14 µL from the prepared PCR reaction mix (Table 2.8) were pipetted into a 96-well plate in triplicates. To each well 1 µL cDNA (10 ng) diluted in nuclease-free water was added. The plate was sealed, centrifuged (2 min, 750 x *g*) and qRT-PCR was carried out according to the following protocol (Table 2.9), at the optimised annealing temperatures, in the CFX96 Real-Time PCR machine detection system (BIO-RAD). To confirm the specificity of the product a melt curve was also added.

Table 2.8 PCR reaction mix

Reagents	Volume added/well (µL)
SYBR green master mix*	7.5
Forward-primer	1.5
Reverse-primer	1.5
ddH_2O	3.5
TOTAL	14

*SYBR-Green master mix: iTaq DNA polymerase, dNTP mix, $MgCl_2$, SYBR green dye, enhancer and fluorescein (Eurofins).

Table 2.9 PCR programme

Number of cycles		Duration	Temperature (˚C)
1		3 minutes	95
x40	Denaturation	10 secs	95
	Annealing	30 secs	Variable temp
	Extension	30 secs	72
Melt curve		Increments of 0.5˚C increase every 5 seconds	65-95

2.6 Next-generation sequencing

RNA was extracted from 15 medulloblastoma-derived exosome samples as described above in section 2.5.1 and sent to Qiagen Genomic Services (Hilden, Germany) where the subsequent steps of NGS were performed. In addition 16 CSF samples were sent to Qiagen Genomic Services where exosomes and exosomal RNA was isolated and again the subsequent steps of NGS were performed.

2.6.1 Library preparation and miRNA sequencing

The library preparation was done using the QIAseq miRNA Library Kit (QIAGEN). A total of 5 µl total RNA was converted into miRNA NGS libraries. Adapters containing UMIs were ligated to the RNA. Then RNA was converted to cDNA. The cDNA was

amplified using PCR (22 cycles) and during the PCR indices were added. After PCR the samples were purified. Library preparation QC was performed using either Bioanalyzer 2100 (Agilent) or TapeStation 4200 (Agilent). Based on quality of the inserts and the concentration measurements the libraries were pooled in equimolar ratios. The library pool(s) were quantified using qPCR. The library pools were then sequenced on a NextSeq500 sequencing instrument (Illumina; SY-415-1002) according to the manufacturer instructions. Raw data was de-multiplexed and FASTQ files for each sample were generated using the bcl2fastq software (Illumina inc.). FASTQ data were checked using the FastQC tool.

2.6.2 Trimming

Cutadapt (1.11) is used to extract information of adapter and UMI in raw reads, and output from Cutadapt is used to remove adapter sequences and to collapse reads by UMI with in-house script.

2.6.3 Mapping and alignment

Mapping of the sequencing data is a useful quality control step in NGS data analysis as it can help to evaluate the quality of the samples. Abundant reads were removed from FASTQ files using Bowtie2 (2.2.2). The filtered FASTQ files were then aligned to the reference genome and to mature miRNA sequences known in miRBase (http://www.mirbase.org/). The mapping results then underwent quality control checks which classified the reads into the following six classes: outmapped, unmapped reads, genome, miRNA, smallRNA and predicted.

2.6.4 Differential expression

Differential expression analysis is performed using the EdgeR statistical software package (Bioconductor, http://bioconductor.org/). For normalization, the trimmed mean of M-values method based on log-fold and absolute gene-wise changes in expression levels between samples (TMM normalization) was used.

2.7 3’ UPX next generation sequencing

In addition to miRNA sequencing, the mRNA cargo of medulloblastoma-derived exosomes was determined using 3’ UPX sequencing, a method of NGS used for low input samples. Sequencing is one-directional from the 3’ end of RNA near the poly-A tail.

2.7.1 Library preparation and 3’ mRNA sequencing

Library preparation was performed using QIAseq® UPX 3' Transcriptome kit (QIAGEN, 333088). A total of 10 ng of purified RNA was converted into cDNA NGS libraries. During reverse transcription, each cell was tagged with a unique ID and each RNA molecule with a unique molecular index (UMI). Universal amplification was then performed to ensure DNA fragments containing Cell ID and UMIs were sufficiently amplified for NGS. Quality control was then performed to determine sample concentration and purity using either Bioanalyzer 2100 (Agilent) or TapeStation 4200 (Agilent), libraries were pooled and quantified by qPCR. The library pools were sequenced on a NextSeq 500 desktop sequencer (Illumina; SY-415-1002) according to the manufacturer’s instructions. Following sequencing, raw data was de-multiplexed and FASTQ files for each sample were generated using bcl2fastq software (Illumina).

2.7.2 Primary sequencing analysis

Raw sequencing data analysis was performed using QIAGEN GeneGlobe bioinformatics tool. Cells were de-multiplexed using the unique cell ID’s, the 3’ poly-A region was then trimmed and reads were aligned to the human reference genome (GRCh38) using STAR splice aware aligner (Dobin *et al.*, 2013). The aligned genes were annotated to gene regions and UMIs were counted for each gene.

2.7.3 Secondary differential analysis using DESeq2

The Bioconductor package DEseq2 (Love, Huber and Anders, 2014) was used for differentially expression analysis of the raw UMI count data. DESeq2 is a method for differential analysis of count data, using shrinkage estimation for dispersions and fold

changes to improve stability and interpretability of estimates. This enables a more quantitative analysis focused on the strength rather than the mere presence of differential expression.

2.8 miRNA and mRNA next-generation sequencing analysis

2.8.1 Unsupervised analysis

Qiagen performed unsupervised analysis of the miRNA and mRNA sequencing results for each sample. Principal Component Analysis (PCA) was performed on DESeq2 counts to reduce the dimensions of large data sets and is a useful tool to explore sample classes arising naturally, based on the expression profile. In addition, heatmaps were generated to show the hierarchical clustering of samples using the top 50 most differentially expressed genes or miRNAs.

2.8.2 Differentially regulated miRNA or mRNAs

Differential gene expression analysis was performed to identify significantly up and down-regulated genes or miRNAs within metastatic, primary, or normal groups. Significant mRNAs or miRNAs were filtered based on fold change (Log2) and FPKM (miRNA) or UMI (mRNA) values. Lists of miRNAs/mRNAs produced were input into the Gene List Venn Diagram online tool (bioinformatics.org/gvenn) to identify overlaps.

2.8.3 FunRich

FunRich software (http://www.funrich.org/), an open access, standalone functional enrichment and network analysis tool, was used to conduct enrichment analysis with Fishers exact test to generate *p*-values.

2.8.4 Miranda database analysis for target gene prediction

Utilizing Miranda database analysis, target gene prediction was performed on the candidate miRNAs that were differentially associated with metastatic-derived exosomes. Analysis was based on experimentally validated and computationally predicted gene targets.

2.8.5 Gene set enrichment analysis

To assess the potential role of exosomal genes in the context of medulloblastoma tumour biology, pathway enrichment analysis was conducted using Gene Set Enrichment Analysis (GSEA) (software.broadinstitute.org/gsea).

Gene sets used in this study included the Kyoto Encyclopedia of Genes and Genomes (KEGG) and Gene Ontology (GO) biological processes gene sets. Significance in overlaps was determined using an uncorrected p-value and a q-value (a p-value adjusted using the Benjamini-Hochberg False Discovery Rate (FDR) approach) to correct for multiple testing.

2.8.6 Patient dataset analysis

Genomic analysis of large-scale publically available datasets was obtained from R2: Genomics Analysis and Visualisation Platform (http://r2.amc.nl) for a number of large-scale medulloblastoma datasets. Information for each dataset used in this study can be found in Table 2.10.

Table 2.10 Gene expression datasets utilized in this study

Data set	Sample type	Number of samples	Platform	Reference
Cavalli	Medulloblastoma	763	hugene11t	Cavalli et al., 2017
Pfister	Medulloblastoma	223	u133p2	Northcott et al., 2017
Roth	Normal Cerebellum	9	u133p2	Roth et al., 2006
Harris	Normal brain	44	u133p2	n/a

2.9 Statistical analysis

All experiments were performed at least in biological duplicates. Data are presented as means ±SEM. Multiple comparisons were analysed by one or two-way ANOVA. A value of $p \leq 0.05$ was considered statistically significant. All statistical analyses were performed using GraphPad Prism 8.1.2 software.

Chapter 3

Isolating and characterising medulloblastoma extracellular vesicles

Chapter 3. Isolating and characterising medulloblastoma extracellular vesicles

3.1 Introduction

Tumours cells are classically known to communicate via direct cell-to-cell contact and the secretion of soluble proteinaceous factors such as proteases and cytokines. Alternative, novel mechanisms, which promote tumour progression, have recently been described. New components of the tumour secretome thought to be involved in cancer progression, including exosomes, have been identified (Dai *et al.*, 2020). Exosomes are nanometre sized vesicles of endocytic origin that carry a variety of molecules including proteins, lipids, mRNA and microRNA (Théry, Zitvogel and Amigorena, 2002). Cancer cell-derived exosomes have been shown to participate in crucial steps in metastatic spread of a primary tumour, ranging from oncogenic reprogramming of malignant cells to formation of pre-metastatic niches (Dai *et al.*, 2020). These affects are achieved through the mediation of intercellular cross-talk and subsequent modification of both local and distant microenvironments.

At the outset of this project only two medulloblastoma exosome studies had been reported (Epple *et al.*, 2012; Bisaro *et al.*, 2015). Both studies focused on exosomes derived from SHH cell lines. More recently the role of exosomes in medulloblastoma progression has been explored (S. Huang *et al.*, 2020; Zhu *et al.*, 2020), including the characterisation of exosomes from Group 3 cell lines. However, the isolation and characterisation of exosomes from matched primary and metastatic paired cell lines remains unstudied; thus the thorough characterisation and study of exosomes from Group 3 and Group 4 cell lines is a novel avenue of research.

The first aim of this chapter was to optimise a reliable method whereby sufficient amounts of high quality exosomes could be routinely obtained. To achieve this, the following objectives were addressed:

- Establish a method for the reproducible isolation of extracellular vesicles

- Optimise cell culture media to establish quality control measures for exosome preparations
- Characterise exosomes based on their morphology, size and protein content

In the second part of this chapter, the functional influence of released exosomes on medulloblastoma migration and invasion was investigated.

3.2 Medulloblastoma cells release two distinct populations of extracellular vesicles

Exosomes and microvesicles have been successfully isolated from cell supernatant and body fluids. The original protocol used for exosome isolation involved multiple centrifugation and ultracentrifugation steps (Théry *et al.*, 2006). Over the years, several modifications to this protocol have been made (Menck *et al.*, 2015). However, further optimisation of the exosome isolation protocol for medulloblastoma cell lines was still required to obtain exosome preparations free from serum contaminants.

An ultracentrifugation method was employed, based upon previously published protocols (Théry *et al.*, 2006; Menck *et al.*, 2015), which were reported to result in isolation of two distinct populations - namely microvesicles and exosomes. The application of this method to cell culture supernatants from CHLA-01 and CHLA-01R medulloblastoma cell lines was the subject of previous research by the author of this thesis (Jackson, MRes Thesis 2017).

In that previous work, transmission electron microscopy (TEM) revealed two distinct populations of extracellular vesicles; 1) microvesicles consisting of a population of heterogeneous, large vesicles with a diameter of >150 nm which neither contained cell organelles nor fragmented DNA (Figure 3.1A) thereby excluding the presence of apoptotic bodies; 2) exosomes which were spherical in morphology with vesicle diameters <100 nm (Figure 3.1B). To further support these findings, the preparations were analysed using nanoparticle tracking analysis (NTA) which determined particle number and size. NTA revealed exosomes had a modal particle size of ~100 nm and

microvesicles a modal particle size of ~200 nm. Exosome samples have several other peaks at larger sizes, however these are seen at much lower concentrations. In comparison, microvesicle samples have a much more heterogeneous spread of peaks at larger sizes (above 300 nm) (Figure 3.1C-F).

Protein and RNA yields were compared between the different extracellular vesicle populations. The highest amount of exosomal protein and RNA was isolated from CHLA-01R exosomes. These differences were not represented in the amount of protein or RNA isolated from microvesicles, where the yield was consistently low (Figure 3.1G and H). Since low yields would make downstream analysis more difficult, it was decided to focus further investigations primarily on exosomes.

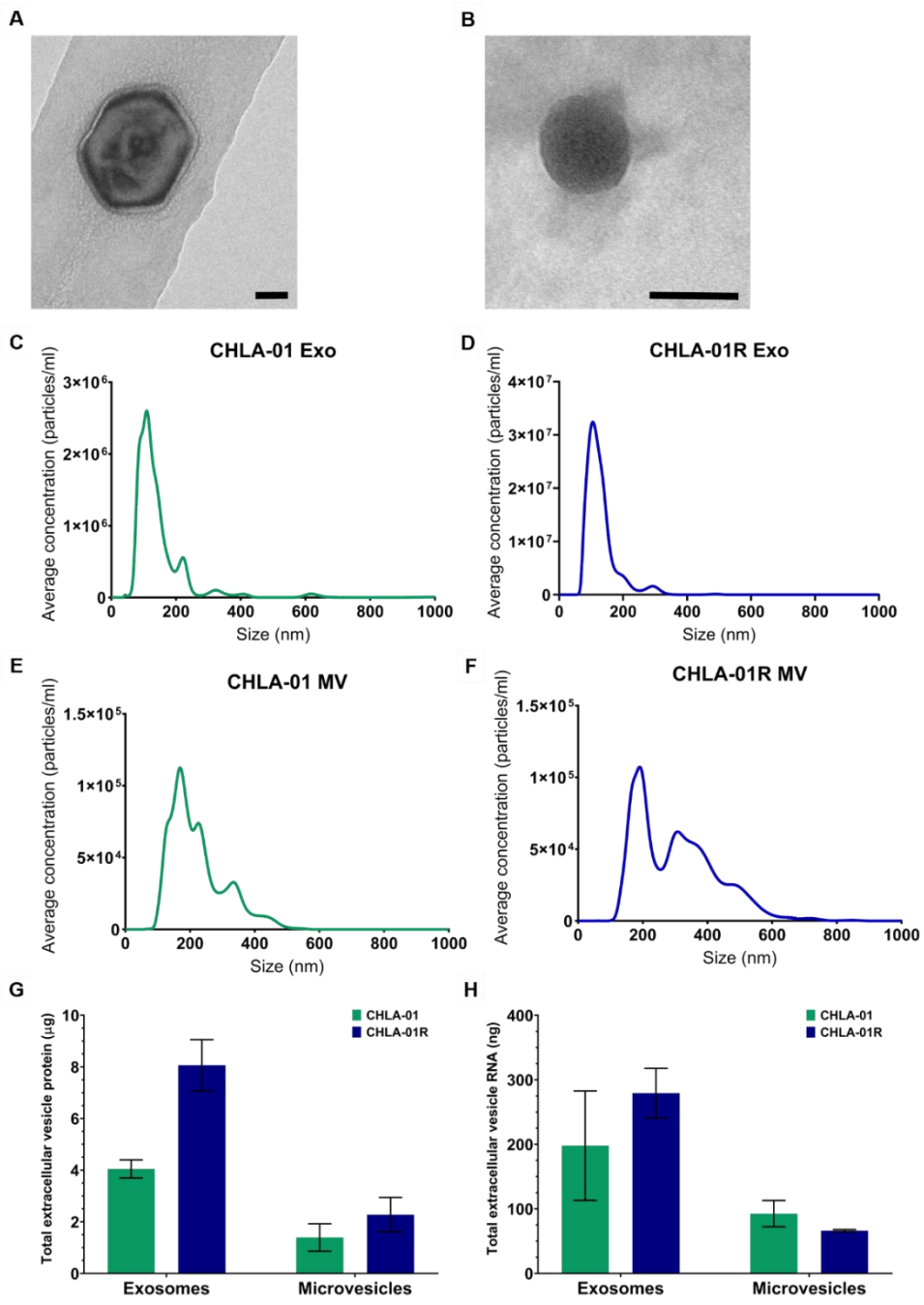

Figure 3.1 Isolation method allows for isolation of distinct populations of extracellular vesicles

TEM images of microvesicles (A) and exosomes (B) preparations showing two different populations of extracellular vesicles (scale bars: 50 nm). Vesicle concentrations and size distributions were verified using Nanoparticle Tracking Analysis (NTA) (C-F). The modal size of isolated exosomes (Exo) is <100 nm. The modal range of microvesicles (MV) is >200 nm. Exosome and microvesicle pellets were lysed and protein was extracted. Protein concentrations were determined by Bradford assay (G). Total RNA was extracted from extracellular vesicles. RNA concentrations were determined by Nanodrop (H). Error bars represent the mean ± SEM of n=≤3 experiments. Figure modified from (Jackson, MRes Thesis 2017).

3.3 Optimisation of medulloblastoma cell culture conditions for exosome isolation

Biological fluids are complex mixtures containing a heterogeneous pool of cells and particles, this poses significant challenges for the isolation of pure exosomes. In contrast to biological fluids, cell culture media gives an opportunity to obtain pure exosomes; it is far easier to control for the presence of co-isolates. However, studying cell lines *in vitro* can be challenging due to the varied array of culture media used to grow cells. Another major challenge in collecting exosomes from cell cultures is handling large volumes of media to maximise yields. Therefore, medulloblastoma cell lines were chosen to allow the scale-up of exosome isolation, as the cells should be compatible with large scale culture. Typically, 10 x T-75 flasks were needed per exosome isolation.

Nine medulloblastoma cell lines representing three of the four molecular subgroups (SHH, Group 3, and Group 4) were used in this study and are grown in different culture media containing a range of amino acids, vitamins, metal salts and organic compounds mixed with 10-15% w/v foetal bovine serum (FBS). Clinical information as well as cell line details are summarised in Table 3.1

Table 3.1 Characteristics of medulloblastoma cell lines used in this study

Cell line	Subgroup	Metastatic stage	Culture media	Growth type
DAOY	SHH	Non-metastatic (M0)	DMEM + 15% FBS + 1% Sodium Pyruvate	Adherent
UW228-3		Non-metastatic (M0)	DMEM + 10% FBS	Adherent
ONS-76		Metastatic tumours at the right prepontine cistern (M2)	RPMI-1640 + 10% FBS	Adherent
D283 Med	Group 3	Peritoneal metastasis and malignant ascites from laparotomy (M2)	DMEM + 10% FBS	Semi-adherent
HD-MB03		Spinal metastases at diagnosis (M3)	RPMI-1640 + 10% FBS	Semi-adherent
D458*		Metastatic cells from CSF (M+)	DMEM + 10% FBS	Semi-adherent
D425*		Non-metastatic cells from primary tumour (M0)	DMEM + 10% FBS	Semi-adherent
CHLA-01*	Group 4	Non-metastatic primary tumour (M0)	DMEM/F12 + 2% B27 + FGF + EGF	Suspension
CHLA-01R*		Recurrent metastatic cells from pleural fluid (M3)	DMEM/F12 + 2% B27 + FGF + EGF	Suspension

*cell lines with matched primary and metastatic pairs

It is also important to note that the serum generally used for cell culture is unprocessed except for heat inactivation; thus, it would be expected to be contaminated by exosomes of the host from which the serum is drawn. These exosomes, if not depleted from serum, will contaminate the media and therefore bias the experiment. To eliminate serum exosomes, serum was ultracentrifuged overnight. Dynamic light scattering analysis revealed that standard FBS samples show a large amount of bovine exosome and microvesicle sized particles, whereas the FBS exo-depleted sample has a significant reduction in these particles (Appendix Figure 1).

The serum component in general is an ill-defined factor in cell culture media. FBS has previously been shown to induce cell migration and proliferation, therefore we believed FBS could affect exosome release. To test this hypothesis we used four medulloblastoma cell lines which are grown in a range of culture media. The effect of each cell lines “standard” media (Table 3.1) and a more controlled media (supplemented with 2% FBS or B27 only), on exosome production is shown in Figure 3.2. In each case exosome production was defined as protein content in exosomes, normalised to the number of cells from which the exosomes were derived. For all cell lines assessed, media supplemented with high concentrations of FBS resulted in an increase in exosome production compared to controlled media. DAOY cells, whose standard media contained the highest concentration of serum, showed the largest difference in exosome production ($p \leq 0.01$). CHLA-01 cell lines whose standard media contains no serum, showed no significant difference in exosome production between the two different media conditions. However, there was still a slight increase in exosome production which could have been a result of the growth factors EGF and FGF. Our findings strongly suggest that serum enriched media affects exosome production.

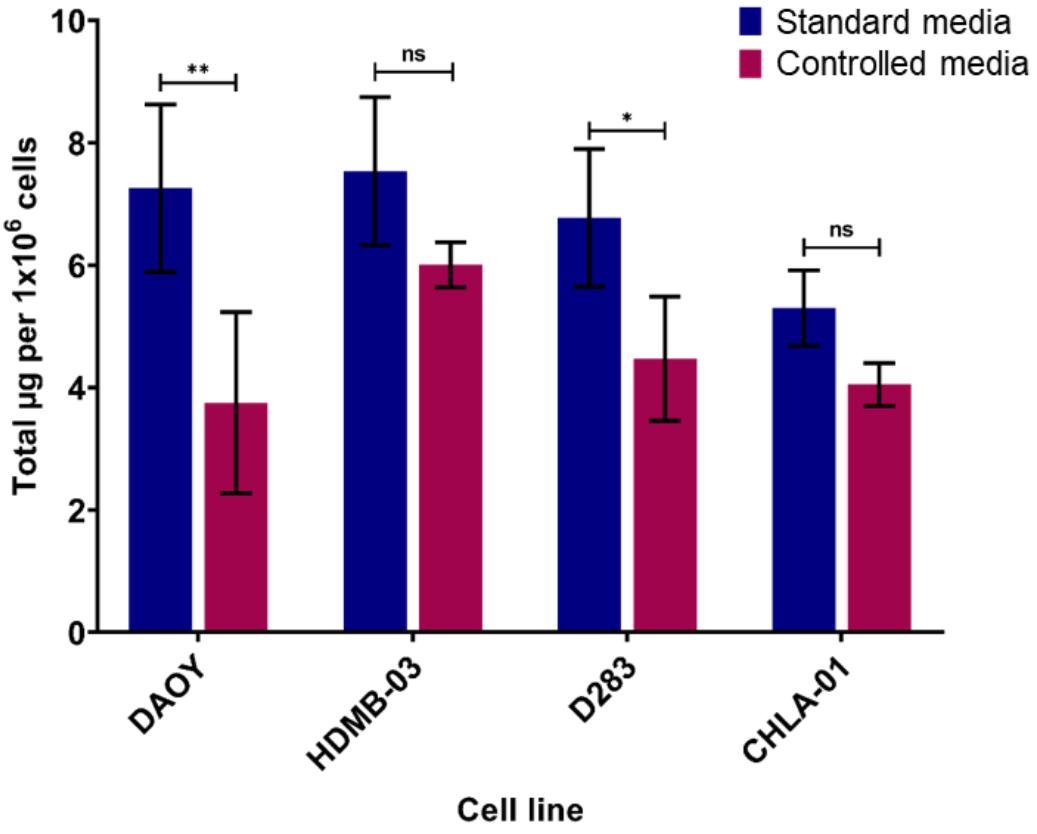

Figure 3.2 Effects of FBS concentration on exosome release

Three different medulloblastoma cell lines, DAOY, HDMB-03 or CHLA-01, were grown in their standard media or controlled media. Total exosome protein amounts were compared for each media condition. In each case exosome production was defined as protein content in exosomes, normalised to the number of cells from which the exosomes were derived. Error bars represent the mean ± SEM of n=3 experiments each containing 3 replicates. Significance was calculated using one-way ANOVA analyses with Sidak's multiple comparisons post-hoc test (*= p≤0.05, **= p≤0.01, ns=not significant).

To allow direct comparisons between medulloblastoma cell lines, our first aim was to optimise culture media so that all cell lines used could be grown under “basal” (controlled) conditions, containing only 2% FBS or B27.

To define the optimal basal conditions for all cell lines, cells were seeded in 96-well plates in either their standard culture media or controlled media with 2% FBS or B27. Growth and cell viability was assessed over a nine-day period post-seeding. Cell lines grown in serum-free media supplemented with B27, failed to grow in these culture conditions (Figure 3.3). Instead, media supplemented with 2% FBS was required for continual growth. All cell lines remained viable for at least seven days regardless of serum concentration (Figure 3.4). In summary, most of the medulloblastoma cell lines used in this study need the presence of serum to grow *in vitro*.

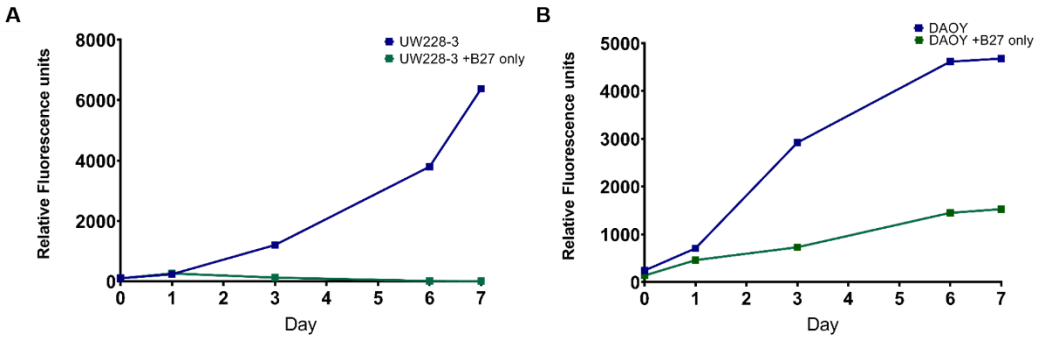

Figure 3.3 Assessment of medulloblastoma cells grown without FBS

(A) UW228-3 and (B) DAOY medulloblastoma cell lines were seeded in 96-well plates in either their standard media or basal media supplemented with B27 only. Growth and viability were monitored across a 7 day time period. n=1 experiments containing ≥3 replicates.

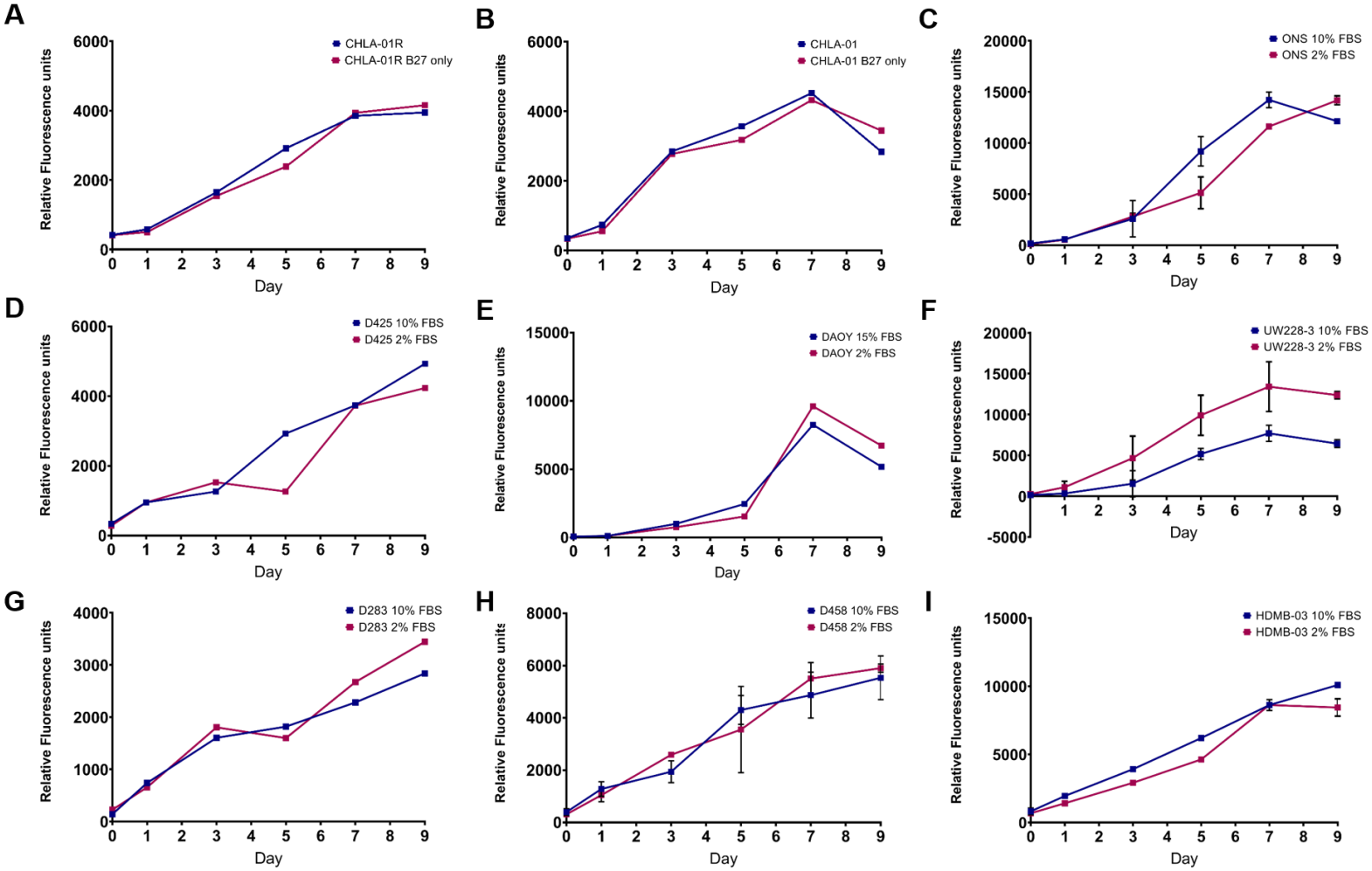

Figure 3.4 Optimisation of medulloblastoma cell culture condition

Nine different medulloblastoma cell lines (A-I) were seeded in 96-well plates in either their standard media or basal media with 2% FBS or B27. Growth and viability was assessed over a nine-day period. Error bars where shown represent the mean ± SEM of n=≥1 experiments each containing ≥3 replicates

3.4 Exosome characterisation

In a 2018 “position statement”, a set of biochemical, biophysical and functional criteria were proposed by the International Society of Extracellular Vesicles (ISEV) (Théry *et al.*, 2018). The aim of this was to standardise the minimal experimental requirements to report the genuine isolation of exosomes. The first of these is the suggestion that two techniques are employed to characterise individual exosomes. For example, showing both electron micrographs and size distribution plots by nanoparticle tracking analysis (NTA). The next is regarding protein content, with the suggestion that 3 or more proteins are reported in at least a semi-quantitative manner. The report suggested the assessment of both transmembrane and intra-luminal proteins that are expected to be present or enriched in exosomes. Additionally, proteins not expected within exosomes should be measured to rule out cellular contamination. These suggestions provide a helpful guideline and were followed in this study, to provide strong evidence that exosome vesicles of good purity had been isolated.

3.4.1 Verification of exosome size and concentration by NTA

Exosomes can be defined by their size: ranging from 30-150 nm diameter (El Andaloussi *et al.*, 2013). Exosomes were isolated from nine medulloblastoma cell lines (Table 3.1), and preparations were analysed using NTA for particle size and concentration (Figure 3.5). Overall, the particles had an average modal diameter of 96.7 nm, which is within the accepted range for exosomes. Furthermore, the histograms showed a uniform distribution giving the appearance of a single population of vesicles being isolated. Together, these data suggest that the isolation procedure was effective in selecting the appropriate sized vesicles. This technique provided a satisfactory first evaluation of exosome size.

It is worth noting that NTA measures particles without distinguishing vesicles from other co-isolates of the same diameter. Therefore, other molecular analyses were also performed to confirm the isolation of exosomes and adhere to the minimal requirement guidelines recommended by ISEV (Théry *et al.*, 2018).

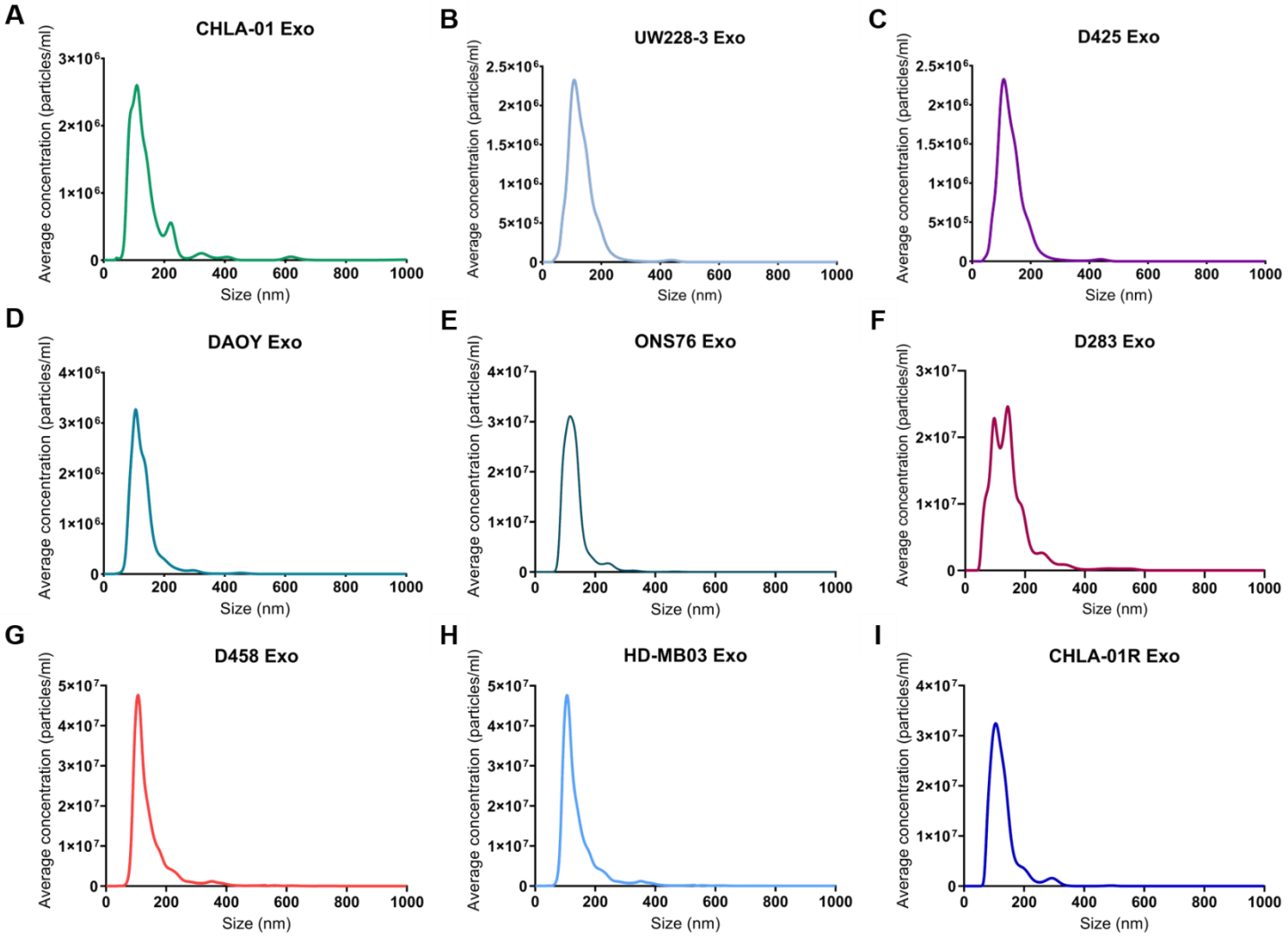

Figure 3.5 Nanoparticle tracking analysis showing exosome diameter and concentration

Quantification and sizing of medulloblastoma exosomes using Nanoparticle tracking analysis (NTA). X-axis represents particle diameter and y-axis represents particle concentration. Overall the particles had an average modal diameter of 96.7 nm, which is within the accepted range for exosomes. Five 60-second videos were recorded for each sample and analysed by the Nanoparticle Tracking Analysis 2.2 software. Data represent the average of at least two independent repeats.

3.4.2 Assessment of technical reproducibility by NanoFCM and NTA

The repeatable measurement of extracellular vesicles size and concentration is one of the key challenges facing the EV field and requires further efforts in order to obtain comparable results using different techniques (Théry *et al.*, 2018; Vogel *et al.*, 2021). Nanoscale flow cytometry (termed NanoFCM) is a more novel technology compared to NTA, which is employed to measure EV particle size distribution and particle concentration. NanoFCM enables flow-cytometry measurements at the sub-micron scale and displays accurate measurements of EVs down to 40 nm (Vogel *et al.*, 2021).

To assess the technical reproducibility of the isolation protocol, exosomes were isolated from four different medulloblastoma cell lines (CHLA-01, CHLA-01R, D425 and D458) and analysed by NTA and NanoFCM. The total particle concentration of replicates between NTA and NanoFCM for all cell lines was consistent with less than 3-fold difference between cell lines (Figure 3.6). In identical samples measured by both methods, NanoFCM generally estimated a slightly higher total particle concentration compared of NTA. The consistency of particle concentration measurements of experimental replicates within the same cell line by two different methods indicate a robust and reproducible isolation procedure.

When comparing particle diameter there was a difference in average modal diameter between the two methods (Figure 3.6), with the average diameter of exosomes measured by NanoFCM being 61.0 nm compared to an average diameter of 93.2 nm measure by NTA, although both measurements are within the accepted range for exosomes.

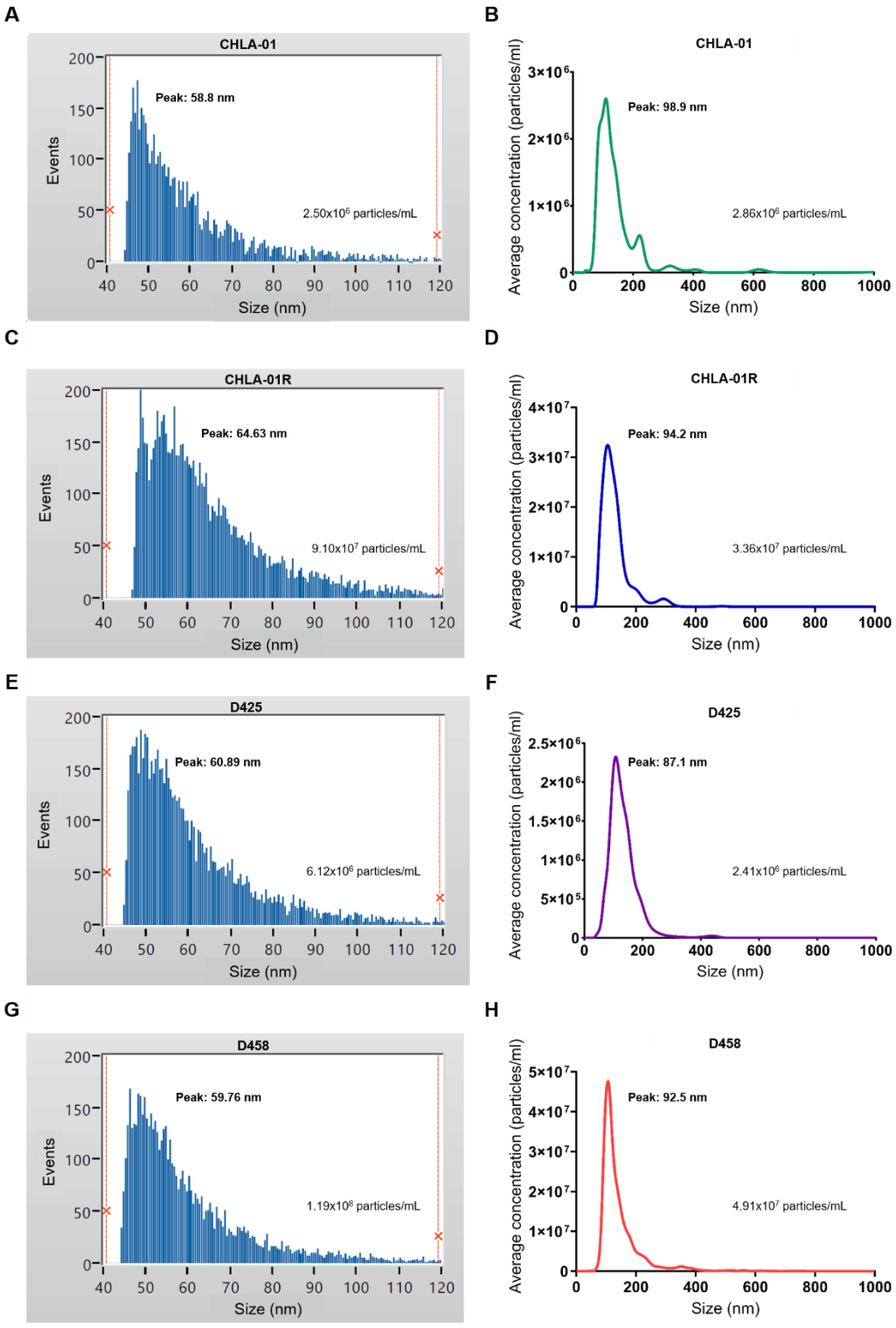

Figure 3.6 Exosome preparations measured by NanoFCM and NTA

Successful exosome isolations from four medulloblastoma cell lines (CHLA-01, CHLA-01R, D425 and D458) were measured by two different methods; NanoFCM (left column) and NTA (right column). Total particle concentration and average modal diameter are numbered on the graphs. NTA data represent the average of at least three independent repeats. NanoFCM represents two independent repeats with similar results.

3.4.3 Verification of exosome size and morphology by transmission electron microscopy

NTA and NanoFCM revealed that exosomes preparations from a range of medulloblastoma cell lines were of the correct size (Figure 3.5; Figure 3.6). However, neither method delivers sufficient resolution to provide any structural detail on the particles present. To provide further morphological detail, transmission electron microscopy (TEM) was employed. TEM has nanometre resolution and can be used to distinguish single exosomes from non-EV particles (Rikkert *et al.*, 2019), and is currently the most widely used method to monitor the quality and purity of extracellular vesicle containing samples (Van Deun *et al.*, 2017).

Isolated exosomes from medulloblastoma cell lines, CHLA-01 and CHLA-01R, were fixed onto formvar-coated carbon EM grids and stained with uranyl acetate prior to visualisation by TEM (Figure 3.7) (sample processing and subsequent images obtained by Dr Zubair Nizamudeen, University of Nottingham). TEM data revealed that medulloblastoma cell lines release a heterogeneous population of “cup-shaped” spherical vesicles, characteristic of exosomes under TEM (Théry *et al.*, 2018). There was some heterogeneity in size (diameters varying between 30-150 nm) and appearance of the structures visualized, but little evidence of non-vesicular contamination (Van Deun *et al.*, 2017). Upon visual inspection, the majority of isolated exosomes appeared >60 nm which is most consistent with the NanoFCM calculated particle size distribution (Figure 3.6).

Collectively, these images confirmed that exosomes of the correct structure and size were isolated. Across the three techniques (NTA, NanoFCM and TEM) exosomes isolated from the primary and metastatic paired cell lines produced a similar size of exosomes.

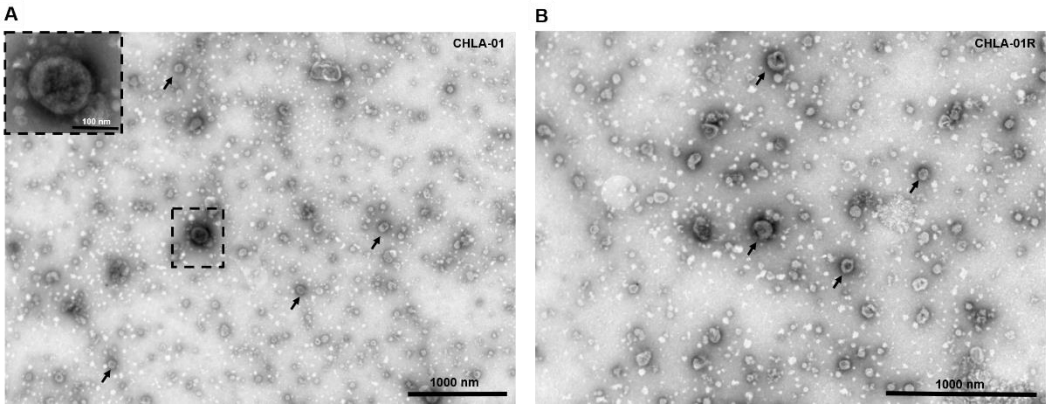

Figure 3.7 TEM images of CHLA-01 and CHAL-01R exosomes

Exosomes isolated by ultracentrifugation from medulloblastoma cell lines were imaged by transmission electron microscopy (TEM). Exosomes isolated from CHLA-01 (A) (insert shows cup-shaped exosome) and CHLA-01R (B) cells depicts multiple cup-shaped structures ranging from 30-150 nm size identified as exosomes, arrows point to exosomes. Representative fields of view from grids obtained by Dr Zubair Nizamudeen, of one experiment.

3.4.4 Verification of exosomes by western blot analysis

To further validate that exosomes were being isolated, analysis of specific proteins was performed. Protein extracts from exosomes were analysed by western blot for the expression of known exosome-enriched markers. Membrane markers included tetraspanin CD9, Epithelial cell adhesion and activation molecule (EpCAM) and annexin V. CD9 is an abundant component of exosomes, which may play a role in the fusion of these secreted membrane vesicles with recipient cells (Khushman *et al.*, 2019). EpCAM was one of the first tumour-associated antigens discovered and is now used to detect tumour-derived exosomes (Langhorst, Reuter and Stuermer, 2005), and annexin V which is commonly used to detect the exposure of phosphatidylserine in the outer membrane of extracellular vesicles (Hemler, 2005). In addition to exosomal membrane markers, the luminal protein ALG-2 interacting proteins X (Alix) is one of the best-established exosome markers due to its role in exosome biogenesis (Théry *et al.*, 2018; Van Niel, D'Angelo and Raposo, 2018). There was positive antibody staining of CD9, Annexin V and Alix in all exosome preps. In contrast EpCAM staining was absent in Group 4, CHLA-01 and CHLA-01R, derived exosomes (Figure 3.8A).

Exosome preparations were also screened for nuclear marker Histone 4 (H4). H4 was present in cell lysates and was undetected in the exosome samples (Figure 3.8B). This suggests that there was no cellular contamination in exosome preparations.

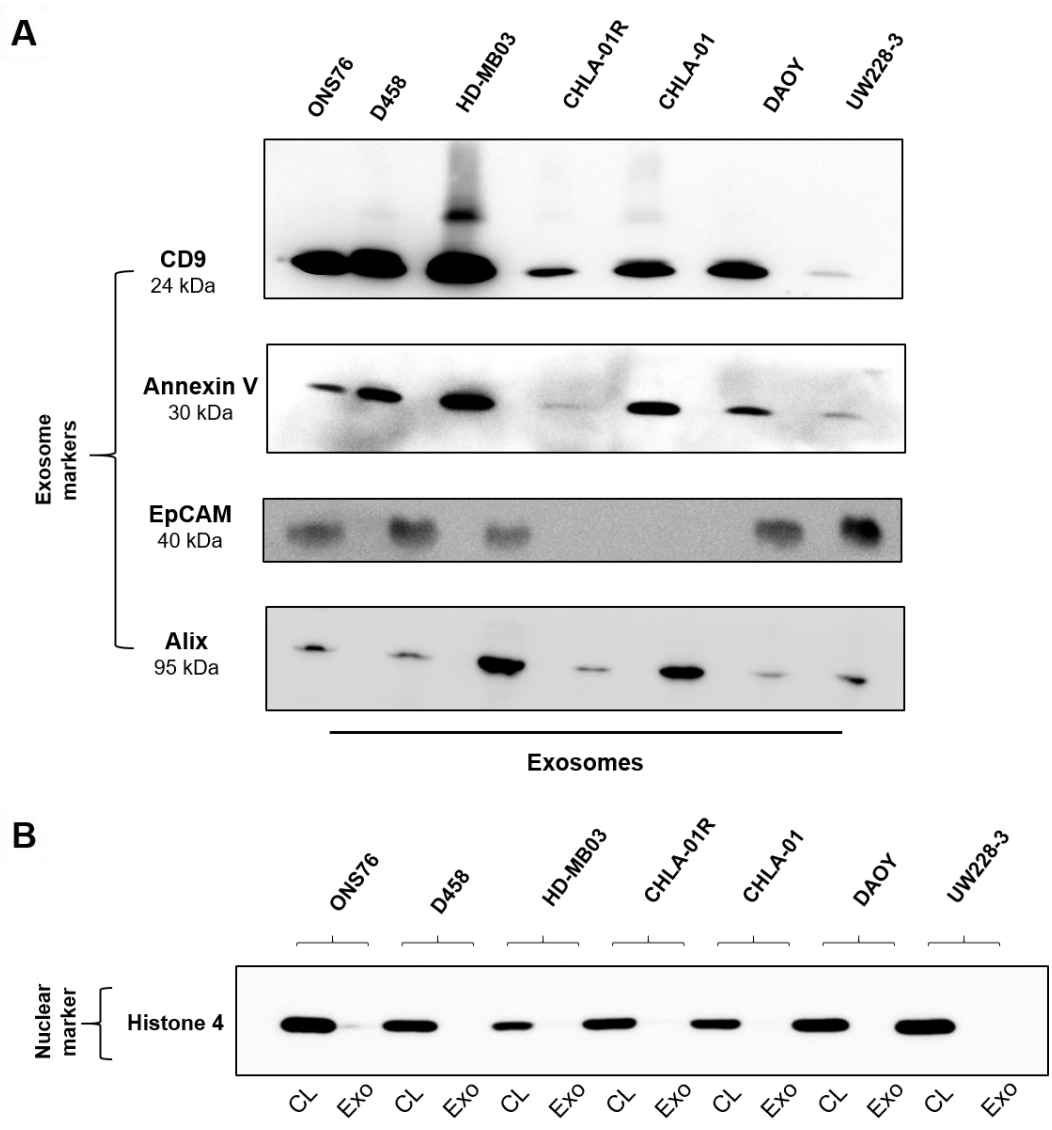

Figure 3.8 Characterisation of medulloblastoma-derived exosomes by western blotting

Exosomes were lysed and protein content was measure by Bradford assay. (A) 20 µg of exosome lysates were loaded onto gels. Samples were then probed with exosome specific antibodies CD9, Annexin V, EpCAM and Alix. (B) 20 µg of exosome lysates and 10 µg of cell lysates were loaded onto gels. The absence of Histone 4 (H4) in exosome samples demonstrates a pure exosome preparation. CL: cell lysate; Exo: exosome lysate. The gel is representative of two independent repeats with similar results.

3.5 Metastatic cells produce more exosomes

Exosomes are secreted by most types of cancers, and one notable feature of cancer cells is that they produce exosomes in greater amounts than normal cells. Several studies have shown that exosome numbers are elevated in the plasma of cancer patients compared to healthy controls, an increase in the levels of extracellular vesicles released correlates with poor prognosis and survival outcome (Baran *et al.*, 2010; Yamamoto *et al.*, 2016). Therefore, we wanted to investigate whether there was a difference between amounts of exosomes released from a series of medulloblastoma cell lines representing different subgroups and metastatic capacity. Among the panel of nine medulloblastoma cell lines (Table 3.1) were those originating from either metastatic (CHLA-01R, D458, HD-MB03, ONS76, and D458) and primary tissue (non-metastatic) (DAOY, UW228-3, D425, CHLA-01).

As well as determining size, NTA also has the capacity to measure particle concentrations. To determine whether metastatic cell lines release more exosomes, total exosomal concentration was measured and was normalized to the number of dissociated single cells producing these exosomes. We observed that the average number of exosomes from 10^6 cells was significantly higher in metastatic cells compared to non-metastatic cell lines (Figure 3.9A), with the lowest concentration of exosomes being consistently produced from UW228-3 cells (2.9-3.4 x 10^6) and the highest from HDMB-03 cells (3.5-3.9 x 10^7).

NTA is currently considered a highly efficient method available for exosome quantification because it does not rely on the detection of specific markers and because exosomes can be suspended in a wide range of solutions. Despite this, there are still important limitations using NTA for exosome quantification. Nanosight instruments have a limited dynamic range for particle concentration measurements. Thus, protein concentration of exosomes were also analysed by Bradford assay, normalised by cell number, and yields were compared between cells of different metastatic status. We observed that the normalised yield of exosomal protein, was

significantly higher when isolated from metastatic cell lines compared to the primary cell lines (Figure 3.9B).

Using both particle concentrations and Bradford measurements, metastatic cells produce more exosomes (either by direct particle counting, or by direct quantification of exosome protein content) relative to primary cells, which might play a vital role in increasing medulloblastoma metastasis.

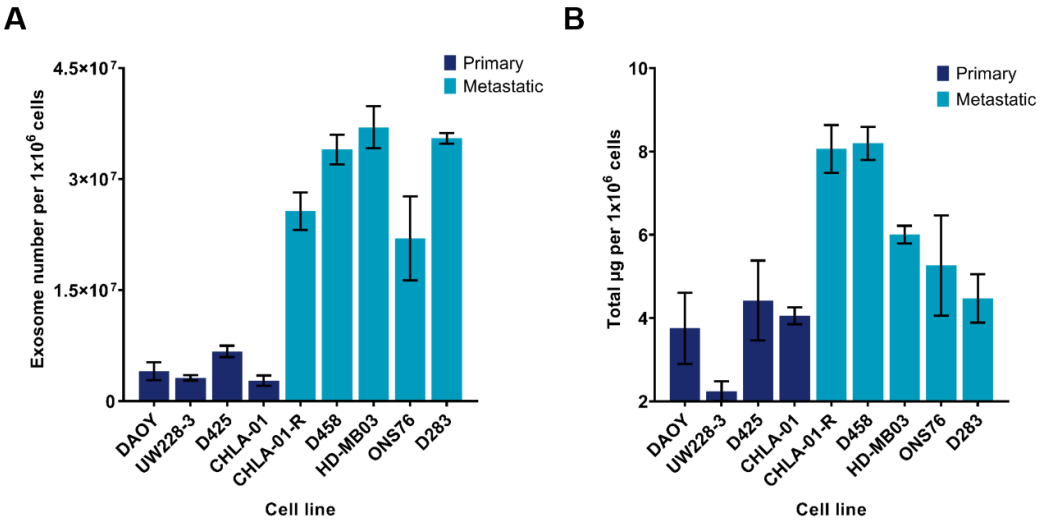

Figure 3.9 Increased exosome production by metastatic medulloblastoma cell lines

(A) Nanoparticle tracking analysis was used to calculate the number of exosomes relative to 10^6 cells. (B) Total protein in exosomes relative to 10^6 cells. The amount of protein isolated from exosomes was measured using Bradford protein assay. Graphs represent the mean ± standard error of at least two independent experiments.

3.6 Functional role of exosomes in medulloblastoma migration and invasion

To examine the functional influence of released exosomes on medulloblastoma migration and invasion, exosomes from cultured cells that represent a range of metastatic or primary tumour origins were isolated. As the Group 3 and Group 4 molecular subgroups have the highest occurrence of metastasis at diagnosis, cell lines were used from these two subgroups. Pairs of cell lines which had a matched primary and metastatic pair from the same patient were selected. The two Group 3 cell lines were D458 and D425. D458 had been isolated from metastatic cells in the patient's CSF. Its matched pair cell line, D425, had been isolated from the same patient's primary tumour. Two Group 4 cell lines used are the matched pair CHLA-01, which was isolated from a primary tumour after surgical resection of the mass in the posterior fossa, and CHLA-01R, derived from a malignant pleural effusion in the lungs of the same patient. These cell lines are valuable in gaining insight into molecular, genetic and proteomic signature changes that occurred between the primary tumour stage and the dissemination to a secondary site.

In order to test the effect of exosomes on cell migration, a modified Boyden chamber transwell model, recapitulating the invasion through the blood-brain-barrier was used (optimised by colleague Dr Macha Aldighieri), a schematic representation of which can be seen in Figure 3.10A. Cells were seeded in the upper compartment and allowed to migrate through an uncoated or coated membrane to a receiver plate. The basement membrane acts as a mechanical barrier between the epithelial and mesenchymal tissues, and only cells able to activate specific migration and invasion pathways can cross the membrane (Xu, Nirwane and Yao, 2019). Collagen IV and Laminin 111 were selected as transwell coatings as they are the most abundant components of the brain ECM, thus would best model the proteins most prevalent at the blood-brain-barrier (Ferro, Heilshorn and Owens, 2020).

Initially the migration of cell lines in the absence of added exosomes was measured. For Group 3 cell lines 10% FBS was added to the receiver plate, creating a chemokine gradient to induce cell migration. For Group 4 cell lines, which are grown without FBS, EGF and FGF were used to create a gradient. After 24 hours, cells were collected from the underside of the transwell insert and from the lower chamber, and cell numbers were quantified using a metabolic activity assay. All cell lines migrated in the transwell assay, and the basement membrane coating led to increased cell migration for Group 4 cell lines (CHLAs). When comparing matched cell line pairs, there was a significant higher level of cell migration in metastatic CHLA-01R cells compared to primary CHLA-01 cells in both the coated ($p \leq 0.01$) and uncoated ($p \leq 0.05$) transwell assay (Figure 3.10B). For Group 3 cell lines, after 24 hours no significant difference in migration was observed (Figure 3.10C).

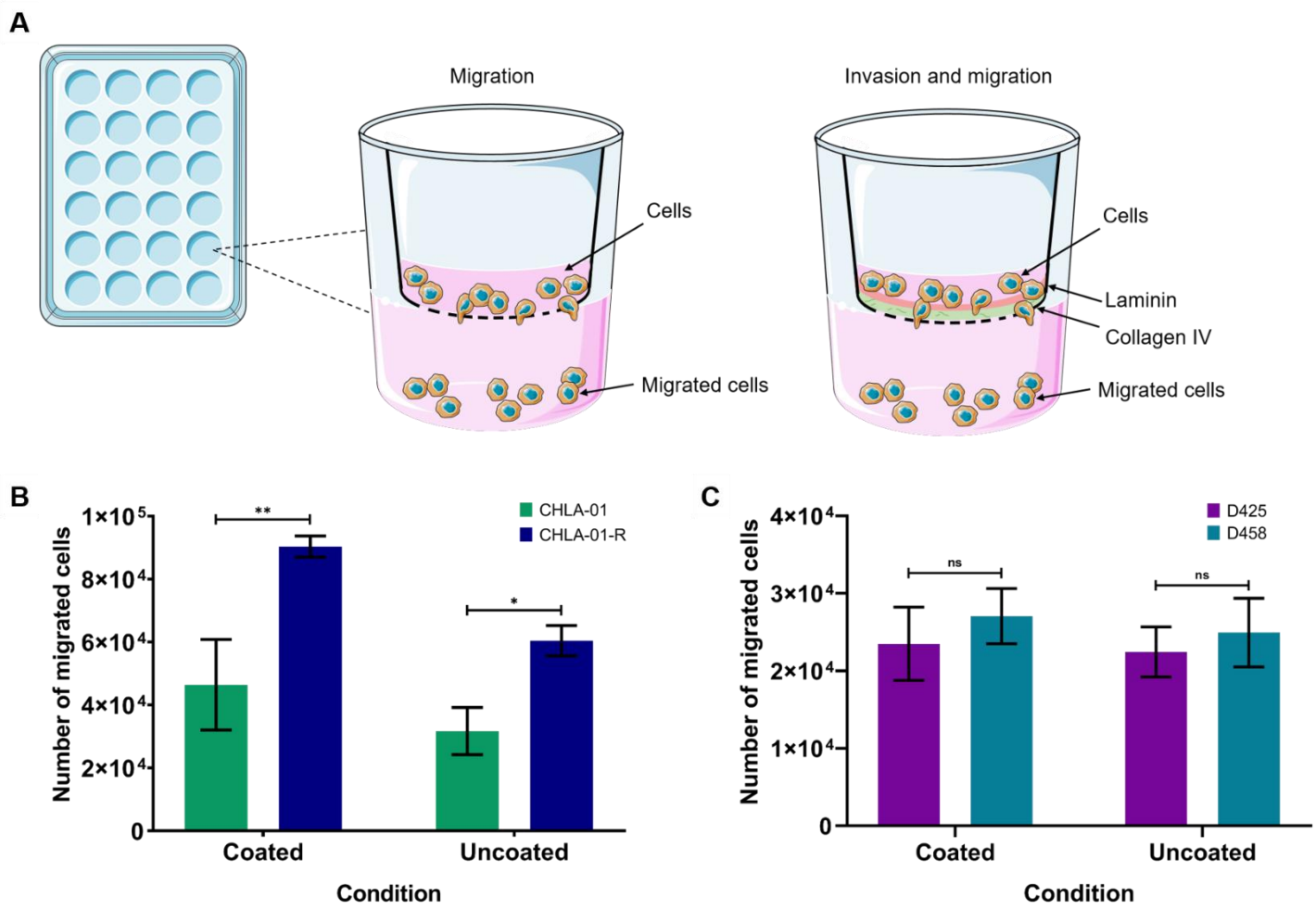

Figure 3.10 Increased invasion and migration capacity of metastatic medulloblastoma cell lines

(A) Schematic representation of transwell migration assay. The migration assay setup is shown for two individual wells, the first representing migration only (uncoated) the second well representing invasion through a Laminin and collagen IV coating, followed by migration into the lower chamber. Matched cell line pairs migrated for 24 hours through uncoated or coated transwell inserts. Cells were collected from the underside of the transwell and from the lower chamber and cell numbers were quantified using a metabolic activity assay. (B) There was a significant increase in cell migration of recurrent CHLA-01R cells compared to primary CHLA-01 cells in both the coated and uncoated transwell assay. (C) After 24 hours there was an increase in migration of the metastatic D458 cells, however the increase in migration was not significant. Results are shown as mean ± standard error of at least three biological replicates. Significance differences in migration was calculated using one-way ANOVA analyses with Dunnett's multiple comparisons post-hoc test (*p≤0.05, **p≤0.01) (ns=not significant).

3.6.1 Stimulation of MB cells with exosomes enhances cancer cell invasion and migration

Since a significant difference in the migration capabilities between a matched pair of Group 4 cell lines (CHLA-01 and CHLA-01R) was observed, it was of interest to determine whether metastatic cell-derived exosomes conferred a phenotype upon less migratory recipient cell lines. To address this question, primary CHLA-01 cells were co-cultured with exosomes isolated from metastatic CHLA-01R cells as well as with the corresponding vesicle-depleted supernatant (supernatant collecting following the final ultracentrifugation step in which the exosomes are pelleted) for 24 hours prior to seeding in the transwell assay. Despite there being no significant difference in cell migration between Group 3 D458 and D425 cell lines (Figure 3.10C), there was still a slight increase in D458 cell migration compared to D425, thus D425 cells were also co-cultured with D458 exosomes. Interestingly, CHLA-01 cells showed significantly (2.7 fold-change, ***$p \leq 0.001$, Figure 3.11B) enhanced tumour migration and invasion in response to exosome addition compared to vesicle-free supernatant. Similarly D425 cells showed a significant (1.52 fold-change, ***$p \leq 0.001$, Figure 3.11C) increase in migration in response to exosome addition.

To determine if the vesicle-free supernatant or PBS (exosomes were resuspended in PBS) altered cell migration, a transwell assay in which CHLA-01 cells had been pre-treated with vesicle-free supernatant or PBS for 24 hours was also performed. Vesicle-free supernatant and PBS had no effect on migration rates of CHLA-01 cells (Figure 3.11D). Taken together, the finding that metastatic-derived exosomes stimulate tumour invasion and migration, while vesicle-free supernatant had no such effect, confirms that exosome induced tumour migration is indeed a specific and not a non-physiological, artificial effect.

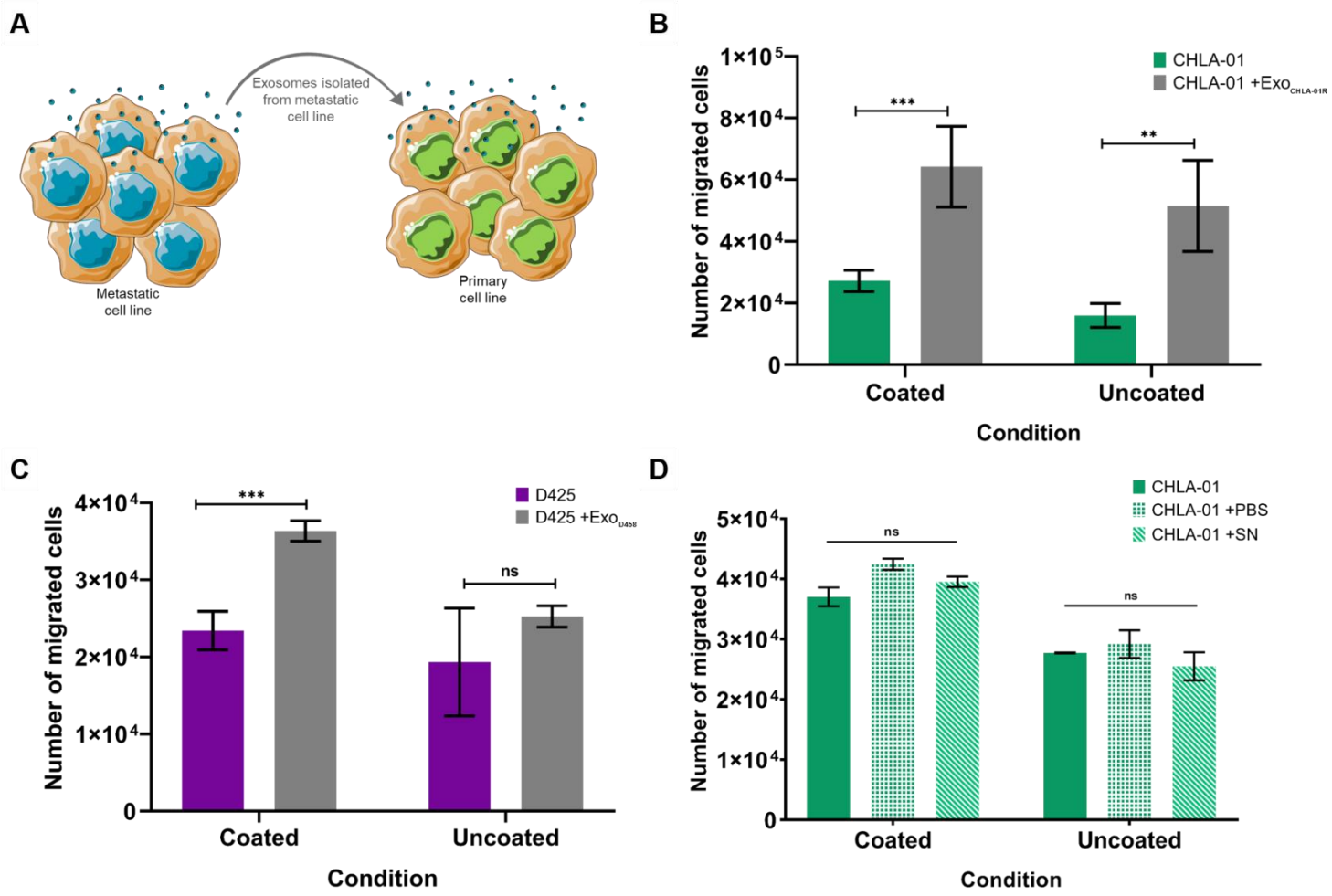

Figure 3.11 Exosomes enhance migration and invasion of primary medulloblastoma cell lines

(A) Schematic representation of exosomes isolated from metastatic cell lines co-cultured with primary medulloblastoma cell lines. (B) Primary CHLA-01 (B) and D425 (C) cell lines were stimulated with their corresponding metastatic derived exosomes as well as with the vesicle-free supernatant for 24 hours prior to seeding in the transwell assay. After 24 hours cells were collected from the underside of the transwell and from the lower chamber and cell numbers were quantified using a metabolic activity assay. Results are shown as mean ± standard error of at least three biological replicates. Significance differences in migration was calculated using one-way ANOVA analyses with Dunnett's multiple comparisons post-hoc test, (**p≤0.01, ***p≤0.001) (ns=not significant). (D) CHLA-01 were pre-treated for 24 hours with PBS, vesicle-free supernatant or normal media and prior to transwell migration assay. Significance differences in migration were calculated using two-way ANOVA analyses with Tukey's multiple comparisons post-hoc test.

3.6.2 Effects of exosome stimulation on medulloblastoma proliferation

To exclude the possibility that the observed migration effect was only due to an influence of exosomes on cancer cell proliferation, CHLA-01 and D425 cells were seeded in 96-well plates and stimulated with metastatic-derived exosomes for 96 hours. At 0, 24, 48, 72 and 96 hours cell proliferation was measured using Prestoblue metabolic activity assay. For CHLA-01 cells there was a significant increase in proliferation (1.6 fold-change, p≤0.05) after 24 and 48 hours after exosome stimulation compared to vesicle-free supernatant (Figure 3.12A). The fold-change in migration after exosome stimulation was 2.7 therefore, despite proliferation accounting for some of the increase in cell numbers, an exosome-dependent increase in migration was also observed. For D425 cells a significant increase in proliferation was observed at 72 hours (1.2 fold-change, p≤0.05, Figure 3.12B), suggestive of a migration effective as well as a component of proliferation.

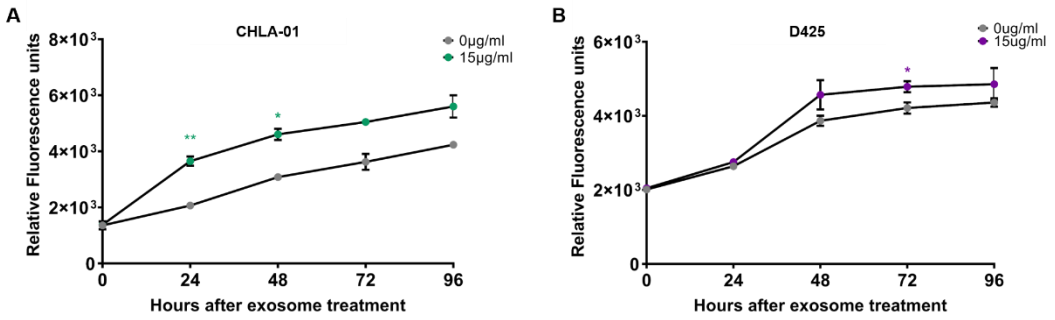

Figure 3.12 Effects of exosome stimulation on medulloblastoma cell proliferation

CHLA-01 (A) and D425 (B) medulloblastoma cells in serum free medium were incubated with corresponding metastatic exosomes for 96 hours. Cell proliferation was measured using Prestoblue metabolic activity assay. Results are shown as mean ± standard error of three biological replicates. Significance differences between exosome treated and untreated were calculated using repeated measures two-way ANOVA analyses with Tukey's multiple comparisons post-hoc test (*p≤0.05, **p≤0.01).

3.6.3 MB exosomes enhance non-malignant cell invasion, migration and proliferation

Since exosomes have been described to transfer malignant characteristics to surrounding benign cells, the influence of exosomes on non-malignant FB83 cells was explored. FB83 cells, derived from human foetal brain tissue, are non-tumorigenic and non-metastatic, and represent the lowest metastatic potential of the cell lines used in this project. As shown in Figure 3.13A, stimulation with metastatic exosomes (derived from CHLA-01R cells) alone was able to induce an invasive phenotype in the benign brain cells ($p \leq 0.01$), suggesting that recipient cells did not need to be predisposed to an invasive phenotype prior to exosome stimulation.

To determine the effect of exosomes on proliferation, FB83 cells were treated with malignant metastatic exosomes derived from CHLA-01R cells for up to 96 hours. The assessment of cell proliferation revealed a significant increase in proliferation at 72 and 96 hours (Figure 3.13B). This again was shorter than the migration assay, therefore we could conclude that we had observed a migration effect in this cell line and not just an increase in proliferation.

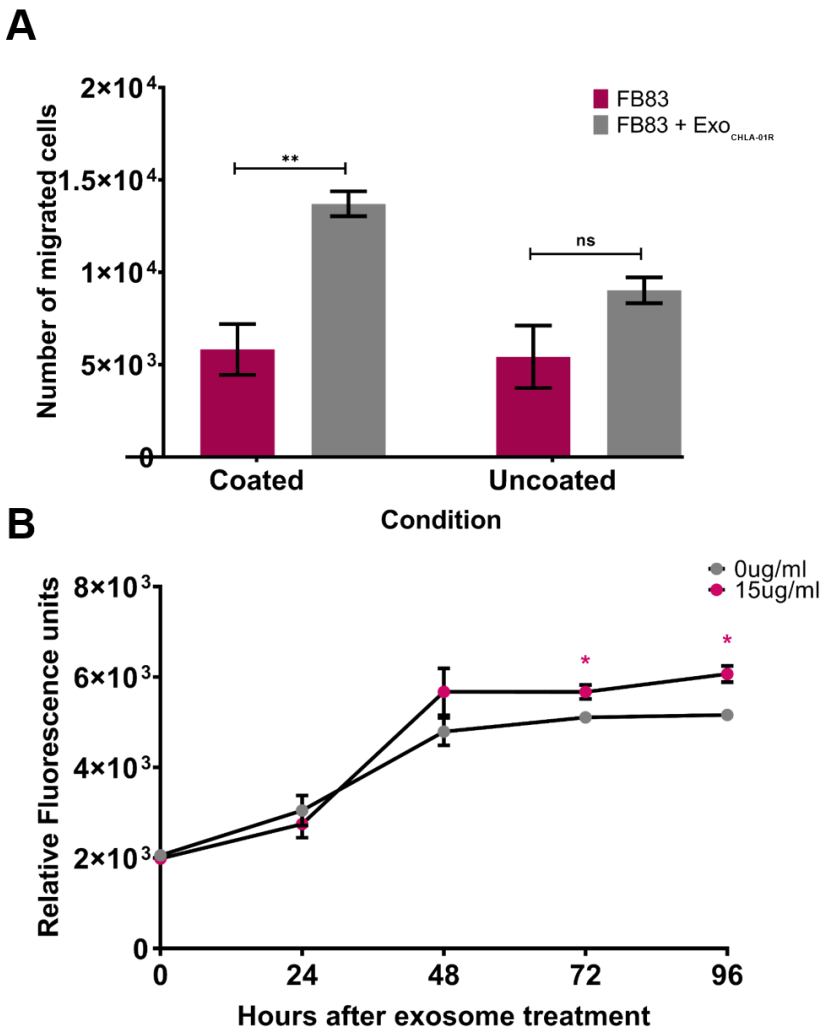

Figure 3.13 Malignant exosomes enhance non-malignant cell line invasion, migration and proliferation

Non-malignant FB83 cells were stimulated with CHLA-01R metastatic-derived exosomes or with vesicle-free supernatant for 24 hours prior to seeding in the transwell assay. After 24 hours cells were collected from the underside of the transwell and from the lower chamber and cell numbers were quantified using a metabolic activity assay. (A) Metastatic exosomes were able to significantly enhance tumour migration and invasion of FB83 cells. Results are shown as mean ± standard error of at least two biological replicates. Significance differences in migration was calculated using one-way ANOVA analyses with Dunnett's multiple comparisons post-hoc test, (**p≤0.01, ns=not significant). (B) FB83 cells in serum free medium were incubated CHLA-01R metastatic exosomes for 96 hours. Cell proliferation was measured using Prestoblue metabolic activity assay. Results are shown as mean ± standard error of three biological replicates. Significance differences between exosome treated and untreated were calculated using repeated measures two-way ANOVA analyses with Tukey's multiple comparisons post-hoc test (*p≤0.05).

3.7 Summary points

- By using electron microscopy and nanoparticle tracking analysis we showed that our protocol isolated medulloblastoma-derived exosomes and microvesicles, which are morphologically distinct. Since microvesicles contained low RNA and protein yields, further studies were focused entirely on exosomes.
- Medulloblastoma cell lines representing three of the four molecular subgroups (SHH, Group 3, Group 4) were successfully cultured in “basal” conditions to allow direct comparisons of exosome numbers.
- Exosome preparations were thoroughly characterised by size, protein content and structure, in keeping with the minimal essential requirements published by Thery *et al.,* 2018.
- A significant difference in the levels of exosomes secreted by metastatic cells compared to primary cells was observed, our first indication that exosomes might play a vital role in medulloblastoma metastasis.
- We demonstrated that metastatic-derived exosomes directly enhanced the migration and invasive potential of primary tumour cells in a heterologous stimulation loop.
- Metastatic exosomes enhanced the invasive capacity of non-malignant human foetal neuronal cells, indicating that recipient cells did not need to be predisposed to an invasive phenotype prior to exosome stimulation.

Chapter 4

EMMPRIN and MMP-2 are involved in the pro-migratory function of exosomes

Chapter 4. EMMPRIN and MMP-2 are involved in the pro-migratory function of exosomes

4.1 Introduction

In Chapter 3, we demonstrated that metastatic-derived exosomes directly enhanced the migratory and invasive potential of primary tumour cells in a heterologous stimulation loop. We next asked what these exosomes are carrying in terms of cargo, which has the capacity to cause this pro-invasive/migratory effect. Therefore, the focus of this chapter was to understand the functional role of exosomes in regard to their effect on the tumour microenvironment and remodelling the matrix, and their immediate effects on the target cells by changing the signalling cascade.

The tumour microenvironment is being increasingly recognised as an important contributor in tumour cell invasion and subsequent migration by secreting metalloproteinases (MMPs) that break down the extracellular matrix (ECM). Induction of MMPs is due, in part, to extracellular matrix metalloproteinase inducer (EMMPRIN), a glycoprotein commonly enriched on the surface of tumour cells and has been associated with tumour progression and poor patient outcome (Sier *et al.*, 2006; Menck *et al.*, 2015). Previous cell culture experiments demonstrated increased MMP release in response to EMMPRIN (Sun and Hemler, 2001), however more recently EMMPRIN has been found in extracellular vesicles of tumour cells and can mediate the MMP-inducing effect (Menck *et al.*, 2015; Colangelo and Azzam, 2020). We therefore hypothesised that medulloblastoma cells secrete EMMPRIN in exosomes, in a manner capable of enhancing the secretion of MMPs in recipient cells and drive processes necessary for tumour progression. We further hypothesised that exosomes contain functional MMPs which could directly degrade the ECM enhancing tumour cell migration.

4.1.1 MMP-2 and EMMPRIN as metastatic markers in medulloblastoma

4.1.1.1 *BSG* and *MMP-2* expression in medulloblastoma patient datasets

EMMPRIN (encoded for by the *BSG* gene) has not been extensively studied in medulloblastoma and the majority of research investigating differential expression of MMPs in medulloblastoma was performed prior to molecular subgrouping. As such, we first wanted to assess candidate gene expression in medulloblastoma patients and study the association between gene expression and survival. MMP-2 and MMP-9 were originally selected due to previous work correlating these MMPs with medulloblastoma metastasis (Rao *et al.*, 2007; Bhoopathi *et al.*, 2012), however MMP-9 protein levels were extremely low in exosomes (Appendix Figure 2), subsequently only MMP-2 was taken forward.

First, *BSG* and *MMP-2* gene expression data across large-scale publicly available patient datasets were analysed. R2: Genomics Analysis and Visualization Platform (http://r2.amc.nl) was used to assess *BSG* and *MMP-2* expression across a human medulloblastoma cohort comprising over 200 samples (Pfister *et al.*, 2009) compared with normal brain tissue (Harris *et al.*, 2014), and differences in gene expression were tested by one-way ANOVA analysis. The data showed highest expression of *BSG* in WNT medulloblastoma samples compared to normal brain, however there was no significant difference between the remaining subgroups compared to normal brain (Figure 4.1A). Correlation between candidate gene expression and patient progression was then explored. The Cavalli dataset, which comprises over 750 patient samples, was utilised to generate Kaplan-Meier survival curves (Cavalli *et al.*, 2017). Strikingly, when medulloblastoma patients were stratified according to mRNA levels at diagnosis, those with higher *BSG* expression had significantly worse 5- and 10-year overall survival than patients with lower *BSG* expression ($p \leq 0.001$; Figure 4.1B), indicative that the expression levels of *BSG* may represent a negative prognostic factor for overall survival in medulloblastoma patients. There was also a slightly higher *BSG* expression

in deceased patients compared to patients who had survived, however this increase was not significant (Figure 4.1C).

Having been shown to correlate with poor patient outcome and higher grade in multiple cancers (Isaacson *et al.*, 2017), it was postulated that expression of MMP-2 would represent a poor prognosis factor in medulloblastoma. Indeed when looking at *MMP-2* expression across the medulloblastoma patient datasets, the data showed higher *MMP-2* expression in medulloblastoma samples compared to normal brain (Figure 4.1D). However, when medulloblastoma patients were stratified according to mRNA levels at diagnosis, those with elevated *MMP*-2 expression displayed a better 5- and 10-year overall survival than patients with low *MMP-2* expression ($p \leq 0.001$) (Figure 4.1E). Conversely, there was significantly higher *MMP-2* expression in deceased patients compared to patients who had survived (**$p \leq 0.01$) (Figure 4.1F).

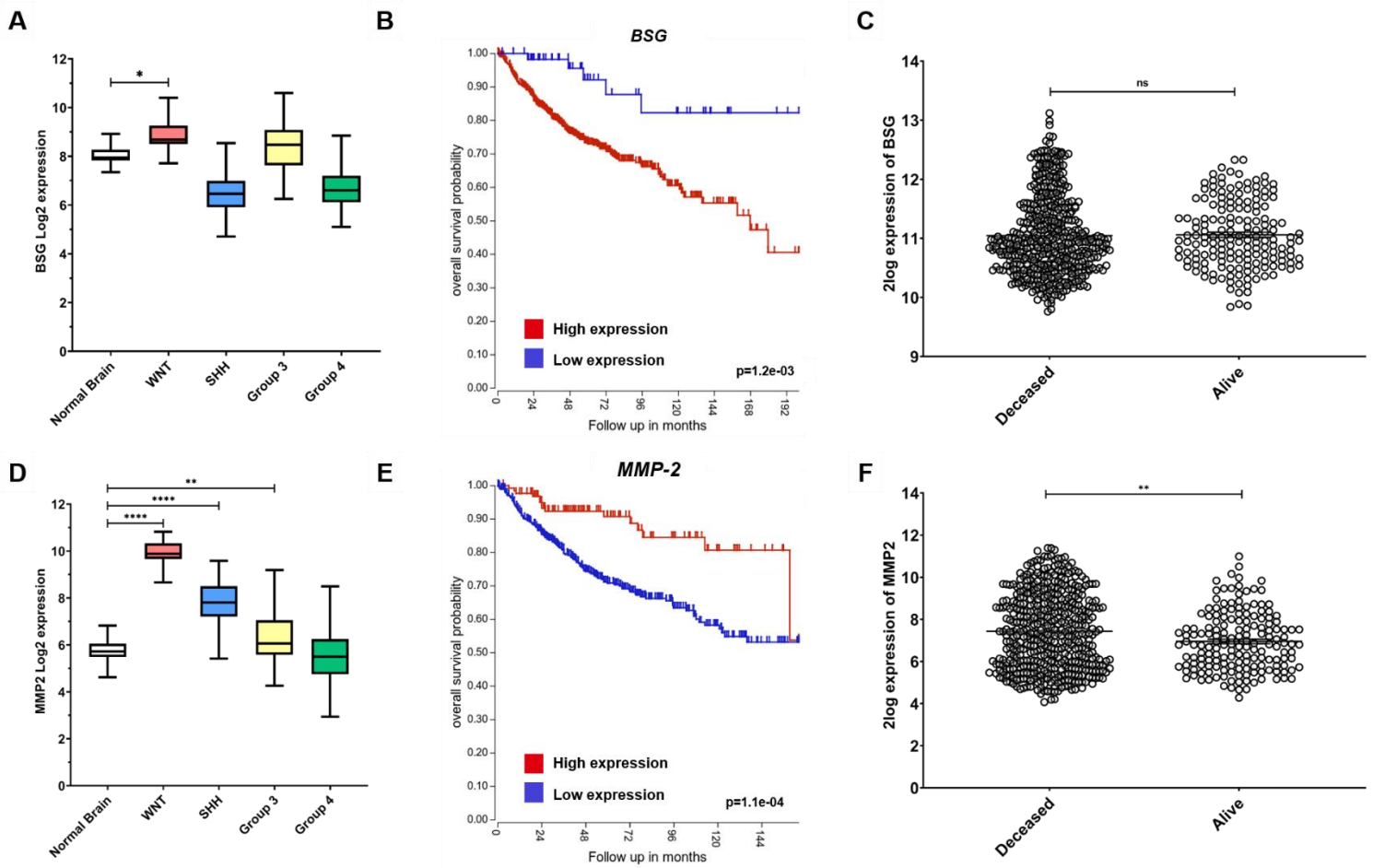

Figure 4.1 *BSG* and *MMP-2* patient gene expression and survival analysis

Gene expression (Log2) of *BSG* and *MMP-2* were assessed on the R2 Genomics Analysis and Visualisation Platform. The MegaSampler function was used to assess *BSG* (A) and *MMP-2* (D) gene expression in two datasets: Harris and Pfister. Harris consisted of normal brain samples (n=44) and served as a normal control against the medulloblastoma samples in the Pfister dataset (WNT: n=17; SHH: n=59; Group 3: n=56; Group 4: n=91). Significant differences in gene expression compared to the normal brain were calculated using the Kruskal-Wallis test with Dunn's multiple comparisons post-hoc test. **p≤0.01, ***p≤0.001, ****p≤0.0001). Kaplan-Meier plots showing overall survival of patients with medulloblastoma all subgroups was assessed for *BSG* (B) and *MMP-2* (E). Log rank test was performed to generate p values (Cavalli 763 cohort). Dot plots comparing *BSG* and *MMP-2* expression in deceased and alive patients. Significance differences was calculated using one-way ANOVA analyses with Dunnett's multiple comparisons post-hoc test, (**p≤0.01, ns=not significant).

Next, *MMP-2* and *BSG* expression levels were assessed in matched primary and metastatic tumours. The Wang dataset (Wang *et al.*, 2015) provides gene expression data from matched primary and metastatic samples from 9 patients. Due to the low sample numbers comprising this cohort, significance was not reached when comparing primary and metastatic expression. However, highest expression of both *BSG* and *MMP-2* were observed in metastatic samples (Figure 4.2 A and B). Interestingly, 7 out of 9 matched pairs displayed an increase in *BSG* mRNA expression in the metastatic tumour compared to the primary tumour (Figure 4.2C). Comparatively, 5 out of 9 matched pairs displayed an increase in *MMP-2* mRNA expression in the metastatic tumour compared to the primary tumour (Figure 4.2D).

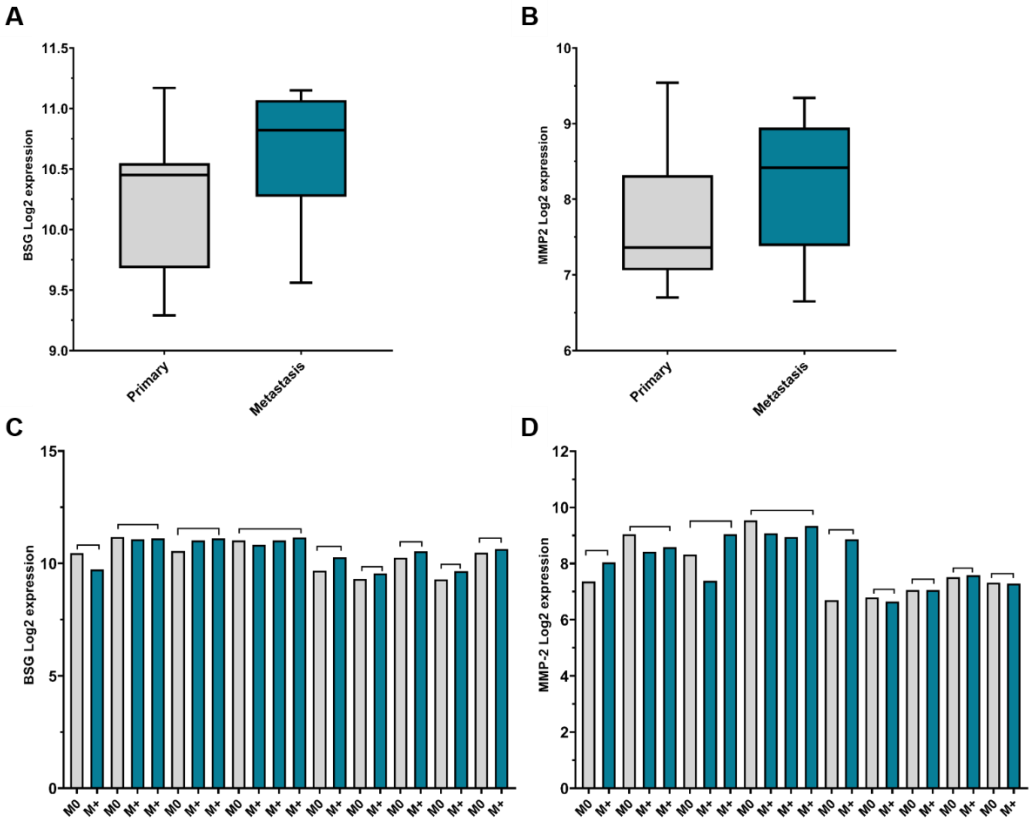

Figure 4.2 *BSG* and *MMP2* gene expression is highest in metastatic patient samples

Gene expression (Log2) of *BSG* (A) and *MMP-2* (B) in a cohort of 9-paired primary-metastatic tumours were assessed using the Wang dataset. Significance was not reached when comparing primary and metastatic expression, however highest expression of both genes were observed in metastatic samples. *BSG* (C) and *MMP-2* (D) expression was found to be frequently elevated in metastatic tumours when compared with the appropriate primary pair. M0 represents primary tumour and M+ represent metastatic. The brackets above the graph define the samples attributed to each patient. n>18.

4.1.2 Analysis of MMP-2 and EMMPRIN expression in medulloblastoma cell lines

Data obtained from the transcriptomic analysis showed *BSG* to be highly expressed across large medulloblastoma patient cohorts and suggested it represents a poor prognosis factor in medulloblastoma. In addition *MMP-2* was also shown to be highly expressed across large medulloblastoma patient cohorts and high expression was observed in paired metastatic samples. Surprisingly, high levels of *MMP-2* expression did not correlate with a worse overall survival, despite strong correlation with metastatic samples. Therefore, to further investigate *BSG* and *MMP-2* as metastatic markers of medulloblastoma, it is important to ensure that the available medulloblastoma cell lines represented an appropriate model for further study and support tentative conclusions from the R2 genomic analysis.

MMP-2 and *BSG* gene expression across a range of medulloblastoma cell lines was determined using SYBR-green real time quantitative PCR (qRT-PCR) and quantified relative to *GAPDH* expression for each cell line. At the gene level, *BSG* and *MMP-2* were found to be expressed in all medulloblastoma cell lines analysed and varied between and within the subgroups (Figure 4.3). Interestingly, expression was observed to be highest in Group 3 and Group 4 cell lines, the two subgroups commonly associated with poor prognosis and higher potential for metastatic dissemination. Both D458 and CHLA-01R were found to express significantly higher *BSG* compared to the SHH cell lines UW228-3, ONS76 and DAOY (***$p \leq 0.001$) (Figure 4.3A). Likewise, a similar pattern was also observed for *MMP-2* expression (**$p \leq 0.01$). However, there was not a consistent metastatic (M+) high, primary (M0) low pattern, as exemplified by the D283 and D425 cell lines (Figure 4.3B).

Interestingly, where pairs of cell lines derived from matched primary and metastatic tumours were available it was noted (Figure 4.3) that the expression of *BSG* was higher in both the metastatic samples; D458 and CHLA-01R were found to express significantly higher BSG compared to their primary counterparts D425 ($p \leq 0.01$) and

CHLA-01 ($p \leq 0.05$), respectively. When comparing *MMP-2* expression between the matched pairs, the most striking differential expression was observed between the Group 4 paired cell lines, with significantly higher expression being observed in the recurrent CHLA-01R cell line ($p \leq 0.01$) (Figure 4.3B). This pattern was not observed in the Group 3 paired cell lines, and no significant difference was seen between the paired primary and metastatic cell lines (Figure 4.3B).

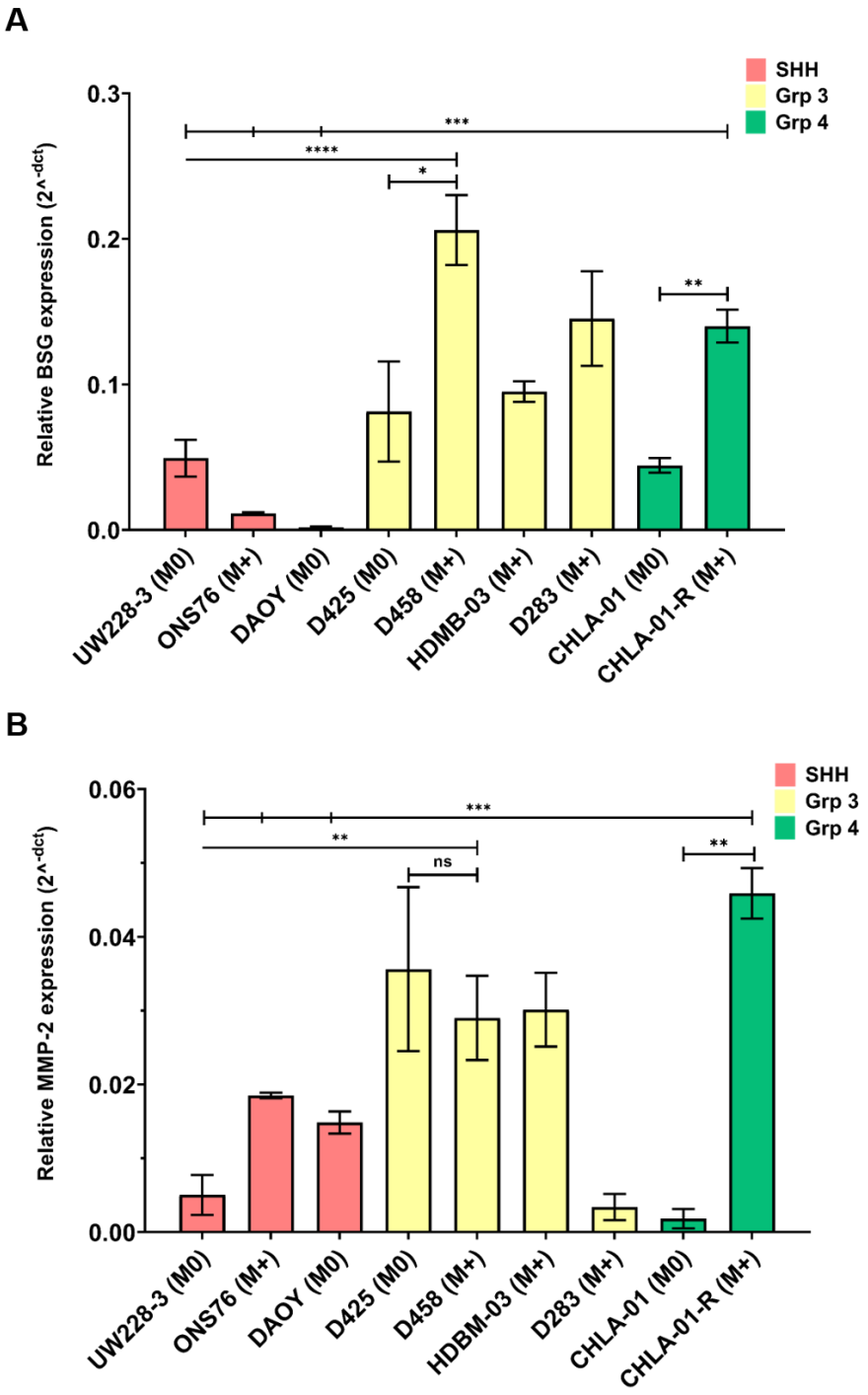

Figure 4.3 Cellular *BSG* and *MMP-2* gene expression across a panel of sub-grouped medulloblastoma cell lines

Relative *BSG* (A) and *MMP-2* (B) gene expression in a larger panel of nine medulloblastoma cell lines covering 3 of the 4 subgroups (SHH, Group 3 and Group 4) with known metastatic staging, was performed by quantitative real-time PCR. Data represent the average of three independent experiments with error bars indicating standard error of the mean (SEM). Significance differences were calculated using one-way ANOVA analyses with Tukey's multiple comparisons post-hoc test, (**p≤0.01, ***p≤0.005, ***p≤0.001). Significant differences in gene expression between matched cell lines (D425 and D458, CHLA-01 and CHLA-01R) were calculated using the Kruskal-Wallis test with Dunn's multiple comparisons post-hoc test (*p≤0.05; **p≤0.01, ns=not significant).

4.1.2.1 EMMPRIN and MMP-2 protein expression in matched medulloblastoma cell lines

The aforementioned transcriptomic analysis suggested *BSG* expression represents a poor prognosis factor in medulloblastoma and subsequent cell line data showed *BSG* levels to be differentially enriched in matched metastatic cell lines compared to primary cell lines. At the gene level, EMMPRIN may therefore represent a strong candidate biomarker for medulloblastoma progression; we aimed to assess whether these findings would also stand true at a protein level.

Aside from EMMPRIN being highly expressed on the surface of various tumour types, a significant biochemical property of EMMPRIN is that it can appear as diverse glycosylated forms, with large variation in molecular weights. Unglycosylated EMMPRIN has a molecular weight of ~32 kDa, whereas the glycosylated form has a molecular weight of ~40-60 kDa. Previous research has suggested that differentiated glycosylation of EMMPRIN exhibits functional relevance in tumour cells. It has been demonstrated that the highly-glycosylated form of EMMPRIN rather than its less glycosylated form is associated with enhancing cell adhesion, cell migration and MMP-1 and MMP-2 production (Sun and Hemler, 2001). We therefore aimed to identify the expression patterns and glycosylation forms of EMMPRIN in our matched medulloblastoma cell lines.

EMMPRIN protein expression across the matched cell lines was assessed by western blot analysis (Figure 4.4). EMMPRIN protein expression was found to be significantly higher in CHLA-01R cells compared to CHLA-01 cells ($p \leq 0.01$) (Figure 4.4B). Similar results were also observed in the metastatic D458 cell lines compared to the primary D425, however significance was not reached. EMMPRIN levels of low-migratory foetal neuronal stem cells (FB83) were also analysed, showing the lowest levels of EMMPRIN compared to all cell lines analysed. Analysis of the protein size revealed that metastatic CHLA-01R and D458 cell lines were significantly enriched with highly glycosylated EMMPRIN compared to the low glycosylation variant of EMMPRIN

(Figure 4.4C). In contrast primary D425 and FB83 cell lines were distinguished by the low glycosylation variant of EMMPRIN, with FB83 cell lines expressing no traceable levels of the high glycosylation variant of EMMPRIN. Surprisingly, the primary cell line CHLA-01 was enriched for the high glycosylated form of EMMPRIN and displayed low levels of the low glycosylation variant of EMMPRIN (Figure 4.4C).

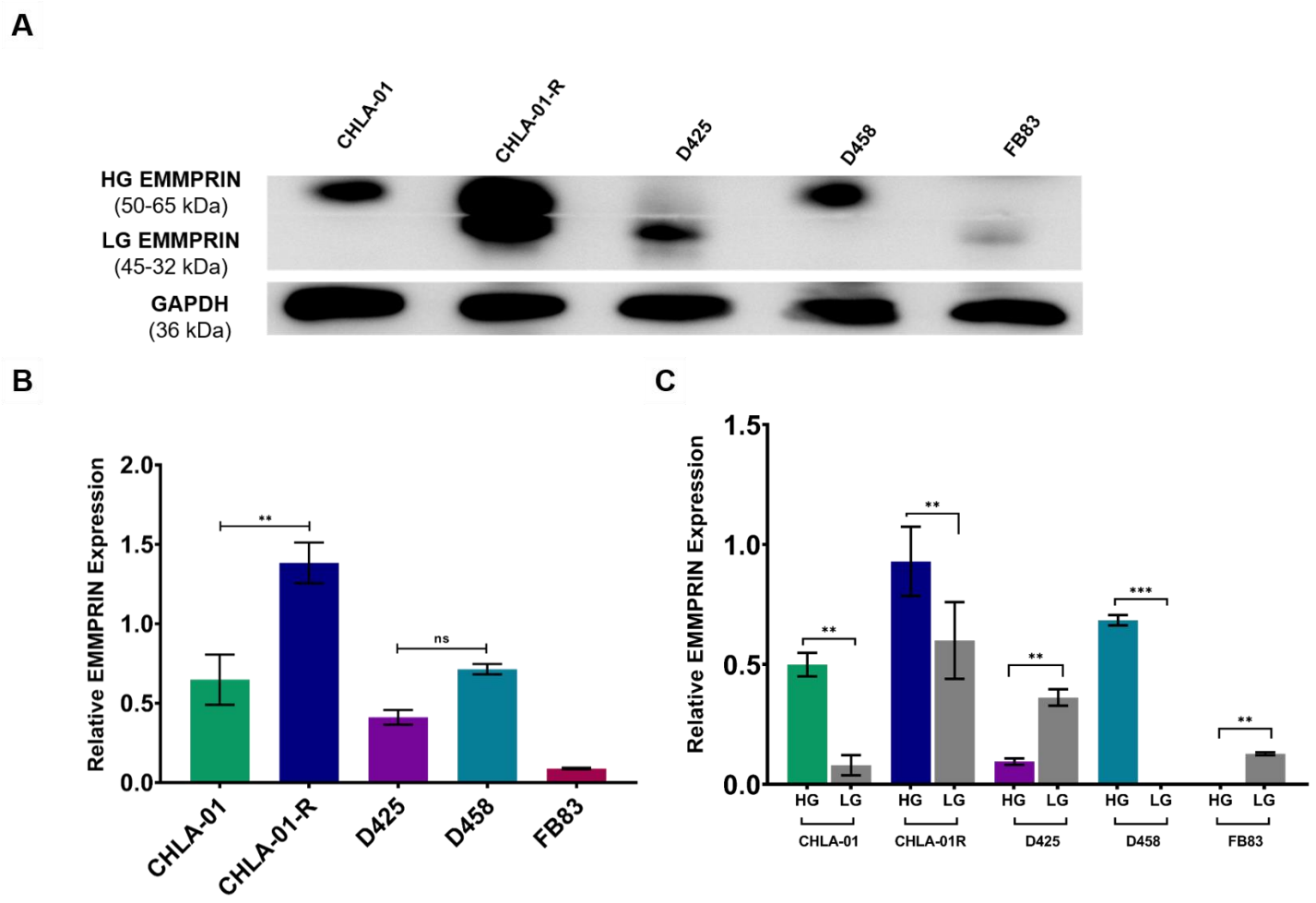

Figure 4.4 Cellular EMMPRIN protein expression correlates with metastatic outcome of matched medulloblastoma cell lines

Relative expression ratio of EMMRPIN and representative western blots. The two pairs of cell lines from subgroups 3 (D425 and D458) and 4 (CHLA-01 and CHLA-01-R), which have a matched primary and metastatic pair from the same patient, were analysed. (A) EMMPRIN protein expression was determined by western blotting and was quantified relative to GAPDH protein expression (B). Relative levels of glycosylation variants were also assessed, high glycosylation (HG) and low glycosylation (LG) (C). Data represent the average of three independent experiments with error bars indicating standard error of the mean (SEM). Significant differences in gene expression between matched cell lines were calculated using the Kruskal-Wallis test with Dunn's multiple comparisons post-hoc test (*p≤0.05; **p≤0.01, ***p≤0.001 ns=not significant).

Differential MMP-2 protein expression in matched medulloblastoma cell lines was also assessed (Figure 4.5). As previously observed *MMP-2* gene expression did not correlate with overall survival (Figure 4.1B), and when comparing matched primary and metastatic cell lines there was not a consistent metastatic high, primary low pattern of expression (Figure 4.3B). However, this pattern was observed at the protein level. MMP-2 protein expression was found to be significantly higher in CHLA-01R cells compared to CHLA-01 cells ($p \leq 0.01$) (Figure 4.5B). In addition MMP-2 protein level was significantly higher in metastatic D458 cell lines compared to the primary D425 ($p \leq 0.05$); perhaps indicative that MMP-2 protein levels may be a more physiologically relevant marker of medulloblastoma metastasis. MMP-2 levels of low-migratory FB83 cells were also analysed, showing the lowest levels of MMP-2 compared to all cell lines analysed.

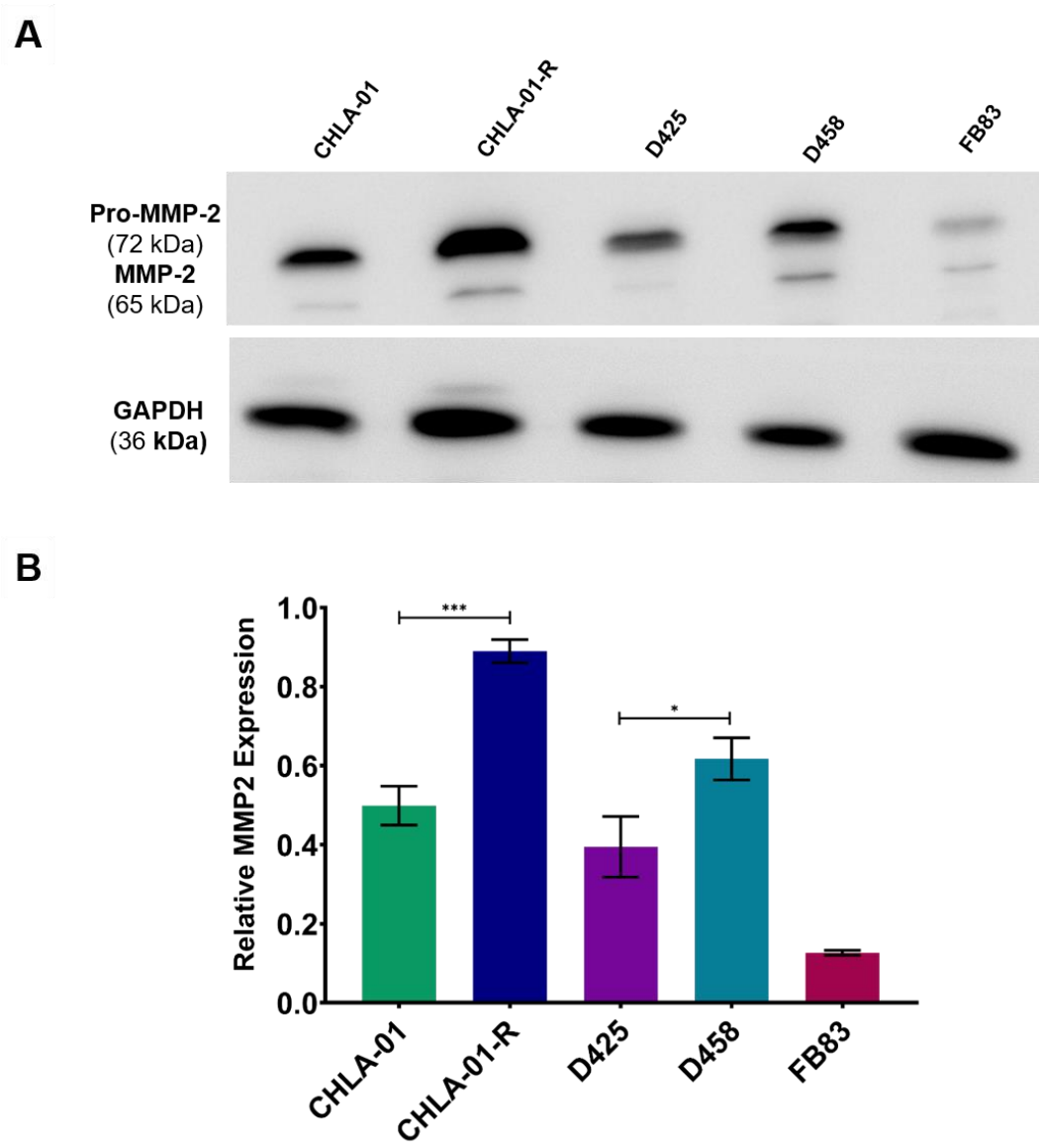

Figure 4.5 Cellular MMP-2 protein expression correlates with metastatic outcome of matched medulloblastoma cell lines

Relative expression ratio of MMP-2 and representative western blotting. The two pairs of cell lines from subgroups 3 (D425 and D458) and 4 (CHLA-01 and CHLA-01-R), which have a matched primary and metastatic pair from the same patient, were selected. (A) MMP-2 protein expression was determined by western blotting and was quantified relative to GAPDH protein expression (B). Data represent the average of three independent experiments with error bars indicating standard error of the mean (SEM). Significant differences in gene expression between matched cell lines were calculated using the Kruskal-Wallis test with Dunn's multiple comparisons post-hoc test (*p≤0.05; ***p≤0.001).

4.2 MMP-2 and EMMPRIN are abundant in pro-invasive exosomes

As shown in Chapter 3, exosomes play an important role in promoting progression of medulloblastoma cells by increasing their invasive and migratory potential. Emerging evidence suggests that tumour exosomal cargoes (protein, mRNA and miRNA) may participate in this progression. A growing number of MMPs have been detected in exosomes, which can modulate the tumour microenvironment by degradation of the ECM as an essential process for tumour dissemination. Having shown that medulloblastoma cell lines exhibit high EMMPRIN and MMP-2 levels and their expression was shown to be differentially enriched in metastatic cell lines compared to primary cell lines, we hypothesised that MMP-2 and its inducer EMMPRIN could be packaged into exosomes for extracellular release, thus contributing to medulloblastoma invasion and migration.

To elucidate the molecular differences underlying the increased invasiveness of medulloblastoma cells after exosome treatments, western blot analysis of exosomes was performed to assess whether the pro-invasive phenotype correlated with increased MMP-2 and EMMPRIN expression. Exosomes isolated from matched medulloblastoma cell lines, D458, D425, CHLA-01 and CHLA-01R, were probed for the expression of MMP-2 and EMMPRIN. Western blot analysis revealed an enrichment of EMMPRIN and MMP-2 in metastatic-derived exosomes (D458 and CHLA-01R) compared to primary-derived exosomes (D425 and CHLA-01) (Figure 4.6). Of note, analysis of EMMPRIN protein size revealed only metastatic CHLA-01R exosomes were enriched with highly glycosylated EMMPRIN compared to the low glycosylation variant of EMMPRIN. In contrast CHLA-01, D458 and D425 exosomes were distinguished by the low glycosylation variant of EMMPRIN. Alix, an established exosome marker, was used as a loading control. Taken together these findings suggest that the differential expression of MMP-2 and EMMPRIN on metastatic and

primary exosomes could explain the pro-invasive phenotype observed from metastatic-derived exosomes.

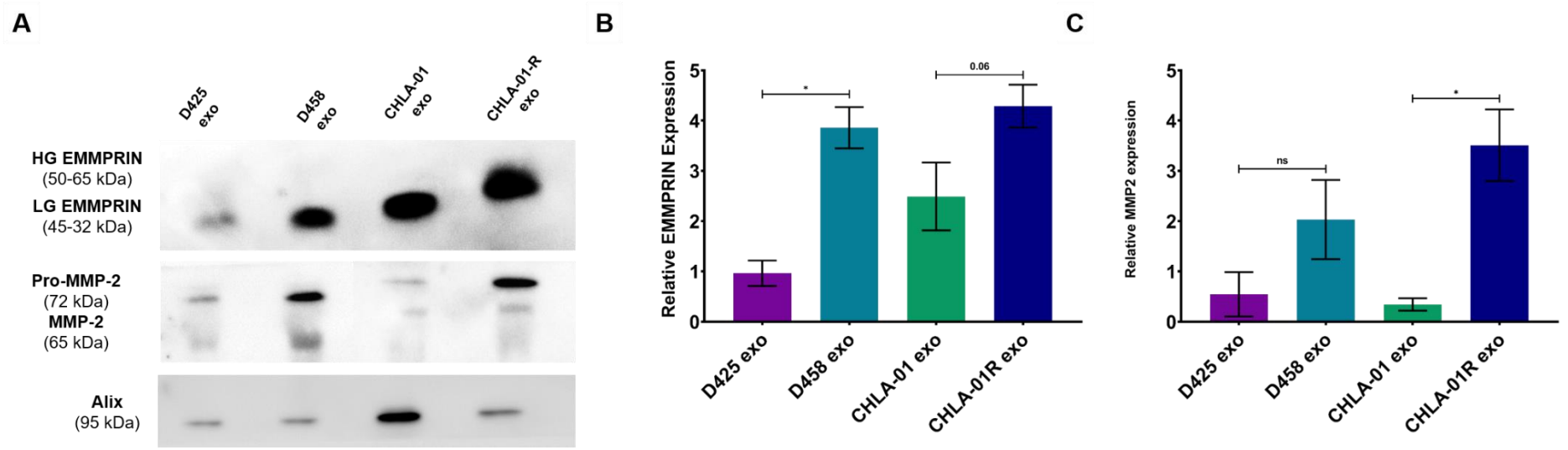

Figure 4.6 Exosomal EMMPRIN and MMP-2 protein are enriched in metastatic-derived exosomes

Relative expression ratio of EMMRPIN and MMP-2 and representative western blotting. The two pairs of cell lines from subgroups 3 (D425 and D458) and 4 (CHLA-01 and CHLA-01-R), which have a matched primary and metastatic pair from the same patient, were selected. (A) EMMPRIN protein expression was determined by western blotting and was quantified relative to Alix protein expression (B). (C) MMP-2 protein expression was determined by western blotting and was quantified relative to Alix protein expression (D). Data represent the average of three independent experiments with error bars indicating standard error of the mean (SEM). Significant differences in protein expression between exosomes derived from matched cell lines were calculated using the Kruskal-Wallis test with Dunn's multiple comparisons post-hoc test (*p≤0.05, ns=not significant).

4.2.1 MMP-2 is co-expressed with EMMPRIN on pro-invasive exosomes

Purified MMP-2 protein exogenously added to culture media in the absence of any carriers promotes cell migration (Tang *et al.*, 2004) and upregulation of EMMPRIN can promote MMP-2 secretion and subsequent cell invasion. Since pro-invasive exosomes promote cell migration and invasion, we predicted exosomes carry MMP-2 and EMMPRIN on their external surface to aid this function. To investigate this hypothesis, flow cytometry of exosomes was carried out.

Exosomes isolated from the metastatic D458 cell line clearly resolved into two populations based upon EMMPRIN expression (49.2% EMMPRIN positive compared to 50.7% EMMPRIN negative) (Figure 4.7B) whereas only a single, lower expressing population was observed in the D425-derived exosomes (1.6% EMMPRIN positive compared to 98.3% EMMPRIN negative) (Figure 4.7A). For MMP-2 expression the difference was more subtle, however again exosomes isolated from the metastatic D458 cell lines clearly resolved into two populations based upon MMP-2 expression (56.2% MMP-2 positive compared to 43.8% MMP-2 negative) and a lower population of MMP-2 expressing exosomes was observed in the D425 exosomes (38.1% MMP-2 positive compared to 61.9% MMP-2 negative) (Figure 4.7C and D). These findings reinforced our hypothesis that EMMPRIN and MMP-2 are enriched on metastatic exosomes and are involved in conveying an exosomal pro-invasive phenotype. Most importantly, we provide evidence that the majority of exosome-associated MMP-2 and EMMPRIN resides on the external surface of exosomes and may explain the increase in medulloblastoma migration after exosome treatment.

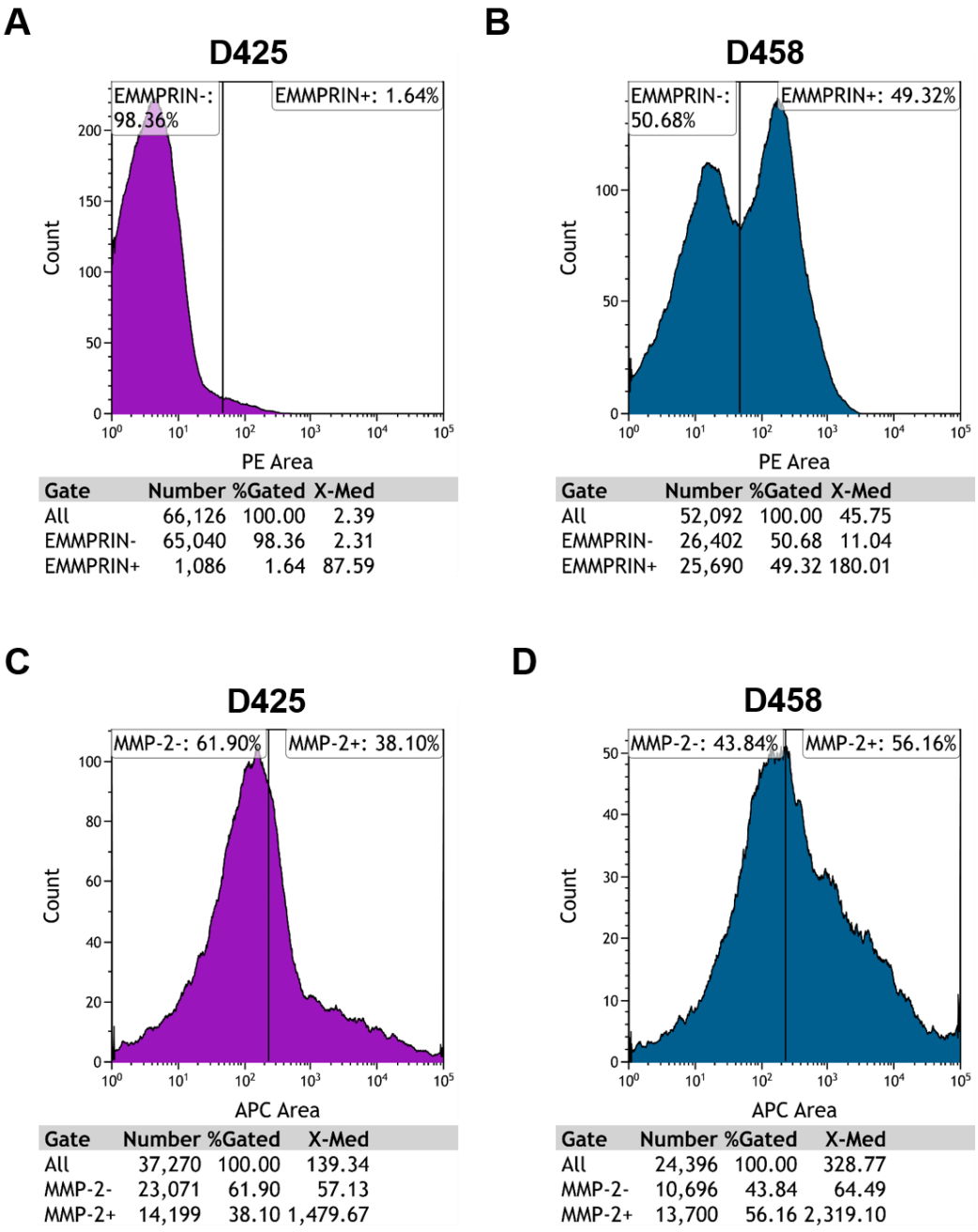

Figure 4.7 Validation of EMMPRIN and MMP-2 protein expression by flow cytometry

Flow cytometry analysis of MMP-2 and EMMPRIN protein expression in medulloblastoma-derived exosomes. Exosomes were labelled with EMMPRIN from primary D425 cell lines (A) and metastatic D458 (B). In addition D425 (C) and D458 (D) exosomes were labelled with MMP-2 One representative experiment out of two performed with similar results is shown.

To elucidate whether EMMPRIN and MMP-2 are expressed independently on exosomes, we performed double staining for EMMPRIN and MMP-2. After gating and analysis, quadrant plots were obtained in which the upper right quadrant represents exosomes expressing high levels of both EMMPRIN and MMP-2. Metastatic D458-

derived exosomes showed a co-expression of EMMPRIN and MMP-2 on 39.7% of all exosomes present, compared to D425 exosomes in which only 6.9% of all exosomes present showed a co-expression of EMMPRIN and MMP-2 (Figure 4.8).

Interestingly, primary D425 exosomes had 71.7% of exosomes expressing neither EMMPRIN nor MMP-2, whereas in metastatic D458 exosomes the percentage of "double-negative" exosomes was far lower (23.3%) (Figure 4.8).

Taken together, these results suggest that EMMPRIN can indeed be acting independently of MMP-2, however MMP-2 appears to be exclusively expressed when EMMPRIN is present on exosomes, and supporting a hypothesis that exosomal EMMPRIN might be involved in the regulation of MMP-2.

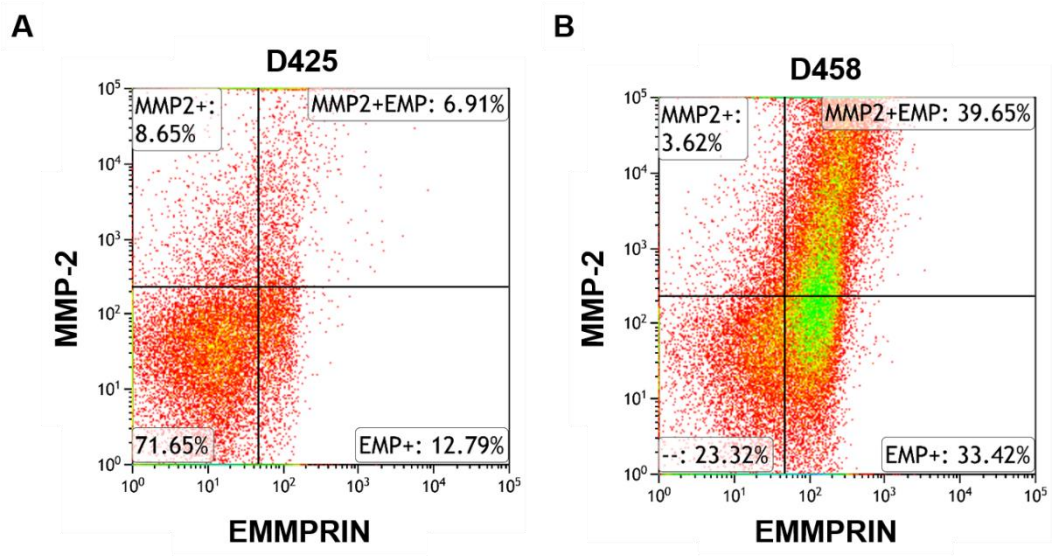

Figure 4.8 MMP-2 is co-expressed with EMMPRIN on pro-invasive exosomes

Flow cytometry analysis of MMP-2 and EMMPRIN protein expression in medulloblastoma-derived exosomes were tested. Pro-invasive exosomes, D458, double labelled with MMP-2 and EMMPRIN (A). Primary-derived exosomes, (D425) were labelled with MMP-2 and EMMPRIN (B). One representative experiment out of two performed with similar results is shown.

4.2.2 MMP-2 is functionally active on exosomes

MMPs can either be bound to the cells membrane or secreted from the cytosol into the extracellular matrix, where they function as modulators of the extracellular space (Isaacson *et al.*, 2017). MMPs are synthesised as inactive proenzymes termed zymogens which require activation prior to being functionally active. Importantly, several MMPs in exosomes have been shown to exhibit proteolytic activities, and can directly contribute to the degradation of ECM proteins in the extracellular space (reviewed by Shimoda and Khokha, 2017). We hypothesised that MMPs on exosomes may degrade the extracellular matrix more effectively, creating a path for tumour cells or exosomes to migrate in the extracellular space.

Zymography is a gel electrophoresis technique in which the levels of the zymogens (pro MMP-2) and their active forms can be detected by their enzymatic digestion of a specific substrate incorporated into the gel. As previously mentioned, MMP-2 is a gelatinase, thus gelatin was incorporated into the zymography gel. To determine whether the exosomal MMP-2 was catalytically active, exosomes suspended in PBS were loaded onto gels and the functional activity of MMP-2 was determined. The zymography assay revealed that D458, D425 and CHLA-01R exosome samples contained functional MMP-2, however MMP-2 appeared absent in primary CHLA-01 exosomes (Figure 4.9). In keeping with western blot results, metastatic-derived exosomes CHLA-01R and D458 demonstrated the highest levels of functional MMP-2 activity compared to the primary CHLA-01 and D425 exosomes (Figure 4.9). In some biological replicates, a functional related gelatinase (MMP-9) was observed but at levels close to the detection limit. The inherent differences in the functional basal levels of exosome-associated MMP-2 present in metastatic-derived exosomes compared to primary exosomes, further suggests that MMP-2 carrying exosomes promotes tumour progression.

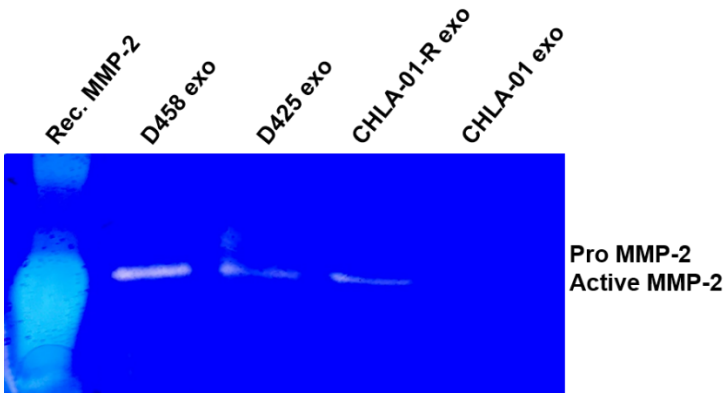

Figure 4.9 Exosomes contain functionally active MMP-2

Gelatin zymography was used for the detections of MMP-2 activity in medulloblastoma-derived exosomes. 5µg of exosomes suspended in PBS were loaded were loaded onto gelatin incorporated zymography gels and the functional activity of the gelatinase, MMP-2 was determined. Proteolysis was detected as a white band. Image representative of three independent repeats.

4.2.3 Pro-invasive exosomes from medulloblastoma cells increase MMP-2 secretion from recipient cells

Our findings on exosome associated MMP-2 and EMMPRIN motivated further evaluation of the functional impact of metastatic exosomes on the progression of primary medulloblastoma cells, and to verify whether their effect on the metastatic properties of primary cells could be attributed to the high levels of MMP-2 and EMMPRIN. Since pro-invasive exosomes were found to express EMMPRIN and MMP-2 at high levels, and the role of exosome-bound EMMPRIN for the induction of MMPs is well established (Redzic *et al.*, 2013; Hatanaka *et al.*, 2014), we investigated MMP-2 secretion by medulloblastoma cells after exosome stimulation. Gelatin zymography was therefore performed to analyse whether exosomes induced recipient cells to secrete MMP-2. CHLA-01 cells, which had very low detectable levels of MMP-2 compared matched CHLA-01R cells (Figure 4.5), were co-cultured with pro-invasive CHLA-01R exosomes for 24 hours, media was removed (removing exosomes) and fresh media was added. After 24 and 48 hours conditioned media was harvested and levels of secreted MMP-2 was assessed by zymography. After pre-conditioning with pro-invasive exosomes we found a time-dependent increase in the levels of

functionally active MMP-2 secreted into the media compared to buffer treated cells. (Figure 4.10).

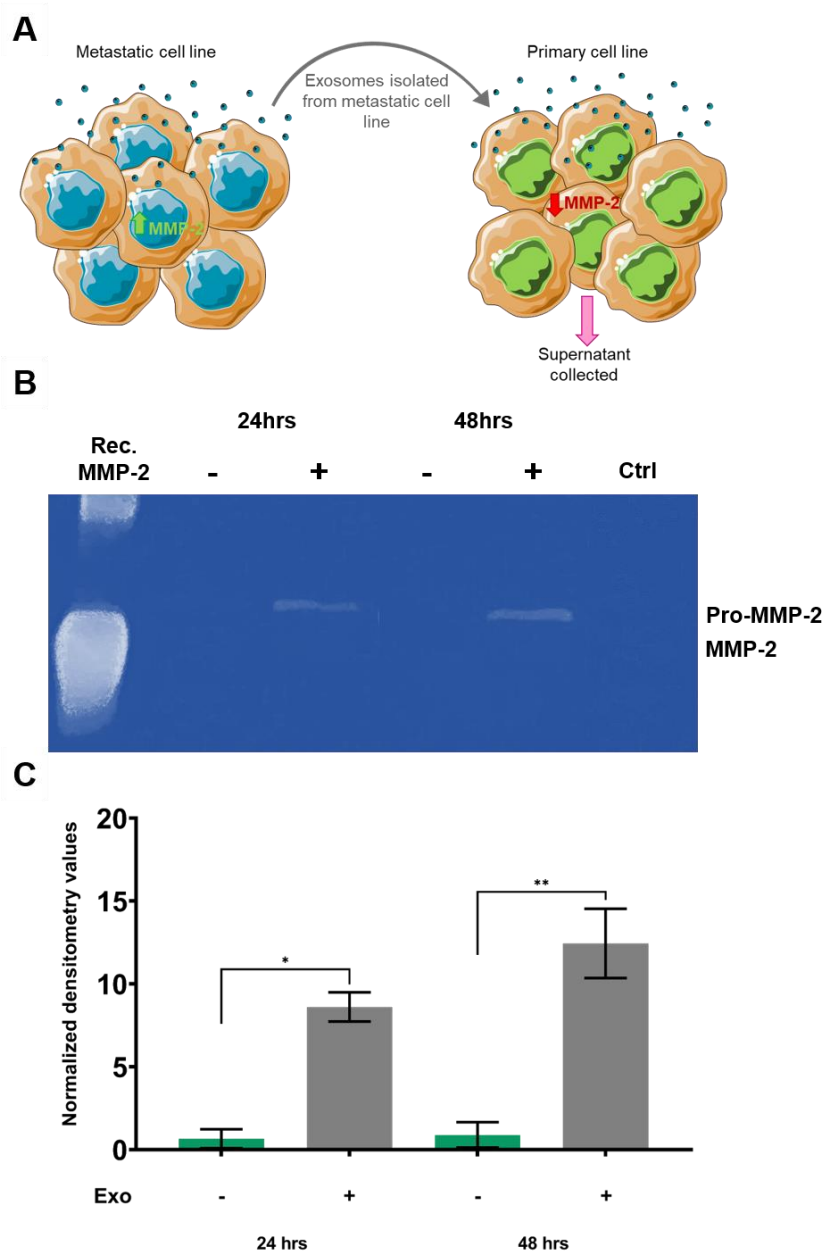

Figure 4.10 Secreted MMP levels from medulloblastoma cells after exosome stimulation

MMP-2 levels in the medium of medulloblastoma CHLA-01 cells recipient of exosomes from metastatic CHLA-01-R cells was determined by gelatin zymography. CHLA-01 cell lines were stimulated with 10 µg of metastatic (CHLA-01R) exosomes, schematic representation (A). After 24 and 48 hours supernatant was collected and loaded onto the gelatin-containing gel. Proteolysis was detected as a white band. MMP-2 levels shown in (B) were quantified and displayed graphically in (C). Data represent the average of two independent experiments with error bars indicating standard error of the mean (SEM). Significance differences was calculated using one-way ANOVA analyses with Dunnet's multiple comparisons post-hoc test, (*p≤0.05, **p≤0.01)

4.3 shRNA knockdown of EMMPRIN and MMP-2 expression

Having established that exosomes from metastatic cells are enriched with EMMPRIN and functional MMP-2, we asked if they are critical for the pro-invasive phenotype of exosomes. Therefore, we performed stable knockdowns of EMMPRIN and MMP-2 via shRNA in D458 and CHLA-01-R cells, because their exosomes showed the highest levels of endogenous MMP-2 and EMMPRIN expression and functional activity.

4.3.1 Optimisation of shRNA knockdowns in medulloblastoma cell lines

Cell lines with stable knockdown of EMMPRIN or MMP-2 were generated through shRNA-mediated gene silencing. As medulloblastoma cell lines exhibit resistance to transduction, we initially started our analysis using HEK293-T cells. The HEK293-T cell line was transduced with a GIPZ lentivirus vector with constructs containing a Turbo GFP reporter under the control of the cytomegalovirus (CMV) promoter, this allowed for visual tracking of transduction and expression. HEK293-T cells were transduced with non-targeting shRNA at a multiplicity of infection (MOI) of 0.3 and 1. Green fluorescence was observed in transduced HEK293-T cells (Figure 4.11). The transduction efficiencies in cells transduced with 0.3 and 1 MOI of non-targeting shRNA, which were calculated by counting green fluorescent cells, were 45 and 90% respectively.

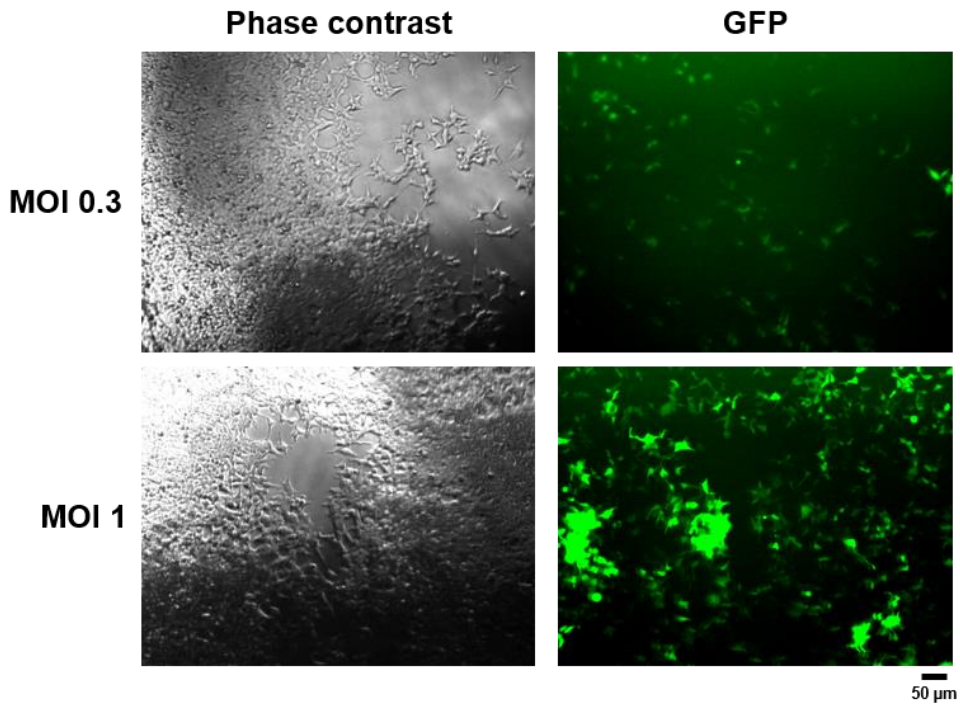

Figure 4.11 Transduction of HEK293-T cells with non-targeting shRNA

Transduction of HEK293-T cells with GIPZ lentivirus vector with constructs containing a Turbo GFP at an MOI of 0.3 and 1. Transduction efficiency of non-targeting shRNA was calculated by counting fluorescent cells.

Subsequently, D458 cells were transduced with non-targeting shRNA at an MOI of 0.5 and 1, 0.5 was selected due to the low transduction efficiency of 0.3 in HEK293-T cells. No green fluorescence was observed in D458 cells after transduction alone, therefore modifications were made to the transduction protocol to facilitate the binding of viral proteins to the receiver cell. The modifications tested included; addition of polybrene, a cationic polymer that can greatly enhance the efficiency of lentiviral infection to mammalian cells by neutralising the charge repulsion between virions and the cell surface, centrifugal inoculation (Abe *et al.,* 1998), or spinoculation, which is known to enhance viral binding and entry into target cells (O'Doherty, Swiggard and Malim, 2000), and a combination of spinoculation with polybrene treatment.

Across all three methods of transduction tested, transduction efficiency obtained varied widely (Figure 4.12). Independent of MOI used, polybrene and spinoculation only resulted in transduction efficiencies of ~2-4%. However, combining polybrene and

spinoculation led to a substantial rise in transduction efficiency, with MOI of 0.3 displaying a transduction efficiency of 40%, and the increased MOI of 1, a transduction efficiency of 80%.

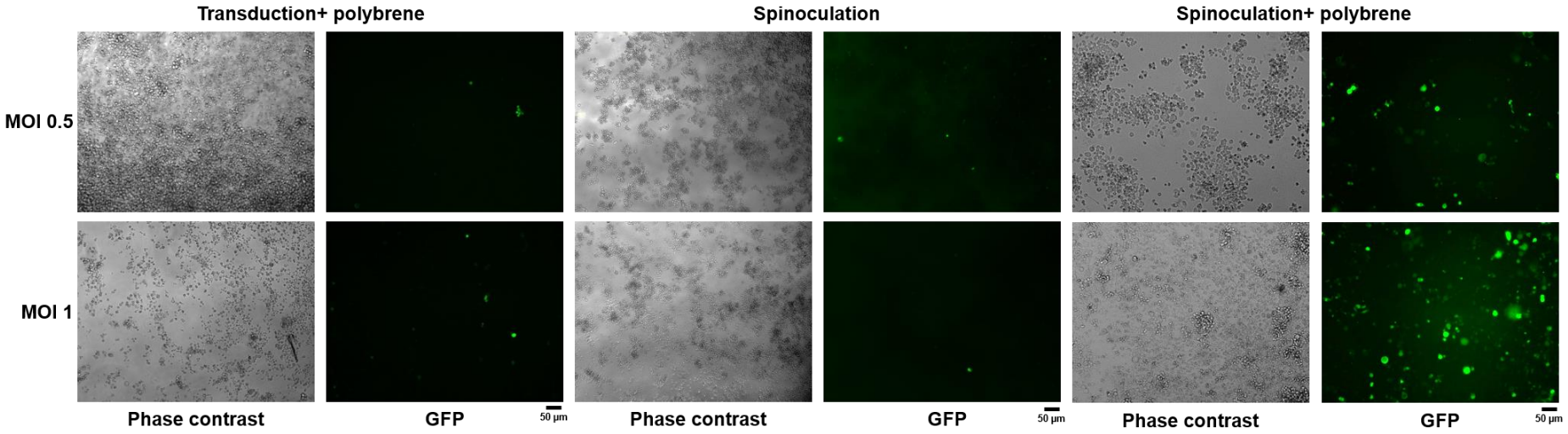

Figure 4.12 Optimisation of shRNA transduction in medulloblastoma cell line D458

Medulloblastoma cell line D458 was transduced with non-targeting shRNA control virus particles. This was done by directly adding the virus to the cell suspension in addition to polybrene (transduction +polybrene), centrifugal inoculation (spinoculation) or spinoculation with polybrene. Microscopic images obtained 4 days after initial transduction were used to calculate transduction efficiency, green fluorescent cells indicate successfully transduced cells. Representative images of an MOI of 1 are shown.

Since polybrene and spinoculation exhibited superior performance in comparison to the other methods tested, this method was used for the subsequent transduction of CHLA-01R and D458 cells. Three shRNA constructs targeting different regions of the *MMP-2* or *BSG* gene were used to create the knockdown cell lines. A non-targeting shRNA was also used to produce non-silencing control cell lines. Transduction yields obtained with different shRNA constructs (A-C for each construct) varied widely. In D458 cell lines, shMMP-2B showed the highest transduction efficiency of ~70% compared to ~30% and ~15% for shMMP-2A and shMMP-2C respectively (Figure 4.13). All BSG constructs displayed high levels of transduction efficiency ranging between 65-90%. Despite CHLA-01R cells being a fully suspension cell line which is commonly reported to exhibit poor transducibilty, all constructs tested for shMMP-2 and shBSG displayed high transduction efficiencies ranging between 60-95% (Figure 4.14). A lower MOI of 0.5 was also tested for all constructs and both cell lines (representative images not shown) resulting in lower transduction efficiency.

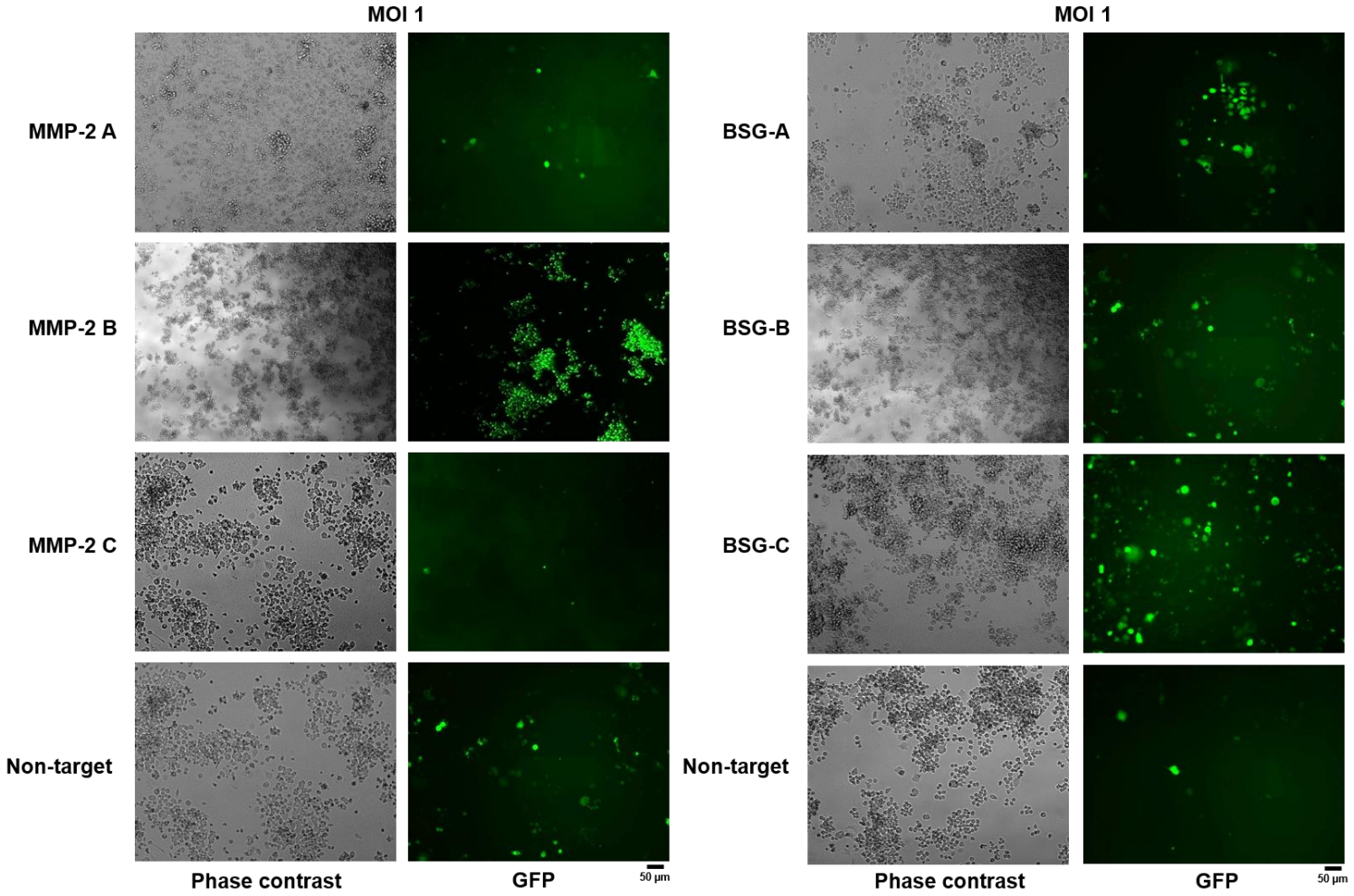

Figure 4.13 Comparison of transduction efficiencies with D458 cells

Medulloblastoma cell line D458 was transduced with three shRNA constructs targeting different regions of the *MMP-2* (left panel) or *BSG* (right panel) gene plus a non-targeting shRNA control. Microscopic images obtained 4 days after initial transduction were used to calculate transduction efficiency, green fluorescent cells indicate successfully transduced cells. Transduction yields obtained with different shRNA constructs (A-C for each construct) varied widely. Representative images of an MOI of 1 are shown.

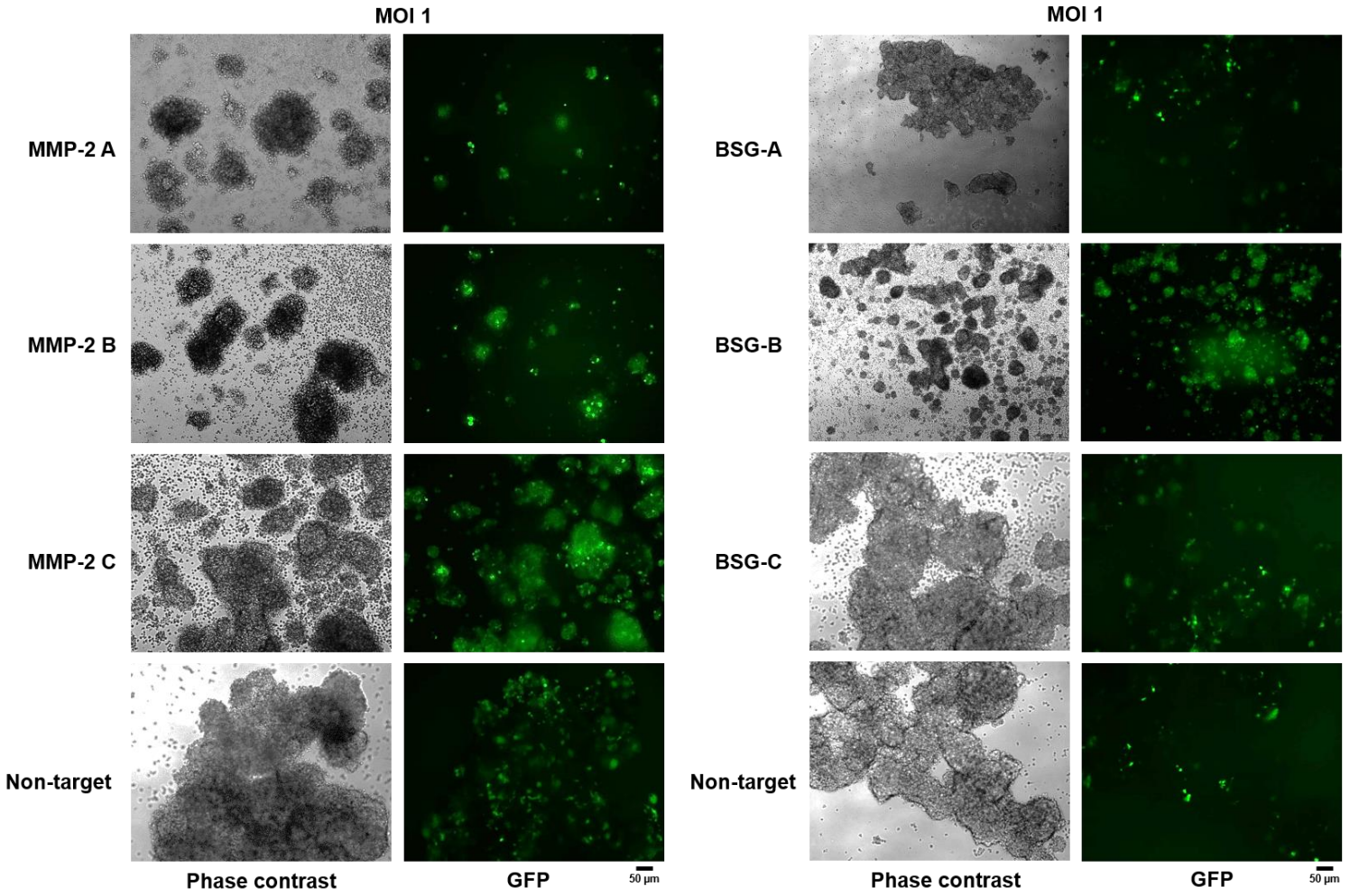

Figure 4.14 Comparison of transduction efficiencies with CHLA-01R cells

Medulloblastoma cell line CHLA-01R was transduced with three shRNA constructs targeting different regions of the *MMP-2* (left panel) or *BSG* (right panel) gene plus a non-targeting shRNA control. Microscopic images obtained 4 days after initial transduction were used to calculate transduction efficiency, green fluorescent cells indicate successfully transduced cells. Transduction yields obtained with different shRNA constructs (A-C for each construct) varied widely. Representative images of an MOI of 1 are shown.

The lentiviral vectors used also delivered puromycin resistance to transduced cells, thus enabling selection of stable cell culture after transduction. Puromycin selection was performed on transduced cells to enable elimination of remaining untransduced cells, resulting in a more homogenous cell population. Optimal dose of puromycin selection for CHLA-01R and D458 cell lines was determined by “kill curves” for each cell line (Figure 4.15), and a concentration of 1 µg/mL was selected to kill all untransfected cells.

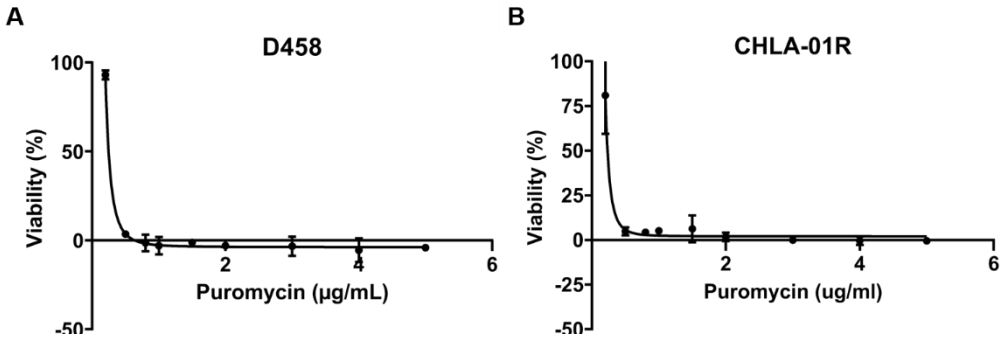

Figure 4.15 Puromycin kill curve for D458 and CHLA-01R cell lines

Kill curves representing the minimal puromycin concentration at which untransfected D458 (A) and CHLA-01R (B) we no longer viable. Viability was expressed as a percentage of surviving cells. A concentration of 1 µg/mL was selected to kill all untransfected cells. Data represent the average of three independent experiments with error bars indicating standard error of the mean (SEM). Dose response curves were generated using non-linear regression analyses

4.3.2 Efficiency of gene silencing

Experimentally, complete knockdown of a gene is difficult to achieve and often some residual expression is observed. To assess the efficiency of gene silencing and to select knockdown cell lines to be taken forward for functional analysis, the gene-knockdown effect was measured at both the transcriptional and translational level.

To validate gene-knockdown efficiency of the different shBSG and shMMP-2 constructs, mRNA and protein expression was analysed across medulloblastoma cell lines transduced with constructs A-C at an MOI of 0.5 or 1 by qRT-PCR and at an MOI of 1 for western blotting. Results were normalised to the non-targeting control. In D458

cell lines, initial mRNA results indicated that constructs shMMP-2A and shMMP-2B at MOI 1 produced the stronger silencing effect, 90% and 70% respectively, compared with shMMP-2C which displayed a knockdown efficiency of 25% (Figure 4.16A). Surprisingly, MMP-2 protein expression in D458-shMMP-2B cells (D458 cell line transduced stably with MMP-2 construct B) appeared higher than expression detected at an mRNA level and much higher expression compared to D458-shNT (D458 cell line transduced stably with non-targeting control), however GAPDH was also high in this sample (Figure 4.16B). In contrast, D458-shMMP-2A showed a marked reduction in MMP-2 protein expression compared to D458-shNT (Figure 4.16B). The silencing effect of EMMPRIN mRNA obtained with the different shRNA constructs varied widely, with D458-shBSG-A cells exhibiting reduced *BSG* expression by 75%, D458-shBSG-B by 20% and D458-shBSG-C by 80% (Figure 4.16C). At the protein level D458-shBSG-C cell line showed the greatest silencing of EMMPRIN compared to the D458-shNT control cells (Figure 4.16D).

In CHLA-01R cell lines, the silencing effect of MMP-2 mRNA by constructs A, B and C showed a knockdown efficiency of 90, 50 and 30% respectively (Figure 4.17A). At a translational level, successful protein knockdown of MMP-2 was achieved in CHLA-01R-shMMP-2A and CHLA-01R-shMMP-2B cells when compared to the CHLA-01R-shNT control, with a slightly greater knockdown being achieved in CHLA-01R-shMMP-2A cells (Figure 4.17B). All constructs were effective at silencing EMMPRIN mRNA expression independent of MOI tested (Figure 4.17C). Only cell lines CHLA-01R-shBSG-B and CHLA-01R-shBSG-C were tested for the effective knockdown of EMMPRIN protein expression, due to the successful results of these constructs observed in D458 cells. Successful protein knockdown of EMMPRIN was observed in cell lines CHLA-01R-shBSG-B and CHLA-01R-shBSG-C when compared to the CHLA-01R-shNT control, with a slightly greater knockdown being achieved by construct C (Figure 4.17D).

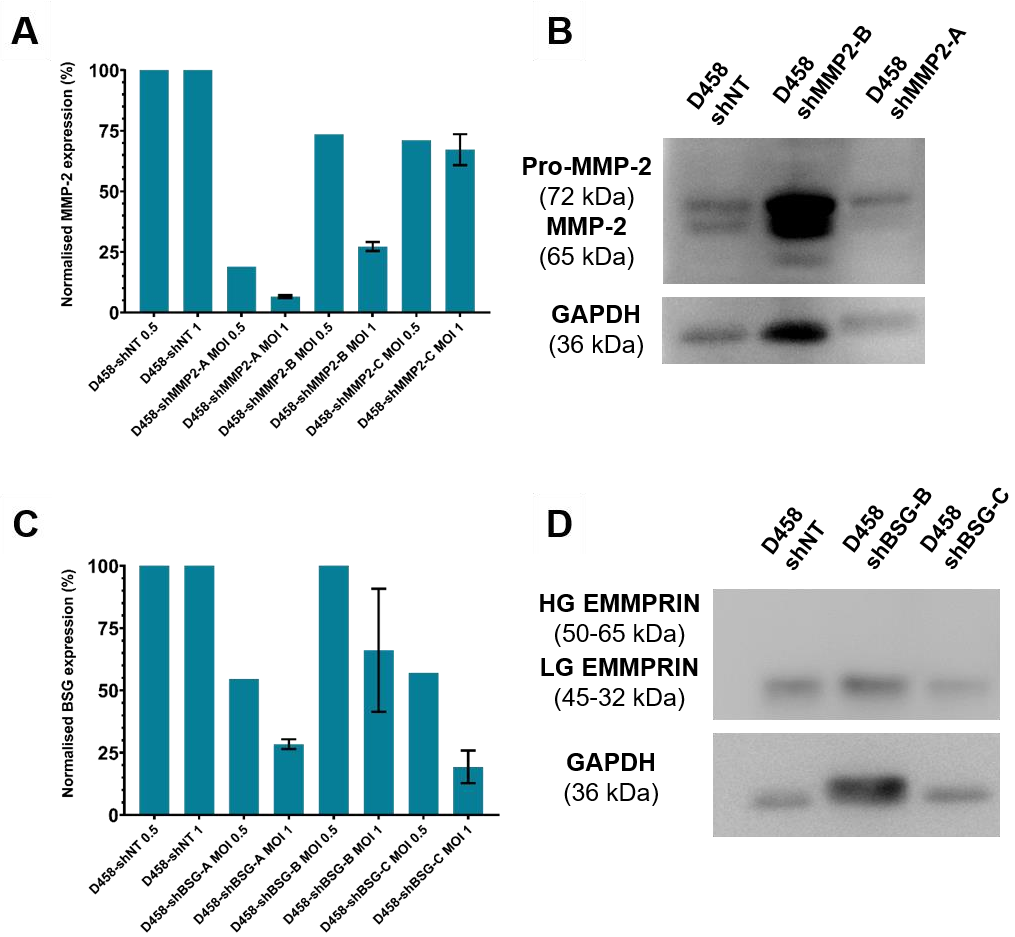

Figure 4.16 Knockdown efficiency of *MMP-2* and *BSG* constructs in D458 cells

The knockdown efficiency of three different shRNA constructs targeting *MMP-2* in medulloblastoma cell line D458 was analysed by qRT-PCR (A) and western blot (B) respectively. In addition, knockdown efficiency of three different shRNA constructs targeting *BSG* was also analysed by qRT-PCR (C) and western blot (D) respectively. GAPDH gene was used as an internal control. Results normalised to non-targeting control cell lines. Data represent the average of at least two independent experiments with error bars indicating standard error of the mean (SEM).

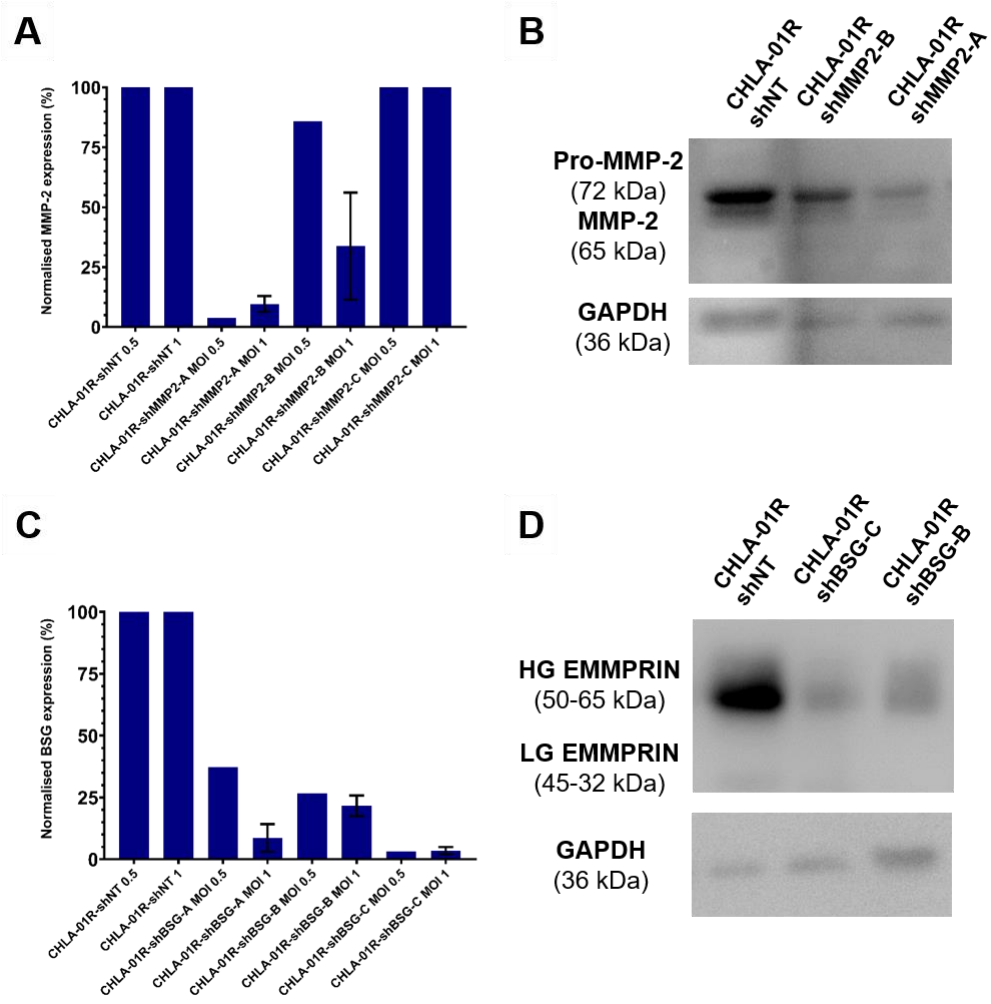

Figure 4.17 Knockdown efficiency of *MMP-2* and *BSG* clones in CHLA-01R cells

The knockdown efficiency of three different shRNA clones targeting *MMP-2* in medulloblastoma cell line CHLA-01R was analysed by qRT-PCR (A) and Western blot (B) respectively. In addition knockdown efficiency of three different shRNA clones targeting *BSG* was also analysed by qRT-PCR (C) and Western blot (D) respectively. GAPDH gene was used as an internal control. Results normalised to non-targeting control cell lines. Data represent the average of at least two independent experiments with error bars indicating standard error of the mean (SEM).

4.3.3 Validation of stable silencing of MMP-2 and EMMPRIN

After initial gene-knockdown validation, it was evident that constructs MMP-2A and BSG-C produced stronger silencing effects in both CHLA-01R and D458 cell lines at both the mRNA and protein expression levels (Figure 4.16 and Figure 4.17). For downstream experiments it is essential that the knockdown of expression is stable. To validate stable silencing using these constructs we analysed the mRNA and protein expression of MMP-2 and EMMPRIN in knockdown CHLA-01R and D458 cell lines over several passages. Figure 4.18A shows a significant reduction in gene expression of *MMP-2* and *BSG* in knockdown CHLA-01R and D458 cell lines compared to non-targeting control cell lines. Consistently decreased levels of MMP-2 and EMMPRIN were also detected at the translational level by western blot analysis, confirming stable knockdown of the candidate genes (Figure 4.18B). In addition, we also analysed MMP-2 secretion and activity in conditioned media from non-targeting control cell lines and D458-shMMP-2 and CHLA-01R-shMMP-2 knockdown cell lines by gelatin zymography. Results indicate that the overall amount of MMP-2 is clearly reduced in the medium of knockdown MMP-2 cells compared with non-targeting controls for both CHLA-01R and D458 cell lines (Figure 4.18).

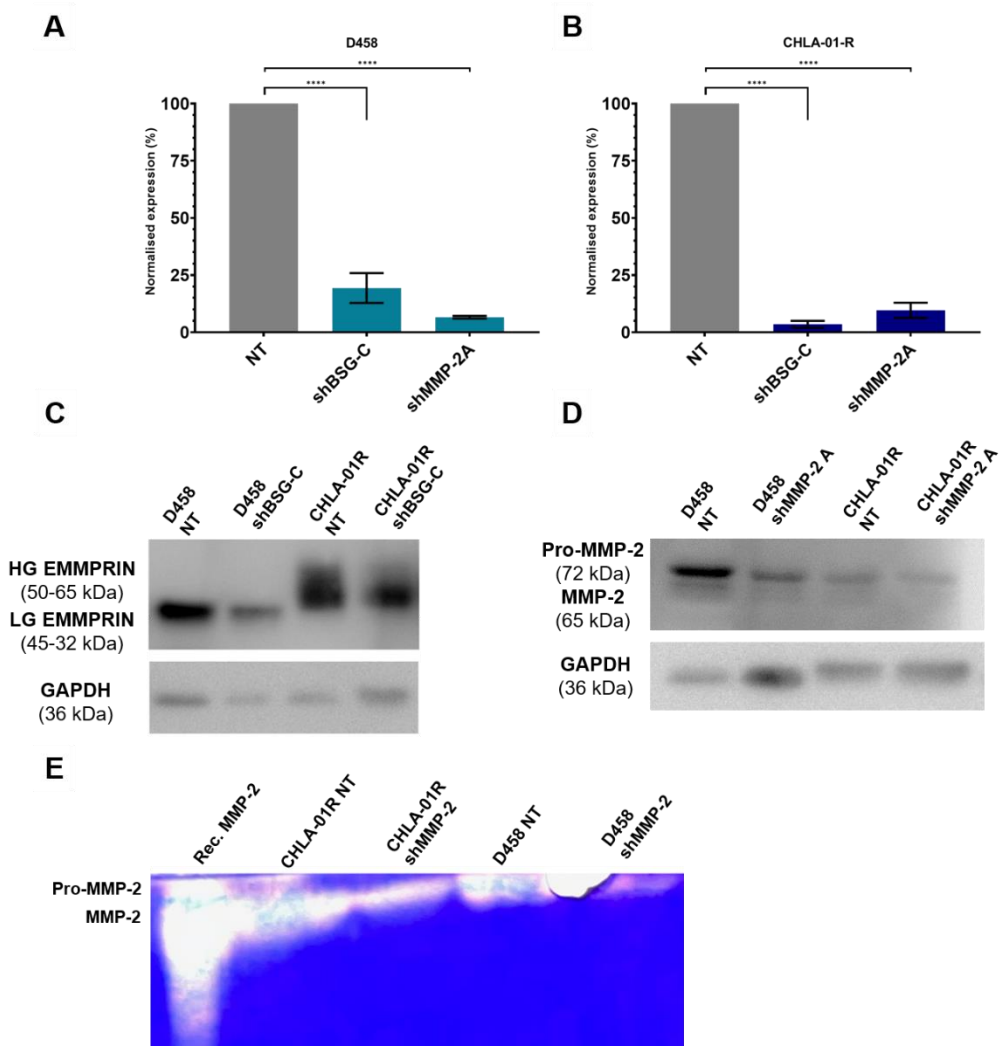

Figure 4.18 Validation of stable silencing of MMP-2 and EMMPRIN gene in medulloblastoma cell lines

Validation of stable knockdown of lentivirus mediated shRNA targeting MMP-2 and EMMPRIN in medulloblastoma cell lines. qRT-PCR analysis of knockdown efficiency in D458 cells (A) and CHLA-01R cells (B) over several successive passages. GAPDH was used as an internal control. Data represent the average of three independent experiments with error bars indicating standard error of the mean (SEM). Significance differences was calculated using one-way ANOVA analyses with Dunnet's multiple comparisons post-hoc test, (****p≤0.001), compared to non-targeting control transduced cell lines (NT). Western blot analysis of EMMPRIN (C) and MMP-2 (D) knockdown efficiency in D458 and CHLA-01R. GAPDH protein was used as an internal control. Data represent one of two independent experiments with similar results. MMP-2 levels in the medium of medulloblastoma CHLA-01R and D458 cell lines after knockdown was determined by gelatin zymography (E). Conditioned media from non-targeting control cells and MMP-2 knockdown cells was collected and loaded onto the gelatin-containing gel. Proteolysis was detected as a white band. Data represent one of two independent experiments with similar results.

4.3.4 Genetic disruption of *BSG* reduces expression of *MMP-2*

As originally reported, EMMPRIN induces the production of MMPs in order to assist tumour invasion and migration (Chandru, Sharada and Manjunath, 2007; Zhu *et al.*, 2012; Huang *et al.*, 2014). It also stimulates the expression of MMPs in a number of cell culture systems (Guo *et al.*, 1997; Caudroy *et al.*, 2002). This prompted us to evaluate the relationship between EMMPRIN and MMP-2 expression in shRNA-treated medulloblastoma cell lines. Using qRT-PCR we investigated the expression of *MMP-2* after gene knockdown of *BSG*, with the assumption that knockdown of *BSG* and its encoded protein EMMPRIN would result in reduction of *MMP-2* mRNA expression in medulloblastoma cell lines. Indeed, genetic disruption of *BSG* significantly reduced the expression of MMP-2 gene expression in medulloblastoma cell lines (Figure 4.19), suggesting *BSG* is required for the production of *MMP-2*.

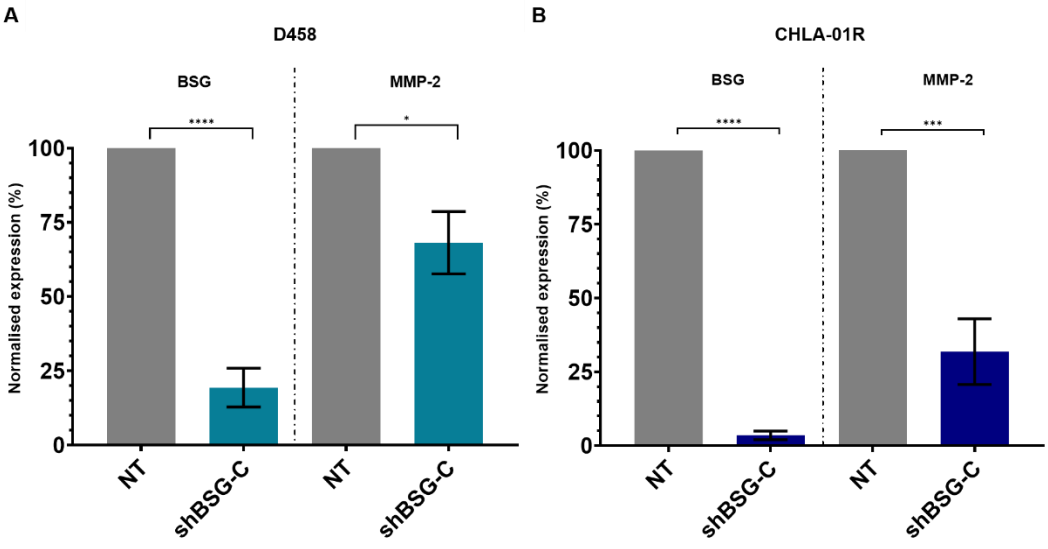

Figure 4.19 Knockdown of EMMPRIN reduces MMP-2 expression in medulloblastoma cell lines

Quantification of relative MMP-2 expression in D458 (A) and CHLA-01R (B) cells after EMMPRIN knockdown. Results normalised to non-targeting control cell lines. Data represent the average of at three independent experiments with error bars indicating standard error of the mean (SEM). Significance differences was calculated using one-way ANOVA analyses with Dunnet's multiple comparisons post-hoc test, (*p≤0.05, ***p≤0.005, ****p≤0.001), compared to non-targeting control transduced cell lines (NT).

4.3.5 Confirmation of EMMPRIN and MMP-2 knockdown in exosomes

Given the observation that exosomes from metastatic medulloblastoma cells, which contained high levels of MMP-2 and EMMPRIN, were capable of changing the phenotype of non-metastatic and benign cell lines, it was of interest to ascertain if MMP-2 and EMMPRIN secreted by/on exosomes is mediating this affect.

Firstly, isolated exosomes from either non-targeting control cells or from CHLA-01R-shBSG, D458-shBSG, CHLA-shMMP-2 and D458-shMMP-2 cell lines were subjected to NTA analysis. Of note, knockdown of *BSG* or *MMP-2* had little effect on either the distribution or the amounts of exosomes secreted by the cells. As shown in Figure 4.20 the size distribution and the concentration of the exosomes collected from knockdown or non-targeting cells were comparable. These findings suggest, knockdown of MMP-2 or EMMPRIN in medulloblastoma cells does not affect the total amount or size of exosomes secreted.

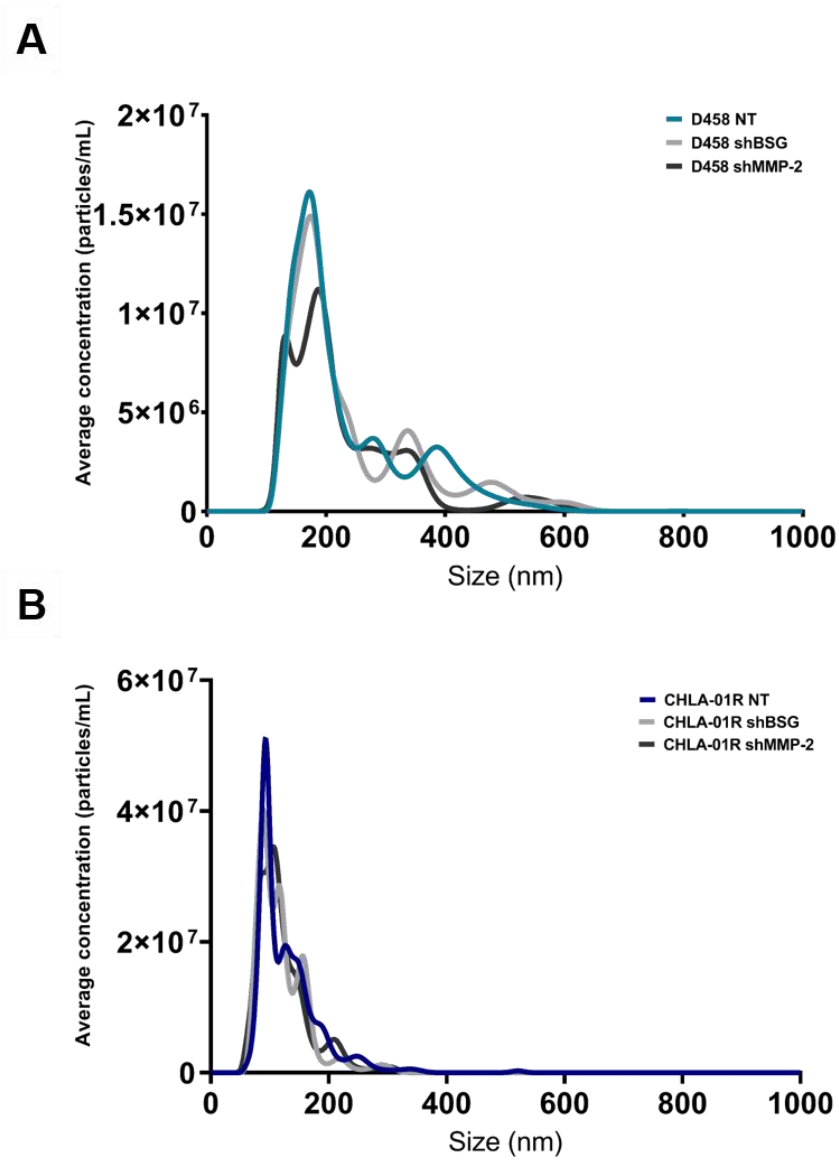

Figure 4.20 Effect of EMMPRIN and MMP-2 knockout on exosome size and secretion

Quantification and sizing of medulloblastoma exosomes using Nanoparticle tracking analysis (NTA). NTA analysis of exosomes isolated from non-targeting (NT) control cells or sh*BSG* and sh*MMP-2* cells. X-axis represents particle size and y-axis represents the mode peak size particle concentration. Five 60-second videos were recorded for each sample and analysed by the Nanoparticle Tracking Analysis 2.2 software. Data represent the average of two independent repeats.

When exosomes from equal numbers of non-targeting or knockdown cell lines were analysed by western blot, there was a significant reduction in expression of EMMPRIN and MMP-2 in exosomes derived from knockdown CHLA-01R cell lines ($p \leq 0.05$) (Figure 4.21). A slight reduction of EMMPRIN and MMP-2 was seen in exosomes derived from knockdown D458 cells however results were not significant (Figure 4.21).

Since earlier gelatin zymography experiments clearly demonstrated an increase in functional MMP-2 on the surface of metastatic exosomes, we also analysed MMP-2 functional activity in exosomes from non-targeting control cells and MMP-2 knockdown cells by gelatin zymography (Figure 4.21E). The zymography assay revealed a reduction of MMP-2 in exosomes isolated from both D458 and CHLA-01R knockdown cell lines compared to exosomes isolated from non-targeting control cells. Taken together these results suggest a significant knockdown of both MMP-2 and EMMPRIN was achieved in exosomes derived from CHLA-01R cell lines and that functional activity of MMP-2 has been reduced in knockdown D458 and CHLA-01R exosomes.

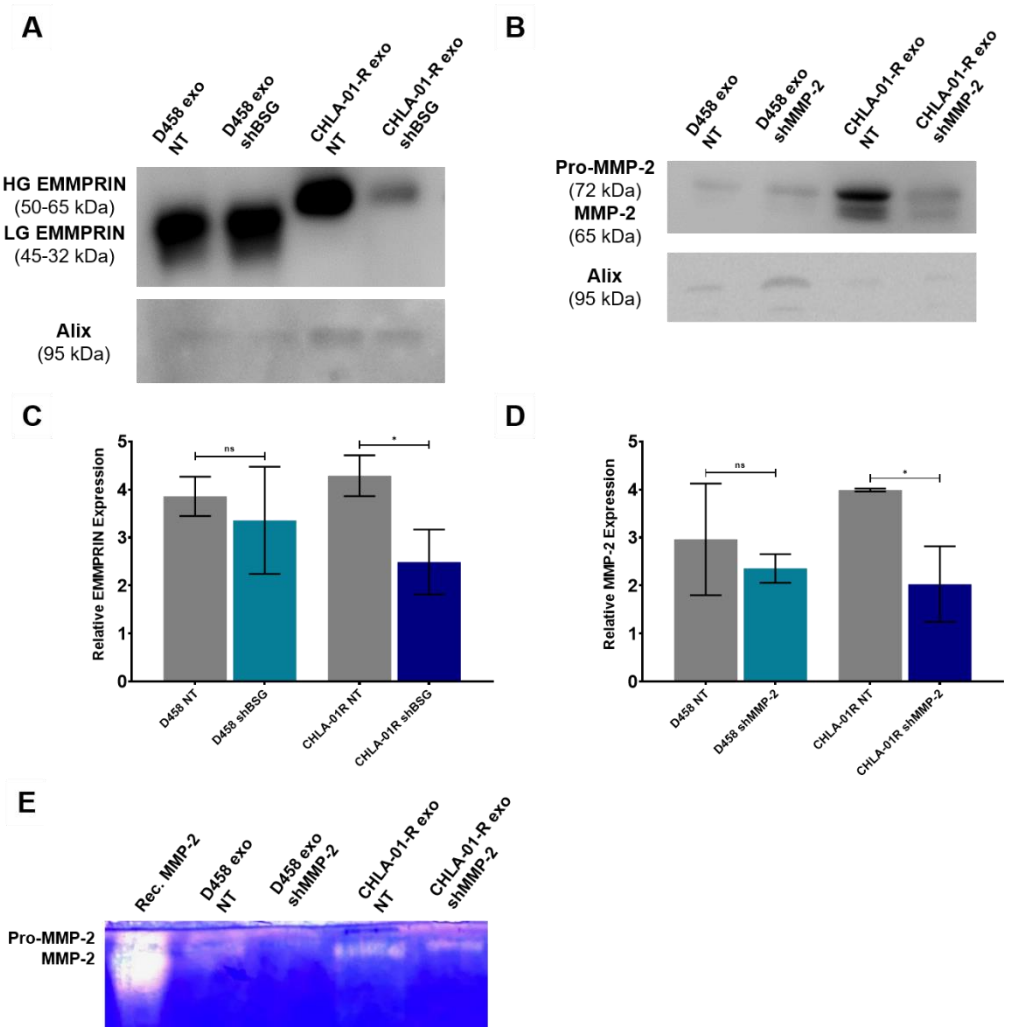

Figure 4.21 Confirmation EMMPRIN and MMP-2 knockdown in pro-invasive exosomes

Effect of EMMPRIN and MMP-2 knockout on exosome marker profile. Validation of knockdown of MMP-2 and EMMPRIN in exosomes derived from transduced CHLA-01 and D458 cell lines. Western blot analysis of exosomes isolated from non-targeting control cell lines (NT), shBSG knockdown cell lines (A) or shMMP-2 knockdown cell lines. Exosomal marker Alix was used as an internal control. Data represent one of two independent experiments with similar results. EMMPRIN protein expression was quantified relative to Alix protein expression (C). MMP-2 protein expression was quantified relative to Alix protein expression (D) Significance differences was calculated using one-way ANOVA analyses with Dunnet's multiple comparisons post-hoc test, (*p≤0.05, ns=non-significant), compared to exosomes from NT control transduced cell lines. Functional MMP-2 levels on exosomes isolated from MMP-2 knockdown CHLA-01R and D458 cell lines was determined by gelatin zymography (E). Exosomes from NT control cells and MMP-2 knockdown cells were loaded onto the gelatin-containing gel. Proteolysis was detected as a white band. Data represent one of two independent experiments with similar results.

4.4 Exosomal MMP-2 increases MMP secretion of recipient cells

To investigate whether exosomal MMP-2 and EMMPRIN played a vital role in the cross-talk between cancer cells, we co-cultured primary D425 and CHLA-01 cell lines with exosomes isolated from knockdown CHLA-01R and D458 cell lines or exosomes isolated from non-targeting controls (Figure 4.22). After 24 hour exosome treatment, media was removed (removing exosomes) and fresh media was added. After a further 24 hours, conditioned media was harvested and levels of secreted MMP-2 was assessed by gelatin zymography (Figure 4.22). For both CHLA-01 and D425 cell lines pre-conditioning with exosomes isolated from non-targeting cell lines, the levels of functionally active MMP-2 secreted into the media was increased compared to PBS buffer treated cells, although for D425 this did not reach significance (Figure 4.22B). In comparison, exosomes from CHLA-shMMP-2 and D458-shMMP-2 knockdown cell lines did not increase the levels of MMP-2 secretion in primary medulloblastoma cell lines. Since EMMPRIN is known to induce MMP-2 production and secretion, we hypothesised that exosomes from EMMPRIN knockdown cell lines would not be expected to induce functional MMP-2 in recipient cells. Surprisingly, when primary medulloblastoma cell lines were pre-conditioned with exosomes isolated from CHLA-01R-shBSG and D458-shBSG cell lines, an increase in MMP-2 function was detected when compared to cells treated with non-targeting control exosomes. However, lower levels of MMP-2 were secreted from receiver cells when treated with exosomes isolated from CHLA-01R-shBSG and D458-shBSG cell lines compared to control exosomes (results were non-significant) (Figure 4.22B). Furthermore, we did not detect the increase of *MMP-2* mRNA expression in primary medulloblastoma cells treated with exosomes from non-targeting shRNA transfected control cells or in cells treated with exosomes from CHLA-shMMP-2 and D458-shMMP-2 knockdown cell lines (Figure 4.23). Together, these results demonstrate that exosomal EMMPRIN can itself initiate some MMP-2 secretion on target cells, however it appears that exosomal MMP-2 creates a positive-forward feedback loop to initiate more MMP-2 secretion in recipient

medulloblastoma cells. Increased levels of secreted MMP-2 would support extracellular matrix degradation, in turn facilitating tumour cell invasion and metastasis.

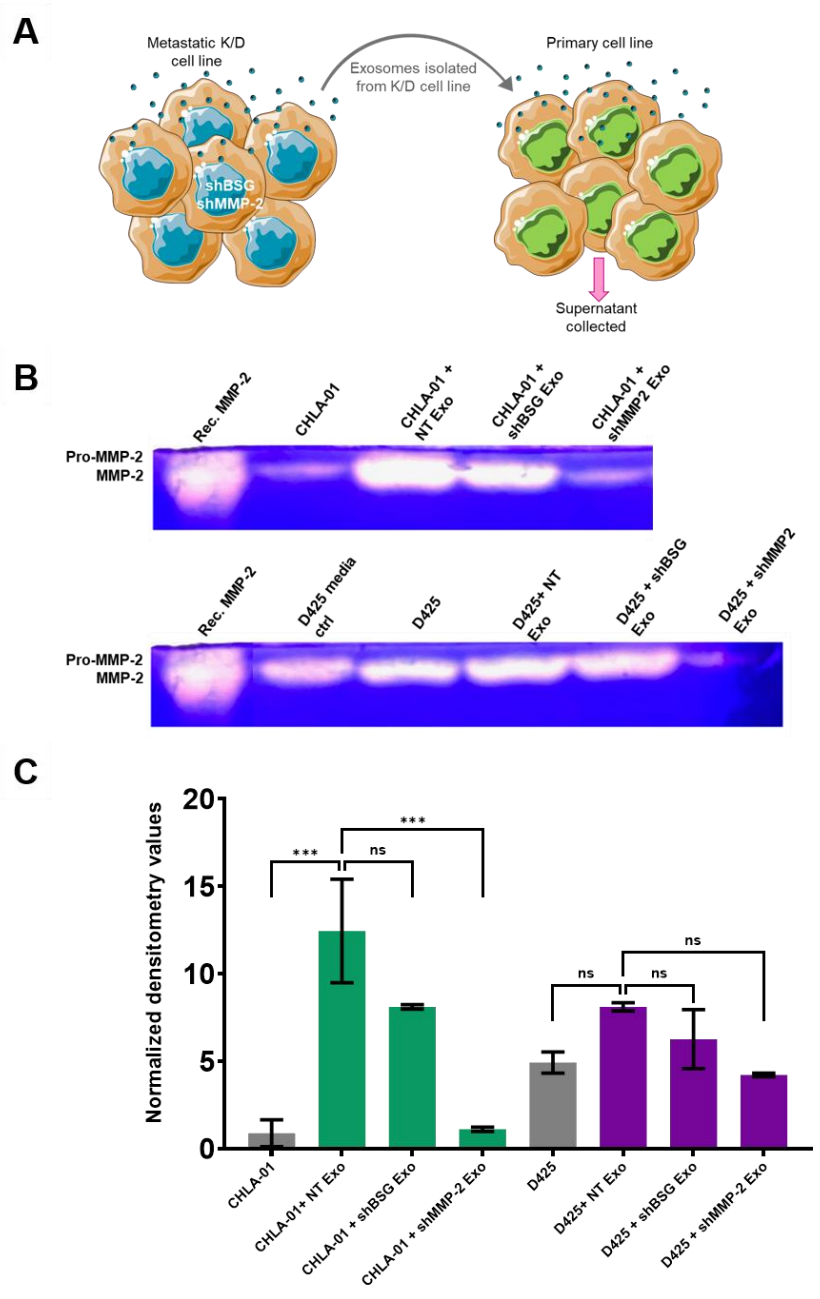

Figure 4.22 Gelatin zymography of conditioned media from cells treated with control or knockdown exosomes

Schematic representation of exosomes isolated from metastatic knockdown cell lines co-cultured with primary medulloblastoma cell lines (A). MMP-2 levels in the medium of CHLA-01 (top image) and D425 (bottom image) cells recipient of exosomes from non-targeting control (+NT exo), knockdown *BSG* (shBSG exo) or knockdown *MMP-2* (shMMP-2 exo) was determined by gelatin zymography. Proteolysis was detected as a white band. MMP-2 levels shown in (B) were quantified and displayed graphically in (C). Significance differences was calculated using one-way ANOVA analyses with Dunnet's multiple comparisons post-hoc test, (***p≤0.005, ns=non-significant), compared to non-targeting control transduced cell lines (NT).

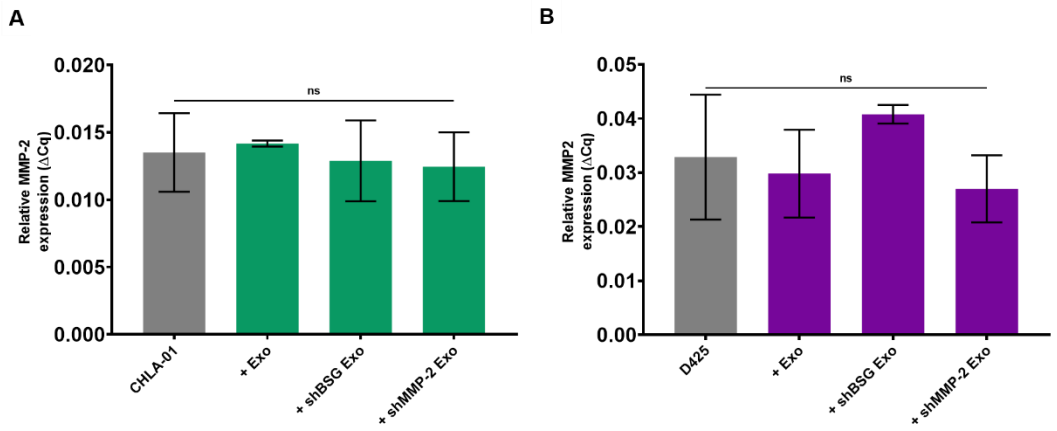

Figure 4.23 No detectable increase in MMP-2 mRNA expression after exosome treatment

MMP-2 mRNA expression levels in CHLA-01 (A) and D425 (B) cells recipient of exosomes from non-targeting control (+exo), knockdown BSG (+shBSG exo) or knockdown MMP-2 (+shMMP-2 exo) was determined by qRT-PCR. Significance differences were calculated using one-way ANOVA analyses with Dunnet's multiple comparisons post-hoc test, (ns=non-significant), compared to untreated control cells (grey).

4.5 Knockdown of MMP-2 and EMMPRIN appears to reduce migration and invasion in metastatic medulloblastoma cell lines

We initially tested if MMP-2 and EMMPRIN are essential for migration and invasion of metastatic medulloblastoma cell lines. Knockdown cell lines were assayed for their ability to migrate through a transwell migration assay.

Knockdown of *BSG* in D458 and CHLA-01R cell lines appeared to reduce migration and invasion compared to non-targeting control cell lines, however the difference was not significant (Figure 4.24A). Whereas, knockdown of *MMP-2* significantly reduced migration of CHLA-01R cell lines ($p \leq 0.05$) compared to control cells (Figure 4.24B). *MMP-2* knockdown also reduced migration of D458 cells compared to non-targeting control cells ($p=0.055$). Results from these experiments implicate both MMP-2 and EMMPRIN in medulloblastoma metastasis, however results regarding MMP-2 appear most convincing.

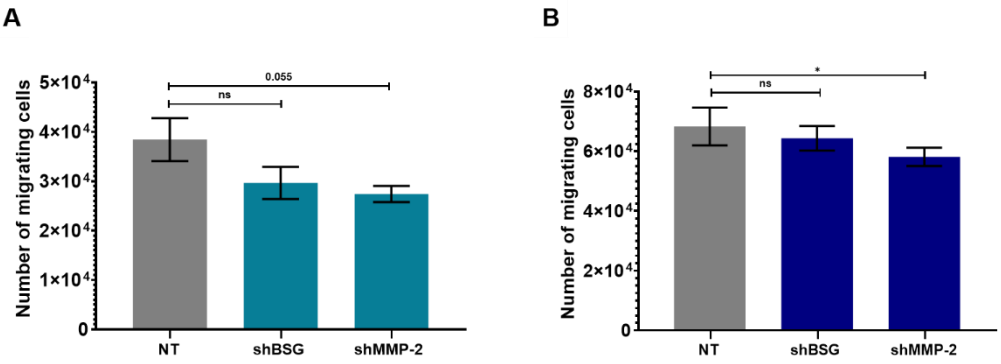

Figure 4.24 Knockdown of MMP-2 and EMMPRIN decreased migration of invasive medulloblastoma cell lines

D458 (A) or CHLA-01R (B) medulloblastoma cell lined migrated through a laminin and collagen coating in a transwell migration assay. After 24 hours cells were collected from the underside of the transwell and from the lower chamber. The number of migrated cells transduced with non-targeting (NT) control shRNA, EMMPRIN shRNA (shBSG) or MMP-2 shRNA were quantified using a metabolic activity assay. Fluorescence readings for each condition were plotted against a standard curve of known cell numbers in order to derive the exact number of migrated cells. Data represent the average of at least two independent experiments with error bars indicating standard error of the mean (SEM). Significance differences between NT controls and knockdowns were calculated using one-way ANOVA analyses with Dunnet's multiple comparisons post-hoc test, (*p≤0.05, ns=non-significant).

4.5.1 Exosomal EMMPRIN and MMP-2 play are implicated in Group 4 medulloblastoma progression

Given the observation that exosomes from metastatic medulloblastoma cell lines significantly increased migration of primary medulloblastoma cell lines (Chapter 3) and knockdown of *MMP-2* and *BSG* slightly reduced migration and invasion of medulloblastoma cell lines (Figure 4.24), it was of interest to ascertain their roles in exosome mediated migration. Primary CHLA-01 cells were co-cultured with exosomes from CHLA-01R-shNT control cells and exosomes isolated from either CHLA-01R-shBSG or CHLA-01R-shMMP-2 cell lines. In addition, primary D425 cells were co-cultured with exosomes from D458-shNT cells and from exosomes isolated from either D458-shBSG or D458-shMMP-2 cell lines. As shown in (Figure 4.25), we found a significant reduction in migration when CHLA-01 cells were pre-treated with exosomes isolated from CHLA-01R-shBSG cells (p≤0.01) and exosomes from CHLA-01R-shMMP-2 cells (p≤0.05) compared to exosomes derived from CHLA-01R-shNT cells. Group 3 D425 cells showed a similar pattern in reduction using exosomes isolated from D458-shBSG or D458-shMMP-2 cell lines compared to exosomes from D458-

shNT cells, however results were not significant. In accordance with the finding of Figure 4.24 that depletion of MMP-2 or EMMPRIN slightly reduced migration of medulloblastoma cells, these results strongly indicate that exosomal MMP-2 and EMMPRIN facilitate the progression of medulloblastoma, this is particularly apparent for Group 4 medulloblastoma.

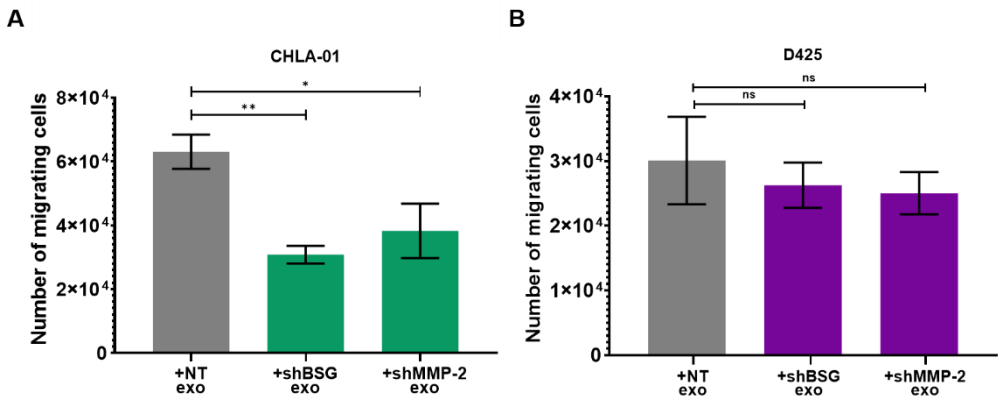

Figure 4.25 Knockdown of exosomal MMP-2 or EMMPRIN reduces pro-invasive phenotype

Exosomes derived from metastatic CHLA-01R or D458 knockdown cell lines were cultured with primary CHLA-01 or D425 cells, respectively. Pre-treated CHLA-01 (B) or D425 (C) cell lines migrated through a laminin and collagen coating in a transwell migration assay. After 24 hours cells were collected from the underside of the transwell and from the lower chamber. The number of migrated cells were quantified using a metabolic activity assay. Fluorescence readings for each condition were plotted against a standard curve of known cell numbers in order to derive the exact number of migrated cells. Data represent the average of three independent experiments with error bars indicating standard error of the mean (SEM). Significance differences between cells receiving non-targeting (+NT exo) exosomes and knockdown exosomes (+shBSG or shMMP-2 exo) were calculated using one-way ANOVA analyses with Dunnet's multiple comparisons post-hoc test, (*p≤0.05, **p≤0.05, ns=non-significant).

4.6 Summary

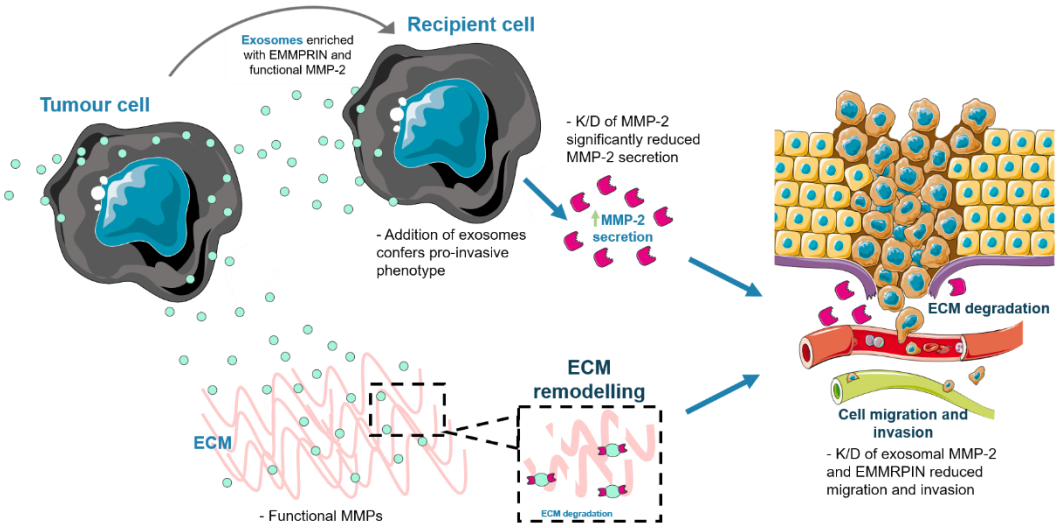

Figure 4.26 Graphical summary

Medulloblastoma-derived exosomes confer a pro-migratory phenotype to recipient cells via transfer of MMP-2 and EMMPRIN.

- Based on patient data sets and matched medulloblastoma cell line pairs, MMP-2 and EMMPRIN were identified as candidate markers of metastatic medulloblastoma.
- Notably, western blot analysis showed that highest expression of exosomal MMP-2 and EMMPRIN correlated with parental cell metastatic status. Flow cytometry analysis also revealed a similar trend, with metastatic exosomes containing more surface-bound MMP-2 and EMMPRIN compared to primary exosomes. In addition, exosomal MMP-2 co-localised with EMMPRIN.
- EMMPRIN and MMP-2 knockdown in metastatic D458 and CHLA-01R cells resulted in a large decrease in EMMPRIN and MMP-2 in exosomes relative to control.
- We found that MMP-2, and to a lesser extent EMMPRIN, in medulloblastoma exosomes played a role in increasing MMP-2 activity in recipient cells, which could be blocked by MMP-2 knockdown, suggesting that exosomes stimulate MMP-2 secretion to the microenvironment to promote medulloblastoma cell invasion and migration.

- We also found that exosomes from metastatic medulloblastoma cell lines increase the migratory phenotype of recipient primary cells, which was blocked by MMP-2 or EMMPRIN knockdown.

Chapter 5

Identifying exosomal mRNAs involved in medulloblastoma progression using next-generation sequencing technologies

Chapter 5. Identifying exosomal mRNAs involved in medulloblastoma progression using next-generation sequencing technologies

5.1 Introduction

Exosomes are shed by cells under both normal and pathological conditions. They contain abundant nucleic acids and proteins from their host cells and are indicative of pathological conditions. Single- and double-stranded genomic DNA as well as mitochondrial DNA has been described to be present, and transcriptomic analyses have catalogued both protein-coding messenger RNA and non-coding-RNAs packaged within exosomes (Théry *et al.*, 2018). In addition, exosomal messenger RNAs (mRNAs) can be translated into proteins once brought into recipient cells, indicating that exosomal mRNAs play a regulatory role in non-cell autonomous signalling (Al-Nedawi *et al.*, 2008). Stabilized within RNA-protein complexes and shielded by a lipid bilayer, exosomal RNAs represent a promising source of diagnostic and prognostic biomarkers for human diseases. Furthermore, exosomes can be isolated from easily attainable biofluids such as blood, CSF and urine, making them attractive targets for diagnostic application (Raposo and Stoorvogel, 2013). There are currently no available biomarkers for medulloblastoma progression, thus the development of early detection strategies for medulloblastoma tumours is essential. Ideal approaches should involve minimally invasive procedures with high sensitivity (Ilyin, Belkowski and Plata-Salamán, 2004). The aim of this chapter was to identify potential exosomal mRNA biomarkers and understand their role in medulloblastoma tumourigenesis by comparing exosomes secreted by a cell line derived from the primary tumour (primary exosomes) to exosomes secreted by a cell line derived from the metastatic tumour (metastatic exosomes) from the same patient. We hypothesized that distinct RNA profiles would be apparent between primary and metastatic exosomes.

5.2 NGS of medulloblastoma-derived exosomes using 3' UPX sequencing

In order to compare differences in exosomal RNA cargo between metastatic- and primary-derived exosomes, exosomal RNA was analysed by 3' QIAseq Ultraplex (UPX) sequencing. To efficiently utilise the samples, it was decided to sequence both the exosomal miRNA and mRNA. Since it was only possibly to obtain a low yield of exosomal RNA, appropriate sequencing methods had to be adopted that would allow for parallel mRNA and miRNA sequencing from the same samples. For miRNA, traditional next generation sequencing (NGS) was adopted, requiring at least 100 ng of RNA per sample. 3' UPX sequencing was used to sequence the remaining RNA. This method is suitable for low input samples and sequences the 3' end of RNA using only the polyadenylated RNAs. The RNA population is converted to a library of cDNA fragments with adaptors attached to one or both ends. These adaptors are used to sequence each cDNA from one or both ends. After sequencing, the reads are aligned to a reference genome to build a transcription map. The advantage of 3' UPX RNA-Seq is that only molecules with a poly-A tail are sequenced, facilitating downstream choices of protein targets to validate.

5.2.1 Optimising exosomal RNA isolation for NGS analyses

In order to perform NGS of medulloblastoma-derived exosomes, it was essential to extract high quality RNA for library preparation and sequencing. However, RNA isolation from exosomes proved particularly challenging due to the low yields of RNA obtained. RNA yield and quality (A_{260}/A_{280} and A_{230}/A_{260} ratios) were therefore compared for exosomal isolation using four different RNA extraction methods: mirVana (Ambion), Nucleospin RNA plus (Agilent), TRIzol (Fisher), miRNeasy micro (Qiagen). Comparisons were performed from exosomes isolated from three different medulloblastoma cell lines. RNA was successfully extracted in most cases except for one Nucleospin RNA plus extracted sample, with the other two samples giving a very low yield, suggesting that this kit may not be suitable for exosomal RNA extraction.

Nanodrop analysis demonstrated that RNA yields were highest from all three cell lines using TRIzol reagent or miRNeasy micro kit compared to mirVana and Nucleospin RNA plus kits (Figure 5.1A). This was also the case when comparing absorbance (A) ratios, with highest A_{260}/A_{280} and A_{230}/A_{260} ratios achieved using TRIzol reagent or miRNeasy micro kit. In general, RNA yield and quality was most consistent when using the miRNeasy micro kit (Qiagen) (Figure 5.1).

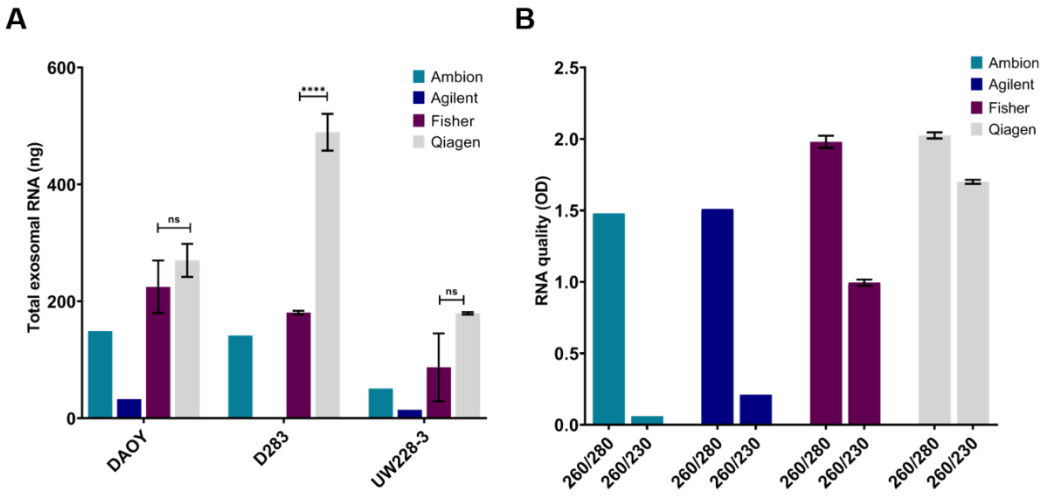

Figure 5.1 Comparisons of RNA quality and yield using different isolation methods

RNA yield (A) and OD_{260}/OD_{280} and OD_{230}/OD_{260} ratios (B) were compared for exosomal isolation using four different RNA extraction methods: mirVana (Ambion), Nucleospin RNA plus (Agilent), TRIzol (Fisher), miRNeasy micro (Qiagen). Comparisons were performed from exosomes isolated from three different medulloblastoma cell lines, DAOY, D283 and UW228-3. Error bars represent the mean ± SEM of n=3 experiments each containing 3 replicates. Significance was calculated using one-way ANOVA analyses with Sidak's multiple comparisons post-hoc test (****= p≤0.0001, ns=not significant).

Next, RNA content of exosomes and their donor cells were examined using capillary electrophoresis (Bioanalyzer) (Figure 5.2). The Bioanalyser instrument was used to measure the size distribution of the extracted RNAs to confirm that exosomes are not contaminated by ribosomal RNAs. Bioanalyzer results comparing RNA in the parental cells versus exosome samples suggested that exosomes appear to contain full-length mRNA transcripts in addition to smaller miRNA fragments, while ribosomal RNAs dominate the signature derived from the parental cells. The broad distribution of RNAs before 18S ribosomal RNA peak indicated that much of the content of the exosomal

RNAs are between 25 and 1000 nucleotides long, highlighting the enrichment of small RNA species.

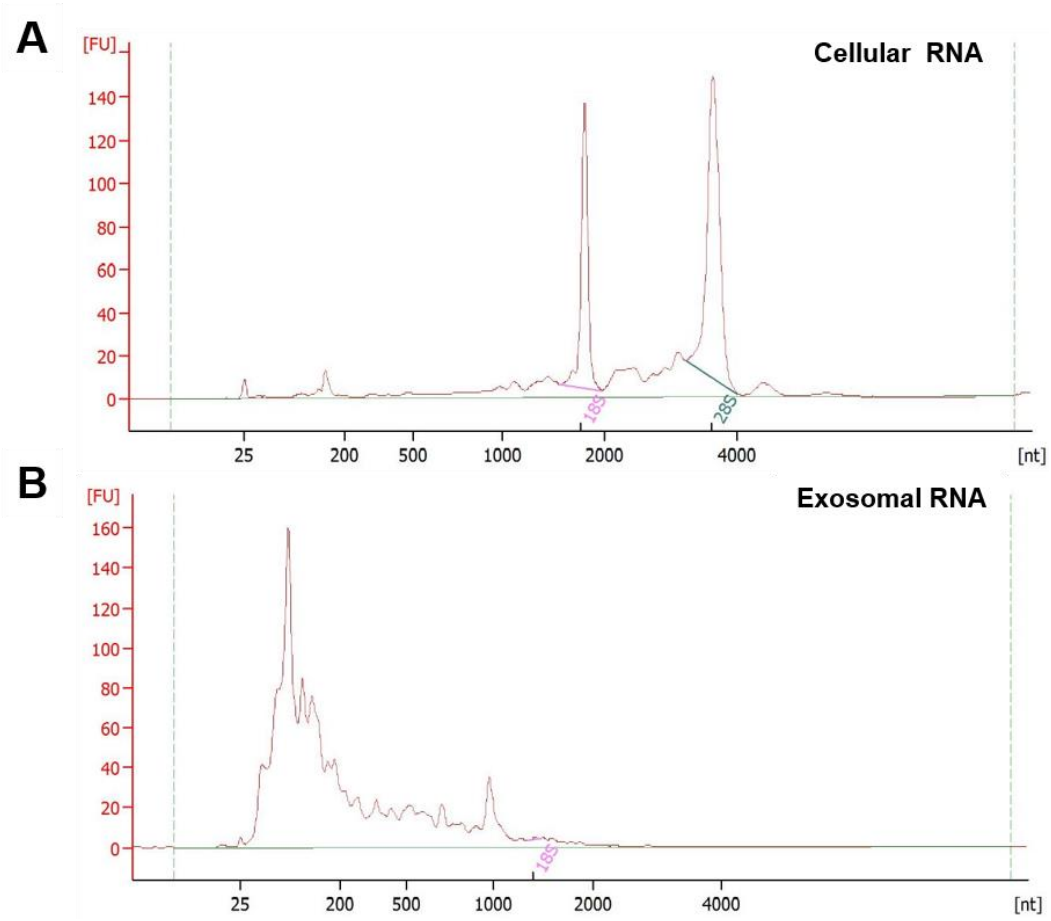

Figure 5.2 Bioanalyzer results of total RNA isolated from exosomes and donor cells

Bioanalyzer electropherogram analysis of exosome and donor cell RNA. Arbitrary fluorescence units (FU) are plotted as a function of RNA size in nucleotides (nt). Total RNA isolated from CHLA-01 cells (A) and total RNA isolated from CHLA-01 exosomes (B) shows the size distribution of RNA. The two dominant peaks in cellular RNA correspond to 18S and 28S rRNA respectively. These ribosomal peaks are absent in the exosomal RNA.

5.2.2 Sample preparation

The experimental workflow for 3’ UPX sequencing is summarised in Figure 5.3. Following RNA extraction using the miRNeasy micro kit (Qiagen), samples were shipped to QIAGEN Genomic Services (Hilden, Germany) where the subsequent steps of NGS were performed. Firstly, quality control of the samples was performed using a TapeStation 4200 RNA high sensitivity assay which quantified the amount of RNA in each sample. Samples with an RNA concentration above 1.4 ng/mL were appropriate for 3' UPX NGS. Table 5.1 provides a summary of the samples prepared for NGS. 15 samples were prepared in total (exosomes derived from 5 cell lines; 2 metastatic, 2 primary, 1 normal/non-malignant, with 3 replicates). For traditional RNA sequencing at least 100 ng of RNA per sample was required, any remaining RNA was used for 3’ UPX sequencing. 14 of the 15 samples had sufficient RNA for both methods of sequencing; however, sample 511 contained the lowest yield of RNA and was therefore only used for RNA sequencing. Following quantification, libraries were prepared and sequenced. Library preparation was performed using the QIAseq® UPX 3' Transcriptome kit. A total of 10 ng purified RNA was converted into cDNA NGS libraries. During reverse transcription, each cell is tagged with a unique ID and each RNA molecule is tagged with a unique molecular index (UMI). After PCR the samples were purified and underwent a second round of quality control. All prepared libraries successfully passed QIAGEN’s internal quality control checks and were sequenced on a NextSeq500 sequencing instrument (Illumina). Following sequencing, raw data was de-multiplexed using the unique IDs and FASTQ files for each sample were generated using the bcl2fastq software. All samples were considered suitable for primary and secondary downstream data analysis.

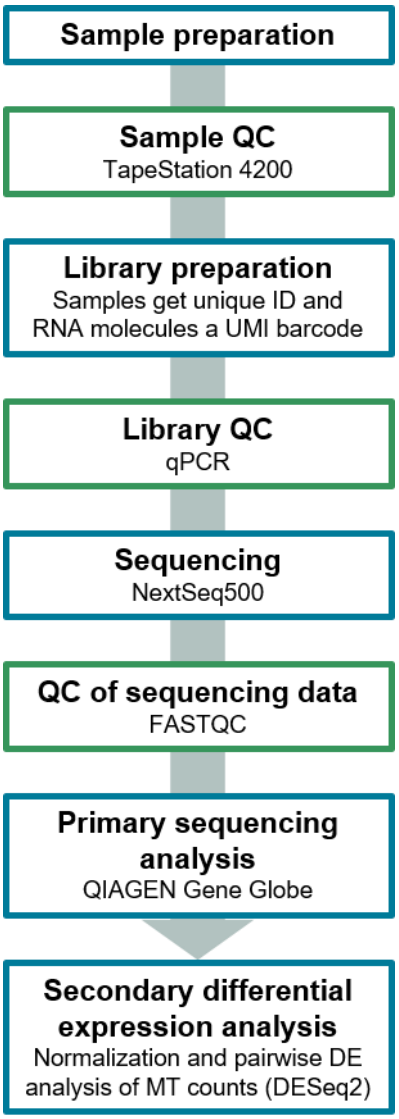

Figure 5.3 Experimental workflow for 3' UPX sequencing

The workflow for the preparation of samples for 3' UPX-sequencing is shown above.

Table 5.1 Summary of the samples prepared for NGS

In total 15 samples were sent for 3' UPX-sequencing. RNA concentration (ng/µL) and total RNA yield (ng) were quantified. 14 of the 15 samples had sufficient RNA for both methods of sequencing; however, sample 511 contained the lowest yield of RNA and was therefore only used for mRNA sequencing.

Sample number	Cell line	Phenotype	RNA conc. (ng/µL)	RNA yield (ng)
500	CHLA-01	Primary	37.80	415.80
501	CHLA-01	Primary	130.80	1111.80
502	CHLA-01	Primary	10.60	109.60
503	CHLA-01-R	Metastatic	19.50	299.00
504	CHLA-01-R	Metastatic	19.90	431.50
505	CHLA-01-R	Metastatic	12.90	267.70
506	D458	Metastatic	57.00	1054.50
507	D458	Metastatic	54.00	864.00
508	D458	Metastatic	10.83	115.60
509	D425	Primary	10.33	110.60
510	D425	Primary	42.70	576.50
511	D425	Primary	9.19	101.10
512	FB83	Normal	20.54	124.10
513	FB83	Normal	10.81	108.60
514	FB83	Normal	10.33	199.00

5.2.3 Mapping of sequence data

Mapping of sequencing data was performed as an additional control step to evaluate the quality of each sample. The total number of reads was 13,374,064, which resulted in 426,513 total UMI's being read after mapping. A summary of the mapping results for each sample is shown in Table 5.2. The reads were classified into four classes:

1) **Total reads:** read pair demultiplexed to each cell identifier. Demultiplexing involves identifying and removing the cell-barcode sequence from one or both reads
2) **Reads aligned to genome:** Trimmed reads of good quality RNA can then be aligned to the reference genome using STAR. STAR identifies the longest sequence which matches one or more sequences to the reference genome.

3) **Reads aligned to ERCC:** reads were next aligned to the external RNA control consortium (ERCC) spike-ins, a set of external RNA spike-in controls enabling performance assessment. In short, spike-in mix is added to RNA samples, and compared to known Spike-In Mix concentrations and ratios, this allows assessment of dynamic range, lower limit of detection, and fold-change responses.
4) **UMIs:** Unique Molecular Index tags counted
5) **Detected genes**

After removing 514 due to its low number of reads, the average number of reads obtained for the remaining samples was 33,000 with a range from 2,000 to 84,000 reads.

Table 5.2 Mapping of 3' UPX NGS sequencing data

Mapping of sequencing data was performed as an additional control step to evaluate the quality of each sample. The number of reads (total, aligned to genome, aligned to ERCC, UMIs and detected genes) for each sample are displayed. Sample 514 contained the lowest number of detected genes and was therefore removed from downstream analysis.

Sample number	Reads total	Reads aligned to genome	Reads aligned to ERCC	UMIs	Detected Genes
500	395419	22439	75	21348	9874
501	188814	3177	30	3083	2423
502	107594	1419	48	1436	1065
503	275701	12973	75	12398	6440
504	155498	4071	53	3928	2654
505	130430	3005	40	2906	2045
506	1029030	69890	174	66741	15698
507	1054328	62215	154	59404	15277
508	78428	3433	37	74001	16216
509	1444538	93628	246	87881	17944
510	1309244	87264	241	84793	17131
512	1249146	78937	227	3279	2463
513	151369	4624	52	4449	3276
514	92548	848	38	866	690

5.3 Characterisation of medulloblastoma exosomal mRNA

To our knowledge, this is the first time mRNA-sequencing analysis of medulloblastoma-derived exosomes has been conducted, with previous studies focusing on protein or miRNA cargo. Therefore, we were initially interested in all gene transcripts identified in exosome samples. The only filters applied to samples were a cut-off of raw UMI count of ≥5.

For Group 3-derived exosomes this resulted in 3,099 gene transcripts being identified from primary exosomes and 1,852 gene transcripts from metastatic exosomes. The gene lists from both phenotypes were compared using Venn diagrams, which showed an overlap of 1,537 genes. For Group 4 samples, fewer gene transcripts were identified. A total of 204 genes were identified in primary exosomes and 82 genes from metastatic exosomes with 43 genes overlapping. Despite fewer genes being identified in Group 4 samples with a raw UMI count of ≥5, most of the identified genes in Group 4 overlapped with Group 3 (Figure 5.4).

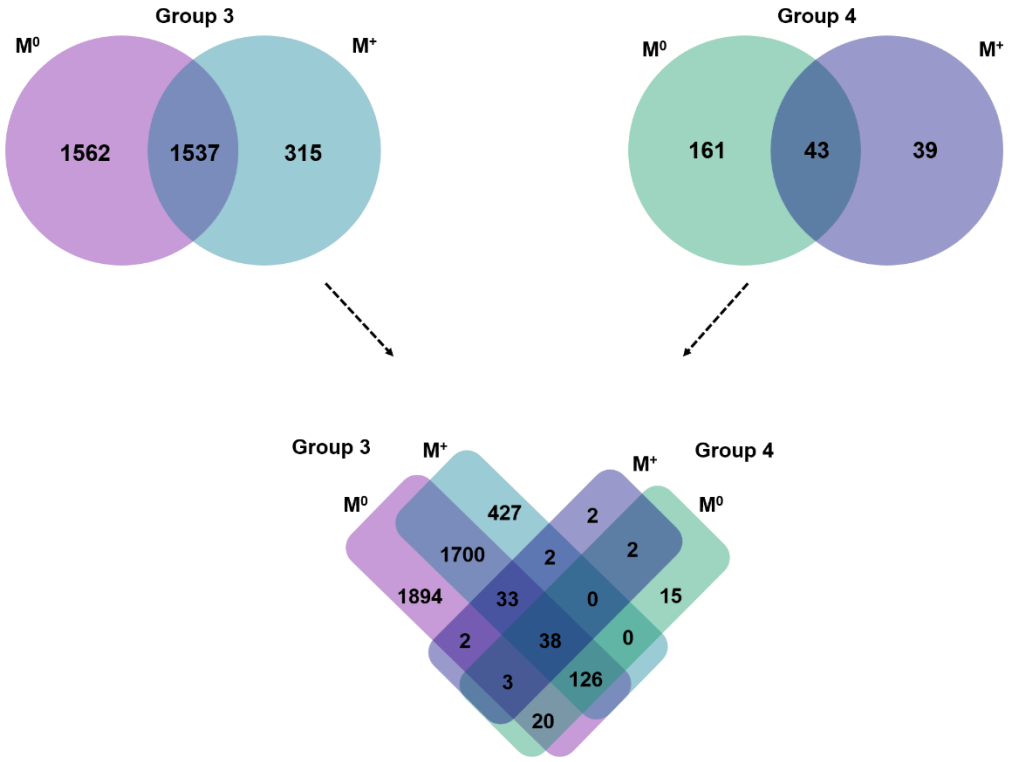

Figure 5.4 All identified gene transcripts prior to differential expression analysis

All gene transcripts identified in exosome samples were analysed (cut-off of raw UMI count of ≥5). Venn diagrams were used to show overlapping gene transcripts between subgroups and phenotypic differences. In Group 3-derived exosomes 3,099 gene transcripts were identified from primary (M^0) samples and 1,852 gene transcripts were identified in metastatic (M^+) exosomes, with an overlap of 1,537 genes. For Group 4 samples, a total of 204 genes were identified in primary (M^0) exosomes and 82 genes from metastatic (M^+) exosomes with 43 genes overlapping. Comparing samples from Group 4 and Group 3 samples, most of the identified genes in Group 4 overlapped with Group 3.

5.3.1 Potential function of exosomal mRNA by cellular compartment

The gene lists from all medulloblastoma exosomes were compiled and Functional Enrichment Analysis Tool (FunRich) software was used to conduct enrichment analysis, Fisher's exact test was performed to generate *p* values. Exploration of the potential compartments in which you would expect the translated mRNAs to have a cellular impact, indicates an enrichment of genes involved in both plasma membrane ($p \leq 0.001$) and cytoplasm functions ($p \leq 0.001$) (Figure 5.5). Other cellular components include axon development ($p \leq 0.005$), cytoskeleton ($p \leq 0.05$) and cell projection.

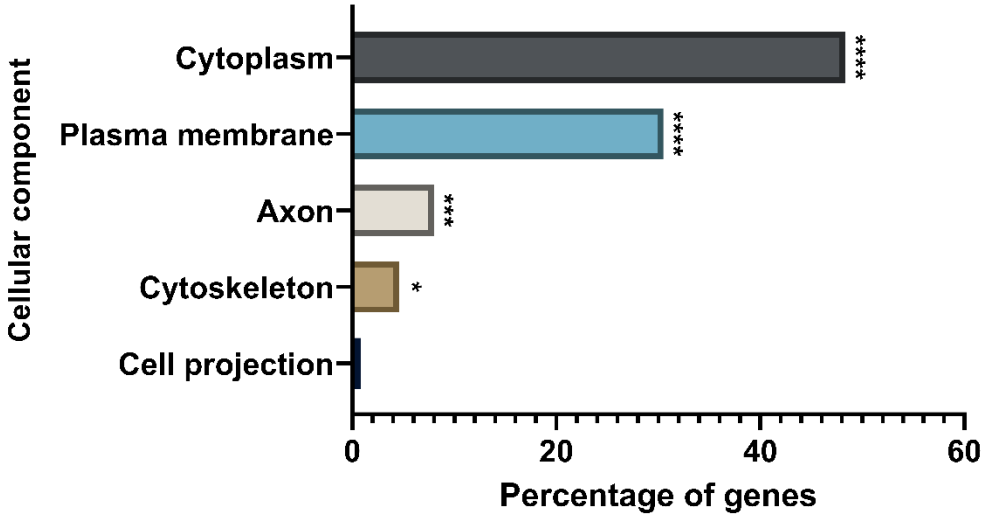

Figure 5.5 Pathway enrichment analysis of mRNAs according to cellular compartment

FunRich software was used to conduct pathway enrichment to explore the potential compartments in which you would expect the translated mRNAs to have a cellular impact, indicates largest enrichment of genes localised to the plasma membrane and cytoplasm. Significance was calculated using Fisher's exact test (*= p≤0.05, ***= p≤0.005, ****= p≤0.001).

5.3.2 Exosomal mRNA pathway analysis

Given that exosomes contain mRNAs which can then be translated to affect biological processes in recipient cells, we used Gene Ontology (GO) analysis to evaluate the potential effects of the exosome-transferred mRNAs on recipient cells. We were keen to see if there was a predicted difference between which biological pathways could be activated by primary-derived exosomes compared to metastatic exosomes and by comparison to normal (FB83). As Group 4-derived exosomes contained fewer gene transcripts, statistical significance was not reached, however similar pathways and processes were still enriched between the subgroups (Appendix Figure 3).

Biological pathway analysis revealed a predominance of genes involved in integrin signalling pathways (Figure 5.6). Integrins and their downstream signalling effectors are involved in regulating the vasculature, angiogenesis, the immune response and the stromal context of metastasis (Hart and Fidler, 1980; Cooper and Giancotti, 2019). It is important to note that enrichment of integrin pathways was absent from normal FB83 samples (Appendix Figure 4).

The top ten GO terms from mRNA identified in Group 3 primary exosomes included; Alpha9 beta1 integrin signalling events ($p \leq 0.001$), Beta1 integrin cell surface interactions ($p \leq 0.001$), Class I PI3K signalling events mediated by Akt ($p \leq 0.001$), mTOR signalling pathway ($p \leq 0.001$) and signalling event mediated by focal adhesion kinase ($p \leq 0.001$) (Figure 5.6A). The top ten GO terms for metastatic Group 3 included; Class I PI3K signalling events mediated by Akt ($p \leq 0.001$), Nectin adhesion pathway ($p \leq 0.001$), Alpha9 beta1 integrin signalling events ($p \leq 0.001$), VEGF and VEGFR signalling network ($p \leq 0.001$) and Cell-Cell communication ($p \leq 0.001$) (Figure 5.6B). The top ten GO terms from mRNA identified in Group 4 primary exosomes included; Integrin family cell surface interactions, Beta1 integrin cell surface interactions, Class I PI3K signalling events mediated by Akt, Insulin pathway and RhoA signalling pathway (Appendix Figure 3). The top ten GO terms for metastatic Group 4 included; Integrin family cell surface interactions, Beta1 integrin cell surface interactions, VEGF and VEGFR signalling network, Class I PI3K signalling events mediated by Akt and Metabolism.

The GO terms that describe the genes identified in normal-derived exosomes displayed no pathway overlap with the medulloblastoma samples (Appendix Figure 4). The genes are described by GO terms for cell cycle regulation, energy production, signal transduction and other normal cell processes necessary for maintaining cell viability.

Taken together, the RNA-seq analysis of all gene transcripts identified in exosomes, provides new insights into the cellular functions and biological pathways regulated by medulloblastoma-derived exosomes.

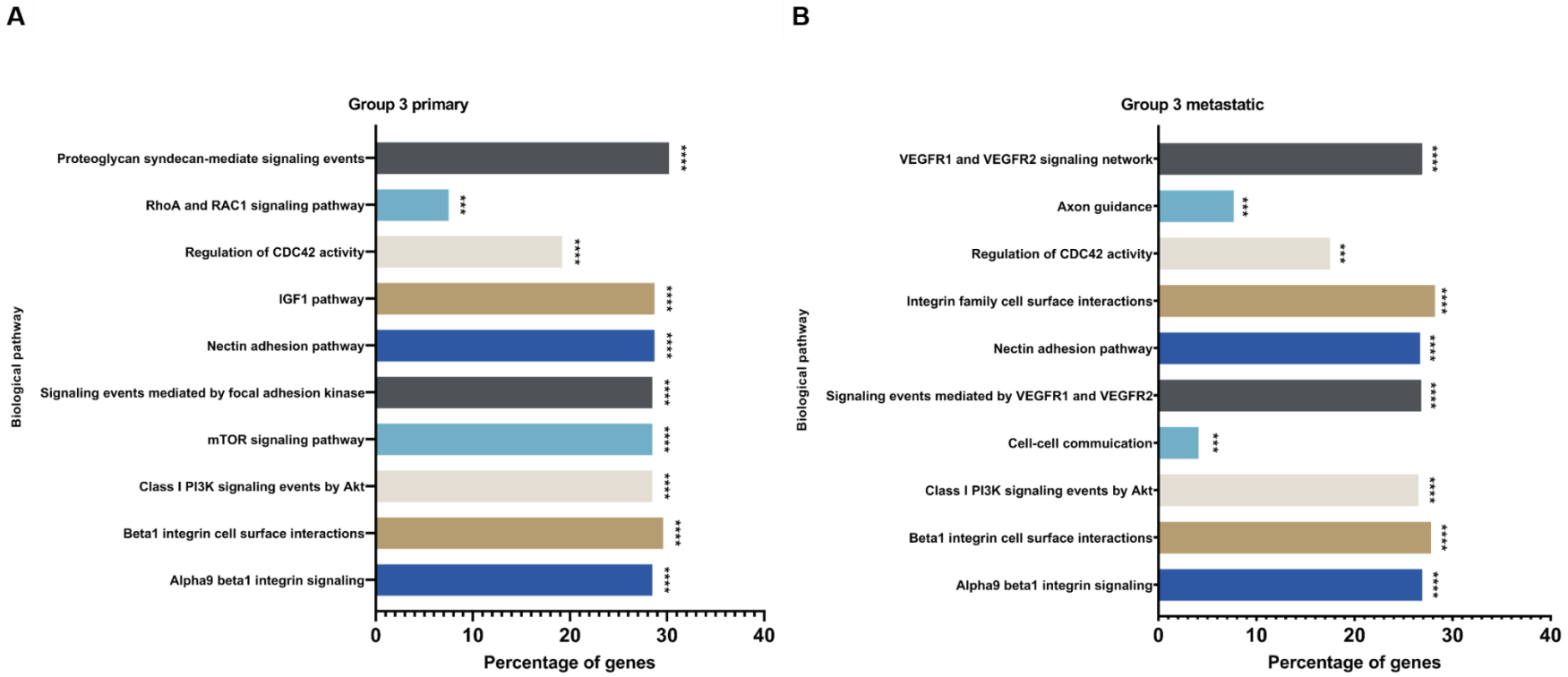

Figure 5.6 Biological pathway analysis targeting by Group 3 exosomal RNA

The characterised major biological pathways potentially targeted by the exosomal mRNA cargo revealed a predominance of genes involved in integrin signalling pathways. Pathway analysis is shown for exosomes derived from Group 3 primary (A) and metastatic (B). Significance was calculated using Fisher's exact test (***= p≤0.005, ****= p≤0.001)

5.4 Differential mRNA profiles between metastatic- and primary-derived exosomes

Whilst analysing all gene transcripts found in exosomes identified common genes lists across phenotype (independent of subgroup), and revealed a predominance of genes involved in integrin signalling pathways. In order to identify specific targets playing a possible role in cell migration and which could be used as biomarkers for metastatic disease, differentially enriched genes across the samples were compared.

To investigate differences in exosomal mRNA profiles between normal, primary and metastatic-derived exosomes, unsupervised transformed gene counts were used to create a heatmap representing the top 50 genes with the largest variance across all samples (Figure 5.7). The heatmap shows unbiased hierarchal clustering of samples; each row represents a gene and individual samples are displayed in columns along the bottom. The colour scale signifies the relative expression level of a gene across all samples. Expression levels above the mean are shown as green and below the mean are red. Firstly, samples clustered based on subgroup, with clustering separating Group 3 from Group 4 samples. In addition, metastatic samples also cluster separately from primary samples, suggesting that metastasis of the tumour is reflected in exosomal mRNA cargo. Of note, the normal FB83-derived exosomes failed to cluster together, however this may be a result of the smaller number of replicates for this group (two independent replicates).

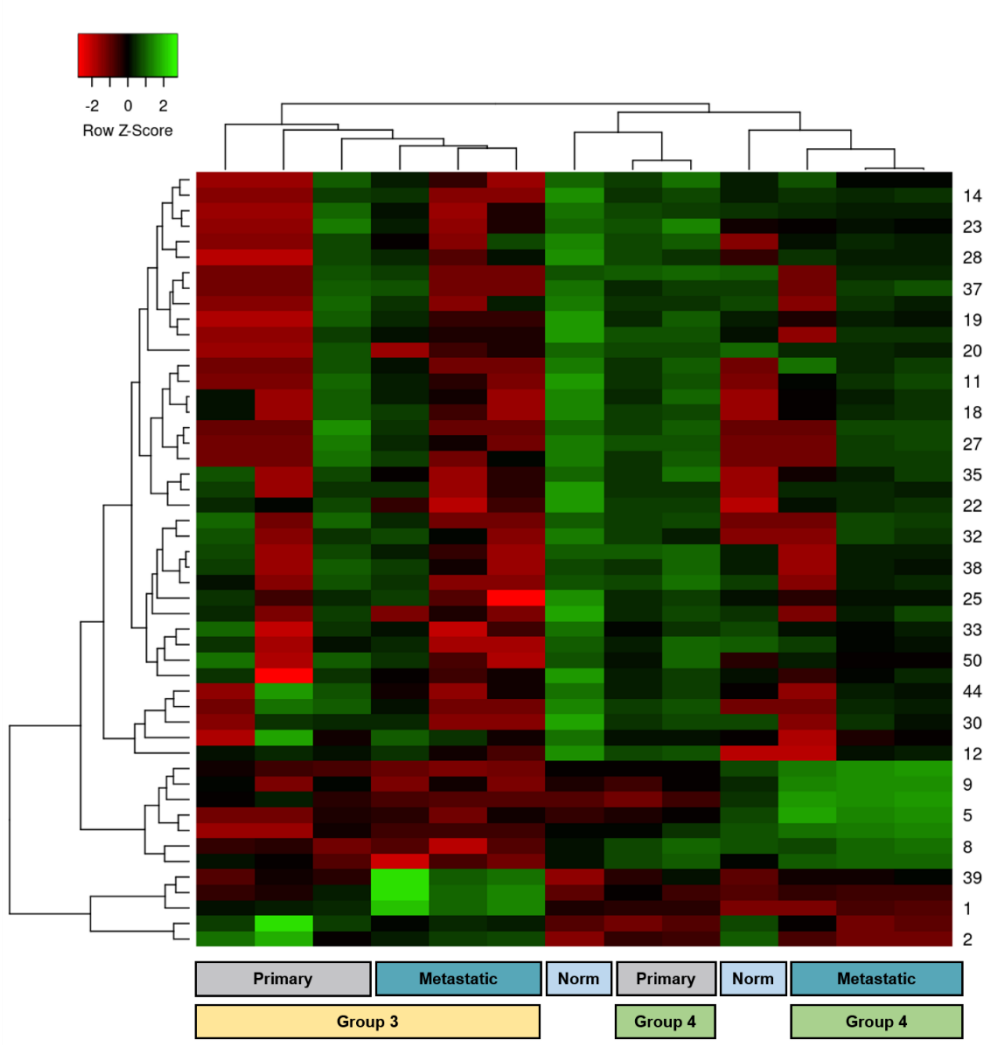

1	CASC19	11	LSAMP	21	SOX2-OT	31	SSH2	41	CASC8
2	MALAT1	12	DMD	22	CCSER1	32	CNTN5	42	NLGN1
3	MT-RNR2	13	PVT1	23	ERBB4	33	GPC5	43	RYR2
4	AL161757.4	14	CASC11	24	ROBO2	34	PARD3B	44	DCC
5	LINC00824	15	RBFOX1	25	SLC39A11	35	CTNNA2	45	RORA
6	OTX2-AS1	16	PCAT1	26	CDH13	36	EXOC6B	46	PCDH15
7	TMEM260	17	NRG1	27	NAALADL2	37	TANC2	47	LUZP2
8	AL161757.5	18	ZFPM2	28	PRKN	38	LRP1B	48	PTPRT
9	CCDC26	19	ROBO1	29	NKAIN2	39	POU5F1B	49	CDH12
10	AC090673.1	20	NRXN1	30	SGCD	40	MALRD1	50	CSMD1

Figure 5.7 Heatmap of unbiased clustering of all samples

Unsupervised transformed gene counts were used to create a heatmap representing the top 50 genes with the largest variance across all samples. The heatmap shows unbiased hierarchal clustering of samples, each row represents a gene and individual samples are displayed in columns along the bottom. The colour scale signifies the relative expression level of a gene across all samples. Expression levels above the mean are shown as green and below the mean are red. Numbers corresponding to the gene names are shown in the table below.

5.4.1 Pathway analysis of metastatic exosomal mRNA

To begin to understand the signalling pathways in the tumour microenvironment that could be impacted by the cellular uptake of exosomes released by metastatic medulloblastoma cells, Gene Set Enrichment Analysis (GSEA) was performed to elucidate which signalling pathways were being regulated in cancer cells (by transfer of mRNA via exosomes). The top 10 gene sets that overlapped with the Kyoto Encyclopaedia of Genes and Genomes (KEGG) gene set database are shown in Table 5.3. Interestingly, when comparing the signalling pathways enriched between the two subgroups, 9 out of the 10 gene sets overlap.

A number of overlapping pathways were shown to be targeted by mRNA enrichment in exosomes, including regulation of actin cytoskeleton and cell adhesion molecules, two key pathways critical to cell migration during processes such as cancer metastasis (Bhowmick *et al.*, 2001). Furthermore, MAPK signalling was identified as being targeted, MAPK has implications in sustained cell proliferation, growth and survival processes in various cancer types (Chapnick *et al.*, 2011). In addition, the MAPK pathway frequently shows aberrant over activity in medulloblastoma tumours, and emerging data strongly implies a role in medulloblastoma cellular migration (Zhao *et al.*, 2015; Van Ommeren *et al.*, 2020). Finally, ErbB signalling pathway was also identified, similarly to MAPK pathway, ErbB has been specifically implicated in medulloblastoma pathogenesis and migration. Overexpression of ErbB in medulloblastoma cell lines significantly increased *in vitro* invasion and cell migration compared to control cell lines, and upregulated expression of downstream MAPK pathway genes and several other pro-metastatic genes in medulloblastoma (Hernan *et al.*, 2003). Taken together, this analysis provides insight into the pathways activated by metastatic exosomes. It is possible that transfer of mRNA via exosomes into recipient cells, activates various metastatic pathways, promoting cancer cell migration and tumour progression.

Table 5.3 Top 10 gene sets differentially regulated in metastatic exosomes compared to primary

Differential gene expression analysis was conducted on samples to generate genes differentially regulated in metastatic exosomes compared to primary exosomes from both subgroups. Gene Set Enrichment Analysis was performed to identify the top 10 gene sets that overlapped with the KEGG gene set database.

Group 3				Group 4			
Gene set name	**Number of gene in overlap**	***p* value**	**FDR q-value**	**Gene set name**	**Number of gene in overlap**	***p* value**	**FDR q-value**
Tight junction	8	7.44E-07	6.92E-05	Axon guidance	6	8.29E-05	3.63E-03
Axon guidance	6	8.29E-05	3.63E-03	Dilated cardiomyopathy	5	1.43E-04	4.44E-03
Regulation of actin cytoskeleton	7	1.88E-04	4.98E-03	Regulation of actin cytoskeleton	7	1.88E-04	4.98E-03
Calcium signalling pathway	6	4.60E-04	1.07E-02	Calcium signalling pathway	6	4.60E-04	1.07E-02
Adherens junction	4	7.15E-04	1.34E-02	Adherens junction	4	7.15E-04	1.34E-02
MAPK signalling pathway	7	7.26E-04	1.34E-02	MAPK signalling pathway	7	7.26E-04	1.34E-02
Phosphatidylinositol signalling system	4	8.33E-04	1.34E-02	Phosphatidylinositol signalling system	4	8.33E-04	1.34E-02
Cell adhesion molecules cams	5	8.66E-04	1.34E-02	Cell adhesion molecules cams	5	8.66E-04	1.34E-02
ErbB signalling pathway	4	1.38E-03	1.97E-02	ErbB signalling pathway	4	1.38E-03	1.97E-02
Pathways in cancer	7	2.24E-03	2.97E-02	Pathways in cancer	7	2.24E-03	2.97E-02

5.4.2 Identification of specific genes associated with metastatic exosomes

While GO analysis identified interesting biological processes which provided insights into the pathways activated by metastatic exosomal genes, the power of RNA-seq analysis comes from the ability to investigate individual genes. Having previously identified that, based on unbiased hierarchal clustering alone, primary exosome samples could be distinctly separated from metastatic exosomes (Figure 5.7), suggesting the metastatic phenotype of the tumour cells is reflected in exosomal RNA cargo, we aimed to identify specific genes associated with metastatic exosomes.

To identify transcripts which were significantly enriched in metastatic exosomes compared to primary exosomes, strict criteria were used; fold differences with a cut-off of log2 fold change threshold of >1 and *P* value of <0.05. Following this criteria, 19 genes were identified that were enriched in metastatic exosomes from Group 3 and 10 genes were identified that were enriched in metastatic exosomes from Group 4. From the identified genes, 5 were enriched in all metastatic-derived exosomes; *POU5F1B, CCDC26, EIF3H, PCAT1* and *PVT1* (Figure 5.8). All gene transcripts enriched in metastatic exosomes from Group 3, Group 4 and combined are summarised in Appendix Table 1-3.

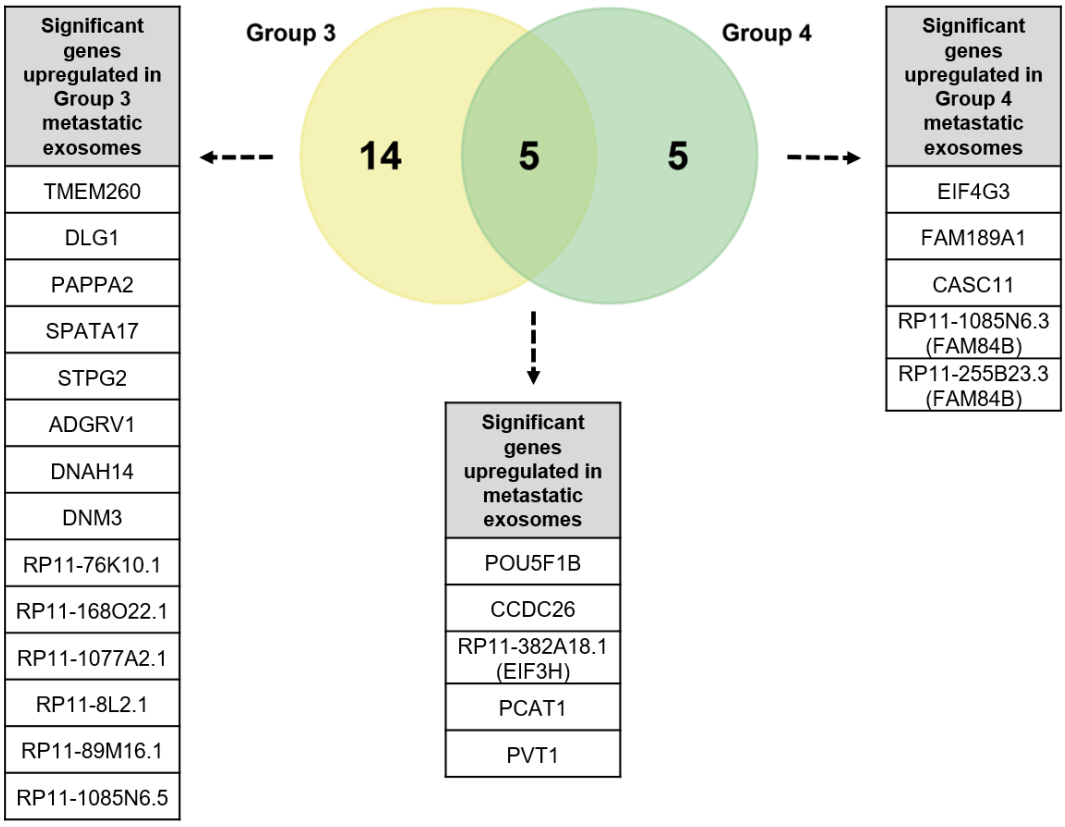

Figure 5.8 Venn diagram comparing enriched genes in metastatic-derived samples

Differential gene expression analysis was conducted to identify genes upregulated in metastatic exosomes compare to primary exosomes. A Venn diagram was constructed showing the overlap between significant upregulated genes (log2 fold change threshold of >1 and *P* value of <0.05) identified in metastatic Group 3 and metastatic Group 4-derived exosomes. 5 enriched genes were shared between the two subgroups.

The Cancer Hallmarks proposed by Hanahan and Weinberg in 2011, gave rise to the idea that the cancer phenotype is characterized by six biological capabilities acquired during a multistep process of cancer (Hanahan and Weinberg, 2011). The six classical cancer hallmarks proposed include; limitless replication potential, insensitivity to growth inhibitors, evading apoptosis, self-sufficiency in growth signals, sustained angiogenesis, and activation of tissue invasion and metastasis. These six hallmarks provide an organizing principle for understanding the complexity and diversity of carcinogenesis. We had previously shown that several mRNAs identified in metastatic exosomes may be involved in activating various metastatic pathways in recipient cells, thus promoting cancer cell migration and tumour progression (Table 5.3). In order to

better interpret our data and infer the potential impact of individual genes, data mining studies, including literature and databases from NCBI, UniProt and NextProt were used to understand the influence of the 24 genes on the six defined hallmarks of cancer.

The 24 genes identified as having mRNAs selectively increased in metastatic exosomes were mapped onto the hallmarks of cancer using their known or predicted functions. Of the 24 genes, 12 were associated to functions compatible with limitless replication, 4 genes to apoptosis, 2 genes to growth signals, 8 genes to invasion and metastasis and 1 gene to angiogenesis. Multiple genes could be included in more than one cancer hallmark, for example *PCAT1*, *PAPPA2* and *POU5F1B* have been linked to replication and invasion and metastasis (Figure 5.9).

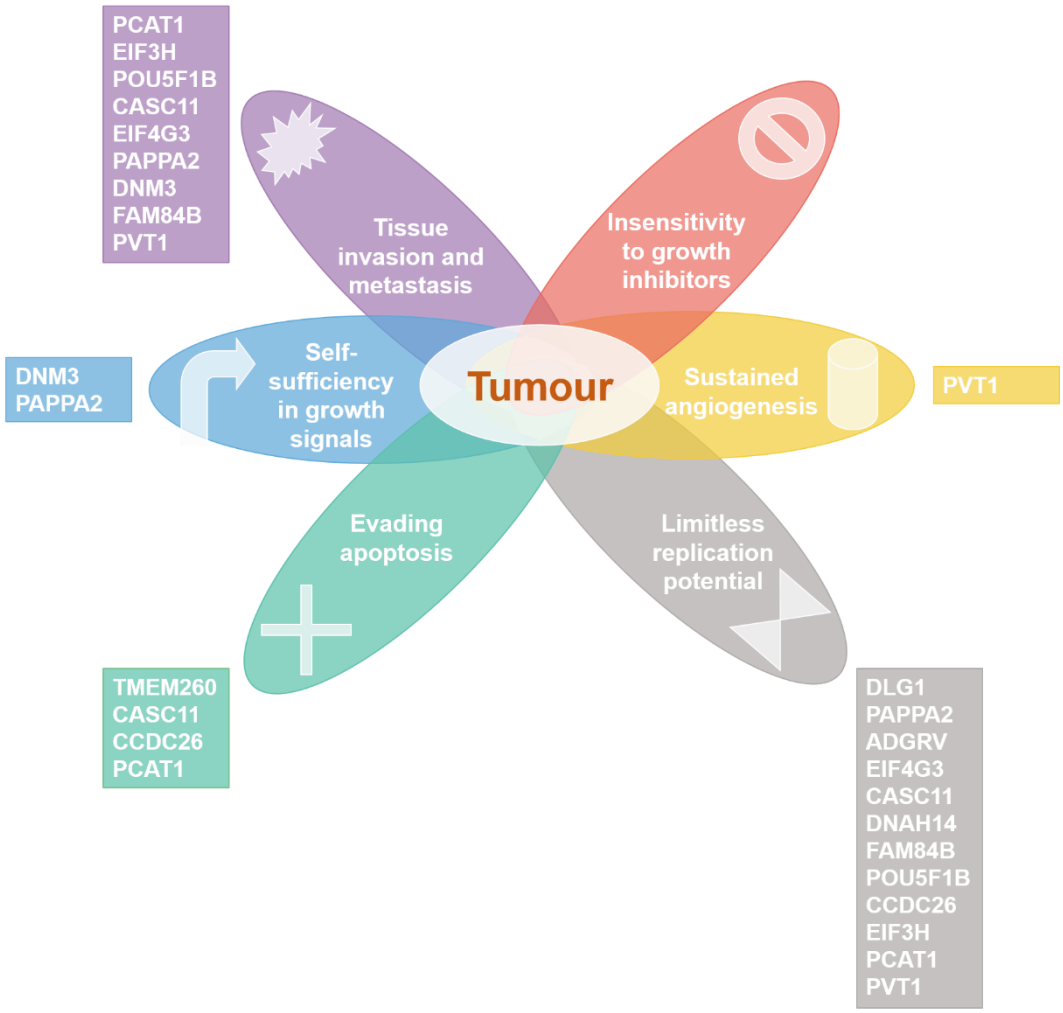

Figure 5.9 Identified metastatic gene signature mapped onto the hallmarks of cancer

The six cancer hallmarks proposed by Hanahan and Weinberg include; limitless replication potential, insensitivity to growth inhibitors, evading apoptosis, self-sufficiency in growth signals, sustained angiogenesis, and activation of tissue invasion and metastasis. The 24 genes identified as having mRNAs selectively increased in metastatic exosomes were mapped onto the hallmarks of cancer using their known or predicted functions.

5.5 Validation of exosome target genes in medulloblastoma patient datasets

Having identified genes enriched in metastatic exosomes compared to primary exosomes, we next wanted to substantiate the importance of these candidates in medulloblastoma patients by determining if their expression correlates with outcome in order to assess their prognostic significance. R2 Genomics Analysis and Visualization Platform was used to analyse a large medulloblastoma patient dataset (Cavalli *et al.*, 2017) for the expression of genes of interest.

5.5.1 Genes identified in metastatic exosomes were found in medulloblastoma patient datasets

The Cavalli dataset was first used to investigate expression levels of the genes among medulloblastoma molecular subgroups (WNT: n=70; SHH: n=223; Group 3: n=144; Group 4: n=326). Significant differences in gene expression between the subgroups were calculated using the Kruskal-Wallis one-way ANOVA with Dunn's multiple comparisons post-hoc test. It was hypothesised that genes which play a role in migration and invasion would be most highly expressed in the most metastatic subgroups, Group 3 and Group 4. For this reason, significant comparisons were only calculated between these two subgroups.

Metastatic Group 3 exosome enriched genes included: *TMEM260, DLG1, PAPPA2, SPATA17, STPG2, ADGRV1, DNAH14 and DNM3* (Figure 5.10A). As there is no patient information for long non-coding genes the expression of genes *RP11-76K10.1, RP11-168O22.1, RP11-1077A2.1, RP11-8L2.1, RP11-89M16.1* and *RP11-1085N6.5* in patient datasets, they were not examined. Expression of all 8 genes analysed was seen across all medulloblastoma subgroups, with high expression levels of *TMEM260, DLG1, PAPPA2, SPATA17, STPG2, ADGRV1* and *DNAH14* being significantly elevated in Group 3 samples compared to other subgroups. In addition, expression of genes; *PAPPA2, SPATA17, STPG2* and *DNM3* were all found to be significantly higher in Group 4 compared with other medulloblastoma subgroups.

Metastatic Group 4 exosome-enriched genes included: *EIF4G3, FAM189A1* and *FAM84B* (Figure 5.10B). Unfortunately, there was no patient data available for long non-coding gene *CASC11*. Again, expression of the three genes was observed in all medulloblastoma subgroups, however no genes were expressed significantly higher in Group 4 patients.

Exosome-enriched genes common in both subgroups included; *CCDC26, PCAT1, POU5F1B* and *EIF3H* (Figure 5.10C). Expression of the four genes analysed was seen across all medulloblastoma subgroups, with *PCAT1* and *POU5F1B* expression levels being significantly elevated in Group 3 compared to other subgroups. Data for long non-coding gene *PVT1* was not available in the Cavalli dataset.

Taken together, based on gene expression analysis between medulloblastoma subgroups, *PAPPA2, SPATA17, STPG2*, *DNM3, PCAT1* and *POU5F1B* were all identified as genes being significantly overexpressed in Group 3 and/or Group 4 patient tumours compared to WNT or SHH tumours. In addition, *PAPPA2, DNM3, PCAT1* and *POU5F1B* have previously been linked with tissue invasion and metastasis (Figure 5.9) and therefore may warrant further investigation.

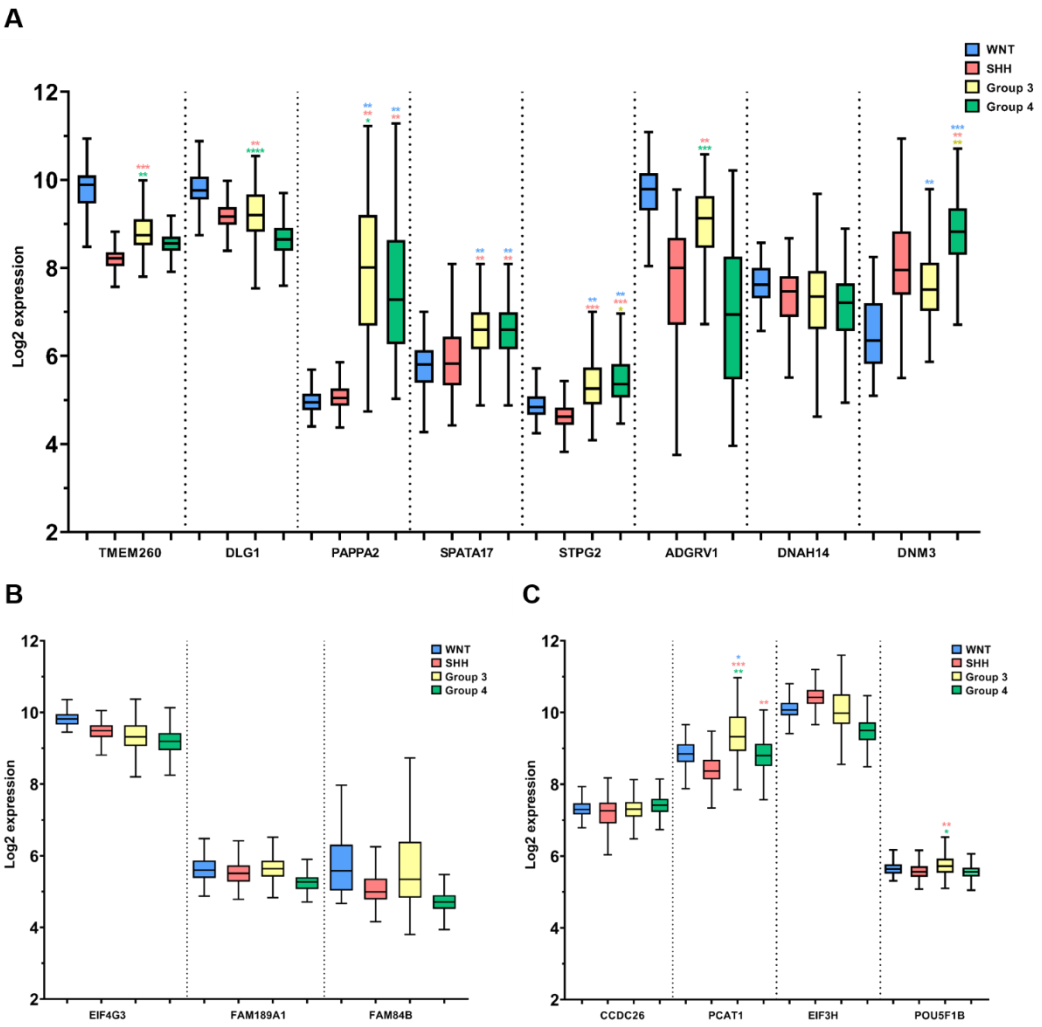

Figure 5.10 The expression of exosome enriched genes in medulloblastoma patient samples

Gene expression (Log2) of genes enriched in exosomes from Group 3 (A), Group 4 (B) and genes found in common (C) were assessed on the R2 Genomics Analysis and Visualization Platform using the Cavalli dataset grouped according to the molecular subgroups. Significant differences in gene expression compared to the Group 3 and Group 4 subgroups were calculated using the Kruskal-Wallis test with Dunn's multiple comparisons post-hoc test. Differences are represented by coloured asterisks of the corresponding subgroup (*p≤0.05; **p≤0.01, ***p≤0.001, ****p≤0.0001).

5.5.2 Highest expression of *PAPPA2*, *STPG2* and *PCAT1* was seen in metastatic tumours

Knowing that metastatic events are more common in Group 3 (46.5%) and Group 4 (29.7%) than in WNT (17.9%) and SHH (19.1%), we analysed the expression levels of the identified genes by comparing metastatic (M^+; n=176) and non-metastatic (M^0 n=397) samples from the Cavalli dataset (Figure 5.11).

When comparing genes which were enriched in Group 3 metastatic exosomes, genes *PAPPA2* (p≤0.001), *SPATA17* (p≤0.05) and *STPG2* (p≤0.001) have significantly elevated expression in metastatic M^+ tumours compared to M^0 tumours (Figure 5.11A). No genes that were identified to be enriched in metastatic Group 4 exosomes showed significantly higher expression in metastatic tumours compared to non-metastatic tumours (Figure 5.11B). Finally, of the genes identified as being enriched in both Group 3 and Group 4 metastatic exosomes, *PCAT1* (p≤0.001) was significantly overexpressed in metastatic patients compared to non-metastatic patients (Figure 5.11C).

Taken together, based on gene expression analysis between medulloblastoma subgroups, *PAPPA2, SPATA17, STPG2*, *DNM3, PCAT1* and *POU5F1B* were all identified as genes being significantly overexpressed in Group 3 and Group 4 patient tumours compared to WNT or SHH tumours. In addition, *PAPPA2, DNM3, PCAT1* and *POU5F1B* have previously been linked with tissue invasion and metastasis (Figure 5.9) and therefore may warrant further investigation.

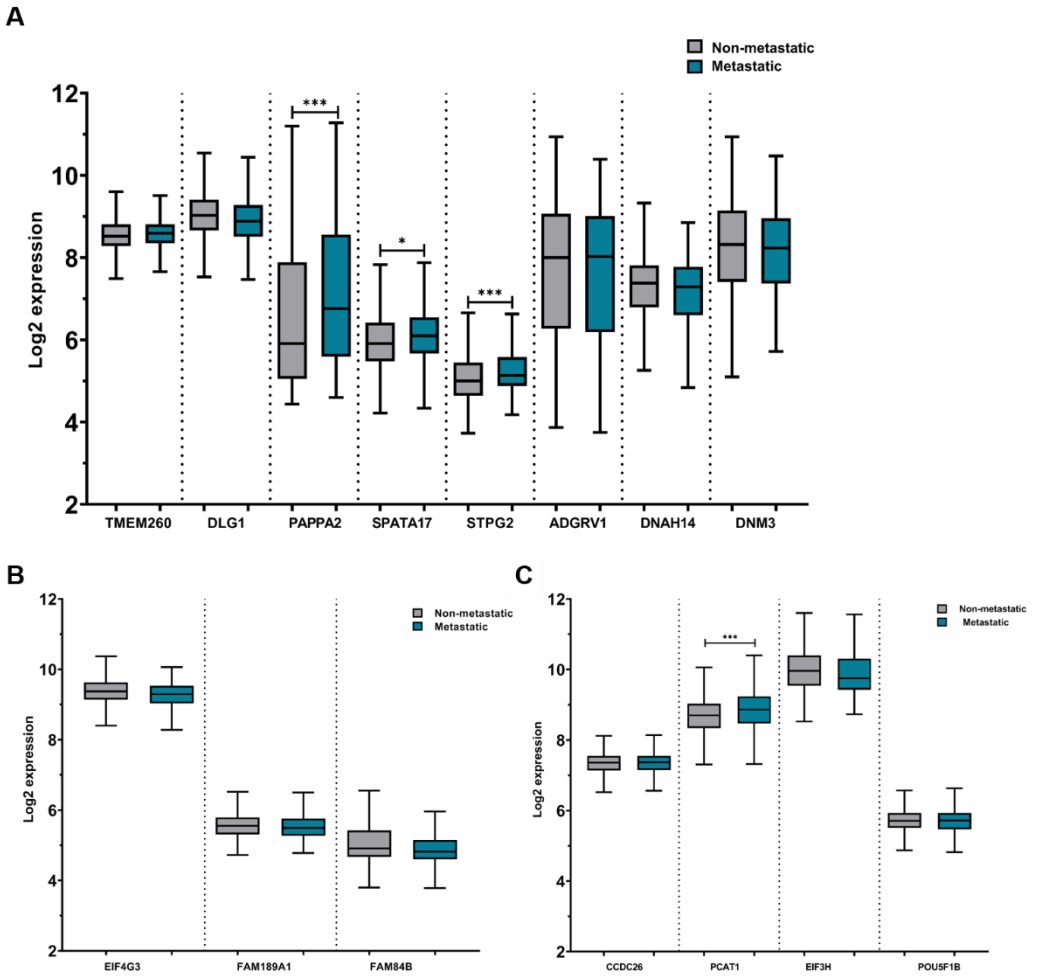

Figure 5.11 The expression of exosome enriched genes in medulloblastoma patient samples

Gene expression (Log2) of genes enriched in exosomes from Group 3 (A), Group 4 (B) and genes found in common (C) in non-metastatic (M0: n=397) and metastatic (M+: n=176) tumours were assessed using the Cavalli dataset. Significant differences in gene expression between metastatic compared to non-metastatic samples were calculated using the Kruskal-Wallis test with Dunn's multiple comparisons post-hoc test (*p≤0.05; ***p≤0.001).

5.5.3 Numerous candidate genes represent a negative prognostic factor for overall survival in medulloblastoma patients

Correlation between candidate gene expression and tumour progression was then assessed. Using the Cavalli dataset, Kaplan Meier curves were used to show the probability of survival of medulloblastoma patients based on high or low expression of particular genes (Figure 5.12). Patients with high expression levels of *DLG1, PAPPA2, ADGRV1* and *DNM3* in tumours had significantly worse 5- and 10-year overall survival outcome than patients with low expression levels, suggesting that these genes may

represent a negative prognostic factor for overall survival in medulloblastoma patients. Comparatively, patients with elevated expression of *TMEM260, SPATA17, STPG2* and *DNAH14* did not display significantly worse overall survival compared to patients with low expression of these genes, indicative that expression levels of these genes do no correlate with patient outcome.

When comparing genes which were enriched in Group 4 metastatic exosomes, high expression of *EIF4G3* and *FAM189A1* in medulloblastoma patient tumours had significantly worse survival outcome compared to patients with low expression levels. In contrast, high expression levels of *FAM84B* were not associated with significantly worse overall survival. Lastly, of the genes identified as being enriched in both Group 3 and Group 4 metastatic exosomes, only patients with high expression levels of *POU5F1B* in tumours had significantly worse 5- and 10-year overall survival outcomes than patients with low expression levels, suggesting that *POU5F1B* may represent a negative prognostic factor for overall survival in medulloblastoma patients. High gene expression levels of *CCDC26* and *PCAT1* also correlated with worse patient overall survival, however results did not reach significance. Comparatively, patients with high expression levels of *EIF3H* did not display significantly worse overall survival than patients with low *EIF3H* expression. Taken together, these observations led to the selection of candidates whose expression was elevated in Group 3 and/or Group 4 subgroups, which were overexpressed in metastatic patients compared to non-metastatic patients, or had been identified as being an independent predictor of patient overall survival. Genes identified following this criteria, may have been packaged into metastatic exosomes to facilitate migration and invasion, additionally exosomes containing high levels of candidate genes could be used as prognostic markers. Based on this criteria *PAPPA2*, *PCAT1* and *POU5F1B* were selected for further validation. When comparing back to previous analyses across all exosome samples sequenced, *PCAT1* and *POU5F1B* were identified in the top 50 genes with the largest variance across all samples (Figure 5.7), and had previously been identified as being linked with tissue invasion and metastasis (Figure 5.9).

A

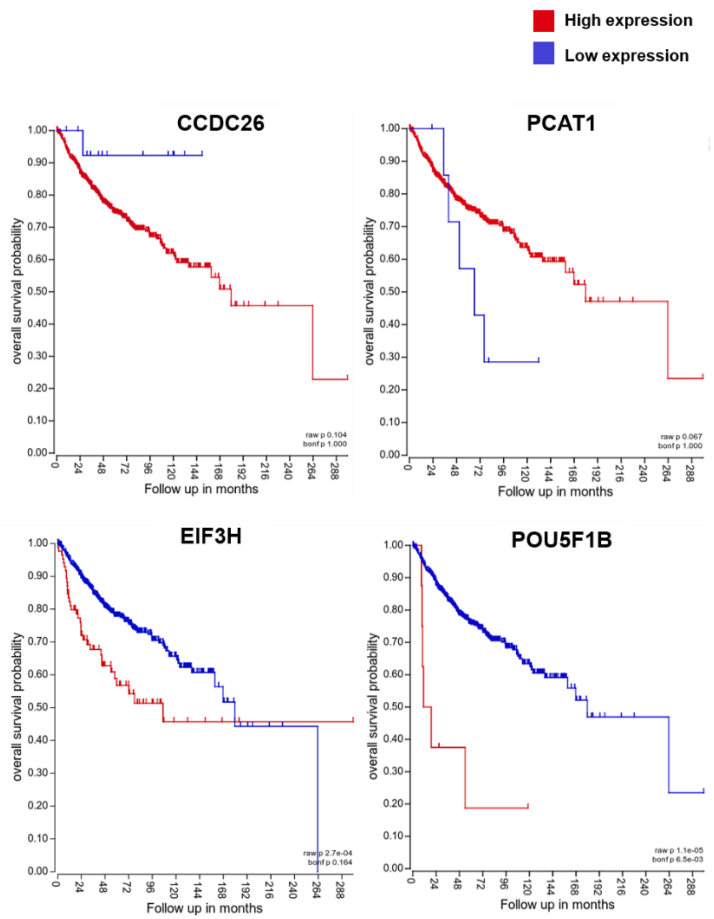

B

Gene	Overall survival based on expression
TMEM260	Low is worse p=2.4e-04
DLG1	High is worse p=1.5e-04
PAPPA2	High is worse p=6.1e-06
SPATA17	Low is worse p=0.021
STPG2	Low is worse p=0.053
ADGRV1	High is worse p=0.015
DNAH14	Low is worse p=1.0e-03
DNM3	High is worse p=0.012
EIF4G3	High is worse p=3.4e-03
FAM189A1	High is worse p=0.015
FAM84B	Low is worse p=0.017
CCDC26	High is worse p=ns (p=0.104)
PCAT1	High is worse p=ns (p=0.067)
RP11-382A18.1 (EIF3H)	Low is worse p=2.7e-04
POU5F1B	High is worse p=1.1e-05

Group 3
Group 4
Combined

Figure 5.12 Kaplan-Meier overall survival for medulloblastoma patients according to expression of identified genes

Kaplan-Meier overall survival analysis of high and low expression of the identified genes in medulloblastoma patients on the R2 Genomics Analysis and Visualization Platform using the Cavalli dataset. (A) Example of Kaplan-Meier plots for all genes enriched in both Group 3 and Group 4 exosomes (combined). (B) Summary of Kaplan-Meier plots for all identified genes. Log rank test was performed to generate *P* values.

5.6 Identification of exosomal markers in metastatic samples

The gene expression data from this study offers an abundance of information, which can be interpreted in numerous different ways. To remain in line with the aim of identifying target genes in exosomes that play a role in medulloblastoma progression, NCBI literature and Exocarta databases were used to answer the following questions regarding candidate genes *POU5F1B, PCAT1* and *PAPPA2*:

1. Does the identified gene have a role in cancer progression and metastasis?
2. Is there any evidence for this gene in extracellular vesicles?
3. Is the identified gene known to play a role in medulloblastoma?

Results of the above questions are summarised in Table 5.4.

Table 5.4 Summary of role of candidate exosomal genes in cancer, extracellular vesicles and medulloblastoma

Gene name, Log2FC, protein function, role in cancer progression and metastasis, evidence in extracellular vesicles and evidence in medulloblastoma for each gene is summarised in the table below.

Gene	Log2FC		Protein function	Role in cancer progression and metastasis	Evidence in extracellular vesicles	Evidence in medulloblastoma
POU5F1B	Combined	1.91	*POU5F1B* (POU Class 5 Homeobox 1B) is a protein coding gene encoding a transcriptional activator and may play a role in carcinogenesis.	Amplification associated with poor prognosis and promotes an aggressive phenotype in gastric cancer (Hayashi et al., 2015) Promotes hepatocellular carcinoma proliferation by activation of AKT (Pan et al., 2018) POU5F1B knockdown suppressed cell proliferation and improved radiosensitivity of oesophageal carcinoma cells (Meng et al., 2018)	POU5F1B gene was detected in microvesicles from medulloblastoma, glioblastoma and fibroblast cells by PCR (Balaj et al., 2011)	High OCT4A/POU5F1 levels drive tumorigenicity and metastatic potential of medulloblastoma cells (Gonclaves da Silva et al., 2017 Expression analysis reveals OCT4 as a predictor of poor clinical outcome in medulloblastoma (Ridini et al., 2012) Amplified POU5F1B gene is an indicator of poor prognosis and a useful biomarker in brain cancers (Zao *et al.,* 2011*)*
	Group 3	1.51				
	Group 4	3.07				
PCAT1	Combined	1.86	*PCAT1* (Prostate Cancer Associated Transcript 1) gene produces a long non-coding RNA that promotes cell proliferation and is upregulated in prostate, colorectal, and other cancers. This RNA negatively regulates the BRCA2 tumour suppressor protein and positively regulates Myc oncoprotein.	PCAT1 is a poor prognostic factor in endometrial carcinoma and associated with cancer cell proliferation, migration and invasion (Zhao et al., 2019) Depletion of PCAT-1 in head and neck cancer cells inhibits tumor growth and induces apoptosis by modulating c-Myc-AKT1-p38 MAPK signalling pathways (Sur et al., 2019)	PCAT1 was present in oesophageal squamous cell carcinoma (ESCC) cell-derived exosomes, was higher in the serum of ESCC patients than those of healthy volunteer donors, and promoted cell growth through exosomes (Huang et al., 2019) Exosomal PCAT-1 overexpression was a prognostic factor associated with poor recurrence-free survival (RFS) of non-muscle-invasive bladder cancer (Zhan et al., 2018)	No evidence in medulloblastoma. PCAT1 knockdown restrained glioma stem cell sphere-formation ability, increased the apoptosis rate and DNA damage under the treatment of radiation. Moreover, knockdown of PCAT1 inhibited cell proliferation (Zhang et al., 2018)
	Group 3	1.68				
	Group 4	3.32				
PAPPA2	Combined	1.07	*PAPPA2* gene encodes a member of the pappalysin family of metzincin metalloproteinases. The encoded protein cleaves insulin-like growth factor-binding protein 5 and is thought to be a local regulator of insulin-like growth factor (IGF) bioavailability.	Acts as an oncogene outside of pregnancy. PAPPA2 overexpression observed in many malignancies (Guo *et al.,* 2018). Accumulating evidence has also shown the oncogenic functions of PAPPA2, including promoting cancer cell proliferation (Boldt and Conover 2011) , migration, invasion and metastasis (Tanaka *et al.,* 2004); thus, PAPPA2 may be a target for chemotherapy.	PAPPA2 mRNA was identified in mesenchymal stem cell-derived microvesicles (Bruno *et al.,* 2009) PAPPA2 protein was detected in urinary derived exosomes (Wang *et al.,* 2012).	No evidence in medulloblastoma Genome-wide association study across pediatric central nervous system tumors implicates shared predisposition and points to 1q25.2 (PAPPA2) and 11p12 (LRRC4C) as novel candidate susceptibility loci (Foss-Skiftesvik *et al.,* 2020)
	Group 3	1.05				
	Group 4	1.85				

5.7 Exosomal *PCAT1*, *PAPPA2* and *POU5F1B*- novel biomarkers in medulloblastoma progression

5.7.1 *PCAT1, PAPPA2* and *POU5F1B* expression levels were up-regulated in medulloblastoma patients and metastatic cell lines

As previously observed, *PCAT1, PAPPA2* and *POU5F1B* display differential expression across medulloblastoma subgroups, with expression levels being significantly higher in Group 3 and/or Group 4 compared to other subgroups (Figure 5.10D). To assess the diagnostic ability of *PCAT1, PAPPA2* and *POU5F1B* in distinguishing medulloblastoma patients from healthy controls, the R2 Genomics Analysis and Visualization Platform R2 genomics was used to compare expression levels of candidate genes in medulloblastoma patients compared to non-tumour normal brain tissue. The MegaSampler function was used to assess gene expression in two datasets: Harris and Pfister. Harris consisted of normal brain samples (n=44) and served as normal control against the medulloblastoma samples in the Pfister dataset, which were categorised into the molecular subgroups (WNT: n=17; SHH: n=59; Group 3: n=56; Group 4: n=91). The Pfister dataset was used in this instance, as the Cavalli dataset is not compatible with the MegaSampler function. Significant differences in gene expression compared to normal brain samples were calculated using the Kruskal-Wallis test with Dunn's multiple comparisons post-hoc test.

PCAT1 expression was significantly elevated in all four molecular subgroups of medulloblastoma compared with normal brain controls (****p≤0.0001) (Figure 5.13A). In addition, *PAPPA2* expression was found to be significantly elevated in group 3 and group 4 molecular subgroups compared to normal brain control samples (****p≤0.0001) (Figure 5.13B). Likewise, *POU5F1B* expression was found to be significantly elevated in WNT, Group 3 and Group 4 subgroups compared to normal brain samples (****p≤0.0001, ****p≤0.001, **p≤0.01 respectively) (Figure 5.13C).

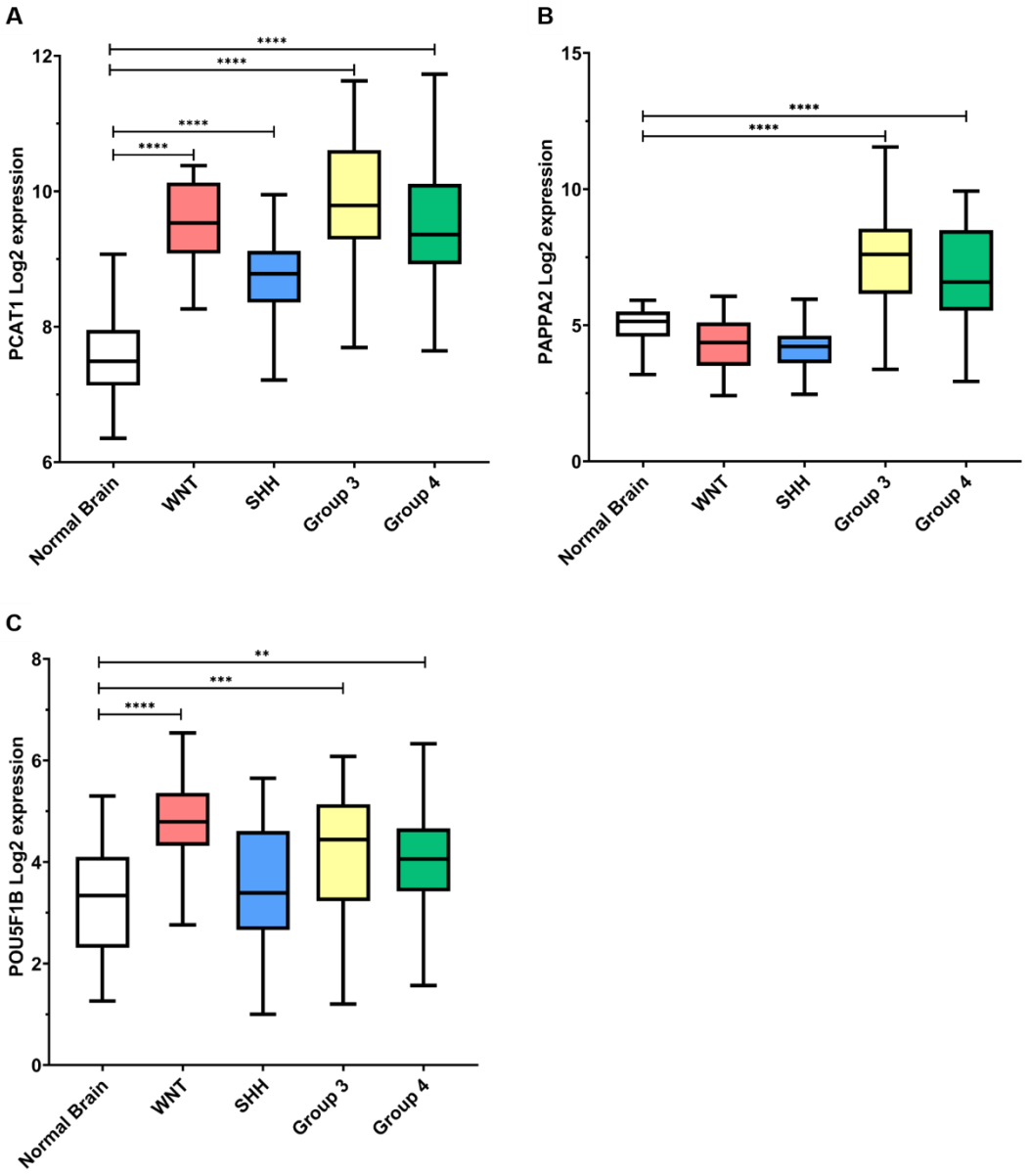

Figure 5.13 ***PCAT1, PAPPA2* and *POU5F1B* patient gene expression analysis**

Gene expression (Log2) of *PCAT1, PAPPA2* and *POU5F1B* was assessed on the R2 Genomics Analysis and Visualisation Platform. The MegaSampler function was used to assess *PCAT1* (A), *PAPPA2* (B) and *POU5F1B* (C) gene expression in two datasets: Harris and Pfister. Harris consisted of normal brain samples (n=44) and served as normal control against the medulloblastoma samples in the Pfister dataset (WNT: n=17; SHH: n=59; Group 3: n=56; Group 4: n=91). Significant differences in gene expression compared to the normal brain were calculated using the Kruskal-Wallis test with Dunn's multiple comparisons post-hoc test (**p≤0.01, ***p≤0.001, ****p≤0.0001).

5.7.2 Exosomal RNA content reflects metastatic cell line status

As previously mentioned, exosomes display several features which make them an ideal source of cancer biomarkers, such as exosomal content reflecting the tumour state and its microenvironment (Kobayashi *et al.*, 2014). The presence of specific cellular protein and RNA from originating cells provides comprehensive information about the tumour. As such, the expression of candidate genes, *PCAT1, PAPPA2* and *POU5F1B,* in corresponding medulloblastoma parental cell lines by qRT-PCR was analysed (Figure 5.14). Unfortunately, *PCAT1* gene expression in medulloblastoma cell lines could not be determined due to failed primers and time constraints.

The pattern of enrichment seen in mRNA sequencing data, showed a similar trend to that of the cellular expression (Figure 5.14) with highest expression of *PAPPA2* and *POU5F1B* being seen in metastatic cell lines (D458 and CHLA-01-R) compared to that in the matched primary cell lines (D425 and CHLA-01). Since, for *PAPPA2* and *POU5F1B* expression exosomal cargo appears to reflect that of parental cell line, they could provide comprehensive information about the metastatic status of medulloblastoma patient tumours. Taken together, these observations suggest *PAPPA2* and *POU5F1B* enriched in metastatic exosomes could be promising markers for medulloblastoma progression.

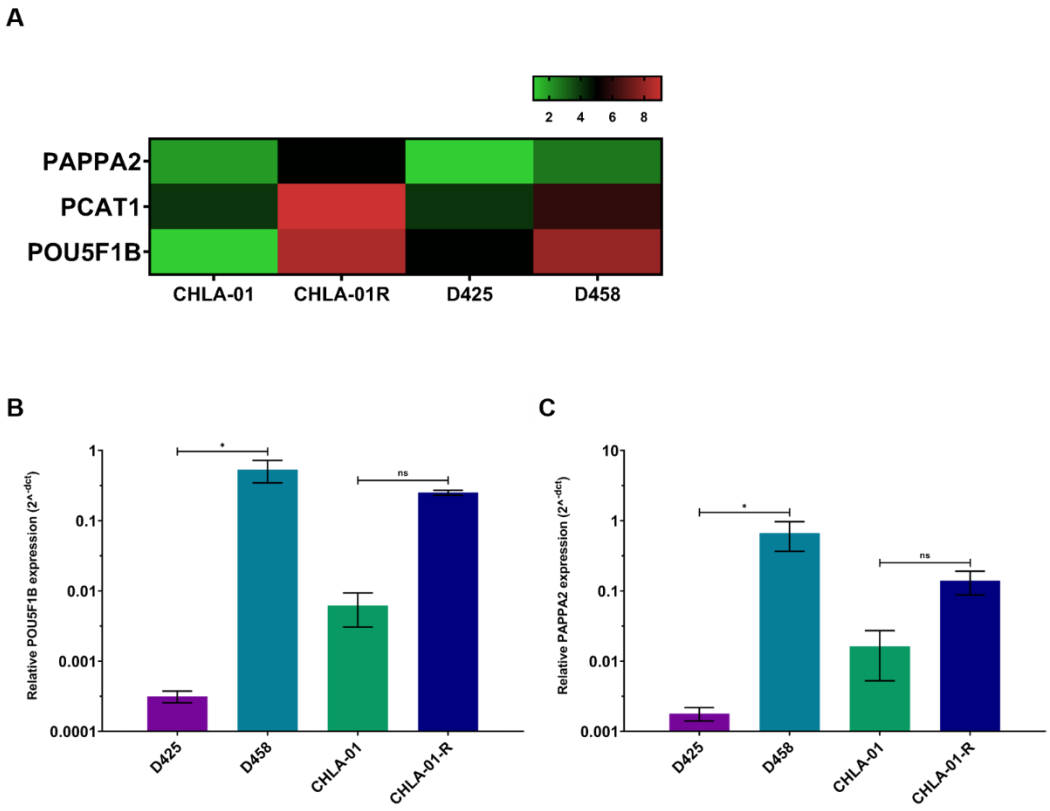

Figure 5.14 Patterns of *PAPPA2* and *POU5F1B* expression in exosomes and their parental cells

PAPPA2 and *POU5F1B* were identified as being enriched in metastatic medulloblastoma-derived exosomes compared to primary exosomes from RNA-sequencing, the colour scale signifies the relative expression level of a gene across the samples (A). (B) *PAPPA2* and *POU5F1B* expression in medulloblastoma parental cell lines D425, D458, CHLA-01 and CHLA-01R was assessed by quantitative real-time PCR. Data represent the average of three independent experiments with error bars indicating standard error of the mean (SEM). Significance was calculated using one-way ANOVA analyses with Sidak's multiple comparisons post-hoc test (*p≤0.05, ns=not significant).

5.7.3 *POU5F1B* and *PAPPA2* can be transferred to medulloblastoma cells by exosomes

In addition to using exosomal mRNA cargo as predictive biomarkers for metastatic medulloblastoma, we aimed to examine whether these exosomes are capable of delivering their RNA content to recipient cells. To determine this, metastatic exosomes with high levels of *POU5F1B* and *PAPPA2* were isolated from donor cells (D458 and CHLA-01R) and co-cultured with primary low expressing *POU5F1B* and *PAPPA2* recipient cells (D425 and CHLA-01) for 24 hours (Figure 5.15A). Expression levels of *POU5F1B* and *PAPPA2* was measured in recipient cells by qRT-PCR and compared to vesicle-free supernatant treated control cells. The results showed that metastatic-derived exosomes can transfer RNA to recipient cells. Expression levels of *PAPPA2* increased in recipient cells CHLA-01 and D425 following exposure of metastatic exosomes (fold-change 1.78 and 3.8 respectively), however results were non-significant (Figure 5.15B). Similarly, expression levels of *POU5F1B* increased in recipient cells CHLA-01 and D425 following exposure of metastatic exosomes (fold-change 2.4 and 4.5 ***$p \leq 0.001$ respectively) (Figure 5.15C). In contrast, there was no increase in expression levels of RNA when recipient cells were treated with vesicle-free supernatant, suggesting that cellular RNAs can be transferred to recipient cells in an exosome-dependent manner.

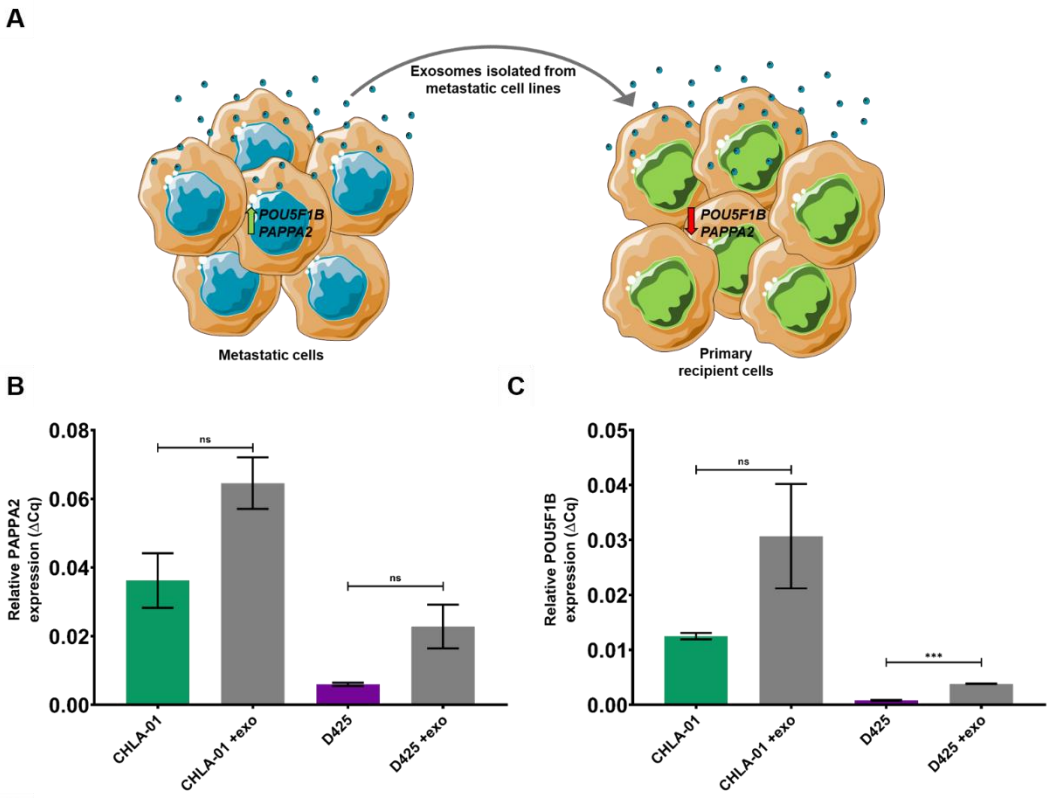

D

Cell line	Gene name	Fold-change
CHLA-01	PAPPA2	1.78
D425		3.8
CHLA-01	POU5F1B	2.4
D425		4.5

Figure 5.15 *PAPPA2* and *POU5F1B* can be transferred to recipient's cells via exosomes

Schematic representation of exosomes isolated from metastatic cells (D458 or CHLA-01R) containing high levels of *POU5F1B and PAPPA2*, co-cultured with primary medulloblastoma cells (D425 or CHLA-01R) containing low levels of *POU5F1B and PAPPA2* (A). *POU5F1B* (B) *and PAPPA2* (C) expression in primary cells was determined by qRT-PCR. Significance differences were calculated using one-way ANOVA analyses with Dunnet's multiple comparisons post-hoc test, (***p≤0.001, ns=non-significant), compared to control cells (grey). (D) Fold-differences were calculated between exosome treated cells compared to vesicle-free supernatant treated control cells. Data represent the average of two independent experiments with error bars indicating standard error of the mean (SEM).

5.8 Summary

- The characterisation of mRNA cargo by NGS sequencing of medulloblastoma exosomes, delineates the targeting of pathways important for medulloblastoma progression and interaction with the surrounding microenvironment.
- Differential gene expression analysis identified numerous mRNA candidates which were significantly enriched in metastatic exosomes compared to primary exosomes. Extensive bioinformatics and literature based evidence identified *PCAT1, PAPPA2* and *POU5F1B* as candidates for further study.
- Investigation of *PCAT1, PAPPA2* and *POU5F1B* expression across large-scale medulloblastoma gene expression datasets correlated elevated expression with poor overall survival and tumour metastasis. In addition, candidate gene expression was higher in medulloblastoma subgroups compared to normal brain controls.
- The pattern of enrichment seen in exosome sequencing data, showed a similar trend to that of the cellular expression, with highest expression of *PAPPA2* and *POU5F1B* being seen in metastatic cell lines; providing further evidence that exosomal cargo appears to reflect that of the parental cell line. Therefore, levels of *POU5F1B* and *PAPPA2* in exosomes may be a useful prognostic marker for medulloblastoma progression.
- Finally, exosomes derived from cells containing high levels of *POU5F1B* and *PAPPA2* can shuttle this RNA to cells to increase recipient cell expression.

Chapter 6

Identifying exosomal miRNAs involved in medulloblastoma progression using next-generation sequencing technologies

Chapter 6. Identifying exosomal miRNAs involved in medulloblastoma progression using next-generation sequencing technologies

6.1 Introduction

In the previous chapter, genes were identified which are likely to be linked to cell migration and medulloblastoma metastasis by comparing exosomal mRNA packaged into metastatic exosomes with matched primary exosomes. As previously mentioned, multiple RNA species have been identified in exosomes. Therefore, to further explore the RNA cargo of medulloblastoma exosomes this chapter aimed to investigate the exosomal miRNA profiles of metastatic medulloblastoma. The identified miRNA profiles were then assessed in patient-derived CSF samples to substantiate their importance in medulloblastoma patients.

MicroRNAs (miRNAs) are a class of highly conserved non-protein encoding, single-stranded RNA molecules of ~20-25 nucleotides in length. They function in gene silencing and post-transcriptional regulation of gene expression (Lee, Feinbaum and Ambros, 1993). In cancer they are often heavily dysregulated and have been implicated in all aspects of carcinogenesis (reviewed by Peng and Croce, 2016). Their presence and intercellular transfer in exosomes has provoked deeper investigation of exosomal miRNAs, as novel non-invasive biomarkers and as intracellular signalling vehicles (Kobayashi *et al.*, 2014; Shi *et al.*, 2015; Bland *et al.*, 2018; Peacock *et al.*, 2018; S. Huang *et al.*, 2020).

Similar to mRNA cargo, profiling studies have revealed that exosomes of different cellular origin contain a unique expression profile and that tumour characteristics of their cell of origin could be detected in exosomes, thus representing a snapshot of the content of the secreting cell (Di Modica *et al.*, 2017). The correlation between tumour-exosome and tumour-cell content is particularly valuable where the ability to conduct a tissue biopsy is limited, such as tumours of the brain or central nervous system. For

example, a study by Shi and colleagues profiling exosomes from the CSF of seventy glioma patients revealed that they contained significantly elevated levels of miR-21 relative to healthy controls, and that exosomal miR-21 levels reflected tumour burden (Shi *et al.*, 2015). Prognostically informative exosomal miRNA signatures have similarly been identified in exosomes derived from; breast cancer patient plasma (Di Modica *et al.*, 2017), human colorectal cancer cell lines (Fu *et al.*, 2018) and exosomes isolated from patients with pancreatobilliary tract cancer (Machida *et al.*, 2016). Taken together, these studies strongly suggest that exosomal miRNAs may serve as non-invasive biomarkers for early disease detection, monitoring or prognosis establishment in cancer.

6.2 Characterisation of medulloblastoma exosomal miRNA by NGS sequencing

In addition to mRNA, miRNA from the same sample of matched primary- and metastatic-derived exosomes was also sequenced. For miRNA NGS we adopted traditional RNA sequencing which required at least 100 ng of RNA per sample.

6.2.1 Sample preparation

The experimental workflow for NGS sequencing is summarised in Figure 5.3. Following sample preparation and quantification as outlined in Chapter 5, libraries were prepared and sequenced. Library preparation was performed using the QIAseq miRNA library preparation kit. A total of 100 ng of purified RNA was converted into cDNA NGS libraries. During reverse transcription, the RNA molecule is tagged with a unique molecular index (UMI). Then RNA was converted to cDNA. The cDNA was amplified using PCR (22 cycles) and during the PCR, indices were added. After PCR the samples were purified and underwent a second round of quality control. All prepared libraries successfully passed QIAGEN's internal quality control checks and were sequenced on a NextSeq500 sequencing instrument (Illumina). Following sequencing, raw data was de-multiplexed and FASTQ files for each sample were generated using

the bcl2fastq software. All samples were considered suitable for primary and secondary downstream data analysis.

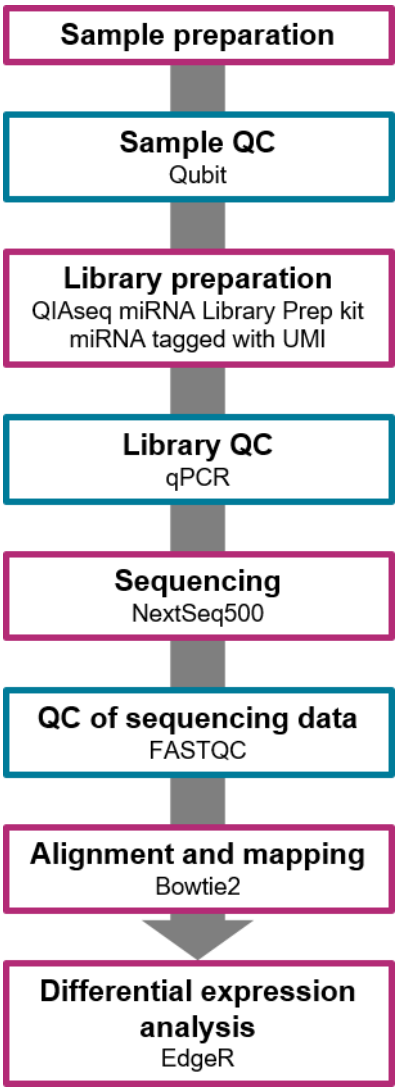

Figure 6.1 Experimental workflow for NGS sequencing

The workflow for the preparation of samples for NGS-sequencing is shown above.

6.2.2 Mapping of sequencing data

Mapping of sequencing data was performed as an additional control step to evaluate the quality of each sample. Typical miRNA sequencing experiments yields approximately 60-90% of the reads mapping to the reference genome. On average 10.9 million UMI-corrected reads were obtained for each sample and the average percentage of mapable reads was 73.0%. Sequencing reads were also mapped using miRBase to identify miRNAs, the percentage of reads that represented miRNAs varied between samples. A summary of the mapping results for each sample is shown in Table 5.2. The reads were classified into the following classes:

6) **miRNA:** maps to mirBase
7) **Genome:** aligning to reference genome
8) **"Outmapped":** For example polyA and polyC homopolymers as well as abundant rRNA and mtRNA sequences
9) **Unmapped reads:** no alignment to reference genome possible

Table 6.1 Mapping of NGS sequencing data

Mapping of sequencing data was performed as an additional control step to evaluate the quality of each sample. The number of reads and mapping results (aligned to miRNA, aligned to genome, outmapped and unmapped).

Sample number	Cell line exosomes derived from	Phenotype	Reads	Mapping results			
				miRNA	Genome	Outmapped	Unmapped
500	CHLA-01	Primary	10,089,710	28.7%	14.8%	36.8%	15.4%
501		Primary	9,952,859	11.8%	16.6%	57.8%	12.7%
502		Primary	12,897,937	5.6%	14.2%	35.2%	39.9%
503	CHLA-01-R	Metastatic	15,580,451	2.2%	27.7%	14.1%	55.6%
504		Metastatic	10,945,110	13.0%	12.4%	51.0%	22.0%
505		Metastatic	14,090,587	8.5%	8.4%	65.4%	14.5%
506	D458	Metastatic	7,358,483	1.6%	8.8%	79.2%	10.2%
507		Metastatic	10,003,686	1.5%	9.4%	63.3%	25.4%
508		Metastatic	12,997,130	1.0%	8.8%	75.7%	14.0%
509	D425	Primary	10,860,129	1.7%	8.8%	74.4%	13.0%
510		Primary	3,217,034	15.6%	14.5%	54.7%	14.5%
511		Primary	8,458,226	2.2%	8.8%	75.9%	11.4%
512	FB83	Normal	12,830,132	8.6%	18.8%	7.4%	59.1%
513		Normal	13,895,169	7.5%	10.1%	39.1%	36.8%
514		Normal	21,833,881	0.3%	27.4%	4.0%	67.5%

6.3 Global miRNA signature correlated with malignant and subgroup status

In order to determine whether exosomal miRNA could be used to distinguish primary from metastatic or malignant from normal, we calculated the biological coefficient of variation (“distance”) of our 14 samples using a multidimensional scaling (MDS) plot. MDS plots create a low-dimensional representation of the samples from a data set. MDS is a useful tool to visualize the level of similarity of each individual sample. If the biological differences between the samples are pronounced, this will describe the dimensions of the variation in the data. This leads to the separation of samples in different regions of a MDS plot corresponding to their biology. However, if other factors such as sample quality introduce more hidden variation in the data, the samples may

not cluster according to the biology. At this point, sample 514 (FB83 sample) was excluded from further analysis as it clustered separately to equivalent samples (Appendix Figure 5), this was in line with mRNA-seq data (Chapter 5, Table 5.1) as sample 514, had the lowest number of detected genes.

To compare miRNA profiles between primary and metastatic exosomes, low-abundance miRNAs were removed (exclusion criteria set at TMM (normalised read counts) ≤10 in at least two replicates). An MDS plot was created to allow a visual overview of how the samples cluster based on miRNA levels (Figure 6.2), all samples from the same subgroup (Group 3 or Group 4) could be grouped together, however looking at all miRNA together did not distinguish between phenotype (metastatic or primary). The MDS plot did however, show a clear separation of normal-derived exosomal miRNA compared to medulloblastoma exosomal miRNA profiles.

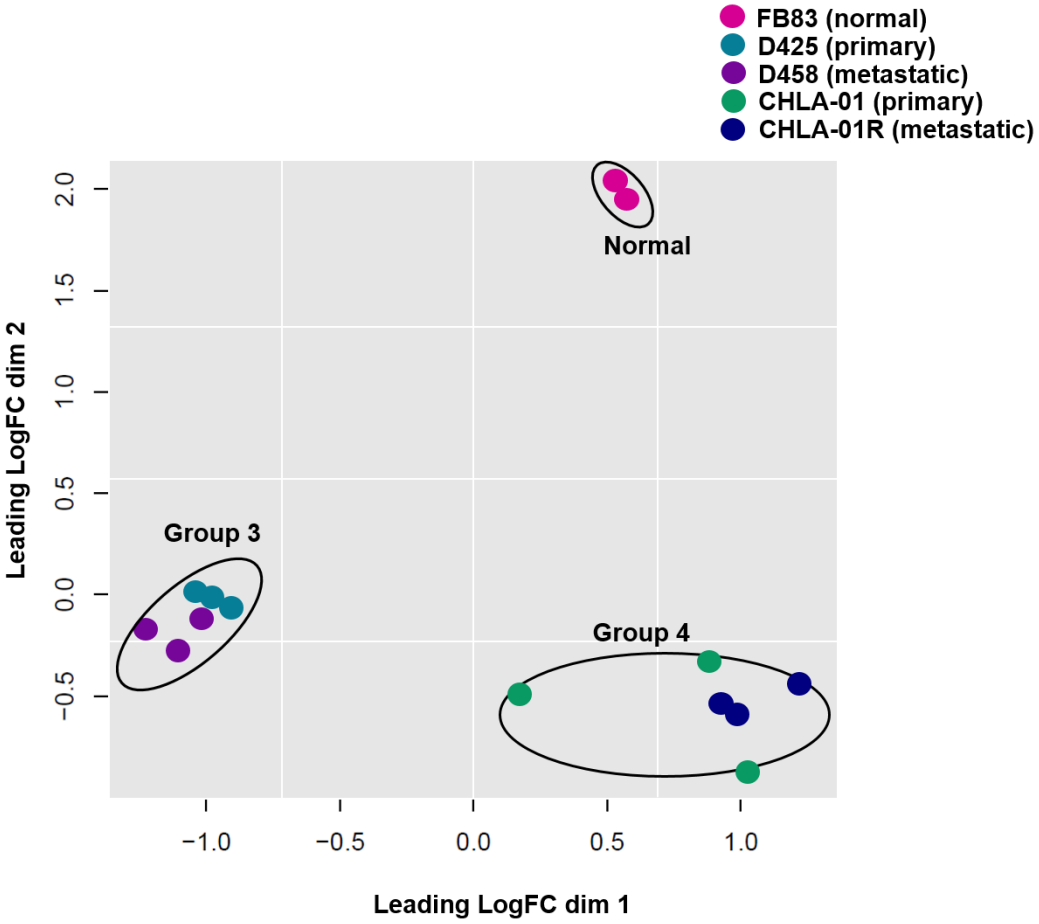

Figure 6.2 Multidimensional scaling plot (MDS) for all samples

The MDS plot was performed on all samples using exosomal miRNA which had a minimum read number of ≤10, the data is normalized with weighted trimmed mean of M-values (TMM) method and an overview of how the samples cluster based on miRNA levels is obtained. The MDS plot shows variation among the RNA-seq samples, distance between the samples indicates dissimilarity.

6.3.1 Visualization of miRNA with large magnitude changes

As we were unable to differentiate exosomal miRNA profiles between metastatic and primary-derived exosomes, we next used a smaller number of miRNAs which had a larger magnitude change to determine if we could discriminate metastatic from primary.

To investigate large differences in exosomal miRNA profiles, unsupervised analyses of the top 50 most differentially expressed miRNA between normal, primary and metastatic-derived exosomes was performed. Here, by including the top 50 miRNAs that have the largest variation across all samples, an overview of how the samples cluster based on this variance is obtained. This generated a heatmap showing unbiased hierarchal clustering of 50 differentially expressed miRNAs, each row represents a miRNA and individual samples are displayed in columns along the bottom (Figure 5.7). The colour scale signifies the relative expression level of a miRNA across all samples. Red represents a miRNA expression level above the mean; green represents a miRNA expression level below the mean. Despite reducing the number of miRNAs analysed to 50 which showed the largest variation between samples, again there was no clear separation between primary and metastatic samples. Aside from one sample, all samples from the same subgroup (Group 3 or Group 4) clustered together, confirming the conclusions drawn from the MDS plot. Again, similarly to the MDS plot, the heatmap showed a clear separation of normal-derived exosomal miRNA compared to medulloblastoma exosomal miRNA profiles. Taken together, these observations suggests that exosomal miRNA cargo might be useful to detect and possibly subgroup medulloblastoma disease.

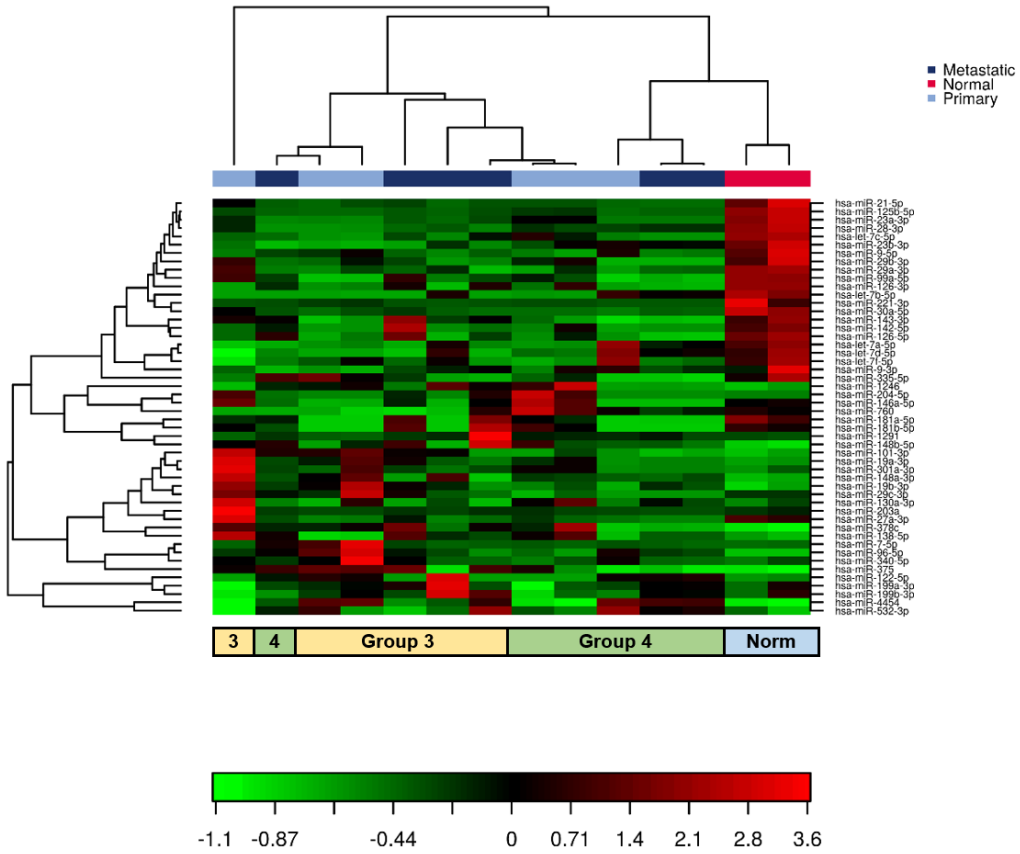

Figure 6.3 Heatmap of unbiased clustering of all samples

Unsupervised transformed miRNA counts were used to create a heatmap representing the top 50 miRNA with the largest variance across all samples. The heatmap shows unbiased hierarchal clustering of samples, each row represents a gene and individual samples are displayed in columns along the bottom. The colour scale signifies the relative expression level of a gene across all samples. Expression levels above and below the mean are displayed in green and red, respectively.

6.3.2 Identification of specific miRNA associated with metastatic exosomes

After having established that differentially expressed exosomal miRNA profiles could discriminate between medulloblastoma cell lines compared to normal controls but not specific phenotypes (metastatic or primary), we next looked at specific miRNA which were associated with metastatic exosomes, and could therefore potentially be associated with medulloblastoma metastasis.

When looking at differential expression between the subgroups, after normalisation, a total of 403 miRNA were shown to display differential levels of expression between primary and metastatic exosomal miRNA in Group 3. For Group 4, there were 441 miRNA which had differential levels of expression between primary and metastatic and a total of 447 miRNA were demonstrated to exhibit different levels of expression in medulloblastoma-derived exosomes relative to normal control-derived exosomes. In addition we also examined miRNA that were present in high abundance (>200 TMM) in all exosomes. In total 88 miRNA were very abundant in all exosome samples, independent of subgroup, phenotype or malignancy status. Table 6.2 shows the top 10 miRNAs found abundant in all exosomes.

Table 6.2 miRNA most abundant across all samples

The table shows the top 10 miRNAs which were present at high abundance in all samples

miRNA	Average TMM
miR-30d-5p	981
miR-20a-5p	794
miR-378a-3p	834
miR-148b-3p	641
miR-34a-5p	656
let-7f-5p	2174
let-7i-5p	3210
miR-26b-5p	960
miR-25-3p	2205
miR-151a-3p	508

In order to identify specific miRNAs associated with metastatic-derived exosomes, fold differences were calculated between metastatic- and primary-derived exosomes, with a cut-off of log2 fold change threshold of >1 in either direction and *p* value of ≤0.05. Using this approach, we identified 30 miRNAs significantly enriched and 54 miRNAs significantly depleted in Group 3 metastatic exosomes (Figure 5.8). In Group 4 metastatic exosomes, we identified 35 enriched and 83 depleted miRNAs compared to Group 4 primary exosomes. Interestingly, 14 were enriched in all metastatic-derived exosomes and 8 were depleted in all metastatic-derived exosomes (Figure 6.5).

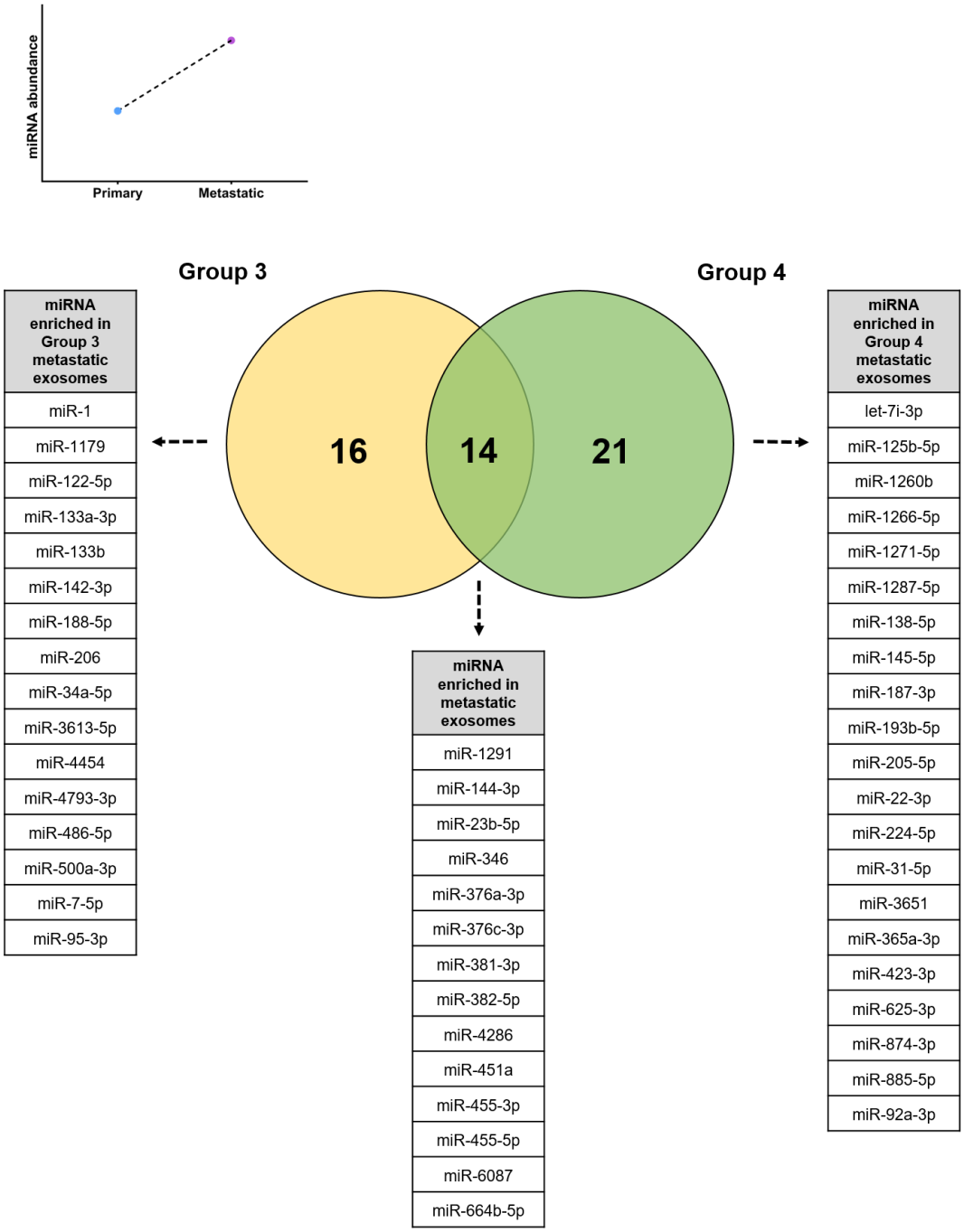

Figure 6.4 Venn diagram comparing enriched miRNA in metastatic exosomes

Differential miRNA expression analysis was conducted to identify miRNA enriched in metastatic exosomes compare to primary exosomes. Line graph represents direction of enrichment between primary and metastatic exosomes. A Venn diagram was constructed showing the overlap between significant enriched miRNA (log2 fold change threshold of >1 and *P* value of <0.05) identified in metastatic Group 3 and metastatic Group 4-derived exosomes.

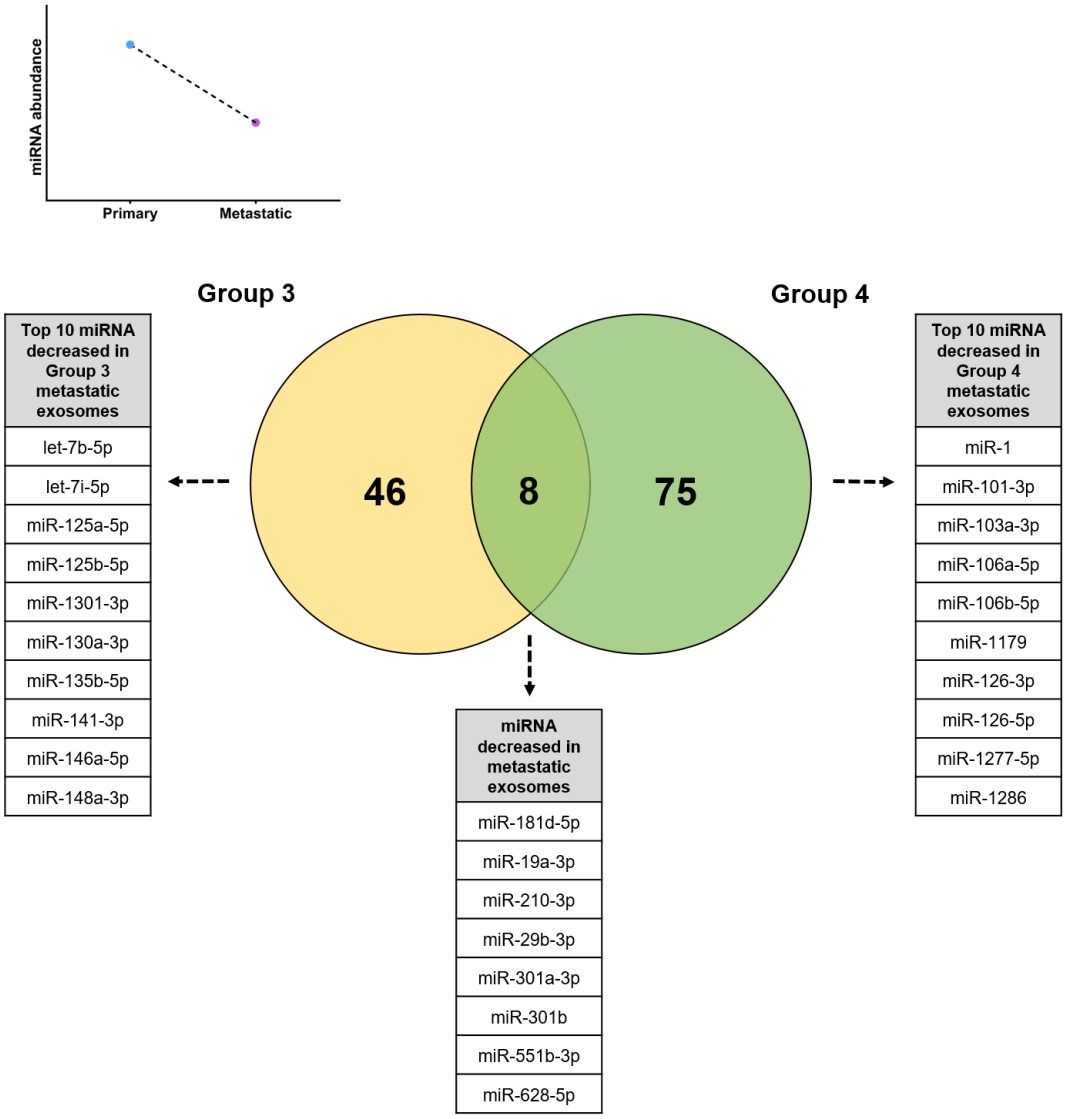

Figure 6.5 Venn diagram comparing decreased miRNA in metastatic exosomes

Differential miRNA expression analysis was conducted to identify miRNA decreased in metastatic exosomes compare to primary exosomes. A Venn diagram was constructed showing the overlap between significant decreased miRNA (log2 fold change threshold of >1 and *P* value of <0.05) identified in metastatic Group 3 and metastatic Group 4-derived exosomes. Line graph represents direction of enrichment between primary and metastatic exosomes.

The analysis above looked at miRNAs whose expression changed between primary and metastatic cell-derived exosomes. Additional comparisons aimed to investigate these same miRNAs in normal control cell exosomes to establish if there were any trends in miRNA expression that could be of interest from the perspective of biomarker discovery. Of the 14 miRNA which were significantly enriched in all metastatic exosomes, 8 (miR-451a, miR-144-3p, miR-381-3p, miR-376a-3p, miR-382-5p, miR-376c-3p, miR-346, miR-23b-5p) were also found at significantly lower levels in normal control exosomes compared to all medulloblastoma samples (Figure 6.6). We also looked at miRNAs downregulated in metastatic exosomes, from the 8 which overlapped in all metastatic exosomes, 4 (miR-628-5p, miR-301b, miR-551b-3p, miR-19a-3p) were shown to be significantly higher in normal control samples compared to medulloblastoma samples (Figure 6.7).

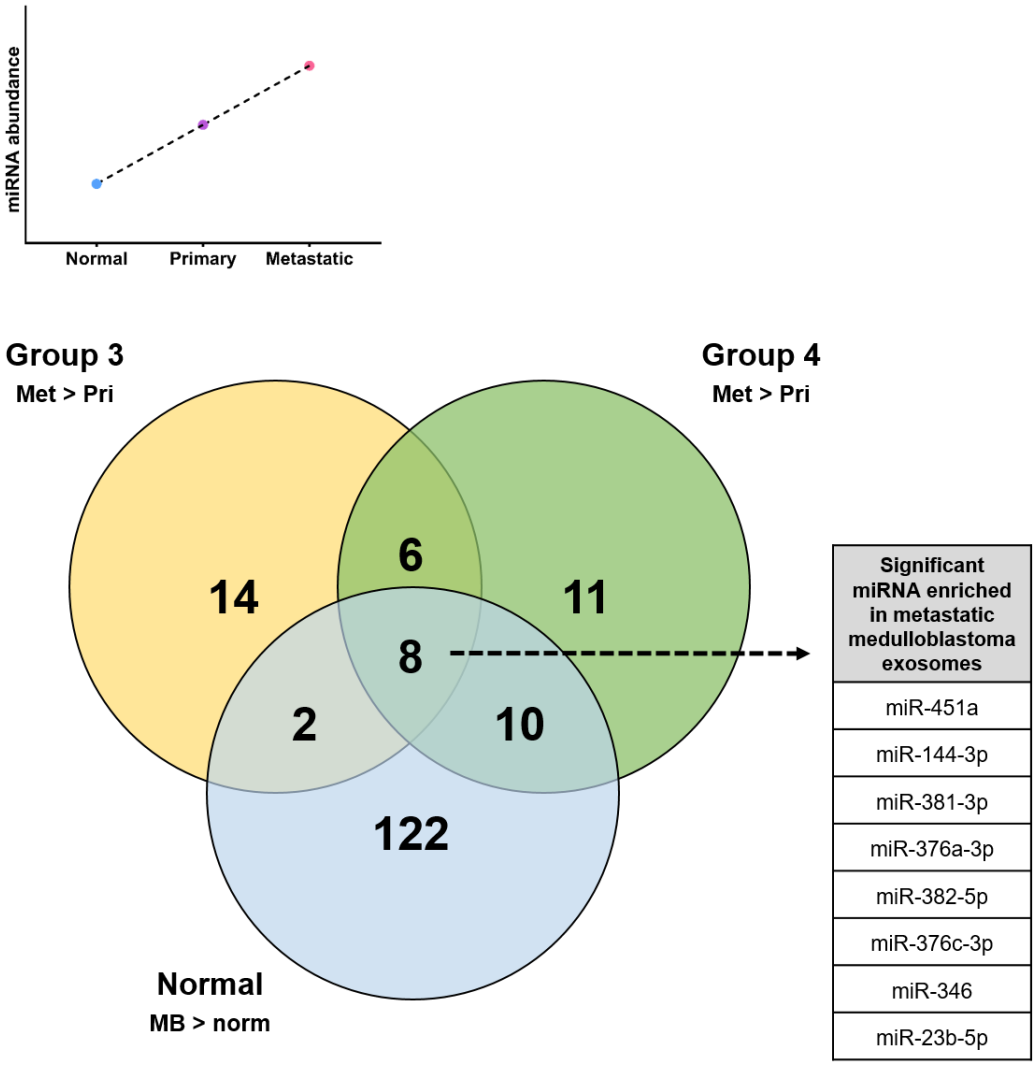

Figure 6.6 Venn diagram comparing enriched miRNA in metastatic exosomes and decreased in normal exosomes

miRNA which were previously identified as being enriched in metastatic exosomes compared to primary, were overlapped with miRNA that were downregulated in normal exosomes compared to all malignant exosomes. Line graph represents direction of enrichment between normal, primary and metastatic exosomes.

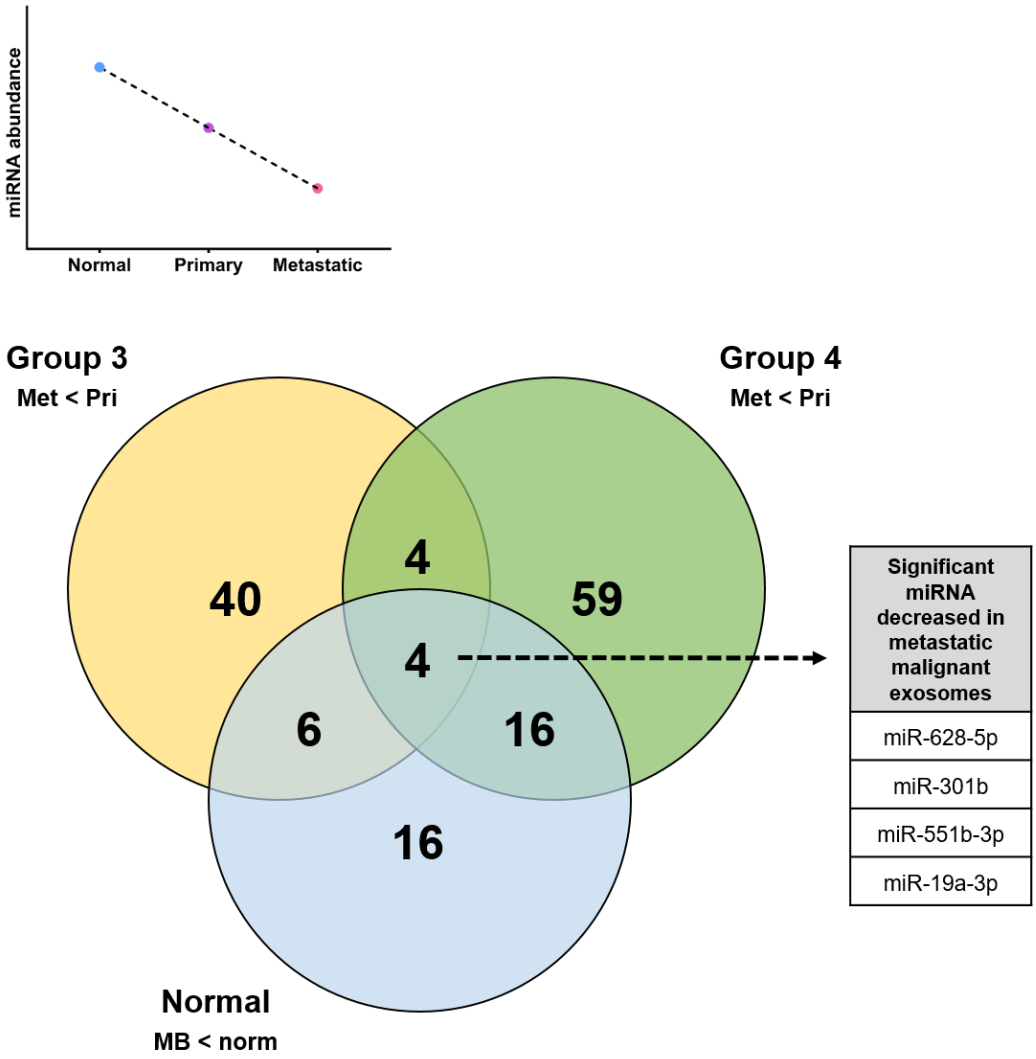

Figure 6.7 Venn diagram comparing decreased miRNA in metastatic exosomes and enriched in normal exosomes

miRNA which were previously identified as being decreased in metastatic exosomes compared to primary, were overlapped with miRNA that were enriched in normal exosomes compared to all malignant exosomes. Line graph represents direction of enrichment between normal, primary and metastatic exosomes.

6.3.3 Functional miRNA pathway analysis

Having identified exosomal miRNAs which may show a progression signature of potential biological interest from control to primary to metastases of the producing cell, pathway enrichment analysis was conducted to explore the potential role these miRNA could play in medulloblastoma tumour progression.

Pathway analysis was performed on the 12 exosomal miRNA (8 enriched and 4 decreased) identified from differential expression analysis. Utilizing miRDB, a database of known and predicted miRNA-target interactions (Chen and Wang 2020), target gene prediction was performed on the candidate miRNAs. The lists generated were inputted into Gene Set Enrichment Analysis (GSEA) to elucidate which signalling pathways were being regulated in cancer cells (by transfer of miRNA via exosomes). GSEA Kyoto Encyclopaedia of Genes and Genomes (KEGG) and Gene Ontology (GO) were assessed with a stringency criteria of Benjamini-Hochberg correction ≤0.05. The KEGG and GO pathways identified as probable downstream targets are shown in Figure 6.8.

The subset of miRNAs were enriched for those targeting genes involved in pathways in cancer and other major cancer-associated KEGG pathways, including cell signalling; MAPK, PI3K/AKT, Wnt and TGF-beta. The KEGG pathway ‘vesicle mediated transport’ had the top number of overlapping genes (Figure 6.8A). In addition, there was an enrichment of pathways related to migration including focal adhesion and regulation of the actin cytoskeleton. Also of note was the heavy enrichment of GO biological processes related to differentiation, locomotion, proliferation and projection organization, events that occur in the process of migration (Figure 6.8).

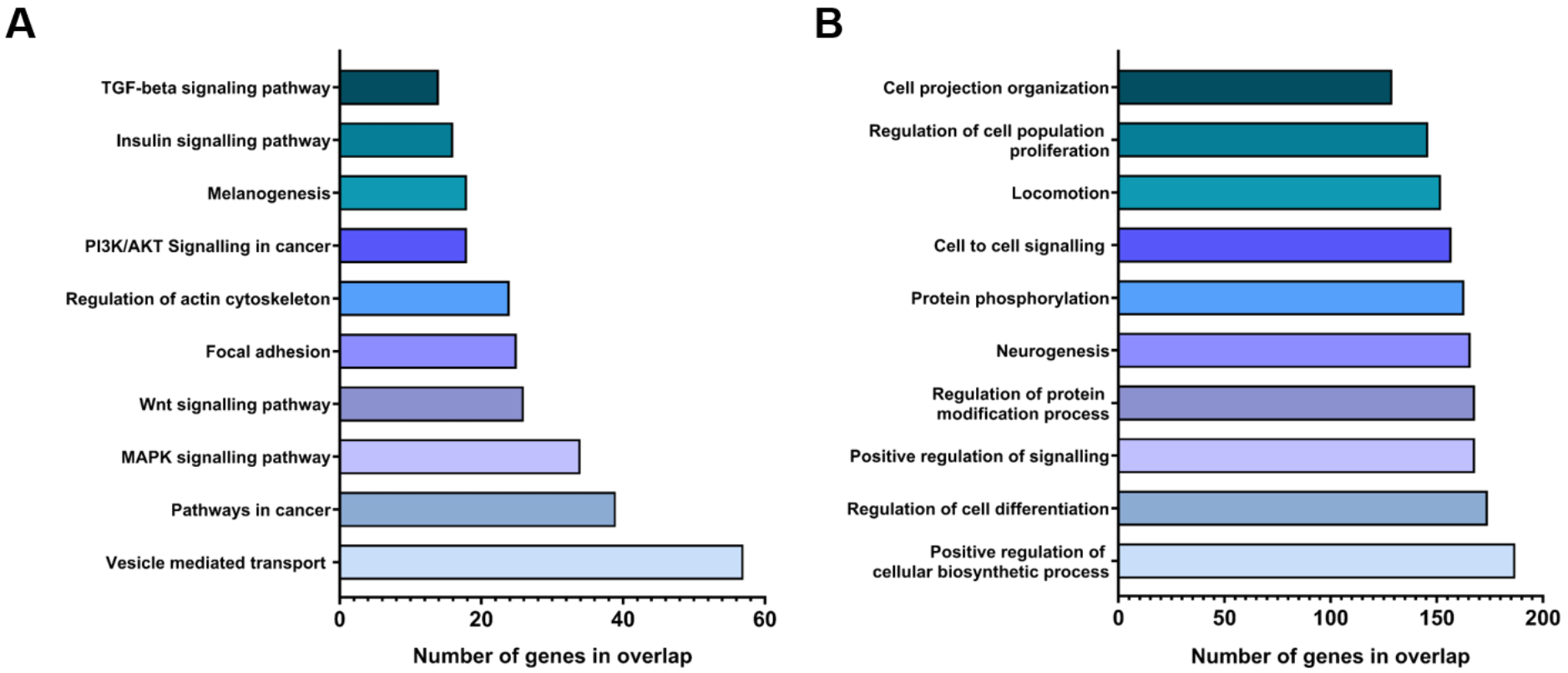

Figure 6.8 Functional analysis of differentially enriched miRNAs in metastatic exosomes

Functional pathway analysis of mRNAs targeted by 12 significantly changing miRNA in metastatic exosomes. Top 10 (A) Kyoto Encyclopedia of Genes and Genomes (KEGG) analysis and (B) Gene Ontology (GO) analysis are shown with the numbers of overlapping genes. All overlaps were significant ($p \leq 0.0001$).

6.4 Differentially enriched miRNA correlate with patient outcome

Having identified a panel of 12 miRNA which are differentially enriched in metastatic-derived exosomes, we next wanted to substantiate the importance of these candidates in medulloblastoma patients, by determining if their expression correlates with outcome in order to assess their prognostic significance. The expression of miRNA in medulloblastoma patients was assessed by analysis of a large medulloblastoma patient dataset (Cavalli *et al.*, 2017) using the R2 Genomics Analysis and Visualization Platform. The Cavalli dataset was used to show the probability of survival of medulloblastoma patients based on high or low expression of one miRNA, using Kaplan Meier curves. Metastasis is associated with poor patient overall survival in medulloblastoma, therefore the aim was to investigate if the 12 miRNA had an effect on patient survival outcome.

For the 8 miRNA whose levels were increased in metastatic exosomes compared to primary and normal samples, patient survival was worse when expression of miR-451a, miR-144-3p, miR-376a-3p, miR-382-5p, miR-376c-3p was high (Figure 6.9). miR-381-3p and miR-346 were not present in the Cavalli dataset, and expression of miR-23b-5p did not significantly correlate with overall patient outcome. Of the 4 miRNA whose levels were decreased in metastatic exosomes compared to primary and normal, miR-638-5p, miR-551b-3p and miR-19a-3p were not present in the Cavalli dataset. miR-301b was found in the dataset and low expression correlated with a worse overall patient survival (Figure 6.9B). These findings further support that the list of identified miRNA may be involved in medulloblastoma progression and their levels may correlate with patient overall survival.

A

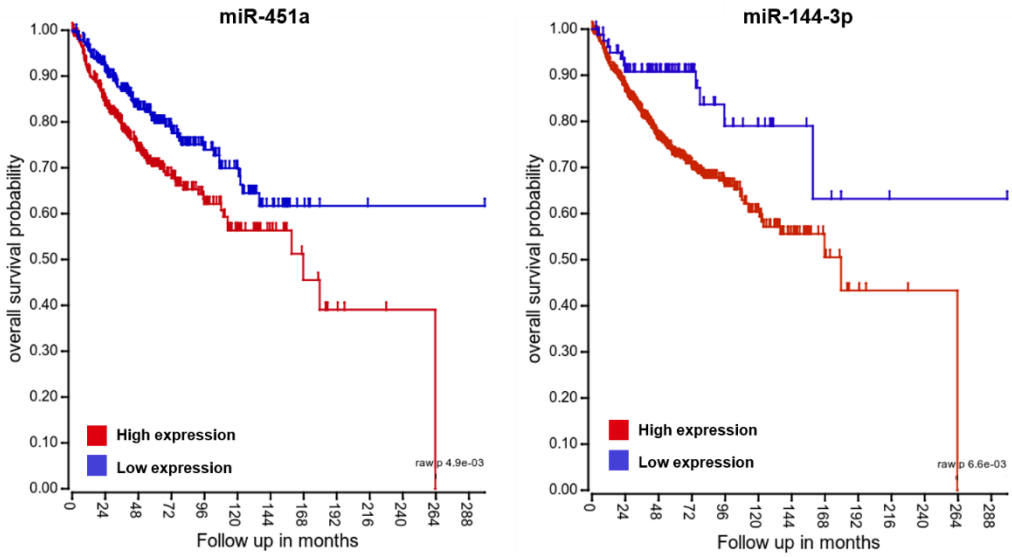

B

miRNA	Overall survival based on expression
miR-451a	High is worse p=4.9e-03
miR-144-3p	High is worse p=6.6e-03
miR-381-3p	Not present in dataset
miR-376a-3p	High is worse p=0.022
miR-382-5p	High is worse p=0.013
miR-376c-3p	High is worse p=0.022
miR-346	Not present in dataset
miR-23b-5p	Not significantly associated with outcome
miR-628-5p	Not present in dataset
miR-301b	Low is worse p=5.6e-03
miR-551b-3p	Not present in dataset
miR-19a-3p	Not present in dataset

Increased in metastatic exosomes

Decreased in metastatic exosomes

Figure 6.9 Kaplan-Meier overall survival for medulloblastoma patients according to expression of identified miRNA

Kaplan-Meier overall survival analysis of high and low expression of the eight identified miRNA in medulloblastoma patients on the R2 Genomics Analysis and Visualization Platform using the Cavalli dataset. (A) Example of Kaplan-Meier plots for miRNAs whose levels were increased in metastatic-derived exosomes. (B) Summary of Kaplan-Meier plots for all identified miRNAs whose levels were significantly increased (green) or decreased (red) in metastatic exosomes. Log rank test was performed to generate *p* values.

6.5 Exosomes in cerebral spinal fluid of medulloblastoma patients

We have identified a significant difference in the abundance of 12 exosomal miRNAs secreted in metastatic medulloblastoma exosomes. We next wanted to apply this candidate set of exosomal miRNA as biomarkers in a clinical setting. To do this, we aimed to validate our findings in cerebral spinal fluid (CSF) of medulloblastoma patients.

6.5.1 Isolation of exosomes from human CSF samples for NGS

Exosome isolation from biofluids is challenging and there is no consensus with respect to the best methodology for isolating exosomes which provides substantial yields with reliable quality (Martins *et al.,* 2018). Throughout this study all exosomes have been isolated by ultracentrifugation (UC) (Chapter 3), however initial attempts revealed low exosomal yields were obtained, as determined by NTA (Figure 6.10A). Indeed, the number of particles was below the NTA detection levels recommended ($1x10^7$ particles/mL). For this reason, the commercial qEV size-exclusion chromatography (SEC) column was also employed to isolate exosomes from CSF samples.

Particle size and concentration was assessed by NTA for exosomes isolated by UC and SEC, in both cases low exosomal yields were obtained, $1.3x10^6$ particles/mL using UC and $5.8x10^5$ particles/mL using SEC. Particle size concentrations using both isolation methods were also assessed, demonstrating the presence of particles with a mean and mode size of around 100 nm, consistent with that of exosomes (Figure 6.10A,B). Furthermore, isolated exosomes were also examined by TEM to assess their morphology, revealing that both techniques successfully isolated exosomes within the expected size range and morphology (Figure 6.10C). Having previously observed exosomal RNA yield to be most consistent using miRNeasy micro kit (Figure 5.1), RNA was isolated and bioanalyses was used to measure RNA integrity and concentration (Figure 6.10D). Unfortunately, RNA yields from both ultracentrifugation and size-exclusion chromatography were too low for NGS-sequencing. As CSF samples were

extremely limited, and due to time restraints, further optimisation was not possible. Therefore, CSF samples were sent directly to QIAGEN for exosome isolation and RNA extraction. Following extraction, the subsequent steps of NGS were performed. All samples were considered suitable for primary and secondary downstream data analysis.

In total 16 CSF samples from paediatric patients with primary, metastatic or recurrent (defined as relapsed disease following previous recurrence) medulloblastoma were prepared for NGS. Table 6.3 provides a summary of the samples.

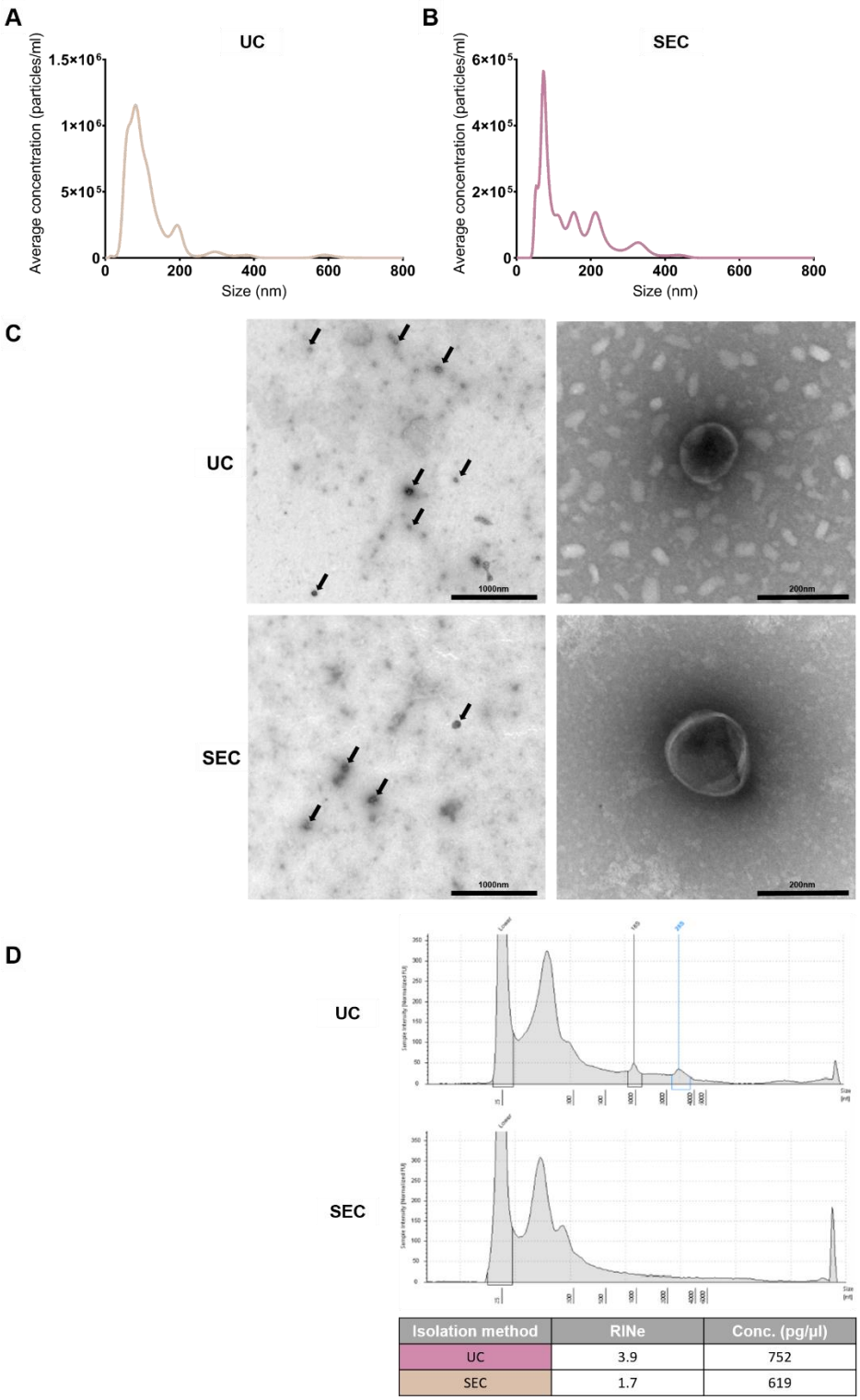

Isolation method	RINe	Conc. (pg/µl)
UC	3.9	752
SEC	1.7	619

Figure 6.10 Characterisation of exosomes derived from medulloblastoma patient CSF

Vesicle concentrations and size distributions were verified using Nanoparticle tracking analysis (NTA) isolated from medulloblastoma patient CSF samples by ultracentrifugation (UC) (A) or size exclusion chromatography (SEC) (B). TEM images of multiple exosomes (left panel) and single exosomes (right panel) isolated by UC or SEC (scale bars: 1000 nm left panel, 200 nm right panel). Exosome pellets were lysed and RNA was extracted. RNA concentrations were determined by bioanalyzer electropherogram analysis. Arbitrary fluorescence units (FU) are plotted as a function of RNA size in nucleotides (nt). Total RNA isolated from exosomes isolated by UC or SEC are shown.

Table 6.3 Patient characteristics of samples prepared for NGS

Sample number	Patient	Gender	Age at sampling	Primary/ Recurrence	Time to recurrence (months)	Phenotype	Molecular subgroup	Histology	Lumbar CSF cytology	Chang's staging
100	1	Male	7	Primary	N/A	Metastatic	Not performed	LCA	Positive	M3
101				Recurrent	Unknown	Metastatic		-	Negative	-
201	2	Male	20	Recurrent	24	Metastatic	Not performed	Classical	Negative	M2
202				Relapsed	12	Metastatic		-	Negative	M2
301	3	Male	5	Recurrent	N/A	Non-metastatic	Group 4	Classical	Negative	M0
302				Relapsed	14	Metastatic		Classical	Negative	M3
400	4	Male	13	Primary	N/A	Non-metastatic	Group 4	Classical	Negative	M0
401				Recurrent	2	Metastatic		Classical	Negative	-
501	5	Male	7	Relapsed	28	Non-metastatic	Group 3	Classical	Negative	M0
600	6	Male	14	Primary	N/A	Non-metastatic	Not performed	-	Negative	M2
601				Recurrent	24	Metastatic				
602				Recurrent		Metastatic				
603				Recurrent		Metastatic				
604				Recurrent		Metastatic				
605				Recurrent		Metastatic				
606				Recurrent		Metastatic				

6.5.2 Visualisation of CSF exosomal miRNA

Principle component analysis, a form of MDS, was performed on miRNA-seq data to visualize the degree of similarity between individual samples. The miRNA profiles of recurrent samples appear similar to each other and cluster on the left hand side of the graph. Interestingly, primary samples 100 and 400 cluster together, clearly separated from their matched recurrent counterparts (101 and 401 respectively). A similar trend was not observed with the remaining matched samples (600 primary and 601-606 recurrent), although sample 601 was clearly separated from the remaining recurrent samples.

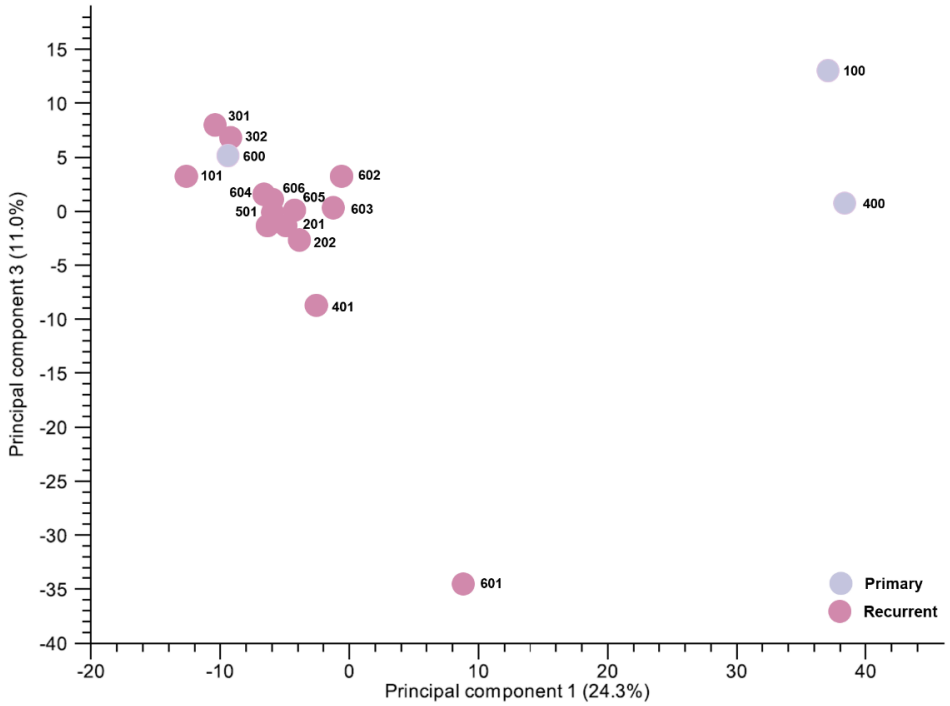

Figure 6.11 Multidimensional scaling of CSF exosomal miRNA

miRNA profiles were compared by multidimensional scaling analysis (MDS). Sample differences are shown by principle component analysis, a form of MDS, with primary samples in lilac and recurrent samples in pink.

6.5.3 Comparison of cell- and patient-derived exosomal miRNA signature

Although exosome isolation methods from cell supernatant and CSF were different, the downstream steps of sample preparation, mapping and differential gene

expression remained consistent (Figure 6.1). It was therefore possible to compare results obtained. As previously ascertained, an average of 10.9 million UMI-corrected reads were obtained for each cell culture-derived exosome sample. For CSF-derived exosomes, an average of 15 million UMI-corrected reads were obtained.

To compare miRNA identified in cell culture-derived (CD) exosomes with miRNA in CSF patient-derived (PD) exosomes, all differentially expressed miRNA from both data sets were compared (Figure 6.12A). A comparison of the two data sets revealed 96% of the miRNA identified in CD exosomes were also reported in PD exosomes. This indicates that although the quantity differed there was almost complete agreement with regard to the type of miRNA identified in CD exosomes, respective to PD exosomes.

In addition to identifying the miRNA types, determining the targets of those miRNAs demonstrates that between the CD and PD exosomes, 99% of predicted gene targets are shared (Figure 6.12B). This data indicates an overlap of genes targeted by the exosomal miRNAs, and this is further supported by comparative cell component and biological pathway analysis (Figure 6.12C,D). Cell component analysis identified a significant enrichment of genes within different cell compartments, targeted by all miRNAs identified in CD and PD exosomes used in the previous comparison. The top five cell compartments showing enrichment of gene targets were: nucleus ($p \leq 0.001$), cytoplasm ($p \leq 0.001$), plasma membrane ($p \leq 0.01$), exosomes ($p \leq 0.05$), and lysosomes ($p \leq 0.05$). Both lists showed a similar percentage of target genes across these five components (Figure 6.12C). This is further exemplified through comparative biological pathway analysis, where a subset of miRNAs differentially secreted in both CD and PB exosomes were enriched for those targeting genes involved in major cancer associated pathways including cell signalling (PI3K-Akt, MAPK and ErbB) and key cellular functions including focal and cellular adhesion (Figure 6.12D). Also of note was the enrichment of miRNA targeting genes involved in signal transduction (VEGF and VEGFR) and cell surface signalling (Alpha9 and Beta1 Integrins) (all $p \leq 0.001$).

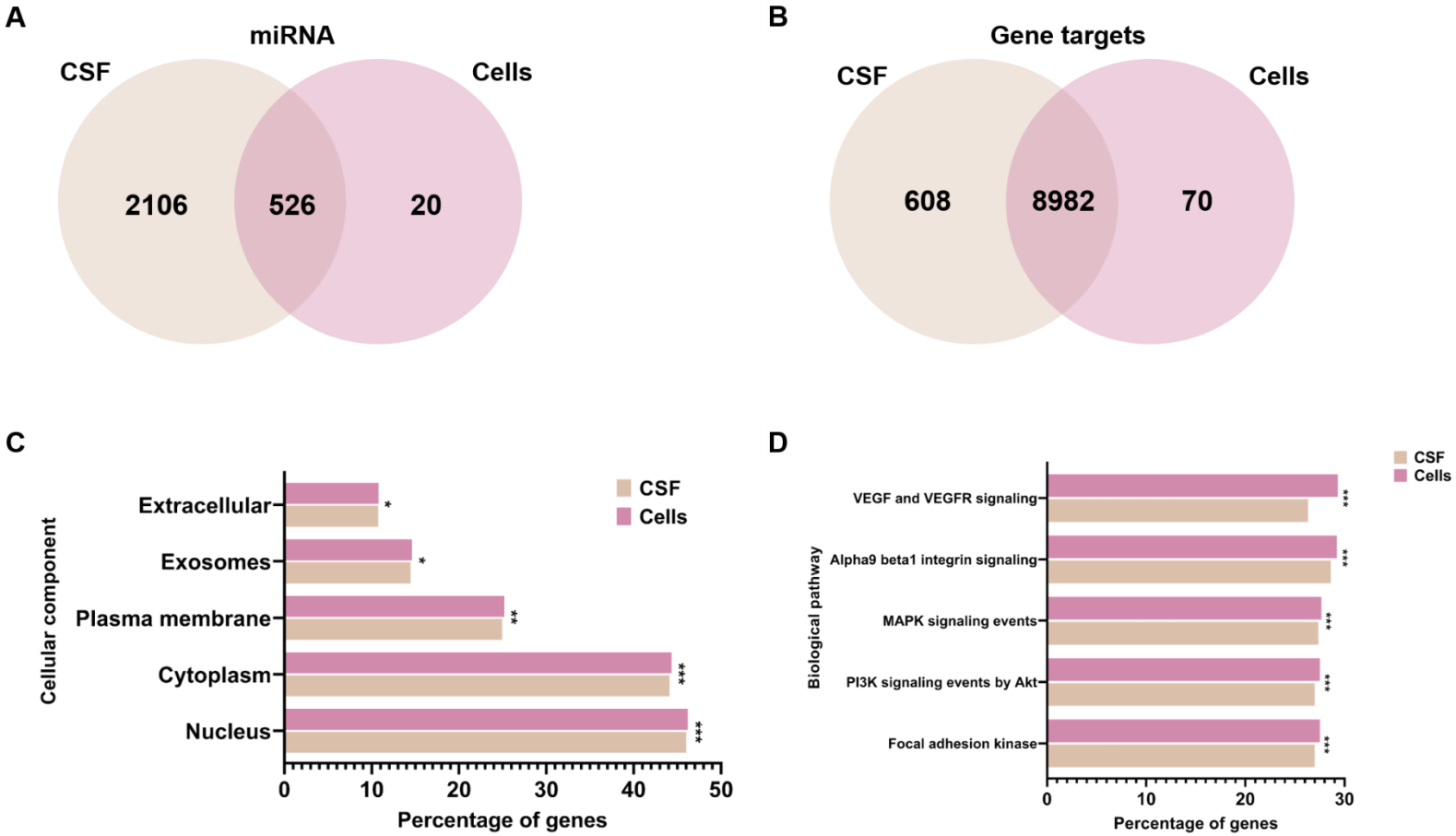

Figure 6.12 Comparative analysis of cell- and patient-derived miRNA signatures

All miRNA transcripts identified in cell derived (cells) and CSF patient derived (CSF) exosomes were compared. (A) Venn diagrams were used to show overlapping miRNA transcripts identified in cells and CSF exosomes. miRDB was utilised to identify miRNA-target genes. Gene lists were created and (B) Venn diagrams were used to identify overlaps in gene targets. Comparative cellular component analysis of the miRNAs from cells and CSF exosomes demonstrate a similar percentage of target genes in the same cellular compartments irrespective of origin (cell derived or CSF patient derived). Comparative biological pathway analysis also showed a similar results. Significance was calculated using Fisher's exact test (*= p≤0.05, ***= p≤0.005, ****= p≤0.001).

6.5.4 Translation to human CSF samples

As a preliminary assessment of the potential for clinical utility of candidate markers in non-invasive CSF samples and to guide the selection of miRNA for future validation, the 12 miRNAs that were identified to show a progression signature in exosomes derived from medulloblastoma cell lines were further evaluated. In particular, miR-144-3p, miR-346, miR-381-3p, miR-382-5p, and miR-451a showed considerable promise. These 5 were previously identified as being significantly enriched in metastatic exosomes compared to primary and normal exosomes. When comparing these transcripts in exosomes from patients with metastatic medulloblastoma, levels were also elevated relative to non-metastatic exosomes (Figure 6.13A). In addition, miR-628-5p had been identified as being significantly decreased in metastatic exosomes compared to primary and normal. When comparing transcripts downregulated in exosomes from patients with metastatic medulloblastoma, levels of miR-628-5p were also decreased relative to non-metastatic exosomes (Figure 6.13B). Importantly, CSF cytology results from all metastatic samples were negative and showed no diagnostic evidence of neoplasia despite positive dissemination observed from post-operative MRI imaging. Taken together, this highlights the potential clinical utility of exosomal miRNA as non-invasive CSF biomarkers for medulloblastoma disease progression.

Surprisingly, expression levels of miR-376a-3p, miR-376c-3p, miR-23b-5p, miR-551b-3p and miR-19a-3p showed opposite expression compared to what had previously been observed in exosomes isolated from cultured cell lines.

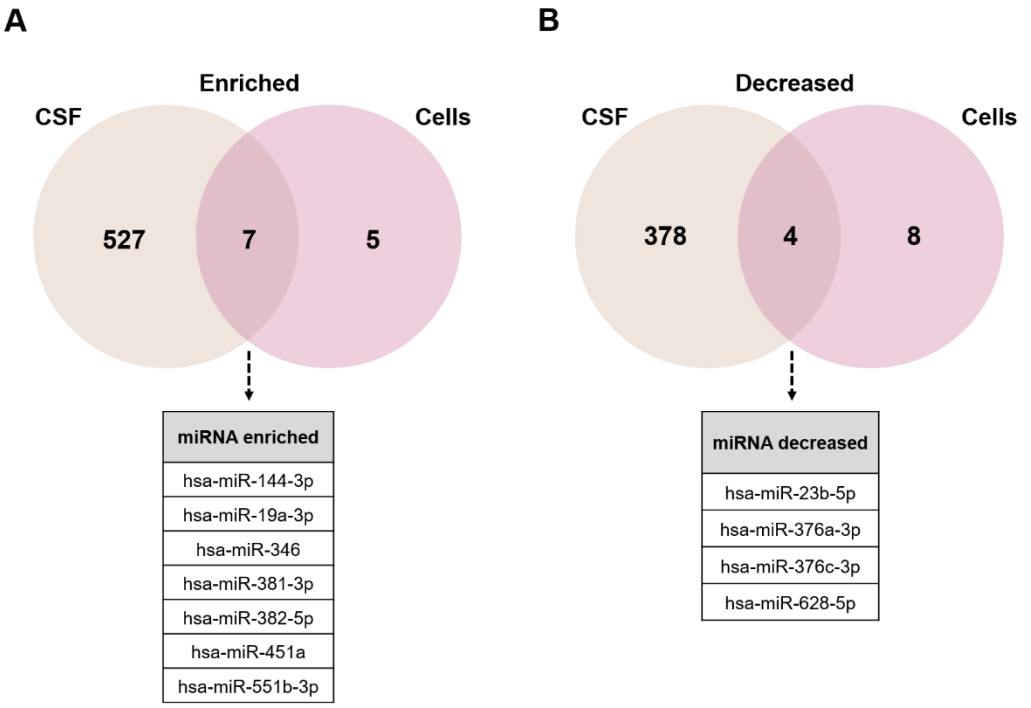

Figure 6.13 Comparison of differentially regulated miRNAs between cell- and CSF patient-derived exosomal miRNAs

All miRNA identified as being enriched in patient CSF exosomes were overlapped with the 12 identified miRNA that were identified to show a progression signature in exosomes derived from cell lines, a Venn diagram was constructed to show overlaps (A). Additionally all miRNA identified as being decreased in patient CSF exosomes were overlapped with the 12 identified miRNA and again a Venn diagram was constructed to show overlap (B).

6.5.4.1 Individual patient analysis

The strength of the patient data used in this study lies in the matched primary and metastatic CSF samples, patient 3, patient 4 and patient 6 (Table 6.3). Upon further review of transcript levels of the candidate miRNA in these three patients, we observed drastically higher levels of miR-382-5p and miR-381-3p in metastatic exosomes from all three patients relative to primary exosomes (Figure 6.14). In addition, transcript levels of miR-346 were present at higher levels in 2 out of 3 metastatic CSF exosomes relative to primary exosomes. miR-628-5p which had been identified as being significantly decreased in metastatic cell-derived exosomes, was completely absent in metastatic exosomes from all three patients and found to be enriched in 2 out of 3 patients primary exosomes (Figure 6.14).

Serial cerebral spinal fluid samples for patient 6 were collected at initial diagnosis and then 22 months later at recurrence, this was followed by multiple collections prior and post administration of intrathecal chemotherapy. Transcript levels of miR-382-5p and miR-381-3p within exosomes from these samples were assessed (Figure 6.15). A substantial increase in levels of both transcripts was observed in sample 2 (recurrence) relative to sample 1 (diagnosis). Of note in both samples from initial diagnosis and at recurrence, CSF cytology was negative despite MRI imaging proving metastatic dissemination (Table 6.3). A drastic reduction in levels of both miRNAs was then observed with ongoing treatment (Figure 6.15). Patient 6 has remained well with no evidence of recurrence on surveillance imaging.

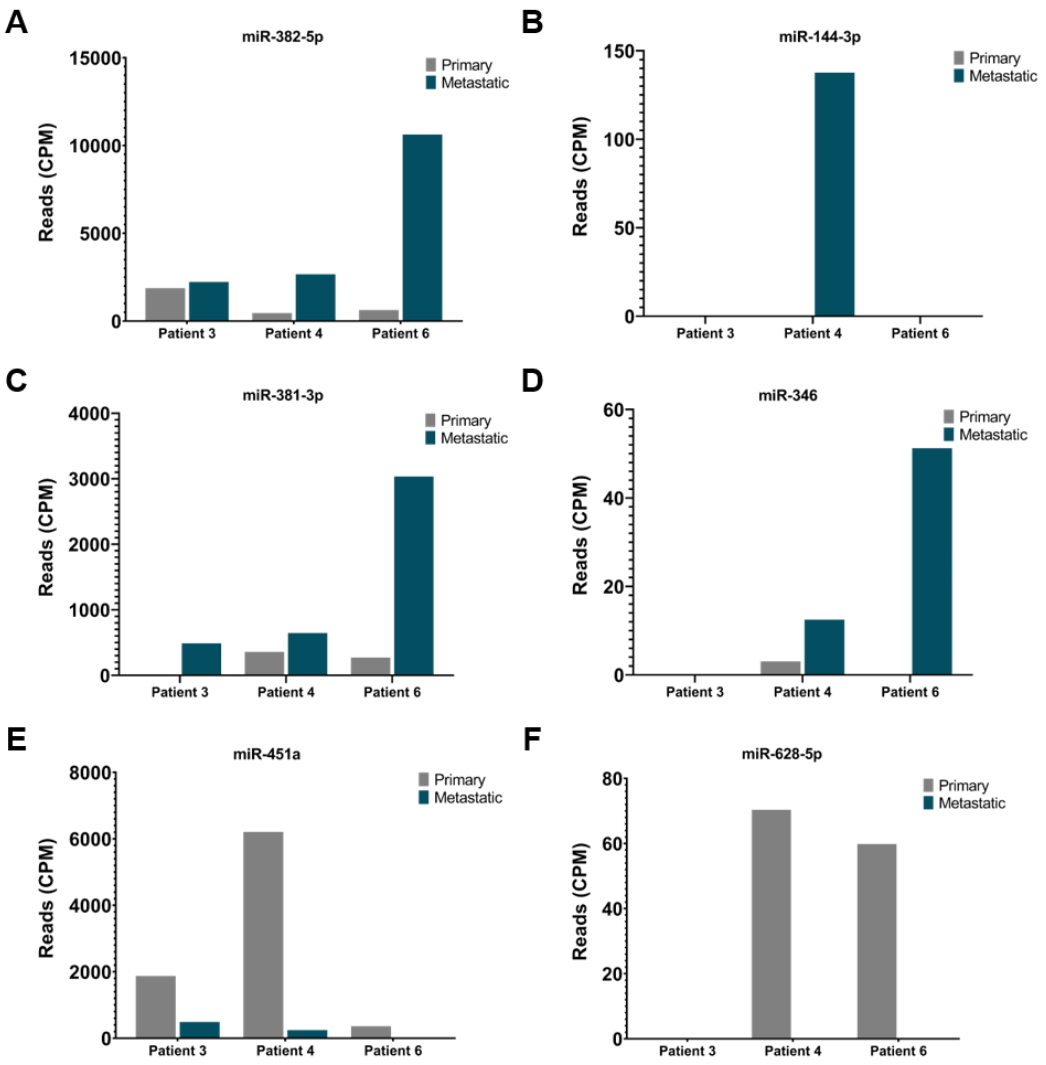

Figure 6.14 Transcript levels of candidate miRNA in exosomes isolated from CSF of matched patients

Counts per millions (CPM) of candidate miRNAs, miR-144-3p, miR-346, miR-381-3p, miR-382-5p, and miR-451a and miR-628-5p were assessed in exosomes isolated from matched primary and metastatic CSF samples

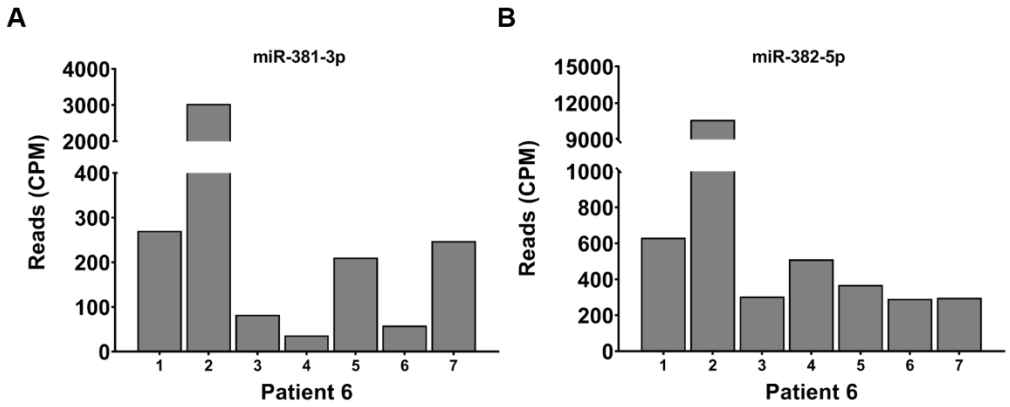

C

Sample no.	Characteristics
1	Initial primary tumour presentation Full surgical resection of tumour
2	22 months later recurrence detected Treatment begins: stereotactic radiosurgery and intrathecal chemotherapy
3	Progressive enlargement of lateral ventricular subependymal lesions despite ongoing intrathecal etoposide
4	Ongoing intrathecal
5	Complete resolution of 2/3 previously demonstrated intraventricular nodules
6	Resolution of all intraventricular nodules
7	Ongoing intrathecal

Figure 6.15 Assessment of miR-382-5p and miR-381-3p in exosomes isolated from serial CSF samples from patient 6

Counts per millions (CPM) of miR-382-5p and miR-381-3p miRNAs were assessed in exosomes isolated from exosomes isolated from serial CSF samples from patient 6 (A). Characteristics of each sample are outlined (B).

6.6 Summary

- Using miRNA NGS technology to characterise exosomal miRNA cargo we have demonstrated a clear pattern of exosomal miRNA secretion that distinguishes metastatic medulloblastoma cells from primary and normal cell lines.
- We identified several miRNA which were differentially secreted in metastatic exosomes relative to primary and normal exosomes, thereby yielding a candidate set of exosomal miRNA for further assessment as biomarkers of medulloblastoma progression and providing new insights into tumour-derived exosome biology.
- Identified miRNA are predicted to be involved in signalling pathways related to tumour progression and migration, including focal adhesion and regulation of the actin cytoskeleton.
- Characterisation of the miRNA content of exosomes isolated from medulloblastoma patient CSF samples revealed 96% of the miRNA identified in cell culture-derived exosomes were also reported in CSF patient-derived exosomes. In addition, 99% of predicted gene targets were also shared, indicating an overlap of genes targeted by the exosomal miRNAs, this was further supported by comparative cell component and biological pathway analysis.
- Importantly, several of the candidate miRNAs (miR-382-5p, miR-381-3p, miR-346, miR-628-5p) were detected at substantially higher levels in CSF of patients with metastatic disease relative to primary medulloblastoma, highlighting the potential clinical utility of exosomal miRNA as non-invasive CSF biomarkers.

Chapter 7

Discussion

Chapter 7. Discussion

Recurrent/metastatic medulloblastoma is a devastating disease with an abysmal prognosis of less than 10% five-year survival. Whilst primary tumours can be classified based on epigenetic and transcriptomic features, there is very little information regarding molecular signatures of metastatic tumours. The secretion of extracellular vesicles (EVs) has emerged as a pivotal mediator for communication in the tumour microenvironment during metastasis. The most investigated EVs are exosomes, nanovesicles secreted by all cell types and able to cross the blood-brain-barrier. The role of exosomes as vehicles for cell-to-cell communication between a tumour and its microenvironment is a relatively new concept, with only limited study of this potential mechanism in medulloblastoma.

Exosomes represent a unique form of information delivery which operates at short and long distances. Tumour-derived exosomes can transfer signals and convey information from tumours to distant tissues and organs. They are present in the circulation and thus have access to all parts of the body. Exosomes have been shown to carry surface components that enable direct contact with recipient cells to activate intracellular signalling. In addition, exosomes interact with the target cell by fusion with the cell membrane followed by transfer of exosomal cargoes (protein, mRNA, miRNA) into the cell cytoplasm.

In this thesis we focussed on how medulloblastoma exosomes influence recipient cells either via extracellular matrix signalling, via surface bound proteins (Figure 7.1, blue box), or the long-term regulation of exosomes via the intracellular delivery of their RNA cargo to recipient cells (Figure 7.1, orange box). Our observations have also highlighted several miRNA which were differentially secreted in metastatic exosomes relative to primary and normal exosomes, thereby yielding a candidate set of exosomal miRNA as biomarkers of increase metastatic potential (Figure 7.1, pink box).

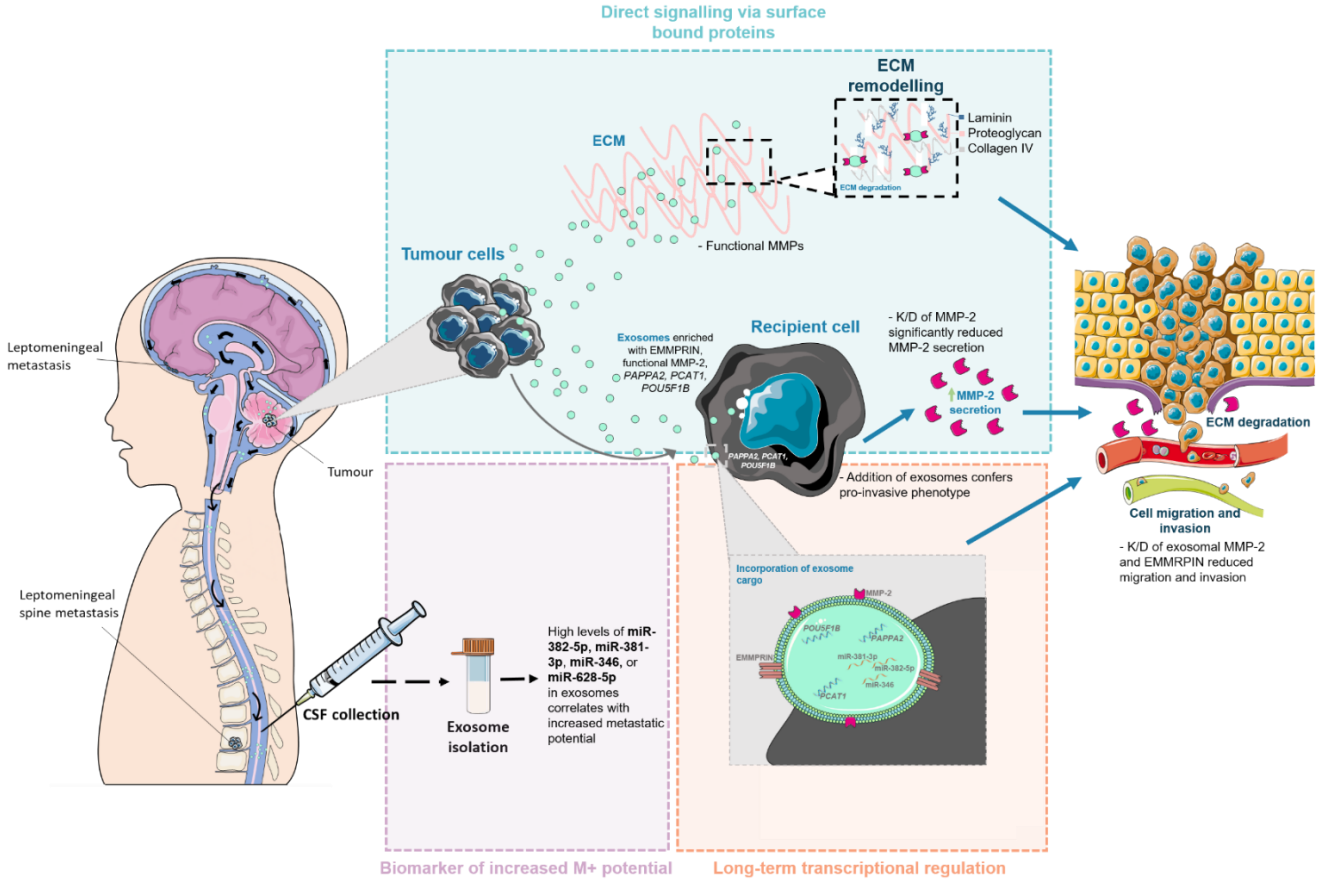

Figure 7.1 Graphical summary: Analysing the role of medulloblastoma exosomes as biomarkers and understanding their functional contribution to metastasis

Schematic diagram showing the functional roles of exosomes in medulloblastoma metastasis, including extracellular matrix signalling, via surface bound proteins (blue box), long-term regulation through the delivery of RNA cargo to recipient cells (orange) and as a CSF-derived biomarkers of increased M^+ potential (pink).

7.1 The role of exosomes in medulloblastoma migration and invasion

7.1.1 Standardising medulloblastoma cell culture conditions for exosome isolations

Media used for cell culture and subsequent exosome recovery from supernatants is a crucial factor in exosome production. All media components have been shown to influence the production and/or composition of exosomes; emphasising the importance of choosing the right components and reporting them on publication (Théry *et al.*, 2018). Of major importance are media components which are highly enriched in proteins and contain EVs, such as FBS (Ludwig *et al.*, 2019). Several studies have demonstrated that vesicles present in the FBS are biologically active and can influence experimental results. Indeed, EVs present in FBS can influence cultured cells phenotype such as migration and proliferation (Shelke *et al.*, 2014; Angelini *et al.*, 2016; Ludwig *et al.*, 2019). Therefore, ISEV guidelines strongly recommend that EVs are removed from FBS prior to use in cell culture experiments (Théry *et al.*, 2018). Despite the clear guidelines on use of exosome-depleted FBS, thus far there are no standardised guidelines regarding the concentration of FBS used in media, and this is usually not reported on publication. Here, we showed that increasing concentrations of FBS were associated with increased levels of secreted exosomes. In line with previous findings, growth factors EGF and FGF also altered exosome production (Zhou *et al.*, 2017). It is therefore crucial to consider cell media compositions when making direct comparisons between cell lines.

Of note, specific miRNAs abundant in FBS, such as miR-122 and miR-1246 have previously been reported to be enriched in cell culture-derived exosomes, even when cells were grown in exosome-depleted FBS; emphasising the potential confounding effects of FBS on results from highly sensitive gene expression profiling. Furthermore, FBS-associated RNA is co-isolated with cell culture-derived extracellular RNA and FBS transcripts can also be taken up by cultured cells (Wei *et al.*, 2016). Importantly,

a study by Shelka and colleagues, concluded that no depletion protocol leads to total FBS-EV elimination. Indeed, an 18-hour ultracentrifugation step to remove FBS (protocol suggested by ISEV guidelines) successfully removed 95% of EV associated RNA, however EVs were still visualised by TEM (Shelke *et al.*, 2014). Therefore, any RNA analysis or cell line cultures grown in high concentrations of FBS, must consider the possible influence of RNA added by EVs derived from FBS. The medulloblastoma cell lines used in this study are grown in varying concentrations of FBS. For this reason, experiments were pursued using cell lines grown in controlled media containing the lowest concentration of exosome depleted-FBS tolerated by medulloblastoma cell lines (no difference in cell viability was observed). This allowed for direct comparisons between cell lines to be detected, and minimised the interference and misinterpretation caused by the co-isolation of FBS EVs and FBS-derived extracellular RNAs.

7.1.2 Isolating and characterising an abundant source of medulloblastoma-derived exosomes

The variation of EV isolation protocols used by different laboratories leads to heterogeneous and unreproducible results (Théry *et al.*, 2018; Royo *et al.*, 2020). In order to obtain comparable results and ensure reproducibility, it is strongly recommended to combine and compare the repeatable measurements of vesicle concentrations using more than one orthogonal method (Vogel *et al.*, 2021). The particle concentration of biological replicates of exosomes isolation from four medulloblastoma cell lines measured by nanoparticle tracking analysis (NTA) and nanoscale flow cytometry (NanoFCM), was consistent. Exosomes were of the expected size (El Andaloussi *et al.*, 2013), confirmed by NTA, NanoFCM and transmission electron microscopy (TEM). The morphology of exosome preparations was also determined by TEM and revealed a heterogeneous population of “cup-shaped” spherical vesicles, characteristic of exosomes under TEM (Théry *et al.*, 2018). In agreement with the known EV markers summarised in 2002 by Clotilde Théry (Théry, Zitvogel and Amigorena, 2002), we confirmed the presence of EV membrane

markers; CD9, EpCAM, and Annexin V, and the EV luminal marker Alix (as recommended by Théry *et al.,* 2018). Furthermore, H4, expressed in the nucleus, was absent in exosome preparations compared to whole cell lysates, indicating that the preparations were free of cellular contamination (Lötvall *et al.*, 2014).

To conclude, the isolation and subsequent characterisation of exosomes undertaken in this thesis is well aligned with the extensive effort undertaken by the EV community to develop reproducible isolation and characterisation methodologies (Lötvall *et al.*, 2014; Théry *et al.*, 2018). This provided the medulloblastoma-derived exosomes, and methodologies of isolation required for subsequent chapters, therefore we could move forward with confidence to test our hypotheses.

7.1.3 Metastatic cells secrete more exosomes

Mounting studies support the notion that exosome levels in supernatant or bodily fluids of patients with cancer are elevated (Baran *et al.*, 2010; Taylor and Gercel-Taylor, 2013; Vasconcelos *et al.*, 2019). In this study we demonstrated for the first time that metastatic medulloblastoma cells secrete markedly more exosomes compared to non-metastatic primary cell lines. For consistency, all particle counts were normalised by cell number. The reasons for increased exosome secretion from metastatic cells are unknown.

A possibility for the differences of exosome secretion from metastatic and primary medulloblastoma cell lines could be associated with Rab GTPases. The Rab GTPase proteins, particularly Rab27a and Rab27b, are strongly implicated in exosome secretion (Ostrowski *et al.*, 2010), and knockdown of Rab proteins have been shown to significantly reduce exosome secretion by tumour cells (Peinado *et al.*, 2012). Research in our lab is investigating the function of Rab proteins in medulloblastoma cell exosome secretion. Preliminary findings have shown high expression of several Rab proteins correlates with cell line metastatic status (Entwistle *et al.*, unpublished data).

Additionally, changes in the cellular microenvironment, including hypoxia or pH alterations induced by chemotherapeutics has also been shown to account for increased exosome secretion by tumour cells (Parolini *et al.*, 2009). A more recently described method of tumour cells altering exosome secretion, involves the often upregulated tumour associated pyruvate kinase type M2 (PKM2) protein, which has been implicated in promoting medulloblastoma growth (Tech *et al.*, 2017). During exosomes secretion, phosphorylated PKM2 forms a dimer structure with protein kinase ability, phosphorylates synaptosome-associated protein 23 (SNAP-23) enabling the formation of SNARE complexes required for the docking and fusion between endosome-containing MVBs and plasma membranes. It was observed that levels of PKM2 were positively correlated with the amount of exosomes released in tumour cells, and knockdown of PKM2 strongly reduced the release of exosomes (Wei *et al.*, 2017).

Whether vesicle fusion and trafficking, or microenvironmental factors, are able to alter exosome secretion, there are numerous reasons which may attribute to the observed differences in exosome secretion between metastatic- and primary-derived cell lines and further studies investigating these avenues are required.

7.1.4 Metastatic exosomes enhance medulloblastoma progression by stimulating tumour cell invasion and migration

Metastatic dissemination is the predominant pathological reason for the mortality of patients with medulloblastoma. Increasing evidence suggests that exosomes serve as key mediators in tumour metastasis (reviewed by Whiteside, 2016). It has been reported that exosomes from highly metastatic tumour cell lines could significantly enhance the migration capability of less migratory recipient cells (Menck *et al.*, 2015). Similarly, the present study revealed that exosomes isolated from migratory medulloblastoma cell lines directly enhanced the invasive potential of less migratory matched primary tumour cells in a heterologous stimulation loop. The effect was

specific to exosomes, since vesicle-free supernatant had no influence on tumour invasion.

Several studies have demonstrated that exosomes are able to transfer malignant characteristics from highly invasive tumour cells to surrounding non-malignant cells (Angelucci *et al.*, 2000; Al-Nedawi *et al.*, 2008). In line with this, the invasive capacity of non-malignant foetal neuronal stem cells was enhanced when stimulated with heterologous exosomes derived from highly migratory medulloblastoma cell lines, indicating that recipient cells did not need to be predisposed to an invasive phenotype prior to exosome stimulation.

7.2 EMMPRIN and MMP-2 proteins mediate exosome induced tumour migration and invasion

7.2.1 MMP-2 and EMMPRIN as markers of increased metastatic potential in medulloblastoma

MMP-2 and EMMPRIN are both correlated to higher grade, aggressiveness and staging in several human cancers, including medulloblastoma (Rao *et al.*, 2007; Chu *et al.*, 2011). We showed that EMMPRIN gene (*BSG*) expression was high across medulloblastoma patient cohorts and represents a negative prognostic factor of medulloblastoma. In addition, despite significance not being reached, a trend towards higher *BSG* expression was observed in metastatic patient samples compared to their matched primary counterparts.

This was further supported by elevated EMMPRIN mRNA and protein in medulloblastoma cell lines with higher metastatic potential. When pairs of cell lines derived from matched primary and metastatic tumours were available, it was noted that the expression of EMMPRIN was higher in both the metastatic samples compared to their primary counterparts. Moreover, we showed that metastatic cell lines were significantly enriched with a highly glycosylated form of EMMPRIN, which is required

for MMP2 activation (Sun and Hemler, 2001), compared to primary and non-malignant cell lines, which were distinguished by the low glycosylation variant of EMMPRIN.

Considering the multi-level regulation of MMP-2 expression, the ambiguity with the gene expression results was not surprising. In fact, when MMP-2 protein expression was assessed, protein expression correlated with metastatic outcome of matched medulloblastoma cell lines. In comparison, gene expression of MMP-2 was often confounding using patient transcriptomic analysis, with patients with elevated *MMP-2* expression displaying significantly better overall survival than patients with low *MMP-2* expression, yet significantly higher *MMP-2* expression was associated with deceased patients compared to patients who had survived. Taken together, this was indicative that MMP-2 protein levels may be a more physiologically relevant marker of increased metastatic potential in medulloblastoma. However, more matched cell lines or the staining of MMP-2 on patient tumour microarrays is required to correlate patient survival and prognosis.

7.2.2 Pro-migratory function of exosomal MMP-2 and EMMPRIN

Although some studies have already demonstrated the tumour-supporting functions of EMMPRIN or MMP-2 in medulloblastoma metastasis, the presence of these proteins on medulloblastoma exosomes has not yet been investigated. In this current study, we have advanced the mechanism of action of MMP-2 and its inducer EMMPRIN in medulloblastoma progression, by demonstrating that MMP-2 and EMMPRIN are associated with secreted exosomes. Importantly, western blot and flow cytometry analysis revealed pro-invasive metastatic exosomes were significantly enriched with membrane-bound EMMPRIN and MMP-2 compared to primary exosomes. It is therefore reasonable to propose that exosomal MMP-2 and EMMPRIN are membrane-bound, this location is required for a protease to exert its proteolytic activity on extracellular proteins.

Activated MMP-2 has a wide range of substrates and can degrade basement membrane collagen IV, elastin, and several other ECM molecules, including interstitial

collagen types I, II, and III, and is therefore associated with ECM remodelling as a prerequisite for cellular invasion and migration (Löffek, Schilling and Franzke, 2011). Our finding, that functional activated MMP-2 is carried by exosomes and released by metastatic cell lines into the extracellular space, reveals a possible mechanism by which MMP-2 may facilitate the breakdown of the ECM. Degradation of the ECM would create routes for medulloblastoma cells to directionally invade into the surrounding environment, and functional MMP-2 on the external surface of exosomes could allow exosomes to reach long distance target locations. Moreover, shRNA-mediated knockdown of EMMPRIN or MMP-2 in exosomes decreased the pro-migratory effect of exosomes on recipient cells. This supported the hypothesis that EMMPRIN and MMP-2 are both proteins that mediate exosome-induced tumour migration and invasion.

The association between exosomal EMMPRIN/MMP-2 and ECM degradation was reinforced by zymography assays, demonstrating that secretion of active MMP-2 was activated in primary medulloblastoma cell lines, upon co-culture with metastatic exosomes enriched with high glycosylated EMMPRIN and MMP-2. Validation of this was provided by a significant reduction in this trans-stimulation when exosomes were isolated from metastatic cell lines stably transfected with EMMPRIN or MMP-2 shRNAs. This is in line with a study from Bernardo and Fridman who demonstrated that pro-MMP-2 is secreted and exported to the cell membrane surface, where upon fusion, is activated by binding with another activated membrane-bound MMP (Bernardo and Fridman, 2003).

7.3 Identification of exosomal mRNA biomarkers of medulloblastoma progression

In the first half of this thesis, we focussed on how medulloblastoma exosomes activate extracellular matrix signalling pathways in recipient cells, via surface bound proteins. However, the intra-vesicular contents of exosomes also includes protein-coding messenger RNA and non-coding RNAs. It has been shown that mRNA content of

exosomes can be translated into functional proteins when brought into the recipient cells (Al-Nedawi *et al.*, 2008). Additionally, exosomal transfer of oncogenic RNA species results in induction of malignant traits in recipient cells (Zomer *et al.*, 2015), indicating a physiological role for exosomal mRNA transfer. With this in mind, we characterised the RNA cargo of exosomes secreted from a pair of matched primary and metastatic medulloblastoma cell lines to identify exosomal RNA biomarkers of increased metastatic potential. Since multiple RNA species have been identified as RNA cargo, both mRNA and miRNA cargo were characterised.

7.3.1 Metastatic mRNA cargo was distinct between primary and metastatic exosomes

Isolating sufficient RNA from exosome samples for downstream analysis is challenging. Therefore, following exosome isolation, we compared the RNA yield and purity resulting from traditional or commercial extraction methods. Overall, RNA yield and quality was most consistent when using the miRNeasy micro kit (Qiagen), producing samples enriched in small RNAs consistent with other reports (Tang et al., 2017) and with undetectable levels of 18s and 28s ribosomal RNA, indicative that the overall exosomal RNA is free of contamination.

Exosomal RNA cargo has been shown to be altered or manipulated under a variety of conditions including cancer progression (reviewed in Zhu *et al.*, 2020). In line with this, we showed an apparent difference in the mRNA profiles of exosomes isolated from metastatic exosomes compared to primary exosomes, based on hierarchal clustering analysis.

Previous findings have also shown that additional mRNAs are packaged into tumour-derived exosomes. For example, in a study comparing exosomal RNA content from plasma of gastric cancer patients versus healthy controls, over 50 additional unique mRNAs were identified in cancer patients compared to healthy control exosomes (Ren *et al.*, 2017). When comparing transcripts identified in medulloblastoma exosomes compared to normal exosomes, a similar trend was not observed, although more

normal exosome samples would be required to confirm this, additionally this was based on cell line data only. However, when comparing levels of gene transcripts (threshold raw UMI count of ≥5), there was a substantial difference between the subgroups. Almost 5000 gene transcripts were identified in exosomes derived from Group 3 medulloblastoma cell lines compared to 243 gene transcripts in Group 4-derived exosomes. A hypothetical reason for this difference could be that Group 4 cell lines have altered pathways which have increased the selectivity of mRNA loading into exosomes. Interestingly, when gene lists were compared, all of the identified genes in Group 4 exosomes overlapped with Group 3, indicative of a potential sorting process. The YB-1 protein has been linked to miRNA sorting into exosomes (Shurtleff *et al.*, 2016), and more recently has been described as a potential mediator of mRNA sorting (Yanshina *et al.*, 2018). Results from our lab have shown that YB-1 is overexpressed in medulloblastoma cell lines, with high expression being observed in CHLA-01 and CHLA-01R cell lines (Taylor *et al.,* unpublished data). Interestingly much lower expression was observed in Group 3 D458 cell lines, however expression of YB-1 has yet to be assessed in the D425 cell lines. These results require further validation, to identify a difference in exosome cargo sorting between different medulloblastoma subgroups.

Despite the differences in transcript levels between exosomes isolated from medulloblastoma subgroups, similar pathways and processes were enriched between Group 3 and Group 4 exosomes; indicating an overlap in pathways targeted by exosomal mRNAs. Characterisation of the mRNA content of all medulloblastoma exosomes delineated the targeting of pathways important for medulloblastoma progression and interaction with the surrounding environment, which is in keeping with the changes in pro-invasive phenotype observed following treatment with metastatic exosomes. Such pathway overlaps were not observed when comparing genes identified in normal exosomes.

7.3.2 Identifying exosomal mRNA markers associated with metastatic progression

Differential expression analysis identified 19 genes which were enriched in metastatic exosomes from Group 3 and 10 genes that were enriched in metastatic exosomes from Group 4. From the identified genes, 5 were enriched in all metastatic-derived exosomes. Since mRNA-seq of medulloblastoma exosomes is a novel avenue of research, identified genes could not be compared against previous findings. The importance of these candidates, were therefore substantiated in medulloblastoma patient datasets. The Cavalli dataset provided information on survival outcome, metastatic status and subtype classification. Investigations of candidate gene expression across the Cavalli patient dataset, correlated high expression of genes, *PAPPA2, POU5F1B,* and *PCAT1* with poor overall survival and tumour metastasis. In addition, candidate gene expression was higher in medulloblastoma subgroups compared to normal brain controls.

Interestingly, metastatic exosomes were enriched with other mRNAs that could have been studied as candidate mediators of medulloblastoma progression, including numerous long non-coding mRNAs. Long non-coding RNAs are a class of RNAs usually greater than 200 nt in length that lack protein-coding potential (Esteller, 2011). Long non-coding RNAs have both oncogenic and tumour-supressing roles and have been demonstrated to modulate metastasis, progression, therapy resistance and clinical outcome in multiple cancer types (reviewed by Prensner and Chinnaiyan, 2011). Emerging evidence has shown that long non-coding RNAs are highly represented in exosomes, and the application of exosomal long non-coding RNAs as biomarkers and therapeutic targets in cancers has attracted interest (reviewed by Wang *et al.*, 2018). Importantly, long non-coding RNAs have also been discovered to be highly expressed in the brain compared to other regions of the human body. In the medulloblastoma field, some long non-coding RNAs have been shown to display prognostic and diagnostic significance. Several long non-coding RNAs have also been

shown to exhibit functional significance and can promote cellular proliferation and metastasis (Joshi and Rajender, 2020). Thus their expression patterns in medulloblastoma exosomes certainly warrant further investigation and validation, and will form on-going bioinformatics work subsequent to this thesis.

7.3.2.1 *PAPPA2* oncogene enriched in metastatic medulloblastoma exosomes

Pregnancy-associated plasma protein-A (*PAPPA*) and its homolog *PAPPA2* comprise the only two known members of the pappalysin family of metzincin metalloproteinases (Laursen *et al.*, 2001). Their encoded proteins are responsible for the proteolytic cleavage of a subset of IGF-binding proteins (IGFBPs) and are thought to be local regulators of insulin-like growth factor (IGF) bioavailability (Faurholdt Gude *et al.*, 2016). PAPPA has been implicated in several types of cancers (Tanaka *et al.*, 2004; Becker *et al.*, 2015) and more recently evidence has also shown the oncogenic functions of PAPPA2, including promoting cancer cell proliferation (Boldt and Conover, 2011), migration and invasion (Guo *et al.*, 2018; Hjortebjerg *et al.*, 2020). There are currently no reports linking *PAPPA2* or *PAPPA* to medulloblastoma. Reports of *PAPPA2* in exosomes is also relatively unstudied, *PAPPA2* mRNA and PAPPA2 protein have previously been detected in extracellular vesicles derived from mesenchymal stem cells and urinary samples (Bruno *et al.*, 2009; Wang *et al.*, 2012).

In the present study, *PAPPA2* was highlighted as a gene of interest with results showing a significant enrichment in Group 4 metastatic exosomes and qRT-PCR analysis revealed *PAPPA2* expression to be highest in metastatic cell lines compared to their primary comparts. In line with this, *PAPPA2* expression was significantly higher in metastatic patient tumours compared to primary tumours ($p \leq 0.001$) and was identified as being a negative prognostic factor for overall survival in medulloblastoma patients ($p \leq 0.0001$).

As previously alluded to, *PAPPA2* is known to promote IGF signalling via direct cleavage of IGFs. IGF signalling is a critical pathway involved in medulloblastoma

dissemination (Del Valle *et al.*, 2002). Additionally it has been described that free (bioavailable) IGF1 in the CSF or at the leptomeningeal surface may induce the expression of various ECM proteases including MMPs, providing a 'feed-forward' mechanism for tumour migration as well as metastasis establishment and growth at the leptomeningeal surface (Svalina *et al.*, 2016). Furthermore, prioritization of IGF signalling as a therapeutic target in medulloblastoma has been proposed (Wu *et al.*, 2012; Svalina *et al.*, 2016).

Recently, using proteomic profiling of exosomes secreted from cardiac progenitor cells (CPC), PAPPA was identified as one of the most highly enriched proteins in CPC exosomes, additionally PAPPA mRNA levels were also elevated in CPC exosomes (Barile *et al.*, 2018). The active from of PAPPA was detected at the surface of these exosomes and was shown to activate IGF-1 via proteolytic cleavage of IGFBP-4. Activation of IGF1 triggers intracellular signalling via ERK1/2 and Akt activation and stimulates increased IGF signalling (Barile *et al.*, 2018). Together with our previous findings whereby exosomes potentiate medulloblastoma migration via an active protease on their surface (MMP-2), it is tempting to speculate that PAPPA2 at the surface of medulloblastoma exosomes may induce augmented IGF signalling of tumour cells to potentiate leptomeningeal dissemination. This hypothesis certainly warrants validation and further studies to test this could lead to the establishment of exosomal *PAPPA2* as a prognostic marker or a diagnostic biomarker for IGF targeted therapy.

7.3.2.2 *OCT4* pseudogene *POU5F1B* abundant in metastatic exosomes

POU5F1B (POU domain class 5 transcription factor 1B) (also termed *OCT4A*), a processed pseudogene that shares 95% homology to OCT4 (Panagopoulos *et al.*, 2008), is frequently amplified in many tumours (Hayashi *et al.*, 2015; da Silva *et al.*, 2017; Pan *et al.*, 2018) and has recently been studied due to its biomarker potential (Zhao *et al.*, 2011).

POU5F1B was one of the most abundant mRNA transcripts observed in metastatic exosomes compared to primary exosomes, and showed promise as a negative prognostic factor in medulloblastoma patient samples (p≤0.0001). *POU5F1B* has not been associated with many EV orientated studies; indeed Vesiclepedia and ExoCarta only list two studies to have identified *POU5F1B* in EVs. However, a lack of isoform discrimination in most studies concerning OCT4 may explain this gap in literature (reviewed by Wang and Dai, 2010). Regardless, one of the two studies identified, verified the presence of elevated levels of *POU5F1B* in medulloblastoma, glioblastoma and fibroblast-derived microvesicles (Balaj *et al.*, 2011), however *POU5F1B* was not pursued further.

In relation to medulloblastoma, OCT4 has been associated as a high predictor of poor clinical outcome and could discriminate patients, that despite being clinically stratified as average-rick, displayed poor overall survival typical of high-risk (Rodini *et al.*, 2012). More recently, overexpression of *POU5F1B* was shown to significantly enhance medulloblastoma cell mobility *in vitro*, as well as aggravating tumour formation and progression including capacity of metastatic spread to the spinal cord *in vivo* (da Silva *et al.*, 2017), suggesting both a prognostic and therapeutic value of *POU5F1B*. Assessing, the levels of *POU5F1B* in patient CSF samples should be explored as a potential prognostic or therapeutic marker when considering medulloblastoma.

7.3.2.3 Oncogenic long non-coding RNA *PCAT1* enriched in metastatic exosomes

Long non-coding prostate cancer associated transcript 1 (*PCAT-1*) is dysregulated and acts as an oncogene in various different cancers. *PCAT-1* has multiple pathological functions and has been implicated in numerous processes correlated with carcinogenesis including proliferation, migration, chemoresistance and apoptosis (Yang *et al.*, 2019; Domvri *et al.*, 2020). Although a role for PCAT1 in medulloblastoma remains unstudied, PCAT1 has been associated with poor prognosis, tumour progression and radioresistance in gliomas (Zhang *et al.*, 2019).

The expression signature of a panel of three urinary exosome derived long-non coding RNAs (*MALAT1, PCAT1* and *SPRY4-IT1*) showed significant clinical value for the diagnosis and recurrence prediction of bladder cancer (Zhan *et al.*, 2018). In line with this, high levels of *PCAT1* have been detected in exosomes isolated from serum of oesophageal squamous cell carcinoma patients compared to healthy controls (Huang *et al.*, 2019) and in the serum of multiple myeloma patients (Shen *et al.,* 2017).

A functional role of exosomal *PCAT1* in carcinogenesis has also been explored; exosomal *PCAT1* was revealed to regulate Kras-associated chemoresistance. Upon silencing of *PCAT1,* exosome-induced cell migration and proliferation were reduced *in vitro* and chemoresistance along with metastatic potential and sustained survival *in vivo* was reduced (Domvri *et al.*, 2020), suggesting a tumour beneficial role for the secretion of *PCAT1* in exosomes.

Our results showed a significant enrichment of PCAT1 in metastatic exosomes compared to primary exosomes. PCAT1 expression was significantly elevated in all medulloblastoma subgroups compared with normal brain controls and was overexpressed in metastatic patients compared to non-metastatic patients, therefore a similar pattern of expression could be expected in matched medulloblastoma cell lines. Taken together, PCAT1 clearly has strong potential as a predictive biomarker relating to metastatic potential in medulloblastoma and should be investigated further.

7.3.3 Metastatic exosomes increased overall transcript abundance of *PAPPA2* and *POU5F1B* in recipient cells

As alluded to previously, several mechanisms have been proposed describing the interactions of exosomes and recipient cells. In the context of exosomal RNA transfer, mRNAs as well as non-coding RNAs can be transferred from cell to cell via mechanisms such as endocytosis (reviewed by Di Liegro, Schiera and Di Liegro, 2017). This was first observed by Valadi *et al.,* who showed that after treatment of human cells with mouse exosomes, mouse mRNA transcripts along with mouse proteins could be found in recipient cells, indicating that not only could mRNAs be

shuttled via exosomes, but they could also be translated (Valadi *et al.*, 2007). More recently, it was demonstrated that kidney tubular cells, which do not normally express interleukin 10 (IL-10), showed elevated expression of IL-10 after treatment with MSC-derived EVs (Ragni *et al.*, 2017). Consistent with these findings, when primary low expressing *POU5F1B* and *PAPPA2* medulloblastoma cells were pre-treated with metastatic exosomes with high levels of *POU5F1B* and *PAPPA2,* we found the abundance of *POU5F1B* and *PAPPA2* was increased in recipient cells, albeit significance was not reached (most likely due to insufficient experimental repeats). Furthermore, there was no increase in expression levels of RNA when recipient cells were treated with vesicle-free supernatant, suggesting that cellular RNAs were being transferred to recipient cells in an exosome-dependent manner. This suggests that mRNA enriched in EVs can be actively shuttled and translated in recipient cells, allowing horizontal transfer of properties from one cell to another. However, it is important to consider that exosomes are enriched in other RNA species including different classes on non-coding RNAs, thus it is likely that a combination of RNAs enriched in EVs has an additive effect on the overall response of the recipient cells, rather than a given mRNA being transferred from one cell to another. Additional studies involving labelling of mRNA transcripts could be beneficial to track RNAs originating from EVs to determine transfer in recipient cells. An example of such was by Probert *et al*., who used 5-Ethynyl Uridine (5EU) labelling to determine exosomal transfer of mRNA and miRNA cargo to osteoblast cells after treatment with prostate cancer-derived EVs (Probert *et al.*, 2019).

7.4 Identification of exosomal miRNA biomarkers through NGS of cell- and patient-derived exosomes

miRNAs are short non-coding single-stranded RNA molecules which function in gene silencing and post-transcriptional regulation of gene expression (Lee et al., 1993). In cancer, they are often heavily dysregulated and have been implicated in all aspects of carcinogenesis (reviewed by Peng and Croce, 2016). Their presence and intercellular transfer in exosomes has provoked deeper investigation of exosomal miRNAs, as novel non-invasive biomarkers and as intracellular signalling vehicles (Rabinowits *et al.*, 2009; Matsumura *et al.*, 2015).

Similar to mRNA cargo, profiling studies have revealed that exosomes of different cellular origin contain a unique expression profile and that tumour characteristics of their cell of origin could be detected in exosomes, thus representing a snapshot of the content of the secreting cell (Di Modica *et al.*, 2017). In line with this, global miRNA signature correlated with medulloblastoma subgroup and malignancy status. Based on multidimensional scaling analysis, there was a clear separation of normal-derived exosomal miRNA compared to medulloblastoma exosomal miRNA profiles, suggesting that malignancy status of the parental cell is reflected in exosomal miRNA cargo and highlighting the diagnostic potential of exosomal miRNA. Moreover, exosomal miRNA content was significantly different between medulloblastoma cell lines, with profiles correlating to the subgroup of their originating cells.

7.4.1 Identification of miRNA-mRNA targets of medulloblastoma exosomes

Several themes emerged with respect to miRNA-mRNA pathway enrichment among the subset of differentially secreted exosomal miRNA. One observation was the enrichment for miRNA regulating genes involved in PI3K/AKT and MAPK signalling pathways. Both the PI3K/AKT and MAPK signalling pathways are key regulators of cellular growth and survival, and aberrant activation of these pathways is commonly observed in multiple cancers and associated with tumour progression and drug

resistance (reviewed by Engelman, 2009). With regards to medulloblastoma, prior investigations have identified that elevated expression of downstream genes of the PI3K/AKT and MAPK signalling pathways are related to poor survival outcome in patients with Group 3 medulloblastoma tumours. Additionally, up-regulation of genes involved in PI3K/AKT signalling were also associated with worst prognosis in Group 4 medulloblastoma tumours (Park *et al.*, 2019). In EVs it has been demonstrated that shuttling of various oncogenic exosomal miRNAs can affect the tumour microenvironment through initiating PI3K/AKT and MAPK signalling pathways in hepatocellular carcinoma, to promote the migration and invasion of non-motile cells through and upregulation of MMPs (He *et al.*, 2015). In this study, we have identified that regulation of these pathways may be mediated by exosomal miRNAs. These findings suggest a novel exosome-driven mechanism through which the tumour can manipulate its microenvironment through initiating pro-tumourigenic signalling pathways.

Secondly, we observed a significant enrichment for exosomal miRNAs targeting a number of pathways related to migration, including focal adhesion and regulation of the actin cytoskeleton. Also of note was the heavy enrichment of biological processes related to differentiation, locomotion, proliferation and projection organization, events that occur in the process of migration. This again is in keeping with the changes in pro-migratory phenotype observed following treatment with metastatic exosomes.

7.4.2 Identifying exosomal miRNAs associated with increased metastatic potential in medulloblastoma

Using differential gene expression analysis, we also identified exosomal miRNA which may show a progression signature of potential biological interest from control → primary → metastatic. Based on this analysis, we found significant differences in the abundance of 12 exosomal miRNAs secreted in metastatic medulloblastoma exosomes, thereby yielding a candidate set of exosomal miRNA for further assessment as metastatic medulloblastoma biomarkers. Importantly, several of the candidate

exosomal miRNA correlated with a worse overall survival in medulloblastoma patient datasets, highlighting the potential clinical utility of the identified miRNA.

As mentioned, at the outset of this project only two exosome studies had been reported, both of which examined the protein cargo of medulloblastoma exosomes and we were not aware of any studies evaluating the miRNA (or any form of RNA) cargo of medulloblastoma exosomes. However, in recent months, two studies focusing on the role of exosomal miRNAs in medulloblastoma progression and the underlying mechanisms involved were released (S. Huang *et al.*, 2020; Zhu *et al.*, 2020). Most similar to our study was by Zhu and colleagues, who used an RNA-seq approach to identify a set of seven exosomal miRNAs originating from aggressive medulloblastoma cells, a selection of which, when transferred into recipient cells, contributed to medulloblastoma cell migration and invasion. In addition, they found that the activation of the ERK/MAPK pathways was likely to be involved in the mechanism by which exosomal miRNAs promote tumour invasion and migration (Zhu *et al.*, 2020). When comparing the identified set of exosomal miRNAs with the set of identified miRNAs in our study, there were no overlaps. This variation in miRNA cargo of exosomes may be a representation of the biological heterogeneity of exosomes, and could further highlight that exosomes of different cellular origin contain a unique expression profile (Crescitelli *et al.*, 2013). However, of the seven miRNAs identified as originating from aggressive medulloblastoma (showed more than a 2-fold difference in Group 3 cell-derived exosomes compared to SHH cells), all miRNAs were identified in our differential expression analysis (Figure 7.2). Although, were not significant when comparing phenotype (metastatic or primary), or when compared to normal control samples. For this reason, they were not taken forward in our analysis. It is of interest to note, that both studies highlighted the involvement of MAPK signalling. However, we further showed that the MAPK pathway remains active in metastatic cells or potentially increases in activity, indicating that exosomes may be biomarkers of pathway activation in aggressive medulloblastoma tumours, which might provide a new therapeutic strategy for metastatic medulloblastoma.

Despite the similarities, the overarching aims between our study and the aforementioned study are substantially different. Zhu and colleagues, identified a panel of miRNAs unique to Group 3-derived exosomes, as compared to one less-migratory SHH cell line (Zhu *et al.*, 2020). This could allow for the subgrouping of a medulloblastoma tumour, however unlike our approach, will not identify drivers of metastasis.

A

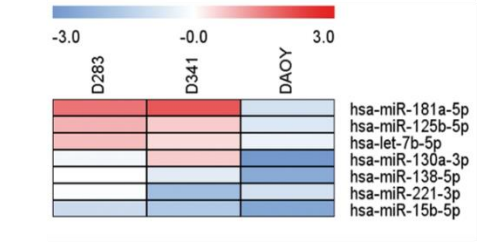

B

miRNA	LogFC (Metastatic V's Primary)
miR-181a-5p	1.12
miR-125b-5p	0.94
let-7b-5p	0.88
miR-138-5p	-0.30
miR-130a-3p	-1.32
miR-221-3p	-1.96
miR-15b-5p	-0.20

Figure 7.2 Comparison of miRNAs between a similar study of medulloblastoma exosomes and data from our study

Heatmap of exosomal miRNA expression in Group 3 cell lines (D283 and D431) compared with SHH cell-derived exosomes (DAOY) from Zhu *et al.,* a similar study of medulloblastoma exosomes (A) Figure taken from (Zhu *et al.*, 2020). Abundance of the same panel of miRNA in data from our study on medulloblastoma exosomes (B).

7.4.3 Exosomes in the CSF of medulloblastoma patients

In the last decade, extracellular vesicles, particularly exosomes, have been increasingly recognised as potential cancer biomarkers which deliver valuable information about the underlying tumour biology. As previously mentioned, they can be easily obtained by non-invasive methods from body fluids such as blood or CSF, this is especially important for cancers where tissue samples are not easily accessible e.g. brain tumours (D'Souza-Schorey Crislyn and Clancy, 2012).

At the start of this thesis, we optimised a method for the reliable, reproducible isolation of exosomes from medulloblastoma cell lines. However, exosome isolation from biofluids is challenging and there is no consensus with respect to the best methodology for isolating exosomes which provides substantial yields with reliable quality (Martins

et al., 2018). Unfortunately, using our method, or a commercially available size-exclusion chromatography method, we were unable to obtain a high enough yield of exosomal RNA required for NGS. As CSF samples were extremely limited, and due to time restraints, further optimisation was not possible, thus CSF samples were sent directly to QIAGEN to perform exosome isolation and NGS. Previous studies comparing exosomes isolated from CSF of glioblastoma patients using ultracentrifugation or exoRNeasy Midi Kit (utilised by Qiagen for our exosome isolations) concluded that both methods are robust and produced consistent and reliable CSF exosome isolations in preparation for miRNA analysis (Akers *et al.*, 2015). It was also noted that the overall distribution of miRNA profiles was similar and independent of the isolation method used (Akers *et al.*, 2015). Therefore, although this was not the method of isolation we hoped to use, we were confident that this chosen isolation method would not be detrimental to the results obtained. Indeed, a comparison of the two data sets revealed 96% of the miRNA identified in cell-derived (CD) exosomes were also reported in CSF patient-derived (PD) exosomes. This not only validates the finding from CD exosomes, but also demonstrates the validity of these cell lines as a model system for medulloblastoma. Further analysis determining the targets of those miRNAs also demonstrated that between the CD and PD exosomes 99% of predicted gene targets are shared. This data indicates an overlap of genes targeted by the exosomal miRNAs, which was further supported by comparative cell component and biological pathway analysis

7.4.4 Potential clinical utility of exosomal miRNAs as non-invasive CSF biomarkers

Due to time restraints, a lack of matched primary tumours and normal control CSF samples, we opted to focus our analyses of CSF miRNAs on substantiating the set of candidate miRNAs identified in our cell lines. Since PD exosomes contained over 4x the amount of miRNA in their exosomes compared to CD exosomes, we reasoned that this restriction would ensure only tumour exosomal miRNAs were being studied for

biomarker purposes. However, the considerable datasets that we have established in this project will now be mined by on-going researchers subsequent to this thesis, and are expected to yield additional data in support of exosomal miRNAs as biomarkers of metastatic medulloblastoma.

Importantly, of the candidate set of miRNA identified in cell-derived exosomes, several (miR-382-5p, miR-381-3p, miR-346, miR-628-5p) were detectable at substantially higher levels in CSF-derived exosomes for a subset of metastatic and recurrent patients, relative to primary and non-metastatic patients, highlighting the downstream clinical potential of exosomal miRNAs as non-invasive CSF biomarkers. This latter finding is important since we are aware of no other studies evaluating exosomal miRNAs (or any other RNA) from CSF as biomarkers of medulloblastoma. Of the three miRNAs identified as showing a progression signature in cell lines and enriched in metastatic CSF patient exosomes, there appeared to be no previous indication of them having a role in medulloblastoma. However, they have all been attributed to oncogenesis and suggested as diagnostic or prognostic markers in other cancer types, as will be explored below.

7.4.4.1 miR-382-5p

miR-382-5p, which in this study was significantly enriched in metastatic cell culture-derived exosomes, compared to primary and normal, and was elevated in metastatic patient-derived exosomes compared to primary. Previous evidence has indicated that miR-382-5p is highly expressed in a variety of tumours, including gastric cancer (Seok *et al.*, 2014), breast cancer (Ho *et al.*, 2017) and oral squamous cell carcinoma (Sun *et al.*, 2019).

The role of miR-382-5p in medulloblastoma progression has not been characterised, however miR-382-5p has been shown to positively regulate Y box-binding protein 1 (YBX1) (Sun *et al.*, 2019). *YBX1* is elevated in medulloblastoma and acts as an oncogene by regulating cellular survival and apoptosis (Dey *et al.*, 2016; Kloetgen *et al.*, 2020). Current work in our lab has also suggested that knockdown of YBX1

increases drug sensitivity to vincristine and cisplatin in medulloblastoma cells (Taylor *et al.,* unpublished data). Therefore, transfer of miR-382-5p via exosomes may target *YBX1*, resulting in enhanced survival and growth of medulloblastoma. Moreover, increased levels of miR-382-5p have been significantly associated with worse overall survival, relapse and metastasis in breast cancer and osteosarcoma (Ho *et al.*, 2017). In this study, upregulation of miR-382-5p was an indicator of poor outcome in medulloblastoma patient datasets. Taken together, these results indicate the potential diagnostic and prognostic value of miR-382-5p in medulloblastoma and may represent a novel target for therapy.

7.4.4.2 miR-381-3p

Similar to miR-382-5p, differential expression analysis showed a strong associating of miR-381-3p with metastatic exosomes in CD and PD exosomes. However, miR-381-3p has been shown to exhibit both tumour suppressor (Yang *et al.*, 2017; Shang *et al.*, 2019) and oncogenic functions (Tang *et al.*, 2011; Zhao *et al.*, 2020), indicating that miR-381-3p may exert its role in both a cell and tissue specific manner. In a study by Tang and colleagues, it was observed that the peripheral blood level of miR-381-3p was found to be significantly higher in brain cancers, including medulloblastoma, compared to normal healthy donors. Levels were also increased with advanced tumour grade, suggesting that miR-381-3p may be a potential diagnostic biomarker for brain tumours. Moreover, overexpression of miR-381-3p using miR-mimics, promoted the proliferation of glioblastoma cells both *in vitro* and in xenograft tumours *in vivo* (Tang *et al.*, 2011).

7.4.4.3 miR-346

miR-346 is a recognised oncogenic miRNA in various cancers (Song *et al.*, 2015). miR-346 has been known to regulate the EMT pathway through targeting *Snail*, which further supresses E-cadherin resulting in increased cell proliferation, invasion and migration. In regards to exosomes, miR-346 was found to be elevated in plasma-

derived exosomes from human ovarian cancer patients, and suggested as a biomarker for disease progression (Wang *et al.*, 2019).

7.4.4.4 miR-628-5p

miR-628-5p was the only miRNA shown to be decreased in malignant exosomes compared to normal exosomes and was decreased in metastatic CSF patient-derived exosomes relative to non-migratory-derived exosomes. miR-628-5p has been reported to be differentially expressed in various cancers, and its expression has mostly been correlated with tumour suppressive functions (Rios-Colon, Deep and Kumar, 2019). Downregulation of miR-628-5p has been evidenced in glioblastoma tissue compared to normal controls (Hua *et al.*, 2012). A later study also revealed miR-628-5p to be beneficial to glioblastoma patient outcome (Li *et al.*, 2013). Furthermore, *Ttk, Cdk2* and *Wee1*, critical members of the cell cycle, were found to be partially regulated by miR-628-5p, suggesting a regulatory role in this cancer (Xie *et al.*, 2019). Transfections with miR-628-5p mimics, decreased cell growth of glioma cell lines, U87 and T98. Additionally, injecting cells with miR-628-5p significantly suppressed glioma tumour growth *in vivo* (Xie *et al.*, 2019). Several studies have also suggested that miR-628-5p could be useful as a cancer biomarker. For example, miR-628-5p levels were significantly lower in serum obtained from prostate cancer patients compared to serum obtained from healthy individuals (Srivastava *et al.*, 2014). In line with these findings, eight patients with colorectal cancer were found to have uniformly downregulated expression of miR-628-5p relative to matched tissue from their normal mucosa (Hamfjord *et al.*, 2012). Taken together, miR-628-5p could be a useful biomarker associated with a more favourable outcome in patients with medulloblastoma, these findings certainly warrant further investigation.

Accumulation of this line of data will hopefully aid medulloblastoma biomarker research but also highlight potential therapeutic targets for medulloblastoma treatment.

7.5 Summary and conclusions

The overall aim of this project was to analyse the role of medulloblastoma exosomes as biomarkers and understand their functional contribution to metastasis. Exosomes are continuously released by all cell types, and increased secretion has been observed in cancer cells. In this thesis, we demonstrated for the first time that aggressive migratory medulloblastoma cells secrete markedly more exosomes compared to less aggressive non-metastatic primary cells, the first indication that exosomes might play a vital role in medulloblastoma metastasis. We showed that metastatic-derived exosomes directly enhanced the migration and invasive potential of less migratory primary tumour cells in a heterologous stimulation loop.

Initially we focussed on how medulloblastoma exosomes interact with the recipient cells utilizing direct extracellular matrix signalling, via surface bound proteins, to activate intracellular signalling pathways. In this context we assessed the expression of tumour-supporting proteins, EMMPRIN and MMP-2. Metastatic exosomes were shown to potentiate medulloblastoma migration via the active protease, MMP-2, on their surface, resulting in degradation of the extracellular matrix (ECM) creating routes for medulloblastoma cells to directionally invade into the surrounding environment. Additionally, functional MMP-2 on the external surface of exosomes could allow exosomes to reach long distance target locations. It was also demonstrated that exosomal MMP-2 and EMMPRIN stimulate medulloblastoma cells to release more MMP-2 into the microenvironment to promote invasion and subsequent migration. Knockdown of these factors partly reduced the invasive potential of exosomes, confirming that MMP-2 and EMMPRIN are pro-migratory factors on exosomes.

The long-term regulation of exosomes via the intracellular delivery of their molecular cargo to recipient cells was also assessed. Using NGS technology to characterise exosomal RNA cargo (mRNA and miRNA) we demonstrated a clear pattern of exosomal RNA cargo that distinguished metastatic medulloblastoma cells from primary and normal cell lines. Further characterisation of the RNA cargo delineated the

targeting of pathways important for medulloblastoma progression and interaction with the surrounding microenvironment, which is in keeping with the changes in pro-migratory phenotype observed following treatment with metastatic exosomes. Differential gene expression analysis of mRNA sequencing data identified *PCAT1, PAPPA2* and *POU5F1B* as highly enriched in metastatic exosomes compared to their matched primary counterpart. The identified genes have all been implicated in cancer progression in various cancer types, and in this study their high expression correlated with poor overall survival and tumour metastasis. Their expression was also elevated in medulloblastoma subgroups compared to normal brain controls, raising the possibility of these candidates as biomarkers for metastatic medulloblastoma, and as potential therapeutic targets for medulloblastoma treatment.

Finally, we identified several miRNA which were differentially secreted in metastatic exosomes relative to primary and normal exosomes, thereby yielding a candidate set of exosomal miRNA for further assessment as biomarkers of increase metastatic potential. Notably, several of the candidate miRNAs (miR-382-5p, miR-381-3p, miR-346, miR-628-5p) were detected at substantially higher levels in CSF of patients with metastatic disease relative to primary medulloblastoma, emphasising the potential clinical utility of these exosomal miRNAs as diagnostic biomarkers.

Taken together, we have demonstrated that medulloblastoma cells release exosomes into the local tumour microenvironment, to create a favourable environment to drive medulloblastoma metastasis, either through extracellular matrix signalling, via surface bound proteins or through intracellular delivery of their RNA cargo to recipient cells. Our observations also highlight the possibility of CSF-derived exosomal miRNAs as biomarkers for metastatic medulloblastoma.

7.6 Future directions

- Aggressive migratory medulloblastoma cells secrete markedly more exosomes with altered cargo compared to primary cells, future work could involve characterising changes in exosome cargo and secretion patterns during cellular stress. Understanding these changes could reveal novel, targetable mechanisms underlying medulloblastoma progression, metastasis, and therapy resistance.
- MMP-2 and EMMPRIN are pro-migratory factors in cell-derived exosomes, to understand the clinical utility of these markers, future work would involve validation in patient-derived exosomes.
- Metastatic exosomes were enriched with other mRNAs that could have been studied as candidate mediators of medulloblastoma progression, including numerous long non-coding mRNAs. Thus, their expression patterns in medulloblastoma exosomes certainly warrant further investigation and validation and will form on-going bioinformatics work subsequent to this thesis.
- The upregulation of several miRNA correlated with poor outcome in medulloblastoma patients, indicating their potential diagnostic and prognostic value. Accumulation of this line of data will hopefully aid medulloblastoma biomarker research but also highlight potential therapeutic targets for medulloblastoma treatment.

References

References

Adachi, E. *et al.* (2016) 'Different growth and metastatic phenotypes associated with a cell-intrinsic change of Met in metastatic melanoma', *Oncotarget*, 7(43), pp. 70779–70793.

Adamson, D. C. *et al.* (2010) 'OTX2 Is Critical for the Maintenance and Progression of Shh-Independent Medulloblastomas', *Cancer Research*, 70(1), pp. 181– 191.

Akers, J. C. *et al.* (2015) 'miRNA contents of cerebrospinal fluid extracellular vesicles in glioblastoma patients', *Journal of Neuro-Oncology*, 123(2), pp. 205–216.

Al-Nedawi, K. *et al.* (2008) 'Intercellular transfer of the oncogenic receptor EGFRvIII by microvesicles derived from tumour cells', *Nature Cell Biology*, 10(5), pp 145-155.

El Andaloussi, S. *et al.* (2013) 'Extracellular vesicles: Biology and emerging therapeutic opportunities', *Nature Reviews Drug Discovery*, 12(5), pp. 347–357.

Angelini, F. *et al.* (2016) 'Foetal bovine serum-derived exosomes affect yield and phenotype of human cardiac progenitor cell culture', *BioImpacts*, 6(1), pp. 15–24.

Angelucci, A. *et al.* (2000) 'Vesicle-associated urokinase plasminogen activator promotes invasion in prostate cancer cell lines', *Clinical and Experimental Metastasis*, 18(2), pp. 163–170.

Atay, S. *et al.* (2014) 'Oncogenic KIT-containing exosomes increasegastrointestinal stromal tumor cell invasion', *Proceedings of the National Academy of Sciences of the United States of America*, 111(2), pp. 711–716.

Azmi, A. S., Bao, B. and Sarkar, F. H. (2013) 'Exosomes in cancer development, metastasis, and drug resistance: A comprehensive review', *Cancer and Metastasis Reviews*. NIH Public Access, pp. 623–642.

Balaj, L. *et al.* (2011) 'Tumour microvesicles contain retrotransposon elements and amplified oncogene sequences', *Nature Communications*, 2(1).

Baran, J. *et al.* (2010) 'Circulating tumour-derived microvesicles in plasma of gastric cancer patients', *Cancer Immunology, Immunotherapy*, 59(6), pp. 841–850.

Barile, L. *et al.* (2018) 'Cardioprotection by cardiac progenitor cell-secreted exosomes: Role of pregnancy-associated plasma protein-A', *Cardiovascular Research*, 114(7), pp. 992–1005.

Becker, M. A. *et al.* (2015) 'A novel neutralizing antibody targeting pregnancy-associated plasma protein-a inhibits ovarian cancer growth and ascites accumulation in patient mouse tumorgrafts', *Molecular Cancer Therapeutics*, 14(4), pp. 973–981.

Bernardo, M. M. and Fridman, R. (2003) 'TIMP-2 (tissue inhibitor of metalloproteinase-2) regulates MMP-2 (matrix metalloproteinase-2) activity in the extracellular environment after pro-MMP-2 activation by MT1 (membrane type 1)-MMP', *Biochemical Journal*, 374(3), pp. 739–745.

Bhoopathi, P. *et al.* (2012) 'MMP-2 mediates mesenchymal stem cell tropism towards medulloblastoma tumors', 18(7), pp. 692–701.

Bhowmick, N. A. *et al.* (2001) 'Transforming growth factor-β1 mediates epithelial to mesenchymal transdifferentiation through a RhoA-dependent mechanism', *Molecular Biology of the Cell*, 12(1), pp. 27–36.

Bi, X. C. *et al.* (2012) 'Extracellular matrix metalloproteinase inducer: A novel poor prognostic marker for human seminomas', *Clinical and Translational Oncology*, 14(3), pp. 190–196.

Bisaro, B. *et al.* (2015) 'Proteomic analysis of extracellular vesicles from medullospheres reveals a role for iron in the cancer progression of medulloblastoma', *Molecular and Cellular Therapies*, 3(1), pp. 1–12.

Bland, C. L. *et al.* (2018) 'Exosomes derived from B16F0 melanoma cells alter the transcriptome of cytotoxic T cells that impacts mitochondrial respiration', *FEBS Journal*, 285(6), pp. 1033–1050.

Boldt, H. B. and Conover, C. A. (2011) 'Overexpression of pregnancy-associated plasma protein-A in ovarian cancer cells promotes tumor growth in vivo', *Endocrinology*, 152(4), pp. 1470–1478.

Bradford, M. M. (1976) ‘A rapid and sensitive method for the quantitation of microgram quantities of protein utilizing the principle of protein-dye binding’, *Analytical Biochemistry*, 72(1–2), pp. 248–254.

Bruno, S. *et al.* (2009) ‘Mesenchymal stem cell-derived microvesicles protect against acute tubular injury’, *Journal of the American Society of Nephrology*, 20(5), pp. 1053–1067.

Campos-Silva, C. *et al.* (2019) ‘High sensitivity detection of extracellular vesicles immune-captured from urine by conventional flow cytometry’, *Scientific Reports*, 9(1), pp. 1–12.

Cancer (2019). Available at: https://www.who.int/health-topics/cancer_1 (Accessed: 16 March 2021).

Caudroy, S. *et al.* (2002) ‘EMMPRIN-mediated MMP regulation in tumor and endothelial cells’, *Clinical and Experimental Metastasis*, 19(8), pp. 697–702.

Cavalli, F. M. G. *et al.* (2017) ‘Intertumoral Heterogeneity within Medulloblastoma Subgroups’, *Cancer Cell*, 31(6), pp. 737-754.e6.

Chambers, A. F., Groom, A. C. and MacDonald, I. C. (2002) ‘Dissemination and growth of cancer cells in metastatic sites’, *Nature Reviews Cancer*, 2(8), pp. 563–572.

Chandru, H., Sharada, A. C. and Manjunath, S. (2007) ‘Expression of matrix metalloproteinase (MMP-2) and extracellular matrix metalloproteinases inducer (EMMPRIN) in benign and advanced breast cancer tissue samples’, *Biomeditsinskaya Khimiya*, 53(4), pp. 461–467.

Chapnick, D. A. *et al.* (2011) ‘Partners in crime: The TGFβ and MAPK pathways in cancer progression’, *Cell and Bioscience*, 1(1), p. 42.

Cheung, K. J. *et al.* (2016) ‘Polyclonal breast cancer metastases arise from collective dissemination of keratin 14-expressing tumor cell clusters’, *Proceedings of the National Academy of Sciences of the United States of America*, 113(7), pp. E854–E863.

Chu, T. *et al.* (2011) ‘Extracellular matrix metalloproteinase inducer is a negative prognostic factor of pediatric medulloblastoma’, *Pathology and Oncology Research*, 17(3), pp. 705–711.

Colangelo, N. W. and Azzam, E. I. (2020) ‘Extracellular vesicles originating from glioblastoma cells increase metalloproteinase release by astrocytes: The role of CD147 (EMMPRIN) and ionizing radiation’, *Cell Communication and Signaling*, 18(1), pp. 1–14.

Colombo, M. *et al.* (2013) ‘Analysis of ESCRT functions in exosome biogenesis, composition and secretion highlights the heterogeneity of extracellular vesicles’, *Journal of Cell Science*, 126(24), pp. 5553–5565.

Cooper, J. and Giancotti, F. G. (2019) ‘Integrin Signaling in Cancer: Mechanotransduction, Stemness, Epithelial Plasticity, and Therapeutic Resistance’, *Cancer Cell*. Cell Press, pp. 347–367.

Crescitelli, R. *et al.* (2013) ‘Distinct RNA profiles in subpopulations of extracellular vesicles: Apoptotic bodies, microvesicles and exosomes’, *Journal of Extracellular Vesicles*, 2(1).

D’Asti, E. *et al.* (2012) ‘Oncogenic extracellular vesicles in brain tumor progression’, *Frontiers in Physiology*, 3, pp. 1–15.

D’Asti, E. *et al.* (2016) ‘Extracellular Vesicles in Brain Tumor Progression’, *Cellular and Molecular Neurobiology*, 36(3), pp. 383–407.

D’Souza-Schorey Crislyn, C. and Clancy, J. W. (2012) ‘Tumor-derived microvesicles: Shedding light on novel microenvironment modulators and prospective cancer biomarkers’, *Genes and Development*, 26(12), pp. 1287–1299.

Dai, J. *et al.* (2020) ‘Exosomes: key players in cancer and potential therapeutic strategy’, *Signal Transduction and Targeted Therapy*, 5(1).

Van Deun, J. *et al.* (2017) ‘EV-TRACK: Transparent reporting and centralizing knowledge in extracellular vesicle research’, *Nature Methods*, 14(3), pp. 228–232.

Dey, A. *et al.* (2016) ‘YB-1 is elevated in medulloblastoma and drives proliferation in Sonic hedgehog-dependent cerebellar granule neuron progenitor cells and medulloblastoma cells’, *Oncogene*, 35(32), pp. 4256–4268.

Diepenbruck, M. and Christofori, G. (2016) ‘Epithelial-mesenchymal transition (EMT) and metastasis: Yes, no, maybe?’, *Current Opinion in Cell Biology*, 43, pp. 7–13.

Dobin, A. *et al.* (2013) ‘STAR: ultrafast universal RNA-seq aligner’, *Bioinformatics*, 29(1), pp. 15–21.

Domvri, K. *et al.* (2020) ‘Exosomal lncRNA PCAT-1 promotes Kras-associated chemoresistance regulation’, 11(29), pp. 2847–2862.

Donovan, M. J. *et al.* (2015) ‘A molecular signature of PCA3 and ERG exosomal RNA from non-DRE urine is predictive of initial prostate biopsy result’, *Prostate Cancer and Prostatic Diseases*, 18(4), pp. 370–375.

Doyle, L. and Wang, M. (2019) ‘Overview of Extracellular Vesicles, Their Origin, Composition, Purpose, and Methods for Exosome Isolation and Analysis’, *Cells*, 8(7), p. 727.

Dudás, J. *et al.* (2018) ‘Nerve growth factor (NGF)—receptor survival axis in head and neck squamous cell carcinoma’, *International Journal of Molecular Sciences*, 19(6).

Dufour, C. *et al.* (2012) ‘Clinical Study Metastatic Medulloblastoma in Childhood: Chang’s Classification Revisited’, *International Journal of Surgical Oncology*, 2012.

Edmondson, R. *et al.* (2014) ‘Three-dimensional cell culture systems and their applications in drug discovery and cell-based biosensors’, *Assay and Drug Development Technologies*. Mary Ann Liebert Inc., pp. 207–218.

Egeblad, M. and Werb, Z. (2002) ‘New functions for the matrix metalloproteinases in cancer progression’, *Nature Reviews Cancer*. European Association for Cardio-Thoracic Surgery, pp. 161–174.

Elmageed, Z. Y. A. *et al.* (2014) ‘Neoplastic reprogramming of patient-derived adipose stem cells by prostate cancer cell-associated exosomes’, *Stem Cells*, 32(4), pp. 983–997.

Engelman, J. A. (2009) ‘Targeting PI3K signalling in cancer: Opportunities, challenges and limitations’, *Nature Reviews Cancer*. Nat Rev Cancer, pp. 550–562.

Epple, L. M. *et al.* (2012) ‘Medulloblastoma exosome proteomics yield functional roles for extracellular vesicles’, *PLoS ONE*, 7(7).

Esteller, M. (2011) ‘Non-coding RNAs in human disease’, *Nature Reviews Genetics*. Nat Rev Genet, pp. 861–874.

ExoCarta: Home - Exosome database (2020). Available at: http://www.exocarta.org/ (Accessed: 16 March 2021).

Faurholdt Gude, M. *et al.* (2016) ‘PAPP-A, IGFBP-4 and IGF-II are secreted by human adipose tissue cultures in a depot-specific manner’, *European Journal of Endocrinology*, 175(6), pp. 509–517.

Ferro, M. P., Heilshorn, S. C. and Owens, R. M. (2020) ‘Materials for blood brain barrier modeling in vitro’, *Materials Science and Engineering R: Reports*, 140, p. 100522.

FIDLER, I. (1970) ‘Metastasis : Quantitative Analysis of Dis- tribution and Fate of Tumor Emboli Labeled’, *J Nat Cancer Inst*.

Friedl, P. (2009) ‘Dynamic imaging of cancer invasion and metastasis: Principles and preclinical applications’, *Clinical and Experimental Metastasis*, 26(4), pp. 269–271.

Fu, F. *et al.* (2018) ‘Circulating Exosomal miR-17-5p and miR-92a-3p Predict Pathologic Stage and Grade of Colorectal Cancer’, *Translational Oncology*, 11(2), pp. 221–232.

Fults, D. W., Taylor, M. D. and Garzia, L. (2019) ‘Leptomeningeal dissemination: A sinister pattern of medulloblastoma growth’, *Journal of Neurosurgery: Pediatrics*, 23(5), pp. 613–621.

FunRich :: Functional Enrichment Analysis Tool :: Home (2019). Available at: http://www.funrich.org/index.html (Accessed: 16 March 2021).

Gabison, E. E. *et al.* (2005) ‘EMMPRIN/CD147, an MMP modulator in cancer, development and tissue repair’, *Biochimie*. Elsevier, pp. 361–368.

Ganji, P. C. N. *et al.* (2011) ‘iRNA-mediated downregulation of MMP-9 and uPAR in combination with radiation induces G2/M cell-cycle arrest in medulloblastoma’, *Molecular Cancer Research*, 9(1), pp. 51–66.

Gonzalez-Avila, G. *et al.* (2019) 'Matrix metalloproteinases participation in the metastatic process and their diagnostic and therapeutic applications in cancer', *Critical Reviews in Oncology/Hematology*. Elsevier Ireland Ltd, pp. 57–83.

González de Vega, R. *et al.* (2019) 'MMP-11 as a biomarker for metastatic breast cancer by immunohistochemical-assisted imaging mass spectrometry', *Analytical and Bioanalytical Chemistry*, 411(3), pp. 639–646.

Grant, B. D. and Donaldson, J. G. (2009) 'Pathways and mechanisms of endocytic recycling'.

Graves, L. E. *et al.* (2004) 'Proinvasive properties of ovarian cancer ascites-derived membrane vesicles', *Cancer Research*, 64(19), pp. 7045–7049.

Greenfield, J. P. and Bilsky, M. H. (2005) 'Neurosurgical interventions for leptomeningeal tumor.', *Cancer treatment and research*. Springer, Boston, MA, pp. 107–119.

Gruenberg, J. and Stenmark, H. (2004) 'The biogenesis of multivesicular endosomes', *Nature Reviews Molecular Cell Biology*. Nat Rev Mol Cell Biol, pp. 317–323.

GSEA | MSigDB | Search Gene Sets (2004). Available at: http://www.gsea-msigdb.org/gsea/msigdb/search.jsp (Accessed: 16 March 2021).

Guo, H. *et al.* (1997) 'Stimulation of matrix metalloproteinase production by recombinant extracellular matrix metalloproteinase inducer from transfected Chinese hamster ovary cells', *Journal of Biological Chemistry*, 272(1), pp. 24–27.

Guo, Y. *et al.* (2018) 'Pregnancy-associated plasma protein a in cancer: expression, oncogenic functions and regulation.', *American journal of cancer research*, 8(6), pp. 955–963.

Gupta, G. P. and Massagué, J. (2006) 'Cancer Metastasis: Building a Framework', *Cell*, 127(4), pp. 679–695.

Hamfjord, J. *et al.* (2012) 'Differential expression of miRNAs in colorectal cancer: Comparison of paired tumor tissue and adjacent normal mucosa using high-throughput sequencing', *PLoS ONE*, 7(4).

Hanahan, D. and Weinberg, R. A. (2011) 'Hallmarks of cancer: The next generation', *Cell*, 144(5), pp. 646–674.

Harris, J. L. *et al.* (2014) 'High-field proton magnetic resonance spectroscopy reveals metabolic effects of normal brain aging', *Neurobiology of Aging*, 35(7), pp. 1686–1694.

Hart, I. R. and Fidler, I. J. (1980) 'Role of organ selectivity in the determination of metastatic patterns of b16 melanoma', *Cancer Research*, 40(7), pp. 2281–2287.

Hatanaka, M. *et al.* (2014) 'Cleaved CD147 shed from the surface of malignant melanoma cells activates MMP2 produced by fibroblasts', *Anticancer Research*, 34(12), pp. 7091–7096.

Hayashi, H. *et al.* (2015) 'The OCT4 pseudogene POU5F1B is amplified and promotes an aggressive phenotype in gastric cancer', *Oncogene*, 34(2), pp. 199–208.

He, M. *et al.* (2015) 'Hepatocellular carcinoma-derived exosomes promote motility of immortalized hepatocyte through transfer of oncogenic proteins and RNAs', *Carcinogenesis*, 36(9), pp. 1008–1018.

Hemler, M. E. (2005) 'Tetraspanin functions and associated microdomains', *Nature Reviews Molecular Cell Biology*, 6(10), pp. 801–811.

Hernan, R. *et al.* (2003) 'ERBB2 up-regulates S100A4 and several other prometastatic genes in medulloblastoma', *Cancer Research*, 63(1), pp. 140–148.

Hjortebjerg, R. *et al.* (2020) 'Pregnancy-Associated Plasma Protein-A2 Is Associated With Mortality in Patients With Lung Cancer', *Frontiers in Endocrinology*, 11, pp. 1–11.

Ho, J. Y. *et al.* (2017) 'MicroRNA-382-5p aggravates breast cancer progression by regulating the RERG/Ras/ERK signaling axis', *Oncotarget*, 8(14), pp. 22443–22459.

Hoshino, A. *et al.* (2015) 'Tumour exosome integrins determine organotropic metastasis', *Nature*, 527(7578), pp. 329–335.

Hua, D. *et al.* (2012) 'A catalogue of glioblastoma and brain MicroRNAs identified by deep sequencing', *OMICS A Journal of Integrative Biology*, 16(12), pp. 690–699.

Huang, G. H. *et al.* (2016) 'Medulloblastoma stem cells: Promising targets in medulloblastoma therapy', *Cancer Science*, 107(5), pp. 583–589.

Huang, L. *et al.* (2019) 'Long noncoding RNA PCAT1, a novel serum-based biomarker, enhances cell growth by sponging miR-326 in oesophageal squamous cell carcinoma', *Cell Death and Disease*, 10(7).

Huang, S. *et al.* (2020) 'Exosomal miR-130b-3p targets SIK1 to inhibit medulloblastoma tumorigenesis', *Cell Death and Disease*, 11(6).

Huang, W. *et al.* (2020) 'Exosomes with low miR-34c-3p expression promote invasion and migration of non-small cell lung cancer by upregulating integrin α2β1', *Signal Transduction and Targeted Therapy*, 5(1), pp. 1–13.

Huang, Z. *et al.* (2014) 'Overexpression of EMMPRIN isoform 2 is associated with head and neck cancer metastasis', *PLoS ONE*, 9(4).

Hugel, B. *et al.* (2005) 'Membrane Microparticles: Two Sides of the Coin', *Physiology*, 20(1), pp. 22– 27.

Ilyin, S. E., Belkowski, S. M. and Plata-Salamán, C. R. (2004) 'Biomarker discovery and validation: Technologies and integrative approaches', *Trends in Biotechnology*, 22(8), pp. 411–416.

Isaacson, K. J. *et al.* (2017) 'Matrix-metalloproteinases as targets for controlled delivery in cancer: An analysis of upregulation and expression', *Journal of Controlled Release*, 259, pp. 62–75.

Ivanov, D. P. *et al.* (2016) 'In vitro models of medulloblastoma: Choosing the right tool for the job', *Journal of Biotechnology*, 236, pp. 10–25.

Joshi, M. and Rajender, S. (2020) 'Long non-coding RNAs (lncRNAs) in spermatogenesis and male infertility', *Reproductive Biology and Endocrinology*. BioMed Central Ltd, pp. 1–18.

Ju, X. Z. *et al.* (2008) 'EMMPRIN expression as a prognostic factor in radiotherapy of cervical cancer', *Clinical Cancer Research*, 14(2), pp. 494–501.

Juraschka, K. and Taylor, M. D. (2019) ‘Medulloblastoma in the age of molecular subgroups: A review: JNSPG 75th Anniversary invited review article’, *Journal of Neurosurgery: Pediatrics*, 24(4), pp. 353–363.

Kaushik, D. K., Hahn, J. N. and Yong, V. W. (2015) ‘EMMPRIN, an upstream regulator of MMPs, in CNS biology’, *Matrix Biology*. Elsevier, pp. 138–146.

Kessenbrock, K., Plaks, V. and Werb, Z. (2010) ‘Matrix Metalloproteinases: Regulators of the Tumor Microenvironment’, *Cell*. Cell, pp. 52–67.

Kessler, A. T. and Bhatt, A. A. (2018) ‘Brain tumour post-treatment imaging and treatment-related complications’, *Insights into Imaging*, 9(6), pp. 1057–1075.

Khushman, M. *et al.* (2019) ‘Exosomal markers (CD63 and CD9) expression and their prognostic significance using immunohistochemistry in patients with pancreatic ductal adenocarcinoma’, *Journal of Gastrointestinal Oncology*, 10(4), pp. 695–702.

Kim, W. *et al.* (2011) ‘The tumor biology and molecular characteristics of medulloblastoma identifying prognostic factors associated with survival outcomes and prognosis’, *Journal of Clinical Neuroscience*, 18(7), pp. 886–890.

Kloetgen, A. *et al.* (2020) ‘Ybx1 indirectly targets heterochromatin-repressed inflammatory response-related apoptosis genes through regulating cbx5 mrna’, *International Journal of Molecular Sciences*, 21(12), pp. 1–17.

Kobayashi, M. *et al.* (2014) ‘Ovarian cancer cell invasiveness is associated with discordant exosomal sequestration of Let-7 miRNA and miR-200’, *Journal of Translational Medicine*, 12(1), pp. 1–12.

Koles, K. *et al.* (2012) ‘Mechanism of evenness interrupted (Evi)-exosome release at synaptic boutons’, *Journal of Biological Chemistry*, 287(20), pp. 16820–16834.

Kool, M. *et al.* (2008) ‘Integrated Genomics Identifies Five Medulloblastoma Subtypes with Distinct Genetic Profiles, Pathway Signatures and Clinicopathological Features’, *PLOS ONE*, 3(8), p. e3088.

Kool, M. *et al.* (2014) ‘Genome sequencing of SHH medulloblastoma predicts genotype-related response to smoothened inhibition’, *Cancer Cell*, 25(3), pp. 393–405.

Koyama, S. (2004) ‘Significance of cell-surface expression of matrix metalloproteinases and their inhibitors on gastric epithelium and infiltrating mucosal lymphocytes in progression of Helicobacter pylori-associated gastritis’, *Scandinavian Journal of Gastroenterology*, 39(11), pp. 1046–1053.

Kulasingam, V. and Diamandis, E. P. (2008) ‘Tissue culture-based breast cancer biomarker discovery platform’, *International Journal of Cancer*. Int J Cancer, pp. 2007–2012.

Laemmli, U. K. (1970) ‘Cleavage of structural proteins during the assembly of the head of bacteriophage T4’, *Nature*, 227(5259), pp. 680–685.

Langhorst, M. F., Reuter, A. and Stuermer, C. A. O. (2005) ‘Scaffolding microdomains and beyond: The function of reggie/flotillin proteins’, *Cellular and Molecular Life Sciences*, 62(19–20), pp. 2228–2240.

Laursen, L. S. *et al.* (2001) ‘Pregnancy-associated plasma protein-A (PAPP-A) cleaves insulin-like growth factor binding protein (IGFBP)-5 independent of IGF: implications for the mechanism of IGFBP-4 proteolysis by PAPP-A’, *FEBS Letters*, 504(1–2), pp. 36–40.

Lee, R. C., Feinbaum, R. L. and Ambros, V. (1993) ‘The C. elegans heterochronic gene lin-4 encodes small RNAs with antisense complementarity to lin-14’, *Cell*, 75(5), pp. 843–854.

Li, H. *et al.* (2017) ‘CD147 and glioma: a meta-analysis’, *Journal of Neuro-Oncology*, 134(1), pp. 145–156.

Li, M. Y., Liu, L. Z. and Dong, M. (2021) ‘Progress on pivotal role and application of exosome in lung cancer carcinogenesis, diagnosis, therapy and prognosis’, *Molecular Cancer*. BioMed Central Ltd, pp. 1–22.

Li, Y. *et al.* (2013) ‘Comprehensive analysis of the functional microRNA-mRNA regulatory network identifies miRNA signatures associated with glioma malignant progression’, *Nucleic Acids Research*, 41(22).

Li, Z. B., Chen, X. and Yi, X. J. (2021) ‘Tumor promoting effects of exosomal microRNA-210 derived from lung cancer cells on lung cancer through the RUNX3/PI3K/AKT signaling pathway axis.’, *Journal of biological regulators and homeostatic agents*, 35(2).

Di Liegro, C. M., Schiera, G. and Di Liegro, I. (2017) ‘Extracellular vesicle-associated RNA as a carrier of epigenetic information’, *Genes*, 8(10).

Liu, J. *et al.* (2020) ‘Immune suppressed tumor microenvironment by exosomes derived from gastric cancer cells via modulating immune functions’, *Scientific Reports*, 10(1), p. 14749.

Liu, W. *et al.* (2020) ‘Hypoxic mesenchymal stem cell-derived exosomes promote bone fracture healing by the transfer of miR-126’, *Acta Biomaterialia*, 103, pp. 196–212.

Löffek, S., Schilling, O. and Franzke, C. W. (2011) ‘Series “matrix metalloproteinases in lung health and disease” edited by J. Müller-Quernheim and O. Eickelberg number 1 in this series: Biological role of matrix metalloproteinases: A critical balance’, *European Respiratory Journal*. European Respiratory Society, pp. 191–208.

Loomis, R. J. *et al.* (2006) ‘Citron Kinase, a RhoA Effector, Enhances HIV-1 Virion Production by Modulating Exocytosis’, *Traffic*, 7(12), pp. 1643–1653.

Lötvall, J. *et al.* (2014) ‘Minimal experimental requirements for definition of extracellular vesicles and their functions: A position statement from the International Society for Extracellular Vesicles’, *Journal of Extracellular Vesicles*, 12, pp. 123-131.

Louis, D. N. *et al.* (2007) ‘The 2007 WHO classification of tumours of the central nervous system’, *Acta Neuropathologica*, 114(2), pp. 97–109.

Louis, D. N. *et al.* (2016) ‘The 2016 World Health Organization Classification of Tumors of the Central Nervous System: a summary’, *Acta Neuropathologica*, 131(6), pp. 803–820.

Love, M. I., Huber, W. and Anders, S. (2014) ‘Moderated estimation of fold change and dispersion for RNA-seq data with DESeq2’, *Genome Biology*, 15(12), p. 550.

Lu, X. and Kang, Y. (2007) ‘Organotropism of breast cancer metastasis’, *Journal of Mammary Gland Biology and Neoplasia*, 12(2–3), pp. 153–162.

Ludwig, N. *et al.* (2019) ‘Isolation and Analysis of Tumor-Derived Exosomes’, *Current Protocols in Immunology*, 127(1), p. e91.

Lv, M. *et al.* (2014) ‘Exosomes mediate drug resistance transfer in MCF-7 breast cancer cells and a probable mechanism is delivery of P-glycoprotein’, *Tumor Biology*, 35(11), pp. 10773–10779.

Machida, T. *et al.* (2016) ‘MIR 1246 and MIR-4644 in salivary exosome as potential biomarkers for pancreatobiliary tract cancer’, *Oncology Reports*, 36(4), pp. 2375–2381.

Martins, T. S. *et al.* (2018) ‘Exosome isolation from distinct biofluids using precipitation and column-based approaches’, *PLoS ONE*, 13(6).

Matsumura, T. *et al.* (2015) ‘Exosomal microRNA in serum is a novel biomarker of recurrence in human colorectal cancer’, *British Journal of Cancer*, 113(2), pp. 275–281.

Menck, K. *et al.* (2015) ‘Tumor-derived microvesicles mediate human breast cancer invasion through differentially glycosylated EMMPRIN’, *Journal of Molecular Cell Biology*, 7(2), pp. 143–153.

Menyhárt, O. and Győrffy, B. (2020) ‘Molecular stratifications, biomarker candidates and new therapeutic options in current medulloblastoma treatment approaches’, *Cancer and Metastasis Reviews*, 39(1), pp. 211–233.

Miklja, Z. *et al.* (2019) ‘Molecular profiling and targeted therapy in pediatric gliomas: Review and consensus recommendations’, *Neuro-Oncology*, 21(8), pp. 968–980.

Di Modica, M. *et al.* (2017) ‘Breast cancer-secreted miR-939 downregulates VE-cadherin and destroys the barrier function of endothelial monolayers’, *Cancer Letters*, 384, pp. 94–100.

Muller, L. *et al.* (2014) ‘Isolation of biologically-active exosomes from human plasma’, *Journal of immunological methods*, 411, pp. 55–65.

Nabeshima, K. *et al.* (2002) ‘Matrix metalloproteinases in tumor invasion: Role for cell migration’, *Pathology International*. Pathol Int, pp. 255–264.

Van Niel, G., D'Angelo, G. and Raposo, G. (2018) 'Shedding light on the cell biology of extracellular vesicles', *Nature Reviews Molecular Cell Biology*, 19(4), pp. 213–228.

Nieuwland, R. *et al.* (2020) 'Rigor and standardization of extracellular vesicle research: Paving the road towards robustness', *Journal of Extracellular Vesicles*, 10(2), p. e12037.

Northcott, P. A. *et al.* (2011) 'Pediatric and adult sonic hedgehog medulloblastomas are clinically and molecularly distinct', *Acta Neuropathologica*, 122(2), pp. 231–240.

Northcott, P. A. *et al.* (2012) 'Medulloblastomics: The end of the beginning', *Nature Reviews Cancer*, 12(12), pp. 818–834.

Northcott, P. A. *et al.* (2019) 'Medulloblastoma', *Nature Reviews Disease Primers*, 5(1).

O'Doherty, U., Swiggard, W. J. and Malim, M. H. (2000) 'Human Immunodeficiency Virus Type 1 Spinoculation Enhances Infection through Virus Binding', *Journal of Virology*, 74(21), pp. 10074–10080.

Offersen, B. V *et al.* (2010) 'Acta Oncologica Matrix metalloproteinase-9 measured in urine from bladder cancer patients is an independent prognostic marker of poor survival'.

Van Ommeren, R. *et al.* (2020) 'The molecular biology of medulloblastoma metastasis', *Brain Pathology*, 30(3), pp. 691–702.

Orr, B. A. (2020) 'Pathology, diagnostics, and classification of medulloblastoma', *Brain Pathology*, 30(3), pp. 664–678.

Ostrowski, M. *et al.* (2010) 'Rab27a and Rab27b control different steps of the exosome secretion pathway', *Nature Cell Biology*, 12(1), pp. 19–30.

Paget, S. (1889) 'The distribution of secondary growths in cancer of the breast.', *The Lancet*, 133(3421), pp. 571–573.

Pan, Y. *et al.* (2018) 'POU5F1B promotes hepatocellular carcinoma proliferation by activating AKT', *Biomedicine and Pharmacotherapy*, 100, pp. 374–380.

Panagopoulos, I. *et al.* (2008) 'A PCR/restriction digestion assay for the detection of the transcript variants 1 and 2 of POU5F1', *Genes Chromosomes and Cancer*, 47(6), pp. 521–529.

Park, A. K. *et al.* (2019) 'Subgroup-specific prognostic signaling and metabolic pathways in pediatric medulloblastoma', *BMC Cancer*, 19(1), p. 571.

Parolini, I. *et al.* (2009) 'Microenvironmental pH is a key factor for exosome traffic in tumor cells', *Journal of Biological Chemistry*, 284(49), pp. 34211–34222.

Paterson, E. K. and Courtneidge, S. A. (2018) 'Invadosomes are coming: new insights into function and disease relevance', *The FEBS Journal*, 285(1), pp. 8–27.

Peacock, B. *et al.* (2018) 'Extracellular vesicle microRNA cargo is correlated with HPV status in oropharyngeal carcinoma', *Journal of Oral Pathology and Medicine*, 47(10), pp. 954–963.

Peinado, H. *et al.* (2012) 'Melanoma exosomes educate bone marrow progenitor cells toward a pro-metastatic phenotype through MET', *Nature Medicine*, 18(6), pp. 883–891.

Peng, Y. and Croce, C. M. (2016) 'The role of microRNAs in human cancer', *Signal Transduction and Targeted Therapy*. Springer Nature.

Pfister, S. *et al.* (2009) 'Outcome prediction in pediatric medulloblastoma based on DNA copy-number aberrations of chromosomes 6q and 17q and the MYC and MYCN loci', *Journal of Clinical Oncology*, 27(10), pp. 1627–1636.

Phoenix, T. N. *et al.* (2017) 'Phoenix et al 2016 medulloblastoma genotype dictate BBB phenotype.pdf', 29(4), pp. 508–522.

Pollack, I. F., Agnihotri, S. and Broniscer, A. (2019) 'Childhood brain tumors: Current management, biological insights, and future directions', *Journal of Neurosurgery: Pediatrics*, 23(3), pp. 261–273.

Pols, M. S. and Klumperman, J. (2009) 'Trafficking and function of the tetraspanin CD63', *Experimental Cell Research*. Academic Press Inc., pp. 1584–1592.

Prensner, J. R. and Chinnaiyan, A. M. (2011) 'The emergence of lncRNAs in cancer biology', *Cancer Discovery*. Cancer Discov, pp. 391–407.

Probert, C. *et al.* (2019) 'Communication of prostate cancer cells with bone cells via extracellular vesicle RNA; a potential mechanism of metastasis', *Oncogene*, 38(10), pp. 1751–1763.

Qu, J. L. *et al.* (2009) 'Gastric cancer exosomes promote tumour cell proliferation through PI3K/Akt and MAPK/ERK activation', *Digestive and Liver Disease*, 41(12), pp. 875–880.

Rabinowits, G. *et al.* (2009) 'Exosomal microRNA: A diagnostic marker for lung cancer', *Clinical Lung Cancer*, 10(1), pp. 42–46.

Ragni, E. *et al.* (2017) 'Extracellular Vesicle-Shuttled mRNA in Mesenchymal Stem Cell Communication', *Stem Cells*, 35(4), pp. 1093–1105.

Ramaswamy, V. *et al.* (2016) 'Risk stratification of childhood medulloblastoma in the molecular era: the current consensus', *Acta Neuropathologica*, 131(6), pp. 821–831.

Rao, J. S. *et al.* (2007) 'MMP-9 SiRNA Induced Senescence Resulting In Inhibition of Medulloblastoma Growth via p16 INK4A and MAPK Pathway', *Cancer research*, 67(10), pp. 4956–4964.

Raposo, G. *et al.* (1996) 'B lymphocytes secrete antigen-presenting vesicles', *Journal of Experimental Medicine*, 183(3), pp. 1161–1172.

Raposo, G. and Stoorvogel, W. (2013) 'Extracellular vesicles: Exosomes, microvesicles, and friends', *Journal of Cell Biology*, 200(4), pp. 373–383.

Redzic, J. S. *et al.* (2013) 'Extracellular Vesicles Secreted from Cancer Cell Lines Stimulate Secretion of MMP-9, IL-6, TGF-β1 and EMMPRIN', *PLoS ONE*, 8(8).

Reed, J. C. (2000) 'Warner-Lambert/Parke Davis award lecture: Mechanisms of apoptosis', *American Journal of Pathology*. American Society for Investigative Pathology Inc., pp. 1415–1430.

Ren, J. *et al.* (2017) 'Characterization of exosomal RNAs derived from human gastric cancer cells by deep sequencing', *Tumor Biology*, 39(4), p. 101042831769501.

Ren, R. *et al.* (2019) ‘Colon cancer cells secrete exosomes to promote self-proliferation by shortening mitosis duration and activation of STAT3 in a hypoxic environment’, *Cell and Bioscience*, 9(1), p. 62.

Rikkert, L. G. *et al.* (2019) ‘Quality of extracellular vesicle images by transmission electron microscopy is operator and protocol dependent’, *Journal of Extracellular Vesicles*, 8(1).

Rios-Colon, L., Deep, G. and Kumar, D. (2019) ‘Emerging role of microRNA 628-5p as a novel biomarker for cancer and other diseases’, *Tumor Biology*. SAGE Publications Ltd, p. 101042831988134.

Robinson, M. H. *et al.* (2019) ‘Upregulation of the chromatin remodeler HELLS is mediated by YAP1 in Sonic Hedgehog Medulloblastoma’, *Scientific Reports*, 9(1), pp. 1–15.

Rochkind, S. *et al.* (1991) ‘Extracranial metastases of medulloblastoma in adults: literature review’, *J Neurol Neurosurg Psychiatry*, 54, pp. 80–86.

Rodini, C. O. *et al.* (2012) ‘Expression analysis of stem cell-related genes reveal OCT4 as a predictor of poor clinical outcome in medulloblastoma’, *Journal of Neuro-Oncology*, 106(1), pp. 71–79.

Royo, F. *et al.* (2020) ‘Methods for Separation and Characterization of Extracellular Vesicles: Results of a Worldwide Survey Performed by the ISEV Rigor and Standardization Subcommittee’, *Cells*, 9(9), p. 1955.

Rudin, C. M. *et al.* (2009) ‘Treatment of Medulloblastoma with Hedgehog Pathway Inhibitor GDC-0449’, *New England Journal of Medicine*, 361(12), pp. 1173–1178.

R2: Genomics Analysis and Visualization Platform. Available at: https://hgserver1.amc.nl/cgi-bin/r2/main.cgi (Accessed: 16 March 2021).

Sakka, L., Coll, G. and Chazal, J. (2011) ‘Anatomy and physiology of cerebrospinal fluid’, *European Annals of Otorhinolaryngology, Head and Neck Diseases*. Elsevier Masson SAS, pp. 309–316.

Sato-Kuwabara, Y. *et al.* (2015) 'The fusion of two worlds: Non-coding RNAs and extracellular vesicles - Diagnostic and therapeutic implications (Review)', *International Journal of Oncology*, 46(1), pp. 17–27.

Savina, A., Vidal, M. and Colombo, M. I. (2002) 'The exosome pathway in K562 cells is regulated by Rab11', *Journal of Cell Science*, 115(12), pp. 2505–2515.

Seo, M. *et al.* (2018) 'Stemness-attenuating miR-503-3p as a paracrine factor to regulate growth of cancer stem cells', *Stem Cells International*, 2018.

Seok, J. K. *et al.* (2014) 'MicroRNA-382 induced by HIF-1α is an angiogenic miR targeting the tumor suppressor phosphatase and tensin homolog', *Nucleic Acids Research*, 42(12), pp. 8062–8072.

Shang, A. *et al.* (2019) 'miR-381-3p restrains cervical cancer progression by downregulating FGF7', *Journal of Cellular Biochemistry*, 120(1), pp. 778–789.

Shelke, G. V. *et al.* (2014) 'Importance of exosome depletion protocols to eliminate functional and RNA-containing extracellular vesicles from fetal bovine serum', *Journal of Extracellular Vesicles*, 3(1), pp. 1–8.

Shi, R. *et al.* (2015) 'Exosomal levels of miRNA-21 from cerebrospinal fluids associated with poor prognosis and tumor recurrence of glioma patients', *Oncotarget*, 6(29), pp. 26971–26981.

Shimoda, M. and Khokha, R. (2017) 'Metalloproteinases in extracellular vesicles', *Biochimica et Biophysica Acta - Molecular Cell Research*, 1864(11), pp. 1989–2000.

Shurtleff, M. J. *et al.* (2016) 'Y-box protein 1 is required to sort microRNAs into exosomes in cells and in a cell-free reaction', *eLife*, 5.

Sidhom, K., Obi, P. O. and Saleem, A. (2020) 'A review of exosomal isolation methods: Is size exclusion chromatography the best option?', *International Journal of Molecular Sciences*. MDPI AG, pp. 1–19.

Sier, C. F. M. *et al.* (2006) 'EMMPRIN-induced MMP-2 activation cascade in human cervical squamous cell carcinoma', *International Journal of Cancer*, 118(12), pp. 2991–2998.

da Silva, P. B. G. *et al.* (2017) 'High OCT4A levels drive tumorigenicity and metastatic potential of medulloblastoma cells', *Oncotarget*, 8(12), pp. 19192–19204.

Simons, M. and Raposo, G. (2009) 'Exosomes - vesicular carriers for intercellular communication', *Current Opinion in Cell Biology*. Curr Opin Cell Biol, pp. 575–581.

Sinha, S. *et al.* (2016) 'Cortactin promotes exosome secretion by controlling branched actin dynamics', *Journal of Cell Biology*, 214(2), pp. 197–213.

Skog, J. *et al.* (2008) 'Glioblastoma microvesicles transport RNA and proteins that promote tumour growth and provide diagnostic biomarkers', *Nature Cell Biology*, 10(12), pp. 1470–1476.

Smith, A. and McCulloh, R. J. (2015) 'Hemopexin and haptoglobin: Allies against heme toxicity from hemoglobin not contenders', *Frontiers in Physiology*. Frontiers Media S.A., p. 187.

Song, G. *et al.* (2015) 'MiR-346 and miR-138 competitively regulate hTERT in GRSF1- and AGO2-dependent manners, respectively', *Scientific Reports*, 5(1), pp. 1–15.

Soo, C. Y. *et al.* (2012) 'Nanoparticle tracking analysis monitors microvesicle and exosome secretion from immune cells', *Immunology*, 136(2), pp. 192–197.

Srivastava, A. *et al.* (2014) 'Circulatory miR-628-5p is downregulated in prostate cancer patients', *Tumor Biology*, 35(5), pp. 4867–4873.

Steinbichler, T. B. *et al.* (2018) 'Epithelial-mesenchymal crosstalk induces radioresistance in HNSCC cells', *Oncotarget*, 9(3), pp. 3641–3652.

Stenmark, H. (2009) 'Rab GTPases as coordinators of vesicle traffic', *Nature Reviews Molecular Cell Biology*. Nature Publishing Group, pp. 513–525.

Sternlicht, M. D. and Werb, Z. (2001) ‘How matrix metalloproteinases regulate cell behavior’, in *Annual Review of Cell and Developmental Biology*. Annu Rev Cell Dev Biol, pp. 463–516.

Sun, J. and Hemler, M. E. (2001) ‘Regulation of MMP-1 and MMP-2 production through CD147/extracellular matrix metalloproteinase inducer interactions’, *Cancer Research*, 61(5),

Sun, L. P. *et al.* (2019) ‘Cancer-associated fibroblast-derived exosomal miR-382-5p promotes the migration and invasion of oral squamous cell carcinoma’, *Oncology Reports*, 42(4), pp. 1319–1328.

Sung, H. *et al.* (2021) ‘Global cancer statistics 2020: GLOBOCAN estimates of incidence and mortality worldwide for 36 cancers in 185 countries’, *CA: A Cancer Journal for Clinicians*, 0(0), pp. 1–41.

Svalina, M. N. *et al.* (2016) ‘IGF1R as a Key Target in High Risk, Metastatic Medulloblastoma’, *Scientific Reports*, 6(June), pp. 1–14.

Tagliatela, A. C. *et al.* (2020) ‘Coronin 1C inhibits melanoma metastasis through regulation of MT1-MMP-containing extracellular vesicle secretion’, *Scientific Reports*, 10(1), p. 11958.

Tanaka, Y. *et al.* (2004) ‘Genetic downregulation of pregnancy-associated plasma protein-A (PAPP-A) by bikunin reduces IGF-I-dependent Akt and ERK1/2 activation and subsequently reduces ovarian cancer cell growth, invasion and metastasis’, *International Journal of Cancer*, 109(3), pp. 336–347.

Tang, H. *et al.* (2011) ‘Interaction of hsa-miR-381 and glioma suppressor LRRC4 is involved in glioma growth’, *Brain Research*, 1390, pp. 21–32.

Tang, Y. *et al.* (2004) ‘Tumor-Stroma Interaction: Positive Feedback Regulation of Extracellular Matrix Metalloproteinase Inducer (EMMPRIN) Expression and Matrix Metalloproteinase-Dependent Generation of Soluble EMMPRIN’, *Molecular Cancer Research*, 2(2), pp. 73–80.

Tang, Y. *et al.* (2005) 'Extracellular matrix metalloproteinase inducer stimulates tumor angiogenesis by elevating vascular endothelial cell growth factor and matrix metalloproteinases', *Cancer Research*, 65(8), pp. 3193–3199.

Taylor, D. D. and Gercel-Taylor, C. (2013) 'The origin, function, and diagnostic potential of RNA within extracellular vesicles present in human biological fluids', *Frontiers in Genetics*, 4(JUL), p. 142.

Taylor, M. D. *et al.* (2012) 'Molecular subgroups of medulloblastoma: The current consensus', *Acta Neuropathologica*, 123(4), pp. 465–472.

Tech, K. *et al.* (2017) 'Pyruvate kinase inhibits proliferation during postnatal cerebellar neurogenesis and suppresses medulloblastoma formation', *Cancer Research*, 77(12), pp. 3217–3230.

Théry, C. *et al.* (2006) 'Isolation and Characterization of Exosomes from Cell Culture Supernatants', *Current Protocols in Cell Biology*, pp. 30:3.22:3.22.1–3.22.29.

Théry, C. *et al.* (2018) 'Minimal information for studies of extracellular vesicles 2018 (MISEV2018): a position statement of the International Society for Extracellular Vesicles and update of the MISEV2014 guidelines', *Journal of Extracellular Vesicles*, 7(1).

Théry, C., Zitvogel, L. and Amigorena, S. (2002) 'Exosomes: Composition, biogenesis and function', *Nature Reviews Immunology*, 2(8), pp. 569–579.

Tian, Y. *et al.* (2020) 'Quality and efficiency assessment of six extracellular vesicle isolation methods by nano-flow cytometry', *Journal of Extracellular Vesicles*, 9(1), p. 1697028.

Tsai, W. C. *et al.* (2013) 'EMMPRIN expression positively correlates with WHO grades of astrocytomas and meningiomas', *Journal of Neuro-Oncology*, 114(3), pp. 281–290.

Valadi, H. *et al.* (2007) 'Exosome-mediated transfer of mRNAs and microRNAs is a novel mechanism of genetic exchange between cells', *Nature Cell Biology*, 9(6), pp. 654–659.

Del Valle, L. *et al.* (2002) 'Insulin-like growth factor I receptor signaling system in JC virus T antigen-induced primitive neuroectodermal tumors - Medulloblastomas', *Journal of NeuroVirology*. J Neurovirol, pp. 138–147.

Vasconcelos, M. H. *et al.* (2019) 'Extracellular vesicles as a novel source of biomarkers in liquid biopsies for monitoring cancer progression and drug resistance', *Drug Resistance Updates*, 47.

Vesiclepedia: Home - Extracellular vesicles database (2018). Available at: http://microvesicles.org/ (Accessed: 16 March 2021).

Vogel, R. *et al.* (2021) 'Measuring particle concentration of multimodal synthetic reference materials and extracellular vesicles with orthogonal techniques: Who is up to the challenge?', *Journal of Extracellular Vesicles*, 10(3).

Wang, L. *et al.* (2020) 'Exosome-transferred LINC01559 promotes the progression of gastric cancer via PI3K/AKT signaling pathway', *Cell Death and Disease*, 11(9), pp. 1–14.

Wang, W. *et al.* (2019) 'The Value of Plasma-Based MicroRNAs as Diagnostic Biomarkers for Ovarian Cancer', *American Journal of the Medical Sciences*, 358(4), pp. 256–267.

Wang, X. *et al.* (2015) 'Medulloblastoma subgroups remain stable across primary and metastatic compartments', *Acta Neuropathologica*, 129(3), pp. 449–457.

Wang, X. and Dai, J. (2010) 'Concise review: Isoforms of OCT4 contribute to the confusing diversity in stem cell biology', *Stem Cells*, 28(5), pp. 885–893.

Wang, Y. H. *et al.* (2018) 'Tumor-Derived Exosomal Long Noncoding RNAs as Promising Diagnostic Biomarkers for Prostate Cancer', *Cellular Physiology and Biochemistry*, 46(2), pp. 532–545.

Wang, Z. *et al.* (2012) 'Proteomic analysis of urine exosomes by multidimensional protein identification technology (MudPIT)', *Proteomics*, 12(2), pp. 329–338.

Wei, Y. *et al.* (2017) 'Pyruvate kinase type M2 promotes tumour cell exosome release via phosphorylating synaptosome-associated protein 23', *Nature Communications*, 8, pp. 1–12.

Wei, Z. *et al.* (2016) 'Fetal Bovine Serum RNA Interferes with the Cell Culture derived Extracellular RNA', *Scientific Reports*, 6, pp. 1–6.

Whiteside, T. L. (2016) ‘Tumor-Derived Exosomes and Their Role in Cancer Progression’, in *Advances in Clinical Chemistry*. Academic Press Inc., pp. 103–141.

Witwer, K. W. *et al.* (2013) ‘Standardization of sample collection, isolation and analysis methods in extracellular vesicle research’, *Journal of Extracellular Vesicles*, 2(1).

Wu, X. *et al.* (2012) ‘Clonal selection drives genetic divergence of metastatic medulloblastoma’, *Nature*, 482(7386), pp. 529–533.

Xie, P. *et al.* (2019) ‘MicroRNA-628-5p inhibits cell proliferation in glioma by targeting DDX59’, *Journal of Cellular Biochemistry*, 120(10), pp. 17293–17302.

Xin, X. *et al.* (2016) ‘CD147/EMMPRIN overexpression and prognosis in cancer: A systematic review and meta-analysis’, *Scientific Reports*. Nature Publishing Group.

Xu, L., Nirwane, A. and Yao, Y. (2019) ‘Basement membrane and blood-brain barrier’, *Stroke and Vascular Neurology*, 4(2), pp. 78–82.

Yamamoto, H. *et al.* (2016) ‘BARHL2 Methylation Using Gastric Wash DNA or Gastric Juice Exosomal DNA is a Useful Marker For Early Detection of Gastric Cancer in an H. pylori - Independent Manner’, *Clinical and Translational Gastroenterology*, 7(7), p. e184.

Yang, X. *et al.* (2017) ‘miR-381-3p suppresses the proliferation of oral squamous cell carcinoma cells by directly targeting FGFR2’, *American Journal of Cancer Research*, 7(4), pp. 913–922.

Yang, Z. *et al.* (2019) ‘PCAT-1: A pivotal oncogenic long non-coding RNA in human cancers’, *Biomedicine and Pharmacotherapy*, 110, pp. 493–499.

Yanshina, D. D. *et al.* (2018) ‘Structural features of the interaction of the 3′-untranslated region of mRNA containing exosomal RNA-specific motifs with YB-1, a potential mediator of mRNA sorting’, *Biochimie*, 144, pp. 134–143.

Ye, L. F. *et al.* (2020) ‘Detection of Prostate Cancer Antigen 3 and Prostate Cancer Susceptibility Candidate in Non-DRE Urine Improves Diagnosis of Prostate Cancer in Chinese Population’, *Prostate Cancer*, 2020, pp.123-131.

Zapotocky, M. *et al.* (2018) 'Differential patterns of metastatic dissemination across medulloblastoma subgroups', *Journal of Neurosurgery: Pediatrics*, 21(2), pp. 145–152.

Zarovni, N. *et al.* (2015) 'Integrated isolation and quantitative analysis of exosome shuttled proteins and nucleic acids using immunocapture approaches', *Methods*, 87, pp. 46–58.

Zhan, Y. *et al.* (2018) 'Expression signatures of exosomal long non-coding RNAs in urine serve as novel non-invasive biomarkers for diagnosis and recurrence prediction of bladder cancer 11 Medical and Health Sciences 1112 Oncology and Carcinogenesis', *Molecular Cancer*, 17(1), pp. 1–5.

Zhang, P. *et al.* (2019) 'Knockdown of long non-coding RNA PCAT1 in glioma stem cells promotes radiation sensitivity', *Medical Molecular Morphology*, 52(2), pp. 114–122.

Zhang, X. *et al.* (2015) 'Exosomes in cancer: small particle, big player.', *Journal of hematology & oncology*, 8, p. 83.

Zhao, C. *et al.* (2020) 'MicroRNA-381-3p Functions as a Dual Suppressor of Apoptosis and Necroptosis and Promotes Proliferation of Renal Cancer Cells', *Frontiers in Cell and Developmental Biology*, 8, p. 290.

Zhao, S. *et al.* (2011) 'Expression of *OCT4* pseudogenes in human tumours: lessons from glioma and breast carcinoma', *The Journal of Pathology*, 223(5), pp. 672–682.

Zhao, X. *et al.* (2015) 'RAS/MAPK activation drives resistance to Smo inhibition, metastasis, and tumor evolution in Shh pathway-dependent tumors', *Cancer Research*, 75(17), pp. 3623–3635.

Zhou, X. *et al.* (2017) 'Exosome production and its regulation of EGFR during wound healing in renal tubular cells', *American Journal of Physiology - Renal Physiology*, 312(6), pp. F963–F970.

Zhu, H. *et al.* (2012) 'EMMPRIN regulates cytoskeleton reorganization and cell adhesion in prostate cancer', *Prostate*, 72(1), pp. 72–81.

Zhu, L. Y. *et al.* (2020) ‘Aggressive medulloblastoma-derived exosomal miRNAs promote in vitro invasion and migration of tumor cells via Ras/MAPK pathway’, *Journal of Neuropathology and Experimental Neurology*, 79(7), pp. 734–745.

Zomer, A. *et al.* (2015) ‘In vivo imaging reveals extracellular vesicle-mediated phenocopying of metastatic behavior’, *Cell*, 161(5), pp. 1046–1057.

Appendices

Appendices

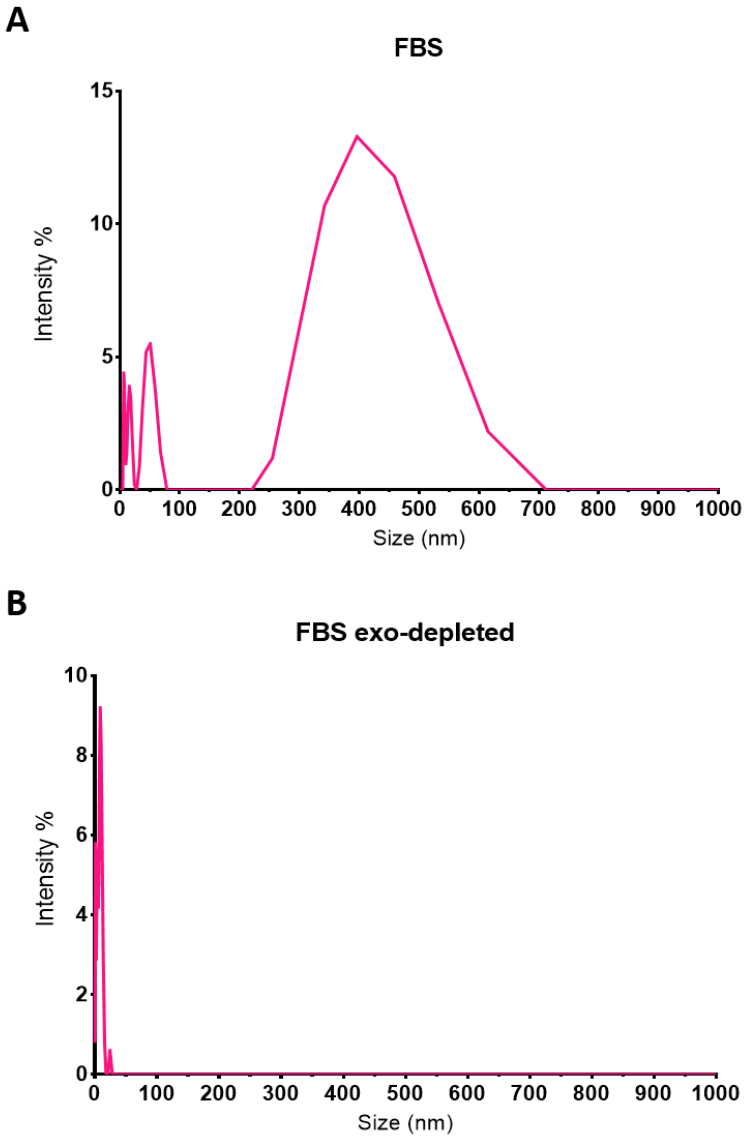

Appendix Figure 1 DLS reading of FBS and exo-depleted FBS

Foetal bovine serum (FBS) is a rich source of exosomes. To ensure we only studied medulloblastoma derived exosomes, FBS was subject to overnight ultracentrifugation at 100,000 x *g*. Normal FBS was then compared with exo-depleted FBS by dynamic light scattering (DLS). (A) Normal FBS showing a range of different particle sizes (B) FBS after ultracentrifugation, showing no measurable bovine exosomes.

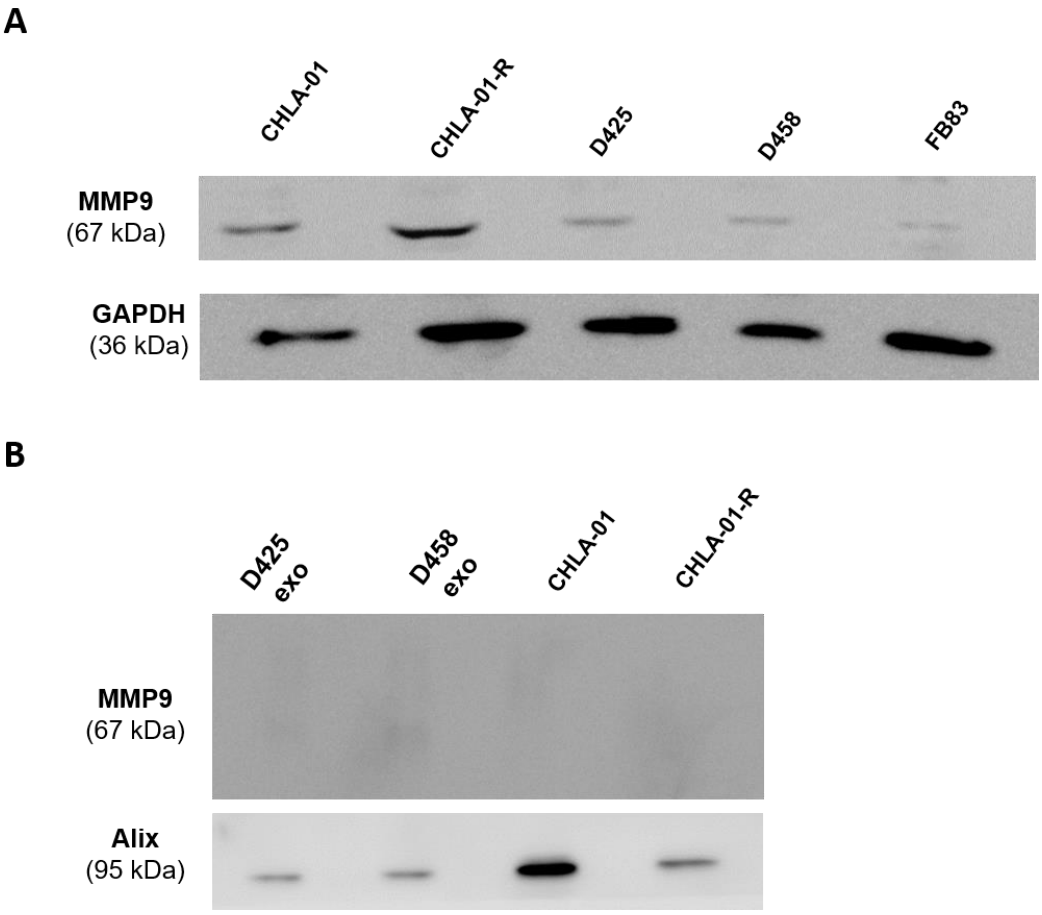

Appendix Figure 2 MMP-9 protein expression in medulloblastoma cell lines and exosomes

The two pairs of cell lines from subgroups 3 (D425 and D458) and 4 (CHLA-01 and CHLA-01-R), which have a matched primary and metastatic pair from the same patient, were selected. (A) MMP-9 protein expression was determined in cell lines by western blotting, GAPDH protein expression was used as an internal control. (B) MMP-9 protein expression was determined in exosomes, Alix was used as an internal control. Data represent one independent experiment.

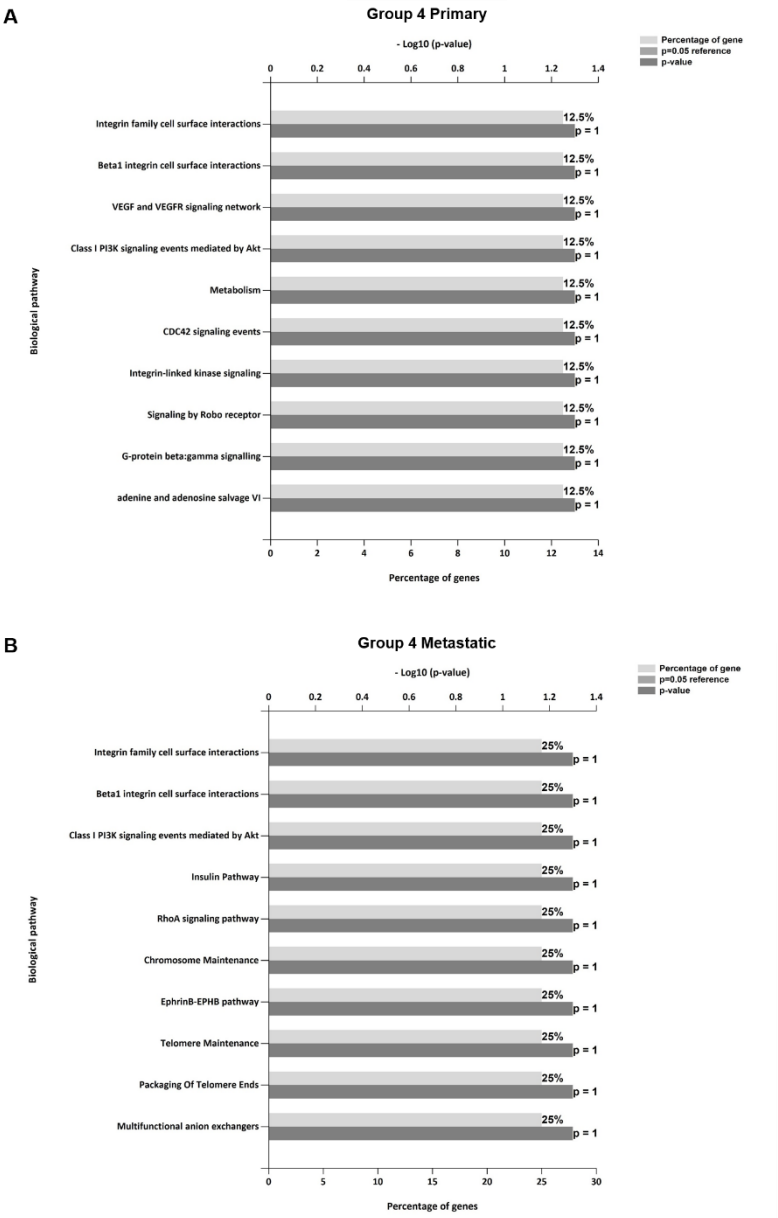

Appendix Figure 3 Biological pathway analysis targeting by Group 4 exosomal RNA

Pathway analysis is shown for exosomes derived from Group 4 primary (A) and metastatic (B). Significance was calculated using Fisher's exact test.

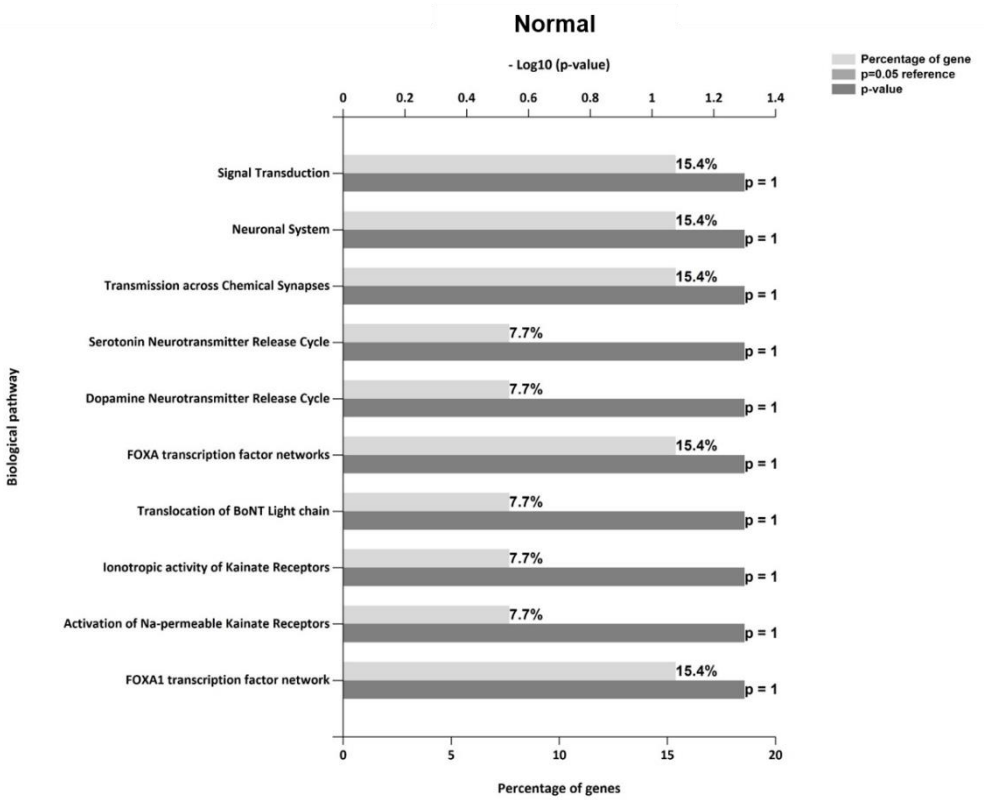

Appendix Figure 4 Biological pathway analysis targeting by normal exosomal RNA

Pathway analysis is shown for exosomes derived from normal exosomes. Significance was calculated using Fisher's exact test.

Appendix Table 1 **Gene transcripts enriched in metastatic exosomes from Group 3**

Gene symbol	Gene name	Gene function
POU5F1B	POU Class 5 Homeobox 1B	The encoded protein is nearly the same length as and highly similar to the POU class 5 homeobox 1 transcription factor (OCT4), has been shown to be a transcriptional activator and may play a role in carcinogenesis
CCDC26	Coiled-Coil Domain Containing 26	RNA Gene, and is affiliated with the lncRNA class. Diseases associated with CCDC26 include Malignant Glioma and Astrocytoma.
RP11-382A18.1 (EIF3H)	Eukaryotic Translation Initiation Factor 3 Subunit H	Protein Coding gene. Diseases associated with EIF3H include Trichorhinophalangeal Syndrome, Type Ii and Trichorhinophalangeal Syndrome, Type I.
PCAT1	Prostate Cancer Associated Transcript 1	This gene produces a long non-coding RNA that promotes cell proliferation and is upregulated in prostate, colorectal, and other cancers. This RNA negatively regulates the BRCA2 tumor suppressor protein and positively regulates Myc oncoprotein.
RP11-1085N6.3 (FAM84B)	Family with sequence similarity 84 member B	Protein coding gene, diseased associated with FAM84B include Lymph node cancer and prostate cancer

Appendix Table 2 **All gene transcripts enriched in metastatic exosomes from Group 4**

Gene symbol	Gene name	Gene function
TMEM260	Transmembrane protein 260	Protein Coding gene. Diseases associated with TMEM260 include Structural Heart Defects And Renal Anomalies Syndrome and Joubert Syndrome
DLG1	Discs Large MAGUK Scaffold Protein 1	May have a role in septate junction formation, signal transduction, cell proliferation, synaptogenesis and lymphocyte activation.
PAPPA2	Pappalysin 2	Encodes a member of the pappalysin family of metzincin metalloproteinases. The encoded protein cleaves insulin-like growth factor-binding protein 5 and is thought to be a local regulator of insulin-like growth factor (IGF) bioavailability
SPATA17	Spermatogenesis Associated 17	Protein coding gene
STPG2	Sperm Tail PG-Rich Repeat Containing 2	Protein coding gene
ADGRV1	Adhesion G Protein-Coupled Receptor V1	Member of the G-protein coupled receptor superfamily. The encoded protein contains a 7-transmembrane receptor domain, binds calcium and is expressed in the central nervous system.
DNAH14	Dynein Axonemal Heavy Chain 14	Dyneins are microtubule-associated motor protein complexes composed of several heavy, light, and intermediate chains
DNM3	Dynamin 3	This gene encodes a member of a family of guanosine triphosphate (GTP)-binding proteins that associate with microtubules and are involved in vesicular transport.
RP11-76K10.1	Long non-coding RNA	Function unknown
RP11-168O22.1	Long non-coding RNA	Function unknown
RP11-1077A2.1	OTX2 Antisense RNA 1 (Head To Head)	RNA Gene, and is affiliated with the lncRNA class.
RP11-8L2.1	Long non-coding RNA	Function unknown
RP11-89M16.1	Long Intergenic Non-Protein Coding RNA 824	RNA Gene, and is affiliated with the lncRNA class. Diseases associated with LINC00824 include Pneumothorax, Primary Spontaneous.
RP11-1085N6.5	(Clone-based (Vega) gene	Function unknown

Appendix Table 3 **All gene transcripts enriched in metastatic exosomes from Group 3 and Group 4**

Gene symbol	Gene name	Gene function
EIF4G3	Eukaryotic Translation Initiation Factor 4 Gamma 3	Involved in mRNA cap recognition and transport of mRNAs to the ribosome. Synthesis of the encoded protein, and this leads to a global increase in protein translation and cell proliferation.
FAM189A1	Family With Sequence Similarity 189 Member A1	Protein Coding gene. Diseases associated with FAM189A1 include Lung Disease, Immunodeficiency, And Chromosome Breakage Syndrome
RP11-1136L8.1 (CASC11)	Cancer Susceptibility 11	RNA Gene, and is affiliated with the lncRNA class. Diseases associated with CASC11 include Astrocytoma and Colorectal Cancer.
PVT1	Pvt1 Oncogene	This gene represents a long non-coding RNA locus that has been identified as a candidate oncogene. Increased copy number and overexpression of this gene are associated with many types of cancers including breast and ovarian cancers, acute myeloid leukemia and Hodgkin lymphoma.
RP11-255B23.3 (FAM84B)	Family with sequence similarity 84 member B	Protein coding gene, diseased associated with FAM84B include Lymph node cancer and prostate cancer

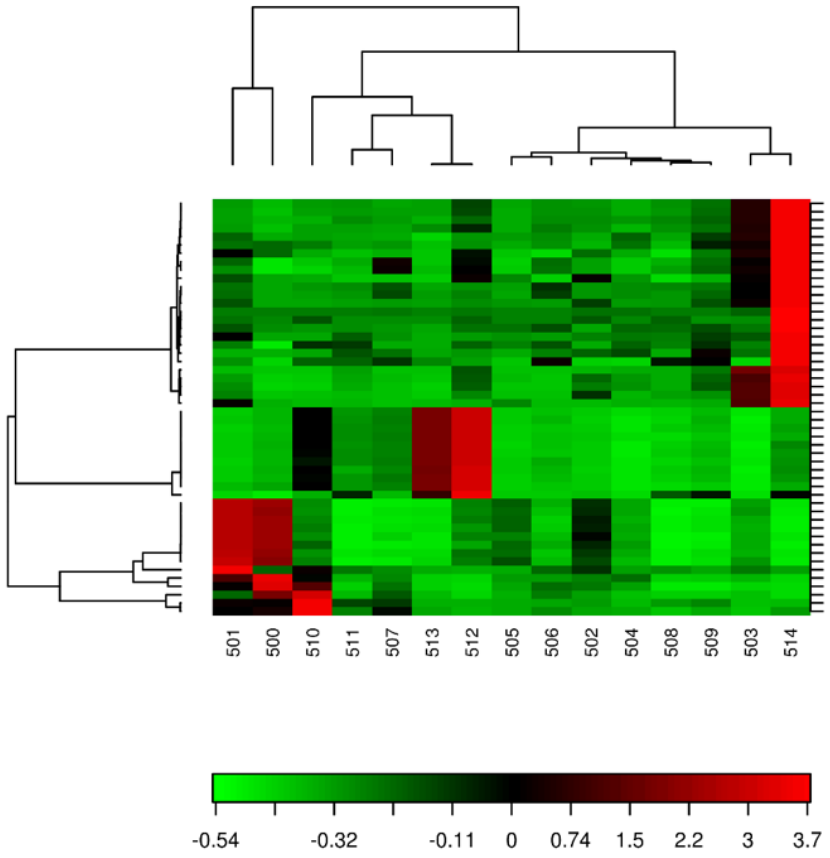

Appendix Figure 5 Heatmap of unbiased clustering of all samples prior to removal of sample 514

Unsupervised transformed miRNA counts were used to create a heatmap representing the top 50 miRNA with the largest variance across all samples. The heatmap shows unbiased hierarchal clustering of samples, each row represents a gene and individual samples are displayed in columns along the bottom. The colour scale signifies the relative expression level of a gene across all samples. Expression levels above and below the mean are displayed in green and red, respectively.

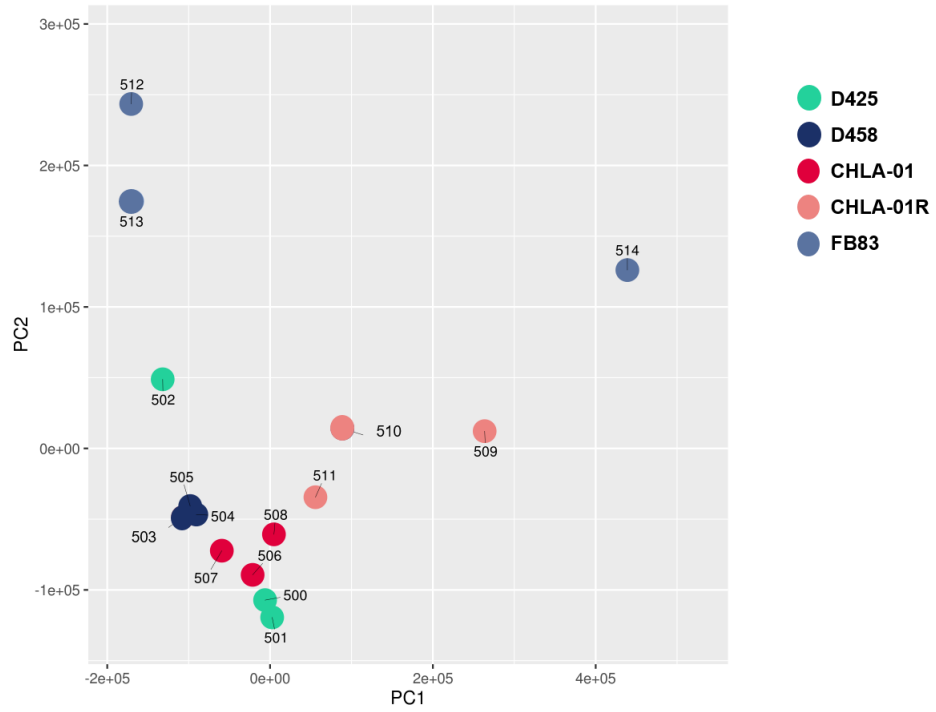

Appendix Figure 6 Principle component analysis for all samples

Principle component analysis (PCA) was performed on all samples using exosomal miRNA which had a minimum read number of ≤10, the data is normalized with weighted trimmed mean of M-values (TMM) method and an overview of how the samples cluster based on miRNA levels is obtained. The PCA plot shows variation among the RNA-seq samples, distance between the samples indicates dissimilarity. FB83 (normal) samples 512 and 513 cluster together away from malignant samples, however sample 514 was separate and was therefore excluded from further analysis.

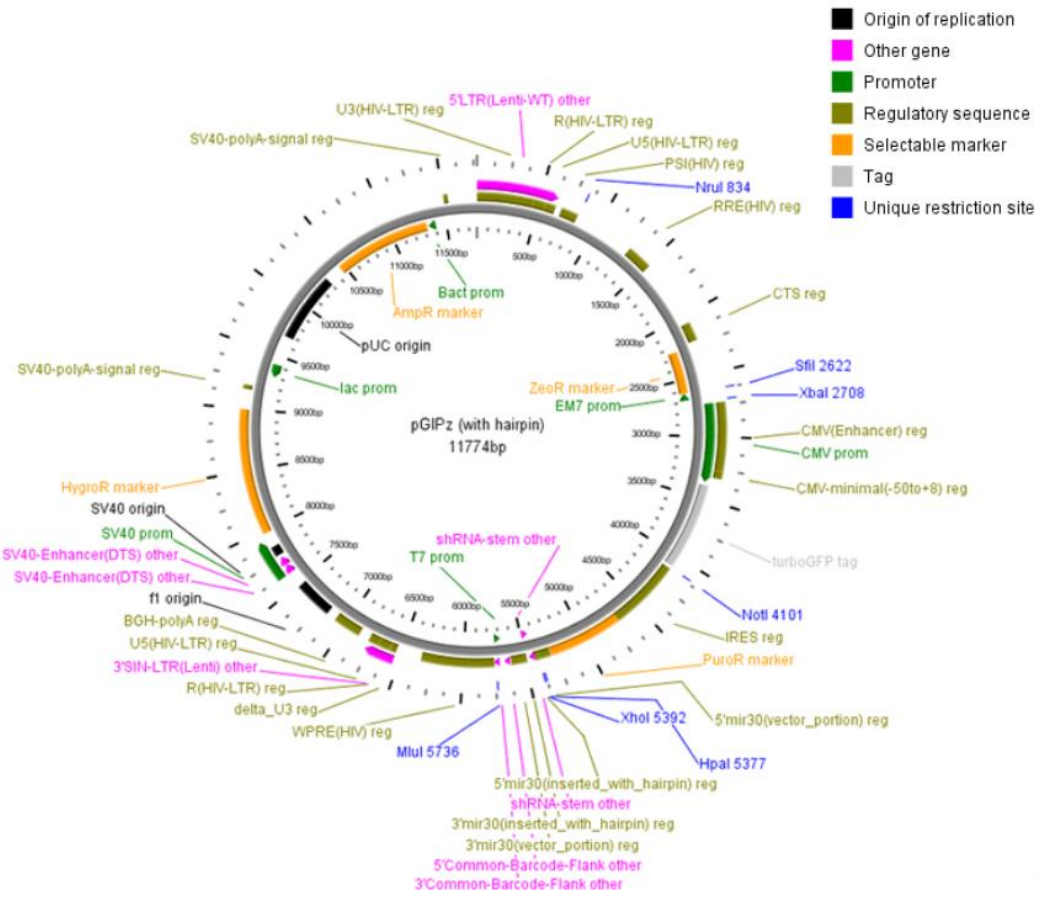

Appendix Figure 7 Lentiviral DNA plasmid map

Cell lines with stable knockdown of *BSG* and *MMP-2* expression were generated though shRNA-mediated gene silencing. GIPZ™ Lentiviral particle starter kits (*BSG*; Horizon Discovery, VGH5526-EG4313, MMP-2; VGH5526-EG682) were used for subsequent transduction of CHLA-01R and D458 cell lines.